

**The development and validation of ultra-thin-film micro-outlet devices  
for spatially constraining local O<sub>2</sub> perturbations to capillaries**

By © Meghan E Kiley, BSc

A Thesis submitted to the School of Graduate Studies in partial fulfillment of the  
requirements for the degree of **Master of Science in Medicine (Cardiovascular  
Sciences)**

Division of Biomedical Sciences, Faculty of Medicine

Memorial University of Newfoundland

**October 2023**

St. John's, Newfoundland, and Labrador

## ABSTRACT

Several local mechanisms for oxygen concentration  $[O_2]$  sensing and blood flow regulation in the microvasculature have been proposed, but existing evidence fails to account for the sensitivity of vascular responses in specific vessels across the physiological range of tissue  $[O_2]$ . We hypothesize that oxygen-mediated blood flow regulation is initiated at the capillary level through oxygen saturation-dependent ATP release from erythrocytes. The purpose of this thesis was to develop and validate a thin-film micro-outlet device that can impose spatially constrained  $O_2$  perturbations at the capillary level to precisely target capillary level regulation. The device was fabricated using soft lithography techniques and high-precision laser cutting. Devices were laser-machined into polyvinylidene chloride film and spun coat with a 100-micrometer thick layer of polydimethylsiloxane. Rats were anesthetized via intraperitoneal injection of sodium pentobarbital; catheters were introduced into the carotid artery for systemic cardiovascular monitoring and jugular vein for supplemental fluids. The extensor digitorum longus (EDL) muscle was blunt dissected, isolated, and reflected over a microfluidic gas exchange chamber (GEC) mounted in the stage of an inverted microscope. The GEC and EDL were coupled with micro-outlet devices of various designs (diameters: 200, 400, 600, 1000  $\mu\text{m}$ ).  $[O_2]$  in the EDL was dynamically manipulated by imposing  $[O_2]$  oscillations while recording intravital video. Our novel composite thin-film micro-outlet devices spatially confined oxygen perturbations to capillaries. Our results demonstrate that our-devices can profoundly manipulate capillary  $SO_2$  and simultaneously alter the hemodynamics in vessels directly overlying the micro-

outlet without affecting capillary  $\text{SO}_2$  at distances greater than 100  $\mu\text{m}$  from the edge of the micro-outlets. All animal protocols were approved by Memorial University's Institutional Animal Care Committee.

Keywords:

*Microcirculation, oxygen transport, blood flow regulation, micro-fluidic device*

## GENERAL SUMMARY

Capillary-level blood flow regulation has been studied, but always with the interaction of higher-level vessels such as arterioles. This thesis focused on analyzing regulatory responses to changing oxygen concentration in capillary networks. We fabricated a gas-based micro-outlet device which allowed direct manipulation of tissue microenvironments by altering gas conditions in confined skeletal muscle tissue regions. Male rats were anesthetized with sodium pentobarbital and a muscle of the hind limb was reflected over a gas exchange chamber combined with a micro-outlet device. Real-time video recordings were taken on the microvasculature of the muscle during varying oxygen conditions. We measured oxygen levels and blood flow through various hemodynamic and oxygen saturation measurements. Our results showed that blood flow increased when oxygen levels were low and decreased when high. This was a consistent finding in all micro-outlet sizes. Interestingly, capillary blood flow responses were observed in our 200- $\mu\text{m}$  micro-outlet, where only 3-6 capillaries overlay the outlet. The results from this size micro-outlet support the concept that oxygen-mediated blood flow is regulated at the capillary level.

## ACKNOWLEDGMENTS

I have been blessed with the support of many people throughout my master's degree experience. I would like to take the time to express my gratitude to the wonderful people who have helped me complete my research project and thesis journey.

First, I would like to say thank you to the wonderful lab members I had the chance to spend many days in the experiment and analysis room with. They dedicated time to helping me be successful in my research project and I could not have done it without them. Reilly Smith, a past lab member, supported me during crucial moments when I began device development and in early stages of my experimental work. I would also like to thank Brenda Wells, a lab member who has supported many of my experiments and answered many of my questions. I am grateful for her calm presence and genuine support always. From day one, Gaylene Russell McEvoy provided me with tremendous guidance throughout my research project, answering countless of my questions, teaching me many lab skills, and giving me reassurance when needed. I am extremely grateful for her support.

Secondly, I would like to thank my committee members, Dr. Bruno Stuyvers and Dr. Anil Zechariah. Their support and insightful advice during committee meetings helped me be successful in my research project.

Additionally, I could not have fabricated my devices without the high precision laser cutting work of mechanical technologists Matthew Fudge and Evan Kearley from Engineering Technical Services of Memorial University.

Finally, I would like to give many thanks to my wonderful, caring supervisor Dr. Graham Fraser, who has been a great teacher, listener, and supporter of me throughout my entire experience. I am very fortunate to have a genuine, empathetic, and enthusiastic supervisor like Dr. Fraser. He is truly passionate about cardiovascular science and our niche field of study; this has provided me with a great learning experience and life lessons to take with me into my future aspirations.

Lastly, I would also like to thank NSERC, CIHR, the School of Graduate Studies, and the Faculty of Medicine Research and Graduate Studies, for providing funding support, as without it this research project would not have been possible.

## TABLE OF CONTENTS

ABSTRACT .....	II
ACKNOWLEDGMENTS .....	VI
LIST OF FIGURES .....	XI
LIST OF APPENDICES .....	XXII
ABBREVIATIONS .....	XXIII
CO-AUTHORSHIP STATEMENT .....	XXVII
CHAPTER 1: INTRODUCTION.....	1
1.1 OBJECTIVES .....	1
1.2 OXYGEN TRANSPORT AS A ROLE OF THE CARDIOVASCULAR SYSTEM.....	4
1.3 MICROCIRCULATION .....	9
1.4 MICROVASCULAR BLOOD FLOW REGULATION .....	15
1.5 MECHANISMS OF OXYGEN-MEDIATED BLOOD FLOW REGULATION AND LOCATIONS OF THE OXYGEN SENSOR .....	22
1.6 MICROVASCULAR PREPARATIONS & MEASUREMENTS .....	33
1.7 MICROFLUIDIC DEVICES USED IN MICROVASCULAR STUDIES.....	50
1.8 SUMMARY .....	62
CHAPTER 2: DEVELOPMENT OF ULTRA-THIN FILM MICRO-OUTLETS FOR SPATIALLY CONSTRAINING LOCAL O <sub>2</sub> PERTURBATIONS TO CAPILLARIES.	63
2.1 INTRODUCTION .....	63

2.2 METHODS .....	68
2.2.1 Computer-Aided Design.....	68
2.2.2 3D Printing Modular Gas Exchange Chamber .....	69
2.2.3 Micro-Outlet Device Fabrication.....	69
2.2.3.1 Fabrication of micro-outlets .....	70
2.2.3.2 Fabrication of composite gas exchange membranes .....	70
2.2.4 Animal Protocol.....	71
2.2.4.1 Instrumentation and physiological monitoring.....	71
2.2.4.2 Surgical isolation of EDL muscle.....	73
2.2.5 Imposed Oxygen Oscillations and Challenges .....	74
2.2.6 Offline analysis using custom MATLAB software .....	77
2.2.7 Hemodynamic and oxygen saturation measurements .....	77
2.3 RESULTS .....	78
2.3.1 Systemic Physiological Measurements .....	78
2.3.2 Results: 400 $\mu\text{m}$ Micro-Outlet Oxygen Oscillation Data .....	83
2.3.3 Results: 400 $\mu\text{m}$ Micro-Outlet Oxygen Challenge Data .....	98
2.3.4 Results: 200 $\mu\text{m}$ Micro-Outlet Oxygen Oscillation Data .....	126
2.3.5 Results: 200 $\mu\text{m}$ Micro-Outlet Oxygen Challenge Data .....	141
2.3.6 Results: 1000 and 600 $\mu\text{m}$ Micro-Outlet Oscillation and Challenge Data .....	169
2.4 DISCUSSION .....	169
2.4.1 Oxygen Oscillations .....	174
2.4.2 Oxygen Challenges.....	180
2.5 ACKNOWLEDGEMENTS .....	185

CHAPTER 3: SUMMARY .....	186
3.1 SUMMARY AND DISCUSSION OF RESULTS .....	186
3.2 LIMITATIONS .....	187
3.3 FUTURE DIRECTIONS .....	188
3.4 FINAL SUMMARY .....	190
REFERENCES .....	192
APPENDIX 1 .....	225
APPENDIX 2 .....	309

## LIST OF FIGURES

Figure 1.1 Basic morphological structure of the microcirculation.....	14
Figure 1.2 Proposed mechanism responsible for oxygen (O <sub>2</sub> ) mediated blood flow regulation at the capillary level.....	32
Figure 1.3 Schematic of a space-time image with visual representation of hemodynamic parameters of a single capillary. ....	45
Figure 1.4 Offline analysis completed with custom matlab software to measure capillary rbc oxygen saturation and hemodynamics.....	47
Figure 1.5 Molar attenuation coefficients of hemoglobin.....	49
Figure 1.6 Three-dimensional computer aided design (CAD) model of a 3D printed gas exchange chamber.....	56
Figure 1.7 Intravital video microscopy setup.....	57
Figure 2.1 Experimental setup of the animal placed on top of the micro-outlet and gas exchange chamber inserted into the microscope stage.....	76
Figure 2.2 200- $\mu$ m micro-outlet device in various forms to be coupled with IVVM. ....	81
Figure 2.3 Comparison of the optical properties obtained in our micro-outlet device with a previous device used in vivo.....	82
Figure 2.4 Capillary rbc oxygen saturation in response to oxygen oscillations for capillaries directly overlying the 400 $\mu$ m micro-outlet. ....	84
Figure 2.5 Capillary rbc oxygen saturation responses in capillaries at various distances outside the 400 $\mu$ m micro-outlet edge. ....	86

Figure 2.6 Capillary hematocrit levels in response to oxygen oscillations for capillaries directly overlying the 400 $\mu\text{m}$ micro-outlet. ....	89
Figure 2.7 Capillary hematocrit values in capillaries at various distances outside the 400 $\mu\text{m}$ micro-outlet edge. ....	91
Figure 2.8 Capillary rbc velocity for capillaries overlying the 400 $\mu\text{m}$ micro-outlet following 4-minute oxygen oscillations. ....	92
Figure 2.9 Capillary rbc velocity for capillaries outside the 400 $\mu\text{m}$ micro-outlet at varying distances from the outlet edge following 4-minute oxygen oscillations. ....	94
Figure 2.10 Capillary rbc supply rate for capillaries overlying the 400 $\mu\text{m}$ micro-outlet following 4-minute oxygen oscillations. ....	95
Figure 2.11 Capillary rbc supply rate for capillaries outside the 400 $\mu\text{m}$ micro-outlet at varying distances from the outlet edge following 4-minute oxygen oscillations. ....	97
Figure 2.12 Capillary rbc oxygen saturation in response to high oxygen challenges for capillaries directly overlying the 400 $\mu\text{m}$ micro-outlet. ....	99
Figure 2.13 Capillary rbc oxygen saturation responses in capillaries at various distances outside the 400 $\mu\text{m}$ micro-outlet edge in response to high oxygen challenges. ....	101
Figure 2.14 Capillary rbc oxygen saturation in response to low oxygen challenges for capillaries directly overlying the 400 $\mu\text{m}$ micro-outlet. ....	102
Figure 2.15 Capillary rbc oxygen saturation responses in capillaries at various distances outside the 400 $\mu\text{m}$ micro-outlet edge in response to low oxygen challenges. ....	104
Figure 2.16 Capillary hematocrit levels in response to high oxygen challenges for capillaries directly overlying the 400 $\mu\text{m}$ micro-outlet. ....	106

Figure 2.17 Capillary hematocrit levels in capillaries at various distances outside the 400 $\mu\text{m}$ micro-outlet edge in response to high oxygen challenges.....	108
Figure 2.18 Capillary hematocrit levels in response to low oxygen challenges for capillaries directly overlying the 400 $\mu\text{m}$ micro-outlet. ....	109
Figure 2.19 Capillary hematocrit levels in capillaries at various distances outside the 400 $\mu\text{m}$ micro-outlet edge in response to low oxygen challenges. ....	111
Figure 2.20 Capillary rbc velocity response to high oxygen challenges for capillaries directly overlying the 400 $\mu\text{m}$ micro-outlet. ....	114
Figure 2.21 Capillary rbc velocity levels in capillaries at various distances outside the 400 $\mu\text{m}$ micro-outlet edge in response to high oxygen challenges. ....	116
Figure 2.22 Capillary rbc velocity response to low oxygen challenges for capillaries directly overlying the 400 $\mu\text{m}$ micro-outlet. ....	117
Figure 2.23 Capillary rbc velocity in capillaries at various distances outside the 400 $\mu\text{m}$ micro-outlet edge in response to low oxygen challenges. ....	119
Figure 2.24 Capillary rbc supply rate response to high oxygen challenges for capillaries directly overlying the 400 $\mu\text{m}$ micro-outlet. ....	120
Figure 2.25 Capillary rbc supply rate in capillaries at various distances outside the 400 $\mu\text{m}$ micro-outlet edge in response to high oxygen challenges. ....	122
Figure 2.26 Capillary rbc supply rate in response to low oxygen challenges for capillaries directly overlying the 400 $\mu\text{m}$ micro-outlet. ....	123
Figure 2.27 Capillary rbc supply rate in capillaries at various distances outside the 400 $\mu\text{m}$ micro-outlet edge in response to low oxygen challenges. ....	125

Figure 2.28 Capillary rbc oxygen saturation in response to oxygen oscillations for capillaries directly overlying the 200 $\mu\text{m}$ micro-outlet. ....	127
Figure 2.29 Capillary rbc oxygen saturation responses in capillaries at various distances outside the 200 $\mu\text{m}$ micro-outlet edge. ....	129
Figure 2.30 Capillary hematocrit levels in response to oxygen oscillations for capillaries directly overlying the 200 $\mu\text{m}$ micro-outlet. ....	131
Figure 2.31 Capillary hematocrit values in capillaries at various distances outside the 200 $\mu\text{m}$ micro-outlet edge. ....	133
Figure 2.32 Capillary rbc velocity for capillaries overlying the 200 $\mu\text{m}$ micro-outlet following 4-minute oxygen oscillations. ....	134
Figure 2.33 Capillary rbc velocity for capillaries outside the 200 $\mu\text{m}$ micro-outlet at varying distances from the outlet edge following 4-minute oxygen oscillations. ....	136
Figure 2.34 Capillary rbc supply rate for capillaries overlying the 200 $\mu\text{m}$ micro-outlet following 4-minute oxygen oscillations. ....	138
Figure 2.35 Capillary rbc supply rate for capillaries outside the 200 $\mu\text{m}$ micro-outlet at varying distances from the outlet edge following 4-minute oxygen oscillations. ....	140
Figure 2.36 Capillary rbc oxygen saturation in response to high oxygen challenges for capillaries directly overlying the 200 $\mu\text{m}$ micro-outlet. ....	142
Figure 2.37 Capillary rbc oxygen saturation responses in capillaries at various distances outside the 200 $\mu\text{m}$ micro-outlet edge in response to high oxygen challenges. ....	144
Figure 2.38 Capillary rbc oxygen saturation in response to low oxygen challenges for capillaries directly overlying the 200 $\mu\text{m}$ micro-outlet. ....	145

Figure 2.39 Capillary rbc oxygen saturation responses in capillaries at various distances outside the 200 $\mu\text{m}$ micro-outlet edge in response to low oxygen challenges. ....	147
Figure 2.40 Capillary hematocrit levels in response to high oxygen challenges for capillaries directly overlying the 200 $\mu\text{m}$ micro-outlet. ....	149
Figure 2.41 Capillary hematocrit levels in capillaries at various distances outside the 200 $\mu\text{m}$ micro-outlet edge in response to high oxygen challenges. ....	151
Figure 2.42 Capillary hematocrit levels in response to low oxygen challenges for capillaries directly overlying the 200 $\mu\text{m}$ micro-outlet. ....	152
Figure 2.43 Capillary hematocrit levels in capillaries at various distances outside the 200 $\mu\text{m}$ micro-outlet edge in response to low oxygen challenges. ....	154
Figure 2.44 Capillary rbc velocity response to high oxygen challenges for capillaries directly overlying the 200 $\mu\text{m}$ micro-outlet. ....	156
Figure 2.45 Capillary rbc velocity levels in capillaries at various distances outside the 200 $\mu\text{m}$ micro-outlet edge in response to high oxygen challenges. ....	158
Figure 2.46 Capillary rbc velocity response to low oxygen challenges for capillaries directly overlying the 200 $\mu\text{m}$ micro-outlet. ....	159
Figure 2.47 Capillary rbc velocity in capillaries at various distances outside the 200 $\mu\text{m}$ micro-outlet edge in response to low oxygen challenges. ....	161
Figure 2.48 Capillary rbc supply rate response to high oxygen challenges for capillaries directly overlying the 200 $\mu\text{m}$ micro-outlet. ....	163
Figure 2.49 Capillary rbc supply rate in capillaries at various distances outside the 200 $\mu\text{m}$ micro-outlet edge in response to high oxygen challenges. ....	165

Figure 2.50 Capillary rbc supply rate in response to low oxygen challenges for capillaries directly overlying the 200 $\mu\text{m}$ micro-outlet. ....	166
Figure 2.51 Capillary rbc supply rate in capillaries at various distances outside the 200 $\mu\text{m}$ micro-outlet edge in response to low oxygen challenges. ....	168
Figure AI.1 Capillary rbc oxygen saturation ( $\text{so}_2$ ) in response to oxygen oscillations for capillaries directly overlying the 1000 $\mu\text{m}$ micro-outlet. ....	237
Figure AI.2 Capillary rbc oxygen saturation responses in capillaries at various distances outside the 1000 $\mu\text{m}$ micro-outlet edge. ....	239
Figure AI.3 Capillary hematocrit levels in response to oxygen oscillations for capillaries directly overlying the 1000 $\mu\text{m}$ micro-outlet. ....	240
Figure AI.4 Capillary hematocrit values in capillaries at various distances outside the 1000 $\mu\text{m}$ micro-outlet edge. ....	242
Figure AI.5 Capillary rbc velocity for capillaries overlying the 1000 $\mu\text{m}$ micro-outlet following 4-minute oxygen oscillations. ....	243
Figure AI.6 Capillary rbc velocity for capillaries outside the 1000 $\mu\text{m}$ micro-outlet at varying distances from the outlet edge following 4-minute oxygen oscillations. ....	245
Figure AI.7 Capillary rbc supply rate for capillaries overlying the 1000 $\mu\text{m}$ micro-outlet following 4-minute oxygen oscillations. ....	246
Figure AI.8 Capillary rbc supply rate for capillaries outside the 1000 $\mu\text{m}$ micro-outlet at varying distances from the outlet edge following 4-minute oxygen oscillations. ....	248
Figure AI.9 Capillary rbc oxygen saturation in response to high oxygen challenges for capillaries directly overlying the 1000 $\mu\text{m}$ micro-outlet. ....	249

Figure AI.10 Capillary rbc oxygen saturation responses in capillaries at various distances outside the 1000 $\mu\text{m}$ micro-outlet edge in response to high oxygen challenges. ....	251
Figure AI.11 Capillary rbc oxygen saturation in response to low oxygen challenges for capillaries directly overlying the 1000 $\mu\text{m}$ micro-outlet. ....	252
Figure AI.12 Capillary rbc oxygen saturation responses in capillaries at various distances outside the 1000 $\mu\text{m}$ micro-outlet edge in response to low oxygen challenges. ....	254
Figure AI.13 Capillary hematocrit levels in response to high oxygen challenges for capillaries directly overlying the 1000 $\mu\text{m}$ micro-outlet. ....	255
Figure AI.14 Capillary hematocrit levels in capillaries at various distances outside the 1000 $\mu\text{m}$ micro-outlet edge in response to high oxygen challenges. ....	257
Figure AI.15 Capillary hematocrit levels in response to low oxygen challenges for capillaries directly overlying the 1000 $\mu\text{m}$ micro-outlet. ....	258
Figure AI.16 Capillary hematocrit levels in capillaries at various distances outside the 1000 $\mu\text{m}$ micro-outlet edge in response to low oxygen challenges. ....	260
Figure AI.17 Capillary rbc velocity response to high oxygen challenges for capillaries directly overlying the 1000 $\mu\text{m}$ micro-outlet. ....	261
Figure AI.18 Capillary rbc velocity levels in capillaries at various distances outside the 1000 $\mu\text{m}$ micro-outlet edge in response to high oxygen challenges. ....	263
Figure AI.19 Capillary rbc velocity response to low oxygen challenges for capillaries directly overlying the 1000 $\mu\text{m}$ micro-outlet. ....	264
Figure AI.20 Capillary rbc velocity in capillaries at various distances outside the 1000 $\mu\text{m}$ micro-outlet edge in response to low oxygen challenges. ....	266

Figure AI.21 Capillary rbc supply rate response to high oxygen challenges for capillaries directly overlying the 1000 $\mu\text{m}$ micro-outlet. ....	267
Figure AI.22 Capillary rbc supply rate in capillaries at various distances outside the 1000 $\mu\text{m}$ micro-outlet edge in response to high oxygen challenges. ....	269
Figure AI.23 Capillary rbc supply rate in response to low oxygen challenges for capillaries directly overlying the 1000 $\mu\text{m}$ micro-outlet. ....	270
Figure AI.24 Capillary rbc supply rate in capillaries at various distances outside the 1000 $\mu\text{m}$ micro-outlet edge in response to low oxygen challenges. ....	272
Figure AI.25 Capillary rbc oxygen saturation in response to oxygen oscillations for capillaries directly overlying the 600 $\mu\text{m}$ micro-outlet. ....	273
Figure AI.26 Capillary rbc oxygen saturation responses in capillaries at various distances outside the 600 $\mu\text{m}$ micro-outlet edge. ....	275
Figure AI.27 Capillary hematocrit levels in response to oxygen oscillations for capillaries directly overlying the 600 $\mu\text{m}$ micro-outlet. ....	276
Figure AI.28 Capillary hematocrit values in capillaries at various distances outside the 600 $\mu\text{m}$ micro-outlet edge. ....	278
Figure AI.29 Capillary rbc velocity for capillaries overlying the 600 $\mu\text{m}$ micro-outlet following 4-minute oxygen oscillations. ....	279
Figure AI.30 Capillary rbc velocity for capillaries outside the 600 $\mu\text{m}$ micro-outlet at varying distances from the outlet edge following 4-minute oxygen oscillations. ....	281
Figure AI.31 Capillary rbc supply rate for capillaries inside the 600 $\mu\text{m}$ micro-outlet following 4-minute oxygen oscillations. ....	282

Figure AI.32 Capillary rbc supply rate for capillaries outside the 600 $\mu\text{m}$ micro-outlet at varying distances from the outlet edge following 4-minute oxygen oscillations. ....	284
Figure AI.33 Capillary rbc oxygen saturation in response to high oxygen challenges for capillaries directly overlying the 600 $\mu\text{m}$ micro-outlet. ....	285
Figure AI.34 Capillary rbc oxygen saturation responses in capillaries at various distances outside the 600 $\mu\text{m}$ micro-outlet edge in response to high oxygen challenges. ....	287
Figure AI.35 Capillary rbc oxygen saturation in response to low oxygen challenges for capillaries directly overlying the 600 $\mu\text{m}$ micro-outlet. ....	288
Figure AI.36 Capillary rbc oxygen saturation responses in capillaries at various distances outside the 600 $\mu\text{m}$ micro-outlet edge in response to low oxygen challenges. ....	290
Figure AI.37 Capillary hematocrit levels in response to high oxygen challenges for capillaries directly overlying the 600 $\mu\text{m}$ micro-outlet. ....	291
Figure AI.38 Capillary hematocrit levels in capillaries at various distances outside the 600 $\mu\text{m}$ micro-outlet edge in response to high oxygen challenges. ....	293
Figure AI.39 Capillary hematocrit levels in response to low oxygen challenges for capillaries directly overlying the 600 $\mu\text{m}$ micro-outlet. ....	294
Figure AI.40 Capillary hematocrit levels in capillaries at various distances outside the 600 $\mu\text{m}$ micro-outlet edge in response to low oxygen challenges. ....	296
Figure AI.41 Capillary rbc velocity response to high oxygen challenges for capillaries directly overlying the 600 $\mu\text{m}$ micro-outlet. ....	297
Figure AI.42 Capillary rbc velocity levels in capillaries at various distances outside the 600 $\mu\text{m}$ micro-outlet edge in response to high oxygen challenges. ....	299

Figure AI.43 Capillary rbc velocity response to low oxygen challenges for capillaries directly overlying the 600 $\mu\text{m}$ micro-outlet. ....	300
Figure AI.44 Capillary rbc velocity in capillaries at various distances outside the 600 $\mu\text{m}$ micro-outlet edge in response to low oxygen challenges. ....	302
Figure AI.45 Capillary rbc supply rate response to high oxygen challenges for capillaries directly overlying the 600 $\mu\text{m}$ micro-outlet. ....	303
Figure AI.46 Capillary rbc supply rate in capillaries at various distances outside the 600 $\mu\text{m}$ micro-outlet edge in response to high oxygen challenges. ....	305
Figure AI.47 Capillary rbc supply rate in response to low oxygen challenges for capillaries directly overlying the 600 $\mu\text{m}$ micro-outlet. ....	306
Figure AI.48 Capillary rbc supply rate in capillaries at various distances outside the 600 $\mu\text{m}$ micro-outlet edge in response to low oxygen challenges. ....	308

LIST OF TABLES

Table 2.1 Mean and standard deviation of systemic animal data for each experimental group based on micro-outlet diameter size. .... 79

Table 2.2 Mean and standard deviation of animal blood gas data for each experimental group based on micro-outlet diameter size used. .... 80

## LIST OF APPENDICES

Appendix 1 .....	225
Appendix 2 .....	309

## ABBREVIATIONS

10X	ten times magnification
2D	two-dimensional
3D	three-dimensional
AA	arachidonic acid
ADP	adenosine diphosphate
ANOVA.	analysis of variance
ATP	adenosine 5' -triphosphate
Ca <sup>2+</sup>	calcium ion
[Ca <sup>2+</sup> ]	calcium concentration
CAD	computer-aided design
cAMP	cyclic adenosine monophosphate
CFTR	cystic fibrosis transmembrane conductance regulator
cGMP	cyclic guanine monophosphate
CO <sub>2</sub>	carbon dioxide
COX-1	cyclooxygenase
EDHF	endothelium-derived hyperpolarizing factor

EDL	extensor digitorum longus
eNOS	endothelial-derived nitric oxide synthase
ET-1	endothelin-1
ETC	electron transport chain
GEC	gas exchange chamber
Gi	heterotrimeric-G
GUI	graphical user interface
Hb	hemoglobin
HCO <sub>3</sub>	bicarbonate concentration
IVVM	intravital video microscopy
L	path length
LDF	laser doppler flowmetry
LMFD	liquid micro-fluidic device
MLCK	myosin light chain kinase
MLCP	myosin light chain phosphatase
N <sub>2</sub>	nitrogen
NIRS	near infrared spectroscopy

NO	nitric oxide
O <sub>2</sub>	oxygen
[O <sub>2</sub> ]	oxygen concentration
OD	optical density
PCO <sub>2</sub>	partial pressure of carbon dioxide
PGI <sub>2</sub>	prostacyclin
PK	protein kinase
PO <sub>2</sub>	partial pressure of oxygen
PDMS	poly(dimethylsiloxane)
PMMA	polymethyl-methacrylate
PQM	phosphorescence quenching method
PSS	physiological salt solution
PVDC	polyvinylidene chloride
RBC	red blood cell
ROS	reactive oxygen species
SAD	sum of absolute difference
SNO	s-nitrosothiol

SNO-Hb      s-nitrosothiol-hemoglobin

SO<sub>2</sub>          oxygen saturation

SR            supply rate

STI          space time image

TCO<sub>2</sub>        total carbon dioxide

μm          micrometer

## CO-AUTHORSHIP STATEMENT

This thesis is structured into 3 chapters. Chapter 1 provides background information relevant to the thesis, chapter 2 is a manuscript describing an original research study, and chapter 3 is a summary chapter.

This thesis contains the following manuscript in preparation:

ME Kiley, RH Smith, BN Wells, GM Russell McEvoy, GM Fraser. Development of thin-film micro-outlet devices for spatially constraining local O<sub>2</sub> perturbations to capillaries. (In preparation for submission to *Microcirculation*).

The project was designed by ME Kiley and GM Fraser. Animal surgeries were completed by ME Kiley and GM Fraser. The gas exchange chamber was three-dimensional (3D) printed by ME Kiley and RH Smith. RH Smith assisted in parts of the development and fabrication process for the ultra-thin film micro-outlet devices. BN Wells and GM Russell McEvoy supported a subset of my experiments. Micro-outlet device fabrication and refinements, data collection, data analysis, interpretation of data, preparation of figures, and writing of the manuscript in this thesis were completed by ME Kiley with support and editorial review by GM Fraser.

---

## CHAPTER 1: INTRODUCTION

### 1.1 OBJECTIVES

The mammalian circulatory system is responsible for transporting blood along the vascular tree to all organs and tissues. Blood is rapidly carried away from the heart through branching arteries that supply the periphery, giving rise to microvascular networks that perfuse organs and tissue. These microvascular networks consist of small vessels with diameters of less than 300 micrometers, including arterioles, venules, and capillaries (Bloch & Iberall, 1982; Segal, 2005). Microcirculation is essential in the body, delivering oxygen and nutrients to tissues while simultaneously removing waste products to ensure normal physiological function (Duling & Klitzman, 1980; Segal, 2005). Arterioles can respond to various intrinsic stimuli, such as oxygen, by modulating their vessel wall diameter through the action of vascular smooth muscle cells that are oriented circumferentially within the vessel walls (Ellis, 2005; Davis, 1993; Tykocki et al., 2017).

The regulation of oxygen ( $O_2$ ) is a critical physiological function that ensures the metabolic demands of organs and tissues in the body are met (Duling, 1970; Golub & Pittman, 2013). The relative oxygen concentration in tissues is an essential metabolic signal for vasomotor changes (Reglin et al., 2009). In the microcirculation, a vasoactive response can be provoked when oxygen levels fluctuate within and outside their normal physiological range (10 – 150 mmHg) (Jackson, 2016). Arterioles vasodilate in response to low  $O_2$  levels, eliciting an increase in blood flow (Sullivan & Johnson, 1981; Dietrich et al., 2000; Ellis, 2005). When  $O_2$  rises above basal levels, arterioles respond by vasoconstricting, causing a decrease in the blood flow rate into capillaries (Duling, 1972,

1974; Hutchins et al., 1974; Sullivan & Johnson, 1981). The microvascular blood flow response is observed when O<sub>2</sub> concentrations in the tissue fluctuate, and the regulation of this response is controlled locally. Indeed, there is evidence to support the role of multiple mechanisms across different vessel types within the microvascular tree (Duling, 1970; Jackson & Duling, 1983; Hester, 1993; Pries et al., 1995; Pittman, 1973; Ellsworth et al., 1994, 2009; Sprague, 2009; Jackson, 2016).

Several local mechanisms for oxygen [O<sub>2</sub>] sensing and regulation have been proposed, but existing evidence fails to account for the sensitivity of vascular responses across the physiological range of tissue [O<sub>2</sub>] and at different locations within the microcirculation (Duling, 1970; Jackson & Duling, 1983; Messina et al., 1994; Pries et al., 1995; Ellsworth et al., 1995; Ellsworth, 2013; Jackson, 2016). It has been proposed that red blood cells (RBCs) act as an O<sub>2</sub> sensor and that oxygen-mediated blood flow is regulated, at least in part, at the capillary level (Bergfeld and Forrester, 1992; Ellsworth & Stein, 1993; Ellsworth et al., 1995; McCullough et al., 1997; Stamler, 1997; Ellsworth, 2004; Gonzalez, 2012; Jackson, 2016). To confirm this mechanism, oxygen-mediated blood flow responses must be quantified at the capillary level while avoiding interaction with other relevant mechanisms in higher-order vessels. Microfluidic devices and gas exchange chambers have been modelled, fabricated, and validated for studying O<sub>2</sub>-mediated microvascular blood flow regulation. Still, the necessary spatial specificity of targeted O<sub>2</sub> perturbations to micro-scale tissue regions has remained a pressing challenge (Sové et al., 2016, 2021; Ghonaim et al., 2011, 2013, 2021).

To further extend the use of microfluidic devices in microvascular research, our focus was to integrate properties of previously developed gas exchange chambers and microfluidic devices to create novel devices with advanced optical and spatial properties. Our goal was to create a device that retained desirable characteristics of previous devices while improving spatial specificity that could be adaptable to multiple microscope setups, research studies and muscle preparations through only minor future adjustments. This novel device, combined with intravital video microscopy (IVVM) and capillary hemodynamic measurements, can help to quantify microvascular blood flow responses when changes in tissue  $[O_2]$  stimulate only a few capillaries or when a single terminal arteriole is selectively targeted.

The work in the current thesis examines oxygen-mediated blood flow regulation at the capillary level in response to changing oxygen concentrations using a gas exchange chamber coupled with an ultra-thin-film micro-outlet device. Our overarching hypothesis is that oxygen-mediated blood flow regulation is initiated at the capillary level through oxygen saturation-dependent ATP release from erythrocytes. We developed a thin-film micro-outlet device that allows spatially constrained oxygen perturbations to be imposed at the capillary level to precisely target associated regulatory mechanisms at this scale.

To address this overarching hypothesis, we sought to develop a novel tool based on the following objectives:

1. Fabricate a composite micro-outlet gas exchange chamber microfluidic device to spatially constrain direct oxygen challenges to microscale regions of skeletal muscle in vivo.
2. Identify the minimum scale at which oxygen-mediated blood flow responses can be provoked using highly localized microvascular scale stimulation.
3. Quantify the capillary/microvascular blood flow response to direct spatially constrained high and low oxygen challenges, and acute oscillations in tissue oxygen concentration.

## 1.2 OXYGEN TRANSPORT AS A ROLE OF THE CARDIOVASCULAR SYSTEM

Oxygen (O<sub>2</sub>) transport through the respiratory and cardiovascular system occurs by convection, and via diffusion of oxygen along gradients between physiological compartments (Ellsworth, 1994; Leach & Treacher, 1992; Goldman & Popel, 2000). Convective transport is defined as the movement of a substance that is contained within a moving fluid (Aroesty & Gross, 1970), versus passive diffusion which is governed by Fick's first law (Federspiel & Popel, 1986; Groebe & Thews, 1990). Fick's law of diffusion can be defined as  $\text{Flux} = -DkA*\Delta P/\Delta x$  which relates mass transport rate (Flux) of a substance from a location of high concentration to an area of low concentration, where  $A$  is the surface area of the exchange surface,  $D$  is the diffusion coefficient,  $k$  is the solubility, and  $\Delta P/\Delta x$  is the concentration gradient (Federspiel & Popel, 1986; Groebe & Thews, 1990). Convective transport functions most efficiently in large tubes and heavily supports mass transport of blood, as the resistance to fluid flow increases rapidly with decreasing

tube diameter, further explained by Poiseuille's Law (Poiseuille, 1846; Suter et al., 1993). Poiseuille's law states that volume flow rate is directly proportional to the pressure gradient divided by the radius raised to the fourth power (Poiseuille, 1846; Suter et al., 1993).

Transporting oxygen into tissues also requires movement through microvascular networks comprised of many tiny tube-like vessels distributed throughout the body. Blood flow becomes relatively slower in microvessels, which helps maximize the time available for oxygen diffusion from capillaries into the surrounding cells. Starting in the lungs, the oxygen cascade involves both convective transport and diffusion that relies on O<sub>2</sub> gradients to diffuse O<sub>2</sub> from one compartment to the next until arriving in the mitochondria where it is consumed (Pittman, 2000; Spires et al., 2013).

Each component of the cardiovascular system is essential for transporting O<sub>2</sub> via the blood to all tissues through branching vascular networks (Pittman, 2005; Dunn, 2016). The cardiovascular system comprises two circuits, the pulmonary and systemic circulation, connected in series through the heart's four chambers. Both circuits are critical in distributing oxygenated blood to meet the body's ever-changing demands (Crystal & Pagel, 2020). Pulmonary circulation is responsible for carrying blood between the heart and lungs where gas exchange and reoxygenation occurs, an early step in O<sub>2</sub> transport (Pittman, 2005). Systemic circulation is responsible for the convective transport of oxygenated blood starting on the left side of the heart through arteries flowing into the periphery and vital organs.

Oxygen transport to tissue cells via the blood, functions by aid from its two components, plasma, and RBCs. Oxygen can reversibly bind to hemoglobin in RBCs and dissolve in the blood's plasma layer (Jensen, 2004). Hemoglobin (Hb) is an allosteric protein consisting of 4 chains, each attached to an iron-porphyrin compound (Friedman, 1985; Popel, 1989; Pittman, 2011). When O<sub>2</sub> binds to hemoglobin, the globin chain changes conformation, enhancing its affinity for oxygen which is fully saturated when four O<sub>2</sub> molecules are bound (Marden et al., 1995). Plasma is responsible for minimal O<sub>2</sub> transport in the blood due to its relatively low solubility, representing less than 2% of total blood O<sub>2</sub> content (Injarabian et al., 2020). As a result, hemoglobin is the primary vehicle for convective transportation of O<sub>2</sub>.

Cooperative binding of O<sub>2</sub> to hemoglobin can be described by the oxygen dissociation curve, which represents O<sub>2</sub> saturation of Hb (SO<sub>2</sub>) at varying partial pressures of O<sub>2</sub> (PO<sub>2</sub>). Specifically, at 50% SO<sub>2</sub>, the PO<sub>2</sub> measures O<sub>2</sub>-affinity for Hb (also expressed as P<sub>50</sub>), which is ~26 mmHg for normal adult human Hb (Ahmed et al., 2020). Further explained by hemoglobin's two forms, taut (T) and relaxed (R), which contribute to the Bohr Effect relationship and affect the binding ability of O<sub>2</sub> (Perutz, 1972; Perutz et al., 1998; Dunn et al., 2016). The Bohr effect describes a shift in hemoglobin's binding affinity for O<sub>2</sub>, which facilitates unloading to meet tissues demands (Malte et al., 2021). The T form has a low affinity for O<sub>2</sub> and promotes its release into circulation in tissues with high levels of CO<sub>2</sub> (Perutz, 1972; Perutz et al., 1998; Safo & Bruno, 2011; Dunn et al., 2016; Ahmed et al., 2020). In the R form, Hb has a high affinity for O<sub>2</sub>, strongly binding to oxygen in areas with low CO<sub>2</sub> (Perutz, 1972; Safo & Bruno, 2011; Dunn et al., 2016). Such forms are

essential regulatory properties of hemoglobin that control O<sub>2</sub> accessibility in various tissue environments and metabolic demands, such as in hypoxia or high-intensity exercise (Perutz, 1972; Yonetani & Laberge, 2008; Safo & Bruno, 2011; Ahmed et al., 2020).

The O<sub>2</sub> cascade pathway begins when O<sub>2</sub> is inspired from the air before moving into the body and the bloodstream. The O<sub>2</sub> we breathe in is transported to the alveoli in our lungs, where blood oxygenation occurs. There is an oxygen pressure (PO<sub>2</sub>) gradient that exists between the alveolar membrane and the pulmonary capillaries (Whiteley et al., 2002, 2003; Roy & Secomb, 2014; Dunn, 2016). Oxygen enters the heart and bloodstream by diffusing across this PO<sub>2</sub> gradient to bind reversibly to hemoglobin in RBCs, forming oxyhemoglobin and oxygenating blood (Weibel, 1984; Dunn, 2016; Jacob et al., 2016). Passive diffusion is most efficient in these instances where short distances between compartments and large O<sub>2</sub> gradients exist.

Large stores of oxygen do not exist in the body; therefore, convection dramatically contributes to the delivery of sufficient O<sub>2</sub> from the atmosphere to tissues where it is consumed. The heart provides the motive force that drives oxygenated blood through the circulatory system as it establishes a pressure gradient to move blood. To obtain this pressure gradient for blood flow through a vessel or an organ, a pressure difference is required between the inflow and outflow of the vessel. The relationship between volumetric blood flow (Q) and pressure differences in a vessel ( $\Delta P$ ) is defined by Ohm's Law ( $Q = \Delta P/R$ ), where R is the resistance to the flow (Q) of blood (Hennig, 1992; Secomb, 2016; Fournier et al., 2021). Therefore, considerable pressure differences are needed to increase blood flow or, alternatively flow can be maintained by decreasing systemic vascular

resistance. This relates to the O<sub>2</sub> supply tissues receive, as when blood flow rate increases, oxygen carried in the blood is moved around the body at a faster rate.

At the microvascular level, O<sub>2</sub> transport is dominated by passive diffusion in peripheral tissues. In these tissues, there is an area between the RBCs in capillaries and the surrounding tissue (parenchymal cells) where the exchange of O<sub>2</sub>, nutrients, and wastes occurs. At this exchange surface, tissue cells are typically positioned less than 150 μm away from the nearest capillary (Augustin et al., 2017; Pias, 2021). Additionally, O<sub>2</sub> diffuses along concentration gradients that exist between individual capillaries and between capillaries and their nearby arterioles and venules that flow in proximity (Duling & Berne, 1970; Swain & Pittman, 1989). These factors allow O<sub>2</sub> to be released from hemoglobin in RBCs into nearby parenchymal cells where mitochondria can consume O<sub>2</sub> to store energy as ATP (Weibel, 1984; Pittman, 2000, 2011).

Oxygen is a requirement of aerobic respiration (ATP production), which functions in the mitochondria within muscle and other tissues (Weibel, 1984). This is where oxidative phosphorylation occurs, a process of the electron transport chain (ETC) and chemiosmosis working together to synthesize ATP. This coenzyme supplies energy to nearly all active metabolic processes (Ellsworth, 1995; Pittman, 2013; Segal, 2005). Oxygen is consumed at cytochrome C oxidase, the terminal electron acceptor within the mitochondrial inner membrane at the end of the ETC (Weibel, 1984; Pittman, 2011). Electron transfers create an electrochemical gradient later used in chemiosmosis along with a water molecule generated by oxygen at the end of the ETC to synthesize ATP. This process is essential for

the body to maintain energy for its metabolic demands, especially in highly oxidative tissues like skeletal muscle during exercise.

Since O<sub>2</sub> is a requirement for cells to produce energy, it needs to be readily accessible in the tissue. A critical PO<sub>2</sub> of ~ 11 mm Hg (Wilson et al., 1979, 1990; Pittman, 2013) is required for the mitochondria to maintain sufficient O<sub>2</sub> consumption and functions. Wilson et al. describes the process that intracellular metabolic factors take to work together to continue a relatively constant O<sub>2</sub> consumption while PO<sub>2</sub> is actively decreasing (Wilson, 1979, 1990). It is below this critical PO<sub>2</sub> level that these metabolic substances (i.e. ADP, cytochrome c) cannot function together and maintain O<sub>2</sub> consumption. This necessary O<sub>2</sub> concentration helps regulate the O<sub>2</sub> supply and demand in the tissues along with ATP generation. If O<sub>2</sub> is not present, the ETC cannot run properly, chemiosmosis will not produce ATP, and cells won't perform their necessary functions to survive.

### 1.3 MICROCIRCULATION

The microcirculation consists of arterioles, capillaries, and venules, the microvessels defined as the circulatory system's exchange vessels. The circulatory system comprises branching vascular networks responsible for transporting blood to all tissues and organs throughout the mammalian body. The circulatory system conducts this transport at the microvascular and macrovascular levels (arteries, veins), composed of large capacitance vessels that transport blood toward or away from organs and tissues. Conduit arteries external to tissue with diameters between 500 – 1000 μm give rise to the microvasculature where the artery branches into first-order arterioles embedded within the

tissue (< 100  $\mu\text{m}$  diameter). First-order arterioles branch distally into second-order arterioles and continue progressively until reaching the terminal arteriole. The terminal arteriole precedes the capillary beds and is responsible for the resistance that determines the blood flow rate into the groups of downstream capillaries it supplies (Berg & Sarelius, 1995; Pries and Secomb, 2011; Murrant, 2017; Murrant & Fletcher, 2022; Jackson, 2021). Arterioles are major resistance vessels embedded in the parenchyma they perfuse that control the distribution of blood by actions of their vascular smooth muscle cells and endothelial cells lining their vascular walls (Duling, 1970; Renkin, 1985; Zweifach & Lipowsky, 1984; Pries & Secomb, 2011; Segal, 2000; Yuan & Rigor, 2010; Jackson, 2016). The structure of a blood vessel is made up of three layers; the tunica intima, an internal layer consisting of the endothelium, a basement membrane, and elastic fibres; the tunica media, a middle layer made up of smooth muscle and elastic fibres, and the tunica externa, consisting of connective tissue and mostly collagen fibres (Pugsley & Tabrizchi, 2000; Martinez-Lemus, 2012), although the layers and components that are present depend somewhat on the vessel type. The arteriole structure contains all three layers, but commonly have only one layer of smooth muscle wrapped circumferentially around the endothelial cells that define the vessel lumen.

Endothelial cells line the heart and vessels of the cardiovascular system, acting as a physical barrier between the blood and the vessel wall (Alberts et al., 2002; Kruger-Genge, 2019). Endothelial cells fulfill many vital functions in microcirculation, which include transporting substances to and from the bloodstream across the vessel wall and releasing vasoactive mediators in response to various stimuli (Pohl & Busse, 1989; Ando

& Yamamoto, 2013). Endothelial cells are connected to smooth muscle cells by gap and myo-endothelial junctions (Hudlicka, 2011). The endothelium is the single layer that composes the capillary wall, as capillaries lack other structural support, like smooth muscle cells.

Capillary networks are interconnected arrangements with a broad surface area and extensive branching, positioning each tissue cell near a capillary. Capillary network architecture supports efficient oxygen transport and nutrient exchange (Hepple, 1997; Baba et al., 1993; Hudlicka, 2011). The proximity, surface area, and single-file flow of red blood cells minimizes the distance between blood and tissue cells, so passive diffusion can occur efficiently as discussed previously in section 1.2. In capillaries, RBCs and plasma directly interact with the endothelium. Lipid-soluble substances such as oxygen and carbon dioxide can quickly diffuse across the 1- $\mu$ m thick layer of endothelial cells lining capillaries.

Blood drains into venules from capillary networks, the microvessel through which blood exits the microcirculation (Emerson & Segal, 1997). A venule's structure comprises endothelial cells surrounded by a basement membrane with elastin fibres and smooth muscle (Hudlicka, 2011). Therefore, venules hold less resistance than arterioles. The venous system is responsible for transporting blood back to the heart. Post-capillary venules, slightly larger than capillaries, converge into larger vessels as they move away and out of organs and into large veins (Eriksson et al., 1972; Emerson & Segal, 1997; Hudlicka, 2011; Latroche et al., 2015). Venules can modulate their vessel diameters, but less is known about their role in blood flow regulation relative to arterioles, which is discussed in section 1.5.

The microvascular morphology associated with each organ and tissue is unique, including specific features related to their role in facilitating the functions of their organ or tissue. Microvascular networks are appropriately structured to ensure sufficient delivery of oxygen and nutrients and waste removal in various capacities. For example, the brain microvasculature contains an extensive dense network of interconnected microvessels organized in parallel to ensure exchange vessels are always near brain tissue cells (Hirsch et al., 2012; Blinder et al., 2013). The brain microvasculature also offers alternate routes for the distribution of blood in the event of a blockage, ensuring oxygen delivery is not impacted (Cassot et al. 2006). In contrast, the kidney, which also has considerable oxygen requirements, contains a complex vasculature composed of highly fenestrated capillaries that facilitate molecule exchange at a higher rate than other capillaries and quickly pass large molecules through their endothelial cells (Nourbakhsh & Singh, 2014). Oxygen is perhaps the most critical substance to be distributed by the blood, especially in the brain and other oxidative tissues where a continuous supply is required.

Skeletal muscle is an active metabolic organ with high oxygen consumption during exercise and is responsible for generating the force required to perform its functions (Emerson & Segal, 1997; Hudlicka & Brown, 2009; Hudlicka, 2011). In skeletal muscle, a microvascular unit comprises the capillaries perfused by a discrete terminal arteriole and collecting venule, representing the smallest functional unit of blood flow regulation (Figure 1.1) (Bloch & Iberall, 1982; Lo et al., 2003; Latroche et al., 2015; Roy et al., 2012). These capillaries run parallel to myofibers in the muscle, and the microvascular bed's architectural arrangement supports these muscle fibres. The microvasculature in skeletal muscle is

essential in metabolism and exercise as it transports oxygen to mitochondria in tissue cells to synthesize ATP for energy. Therefore, as presented in this thesis, skeletal muscle is an ideal model to study blood flow regulation in the microcirculation stemming from changes in oxygen concentration.

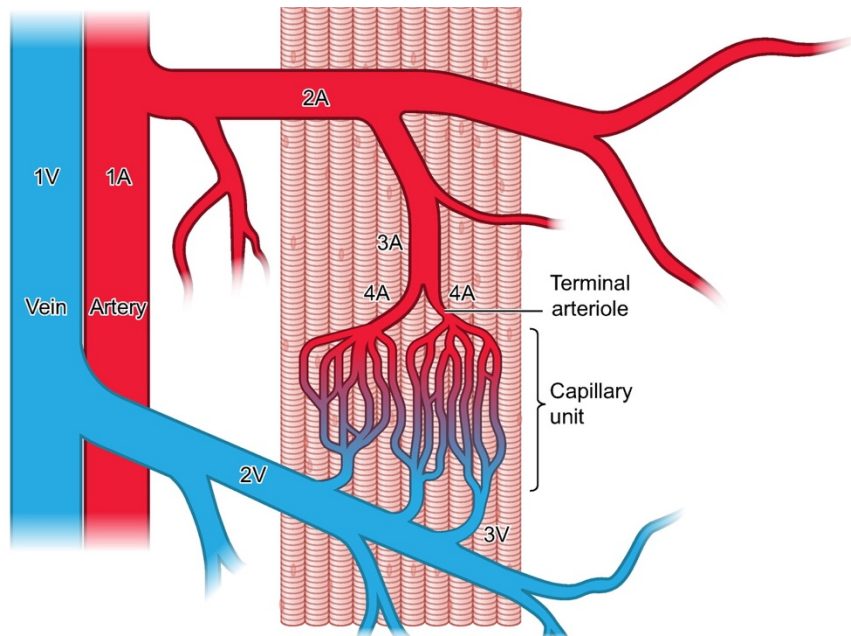


**Figure 1.1 Basic morphological structure of the microcirculation.** Image represents a portion of a microvascular network in skeletal muscle. Image shows the branch orders of the arteriolar (red) and venous (blue) ends of the vasculature and the location of capillary units in relation to the rest of the microvascular network and to skeletal muscle cells. (Image obtained from Murrant & Fletcher, 2022 with permission).

## 1.4 MICROVASCULAR BLOOD FLOW REGULATION

Under normal physiological conditions, all resistance vessels exhibit some degree of smooth muscle contraction that determines their diameter, also known as vascular tone. Vascular tone is the partial constriction of resistance arteries and arterioles due to myogenic tone and sympathetic nerve activity on the vascular smooth muscle of the vessel walls, which is subject to inhibition by local metabolites and O<sub>2</sub> conditions (Tateishi & Faber, 1995b; Joyner & Casey, 2014). The vascular tone of arterioles can be controlled directly or indirectly by smooth muscle cells through sympathetic nerve activity, physical factors, vasoactive metabolites, and conducted responses (Pohl et al., 2000; Schubert & Mulvany, 1999; Segal, 2005; Secomb, 2008; Roy et al., 2012). Several of these associated mechanisms maintain resistance vessel diameters within a functional range (Pohl et al., 2000; Schubert & Mulvany, 1999; Joyner & Casey, 2014).

Sympathetically mediated modulations of vascular tone act via adrenergic receptors on vascular smooth muscle and endothelial cells. Specifically, sympathetic nerve fibres release norepinephrine to constrict the vessel wall by activating  $\alpha$ -adrenergic receptors on smooth muscle (Faber, 1988; Joyner & Casey, 2014). Such receptors exist on the vascular smooth muscle in two types,  $\alpha$ 1-adrenergic receptors, which act on large arteries and  $\alpha$ 2-adrenergic receptors, which are responsible for the constriction of smaller resistance vessels such as arterioles in inactive skeletal muscle (Tateishi & Faber, 1995b). During intense exercise and in flight or fight, the body's hormonal response is to release epinephrine (adrenaline) from the adrenal medulla, stimulated by adrenergic receptors on vascular smooth muscle cells. Adrenaline then acts on  $\beta$ -adrenergic receptors on vascular

smooth muscle and is ligated to mediate a vasodilatory response (Marshall, 1982). Additionally,  $\alpha_2$ -adrenergic receptors can mediate a vasodilatory response when they exist on endothelial cells (Vanhoutte, 2001; Sorriento et al., 2011; Mishra et al., 2018).

The contraction of vascular smooth muscle in resistance arteries and arterioles is directly influenced by the cytoplasmic concentration of free calcium ( $\text{Ca}^{2+}$ ) (Somlyo, 1994, 2004; Pfitzer, 2001; Brekke et al., 2006). Increasing cytosolic  $\text{Ca}^{2+}$  in vascular smooth muscle cells from extracellular compartments results in a  $\text{Ca}^{2+}$ -calmodulin complex to activate the enzyme myosin light chain kinase (MLCK). Activated MLCK phosphorylates myosin light chain, allowing cycling of cross-bridges between actin and myosin, which results in smooth muscle contraction (Somlyo, 1994; Wynne et al., 2009). An opposing mechanism produces vessel relaxation, where the myosin light chain is dephosphorylated by myosin light chain phosphatase (MLCP) (Lai & Frishman, 2005). These control actions of vascular smooth muscle  $[\text{Ca}^{2+}]$  are influenced by various membrane receptors, ion channels, mechanical sensors and signalling molecules that induce changes in vascular tone and blood flow.

The factors that regulate vascular tone do so by modulating cytosolic-free  $[\text{Ca}^{2+}]$  and themselves sensitivity to the contractile proteins. These factors alter cell membrane potential and activate signalling cascades within the vascular smooth muscle by opening and closing potassium ( $\text{K}^+$ ) channels.  $\text{K}^+$  channels are involved in critical regulatory mechanisms and are expressed in both endothelial cells and vascular smooth muscle cells (Dora, 2017; Tycocki et al., 2017). When  $\text{K}^+$  channels open, an outward flux of  $\text{K}^+$  produces a more negative membrane potential, leading to hyperpolarization. Then, voltage dependent

$\text{Ca}^{2+}$  channels close,  $\text{Ca}^{2+}$  influx decreases, and vasodilation occurs. Opposingly, if  $\text{K}^+$  channels close, vasoconstriction occurs.

The endothelium plays a critical role in regulating vascular tone by releasing vasoactive mediators in response to physical and chemical changes, which modulate the opening of  $\text{K}^+$  channels (Busse et al., 1983; Pohl & Busse, 1989; Kaley et al., 1989; Messina et al., 1992). Calcium-activated potassium channels ( $\text{K}_{\text{Ca}}$ ) channels are activated by membrane depolarization, increased intracellular calcium, cGMP-dependent protein kinase G (PKG) and cAMP phosphorylation (Brayden, 1996; Jackson, 2005). Voltage-dependent potassium ( $\text{K}_v$ ) channels are embedded in the plasma membrane of vascular smooth muscle cells. They are also modulated by cAMP vasodilator agonists and open by membrane depolarization (Aiello et al., 1998; Jackson, 2005; Li et al., 2003). ATP-sensitive  $\text{K}^+$  channels are sensitive to changes in the metabolic demand, increasing their open probability when an increased level of ATP and ADP exists in the microenvironment (Jackson, 2005; Quayle et al., 1997). While other vasodilators are produced during exercise, hypoxia and acidosis activate these channels by activating their respective phosphorylation mechanisms (Jackson, 2005; Quayle et al., 1997). Endothelium-derived vasoactive molecules exert their actions using protein kinases (PKG, PKA), to modulate the opening of  $\text{K}_{\text{Ca}}$  channels or protein kinase C (PKC) to slow channel opening as an inhibitory effect (Hu et al., 1991; Ledoux et al., 2006; Minami et al., 1993). Some of these vasoactive molecules include prostacyclin ( $\text{PGI}_2$ ), nitric oxide (NO), endothelium hyperpolarizing factor (EDHF), and endothelin (ET-1).

Several metabolites act on vascular smooth muscle cells to relax or constrict vessel walls. NO is produced from the amino acid, L-arginine, and molecular oxygen by the enzymatic activity of endothelial nitric oxide synthase (eNOS) (Duza et al., 2003; Palmer et al., 1987; Sessa, 2004). The eNOS pathway is activated by acetylcholine and bradykinin, neurotransmitters that increase intracellular  $[Ca^{2+}]$  ions. NO acts on vascular smooth muscle by activating soluble guanylyl cyclase to produce cGMP and PKG, resulting in vasodilation (Denninger & Marletta, 1999; Arnold et al., 1977; Palmer, 1987). Another endothelium-derived vasodilator that can respond to a variety of stimuli is prostacyclin ( $PGI_2$ ), produced from arachidonic acid (AA) through prostacyclin synthase by the cyclooxygenase (COX-1) pathway (Albertini et al., 1996; Luscher & Vanhoutte, 1990; Max et al., 1999; Norel, 2007).  $PGI_2$  acts directly on vascular smooth muscle cells by stimulating adenylate cyclase to increase cyclic AMP (cAMP) to elicit vasodilation (Frisbee et al., 2001; Messina et al., 1992; Lombard et al., 1999; Ngai, 2010). Endothelium-derived hyperpolarizing factor (EDHF) activates potassium channels to hyperpolarize underlying vascular smooth muscle cells and block calcium entry via  $Ca^{+}$  channels for relaxation (Ding et al., 2000; Matthewson & Dunn, 2014). Both NO and  $PGI_2$  can hyperpolarize vascular smooth muscle cells but an additional mechanism exists involving the EDHF (Busse et al., 2002; Budel et al., 2003). However, the specific identity(ies) of EDHF themselves and their associated initiating factors are not fully understood (Chauhan et al., 2003; Si et al., 2006; Feletou & Vanhoutte, 2009). Endothelin-1 (ET-1) is a vasoconstrictor peptide and the most potent endothelin isoform (Wynn et al., 2009). ET-1 is released in the direction of smooth muscle cells to bind Gq-coupled endothelin subtype A (ET-a) receptors to elicit skeletal muscle contraction through inhibition of  $K_{ca}$  channel

actions by PKC (Rubanyi & Polokoff, 1994; Schiffrin & Touyz, 1998; Webb & Haynes, 1995). ET-b receptors exist on both endothelial and vascular smooth muscle cells. In response to changes in transmural pressure, ET-b receptors on vascular smooth muscle cells are activated along with ET-a to elicit vasoconstriction. Although, if ET-1 binds to ET-b on the endothelial cells instead, NO is produced and will mediate the relaxation of the underlying smooth muscle (Kawanabe et al., 2011; Rubanyi & Polokoff, 1994; Schiffrin & Touyz, 1998; Webb & Haynes, 1995). These metabolites may act through slightly different mechanisms, but they can all elicit a vasoactive response in skeletal muscle tissue to promote matching blood supply with metabolic demand.

Vascular wall cells can sense and act on intrinsic forces such as vessel wall shear stress and circumferential wall stress by transmural pressure (Koller & Kaley, 1991; Jimenez et al., 1996; Kotecha & Hill, 2005; Lehoux et al., 2006; Shi & Tarbell, 2011; Jackson, 2020, 2021). Increased blood flow can cause mechanical pressure which exerts a force on the vessel wall endothelial cells, known as shear stress (Hull et al., 1986; Koller & Kaley, 1991). When shear stress is elevated, it initiates a vasoactive response to increase blood flow in upstream conduit vessels, also known as flow-induced vasodilation (Hull et al., 1986; Kuo et al., 1990; Pohl et al., 2000; Li & Xu, 2007). This dilation of resistance arteries and arterioles increases blood flow downstream to enhance nutrient delivery and waste removal in downstream capillaries and post-capillary venules. Increased shear stress elevates endothelial  $[Ca^{2+}]$ , which activates the eNOS pathway; therefore, the flow-induced vasodilation mechanism occurs partly through the actions of nitric oxide (Griffith et al., 1989; Falcone et al., 1993; Shi & Tarbell, 2011). Arterioles also respond to local transmural

pressure increases that stretch their vascular smooth muscle, known as the myogenic response (Bayliss, 1902; Davis et al., 1993, 1999; Korthuis, 2011). In resting conditions, myogenic tone refers to the steady state of vascular smooth muscle contractile activity that occurs in a pressurized vessel, contributing to blood flow distribution to and within tissues (Schubert & Mulvany, 1999; Jackson, 2020). However, when transmural pressure increases, it activates mechanosensitive ion channels to increase muscle contraction through membrane depolarization and intracellular  $[Ca^{2+}]$  increase in smooth muscle promoting vasoconstriction (Schubert & Mulvany, 1999; Carlson et al., 2005).

Endothelial cells contribute to the conduction and integration of local vasodilatory signals facilitated by cell-to-cell communication along the microvascular endothelium (Ellsworth, 2013, Segal & Duling, 1987,1989; Dietrich & Tyml, 1992).  $K^+$  channels assist in the propagation of a stimulus over a distance via electrical coupling among vascular smooth muscle and endothelial cells, known as a conducted response (Segal, 1989; Ngo et al., 2013; Dora, 2016, 2017). Such cells are tightly connected in small arterioles via gap junctions expressing connexin channels. The connexin channels provide direct communication between cells and enable the spread of endothelial hyperpolarization to smooth muscle cells (Emerson & Segal 2000; Dora, 2010). Local vasodilation of arterioles by metabolite actions in extracellular space ( $K^+$ , Adenosine) can initiate a conducted response upstream to feed arteries to increase arteriolar and capillary perfusion (Bagher & Segal., 2011; Beach et al., 1998; Diep et al., 2005; Hungerford et al., 2000; Segal & Duling., 1986; Segal, 1991; Takano et al., 2005; Ngo et al., 2010). Metabolic

demand fluctuations that elicit local vasodilation are insufficient without upstream conducted responses that direct blood flow increases to fully support tissue needs.

Metabolic demand is an essential determinant of skeletal muscle blood flow regulation between tissue regions. The diameter of the arteriolar walls is modulated to adjust resistance and therefore blood flow to meet tissue needs. As mentioned above, skeletal muscle arterioles exhibit basal tone that maintains a low blood flow rate under resting conditions. However, this sympathetic vasoconstriction is reversed during exercise, through actions of vasodilatory metabolites (e.g., Adenosine) to direct blood flow into active skeletal muscle tissue, via processes collectively termed functional sympatholysis (Anderson et al., 1991; Doyle & Duling, 1997; Furchgott, & Zawadzki, 1980; Hearon et al., 2020). Skeletal muscle capillary perfusion can be increased up to 100-fold through coordinated vasodilation of supplying arterioles to increase oxygen delivery into active muscle fibres (Korthuis, 2011; Attrill, 2019). This elevated tissue activity and blood flow during exercise generally is referred to as active, or functional hyperemia which dynamically adjusts to match the oxygen demands of tissues (Marvar et al., 2007; Samora et al., 2008; Sindler et al., 2009).

Oxygen is an essential component of local blood flow regulation in skeletal muscle as oxygen supply is closely matched to the oxygen demands of tissue (Sparks, 1980; Rowell, 2004; Saltin, 2007; Laughlin et al., 2012; Golub & Pittman, 2013). For example, endothelial cells release NO and PGI<sub>2</sub> under hypoxic conditions to regulate blood flow and oxygen delivery through vasodilatory actions (Pohl & Busse, 1989; Hellsten et al., 2012). To what extent oxygen is involved in regulating blood flow has yet to be fully described. Still, many

studies have focused on determining the mechanism and location responsible for regulating oxygen-mediated blood flow, as outlined in the following section.

## 1.5 MECHANISMS OF OXYGEN-MEDIATED BLOOD FLOW REGULATION AND LOCATIONS OF THE OXYGEN SENSOR

Oxygen ( $O_2$ ) regulation is a physiological function required to maintain the body's metabolic demands. Oxygen supply is directly proportional to the oxygen demand in essential tissue or organs such as the skeletal muscle, kidneys, and the brain (Sparks, 1980; Emerson & Segal, 1997; Golub & Pittman, 2013). In the microcirculation, a vasoactive response occurs when oxygen levels change, leading to vasoconstriction in the presence of high  $[O_2]$  (Duling, 1972; Hutchins et al., 1974; Welsh & Segal, 1998; Frisbee & Lombard, 2002) and vasodilation in the presence of low  $[O_2]$  (Pittman & Duling, 1973; Fredricks et al., 1994a; Frisbee et al., 2002). The control response associated with changing  $[O_2]$  suggests an oxygen sensor exists, yet there are several potential candidates (Jackson, 2016). Some studies indicate that an  $O_2$  sensor lies within microvascular vessels (Pittman & Duling, 1973; Duling 1974; Jackson & Duling., 1983; Jackson, 1987; Ellsworth & Pittman, 1990; Pries et al., 1995; Hester, 1993; Messina et al., 1994). In contrast, other evidence suggests that the sensor resides in the tissue surrounding microvessels (Haddy & Scott., 1968; Harder et al., 1996; Jackson & Duling, 1983; Storch et al., 2015). Although multiple hypothetical sensors and mechanisms are involved, there remains many unanswered questions regarding the sensing and control of blood flow in skeletal muscle microcirculation in response to changing  $[O_2]$ .

The microvascular control of oxygen supply to tissue cells requires a precise localized sensor coupled with one or more mechanisms that can be activated with the speed and sensitivity needed to titrate supply under physiological conditions. Duling & Berne discovered a longitudinal PO<sub>2</sub> gradient that exists along the arteriolar tree, suggesting a location for oxygen control (Duling & Berne, 1970). For oxygen to be involved directly with regulating vascular function, local O<sub>2</sub> tension of the vascular smooth muscle cells must be altered by supply and demand changes, and the PO<sub>2</sub> must be in a range where alterations of smooth muscle cell contractility can occur (Duling, 1972). The sensitivity of individual arterioles to oxygen tension has been analyzed in the search for determining the location responsible for sensing oxygen demands (Duling & Berne, 1970; Duling, 1972, 1974; Pittman & Duling, 1973; Jackson, 1987).

The contractile state of the arterioles' vascular smooth muscle shifts based on the tissue's oxygen supply. Based on this understanding, it was proposed that the vascular smooth muscle or an arteriole component could sense O<sub>2</sub> changes. Experimentally, arterioles vasoconstrict when exposed to high PO<sub>2</sub> solutions overlying muscle tissue preparations (Duling & Berne, 1970; Duling, 1972; Hutchins et al., 1974; Welsh & Segal, 1998; Frisbee & Lombard, 2002). This arteriolar vasoactive response to O<sub>2</sub> supports such a proposal, however, these studies failed to determine whether oxygen directly or indirectly affects vascular smooth muscle in the arteriolar wall (Duling, 1972). To understand the sensitivity of individual arterioles for sensing O<sub>2</sub>, intravital studies compared the vasoactive responses to PO<sub>2</sub> changes when individual cheek pouch arterioles were stimulated versus the entire tissue (Duling, 1974). Neither the arteriolar wall response from manipulations by

altering the PO<sub>2</sub> of fluid-filled micropipettes, nor the response from in situ perfusion of arteriole segments showed arteriolar O<sub>2</sub> reactivity in the vessel wall (Duling; 1974; Jackson, 1987). In contrast, vasoconstriction was induced when PO<sub>2</sub> was increased within the superfusion solution flowing over an entire cheek pouch (Duling, 1974; Jackson, 1987). Therefore, these groups concluded that individual vessels could not directly sense and respond to O<sub>2</sub> changes, suggesting control occurred elsewhere, potentially involving the parenchymal cells (Duling, 1974; Jackson, 1987; Duling & Pittman, 1975).

Experimental protocols have been developed to focus on multiple areas in the microcirculation to examine potential locations of O<sub>2</sub> sensing. Jackson & Duling utilized rodent models with and without a parenchyma to quantify the involvement of parenchymal cells near capillaries and arterioles in oxygen-mediated regulation (Jackson & Duling, 1983). O<sub>2</sub> reactivity responses were observed in the hamster cheek pouches with their parenchyma removed, providing no support for the role of parenchyma in O<sub>2</sub> reactivity (Jackson & Duling, 1983). Still, it suggests arterioles or elements of arterial vasculature and blood may be the site of oxygen sensing within the system. Contradicting evidence exists from intravital studies, suggesting smooth muscle is not involved in sensing O<sub>2</sub> (Jackson, 1987; Messina et al., 1992, 1994). The current literature constitutes numerous examples of contradicting evidence for multiple potential sensors.

The endothelium is a component in the vascular wall that has also been studied for potential involvement in local O<sub>2</sub> sensing. Ex vivo experiments using pressure myography provide supporting evidence for endothelial cells as a potential O<sub>2</sub> sensor, in arteries, large arterioles, and first-order cremaster arterioles (Busse et al., 1983, 1984; Jackson, 1987;

Messina et al., 1992,1994; Fredricks et al., 1994a, 1994b; Ward, 1999; Frisbee et al., 2001a, 2001b, 2001c). Although, a large quantity of the data was collected in conduit arteries rather than at the microvascular level. However, pressure myography using rat gracilis muscle feed arteries lacking an endothelium displayed some O<sub>2</sub> reactivity in a PO<sub>2</sub> range of 10 - 150 mmHg (Frisbee et al., 2002). Although, it is important to consider that data collected at high PO<sub>2</sub> of 150 mmHg in arterioles is above the physiological range. Experimental work on rat cremaster arterioles with intact endothelium did not affect myogenic tone when PO<sub>2</sub> changed (Tateishi & Faber, 1995a; Kerkhof et al., 1999). The main comparison between studies that support endothelial cells as an O<sub>2</sub> sensor and ones that did not, were the presence of luminal flow only in studies with evidence supporting endothelium dependent O<sub>2</sub> reactivity (Jackson, 2016). Additionally, IVVM data described earlier did not support endothelial cells as the sensor for mediating arteriolar O<sub>2</sub> reactivity (Duling, 1974; Jackson, 1987). A critical difference in these studies was that vessels with diameters > 50 µm were used in ex vivo work. In contrast, vessels smaller than 40 µm in diameter were observed in intravital studies. The varying results obtained from in vivo studies lack significant support for the arteriolar smooth muscle cells or endothelial themselves to act as an O<sub>2</sub> sensor.

Along with the location of this proposed sensor, the mechanism regulating oxygen-mediated blood flow and smooth muscle tone remains to be determined. Endothelium-derived vasodilators prostacyclin and nitric oxide have been studied for their involvement in O<sub>2</sub> regulation. PGI<sub>2</sub> has been shown to mediate the dilation of arteries and large arterioles to a reduction in PO<sub>2</sub> from 150 mmHg to 20 - 50 mmHg (Busse et al., 1983, 1984; Fredricks et al. 1994a, 1994b; Frisbee et al., 2001b, 2001c, 2002). Although, the role

of PGI<sub>2</sub> in mediating arteriolar O<sub>2</sub> reactivity remains unclear (Messina et al., 1992). O<sub>2</sub> reactivity was analyzed in rat skeletal muscle by observing responses pre- and post-removal of the endothelium, and while a prostaglandin inhibitor, indomethacin, was administered (Messina et al., 1992). Arteriolar O<sub>2</sub> reactivity was present in all three experimental protocols, suggesting prostaglandins did not directly sense O<sub>2</sub> changes. Isolated rat cremaster muscle arterioles vasoconstrict at high PO<sub>2</sub> (150-600 mmHg) by reducing PGI<sub>2</sub> synthesis, supporting endothelial cells' role in regulating blood flow at elevated tissue oxygen tension (Messina et al., 1994). Although, contrasting evidence exists showing that inhibiting cyclooxygenase in various intravital muscle preparations did not affect arteriolar O<sub>2</sub> reactivity (Jackson, 1986; Pries et al., 1995; Ngo et al., 2013). Therefore, the mechanism and role of endothelium as an O<sub>2</sub> sensor are still unclear.

The involvement of NO in arteriolar O<sub>2</sub> reactivity has been extensively studied. Several *ex vivo* studies provided evidence to support PO<sub>2</sub>-dependent vasodilation mediated by NO in rabbit aortas and femoral arteries when exposed to low PO<sub>2</sub> perfusing solutions (Pohl & Busse, 1987), in hamster carotid arteries when PO<sub>2</sub> was reduced from 150 to 20-30 mmHg (Jackson, 1987), and in rat spinotrapezius muscle and intestinal arterioles *in situ* (Nase et al., 2003; Pries et al., 1995). However, intravital studies obtained contrasting evidence that showed the inhibition of NO synthesis did not affect the ability of arterioles to vasodilate under low O<sub>2</sub> conditions in hamster cheek pouch (Jackson, 1991) or mouse cremaster muscle (Ngo et al., 2010, 2013; Riemann, 2011). Variability remains in the O<sub>2</sub> reactivity responses, depending on location, preparation, and target mechanism.

More recently, researchers have found evidence supporting erythrocytes as the vascular sensor and regulator of O<sub>2</sub> supply. Erythrocytes contain an essential component of the oxygen transport system, hemoglobin, which is directly influenced by [O<sub>2</sub>]. Erythrocytes' role as an O<sub>2</sub> carrier supports their ability to respond to oxygen demands. It is well established that when RBCs arrive at the arteriole level, they experience an O<sub>2</sub> gradient related to the oxidative metabolic demands of nearby tissue, causing the offloading of oxygen from hemoglobin to trigger a simultaneous increase in blood flow (Ellsworth et al., 1995, 2004).

Three proposed mechanisms exist for how erythrocytes may act as an O<sub>2</sub> sensor. The first mechanism involves a conformational change associated with the desaturation of hemoglobin when exposed to low PO<sub>2</sub> and decreasing the binding affinity of S-nitrosothiol (SNO) to hemoglobin (Stamler et al., 1997). Typically, oxyhemoglobin promotes the binding of NO and cysteine to form S-nitrosohemoglobin (SNO-Hb). It is proposed that when SNO is released in the tissue from oxyhemoglobin, it acts as a vasodilator to increase blood flow and oxygen transport (Jia et al., 1996; Stamler et al., 1997). Although some evidence exists, the role of SNO in vivo remains unclear (Patel, 1999; Gladwin & Schechter, 2004; Gladwin, 2003). The second proposed mechanism involves the ability of deoxyhemoglobin to act as a nitrite reductase, converting nitrite to NO (Patel et al., 1999; Cosby et al., 2003; Gladwin et al., 2004). This mechanism does provide evidence for erythrocytes inducing vasodilation on arterioles locally at low SO<sub>2</sub>. Still, this mechanism does work in the required time and space to control erythrocyte distribution rapidly (Ellsworth et al. 2009). A conducted signalling mechanism is necessary to elicit a

vasoactive response that can travel across the vascular tree and enable communication from capillaries to arterioles to regulate blood flow in response to O<sub>2</sub> (Collins et al., 1998). Neither of the two proposed mechanisms above accounts for this, as there is no evidence for the role of either in conducted responses (Ellsworth et al, 2009).

Lastly, the third and most thoroughly studied mechanism proposed for oxygen-mediated regulation is the release of ATP from erythrocytes (Ellsworth et al., 1995, 2004, 2009, 2013; Stein & Ellsworth, 1993; McCullough et al. 1997; Gonzalez-Alonso, 2002; Sprague, 2009; Hanson et al., 2009; Ellis et al., 2012; Sové et al., 2021). Along with many animal studies, this mechanism has also been proposed in human experiments (Ellsworth, 2000; Gonzalez-Alonso, 2002, 2006 2012; Sprague et al., 2010). Initially, erythrocytes were shown to release ATP under low O<sub>2</sub> levels and were proposed to result in local vasodilation (Bergfeld & Forrester, 1992). Not long after, Stein & Ellsworth confirmed that local vasodilation occurs in the presence of ATP at the arteriole level (Stein et al., 1993). Purinergic receptors were discovered on the endothelium, and the local vasodilation resulted in conducted downstream responses (Stein et al., 1993). Additionally, O<sub>2</sub> content (SO<sub>2</sub>) was shown to be more critical than PO<sub>2</sub> (partial pressure of oxygen) for microvascular regulation, as erythrocytes released signalling molecules to modulate blood flow in response to a drop in internal hemoglobin SO<sub>2</sub> (Stein et al. 1993; Ellsworth et al. 1995). This proposal became more robust when similar response occurred during exposure to decreased pH (Ellsworth, 1995) and mechanical deformation (Sprague, 1998; Wan et al., 2008, 2011), providing further evidence of the erythrocyte's suggested role. Multiple studies showed local vasodilation occurred in the vascular lumen, conducted upstream to

arterioles in the presence of ATP (Kurjiaka & Segal, 1995; McCullough et al., 1997; Dora, 2017). Another study injected ATP into skeletal muscle venules to successfully elicit conducted vasodilation from capillary networks to upstream feed arterioles, increasing erythrocyte flux and thus increase O<sub>2</sub> tension in the tissue (Collins et al., 1998).

If RBCs are responsible for O<sub>2</sub> sensing, a stimulus must initiate their associated signalling pathway. The responsible activator has not been confirmed in the literature. The pathway was believed to be triggered by the desaturation of hemoglobin (Jagger et al., 2001), consistent with earlier findings by Stein & Ellsworth (1993). More recently, it was hypothesized that membrane-bound hemoglobin desaturates, resulting in a conformational change and a local membrane deformation. It is a direct mechanical stimulus activating the Gi protein (Sridharan, 2010b; Wan et al., 2008, 2011). Activation of the Gi protein activates adenylyl cyclase to increase cyclic adenosine monophosphate (cAMP), protein kinase A, and the cystic fibrosis transmembrane inductance regulator to release ATP (Sprague et al., 1998; Sidhuran, 2010b) Therefore, in hypoxic conditions, this signal transduction pathway modulated by RBCs would result in an increased ATP release through pannexin-1 channels binding to purinergic receptors (P<sub>2</sub>Y<sub>2</sub>) on the vascular endothelium (Sridharan et al., 2010a; Needham, 1987; Rubino et al., 1995; Malmjö et al., 1999; Wihlborg et al., 2003). Conducted signalling is believed to occur by the activation of P<sub>2</sub>Y<sub>2</sub> receptors along the vascular endothelium in both arterioles and capillaries. This activates K<sub>ATP</sub> channels and hyperpolarization of endothelial and smooth muscle cells, resulting in conducted vasodilation upstream to increase the supply of O<sub>2</sub>-carrying RBCs (Jackson, 2005; Quayle

et al., 1997; Campbell et al. 1996; Dietrich et al., 2000, 2009; Segal & Duling, 1989; Ellis et al., 2012).

Conflicting evidence and opinions exist for the site of ATP release and the associated mechanisms. It was initially thought that if ATP is released in the arterioles, vasodilation in adjacent smooth muscle cells will occur quickly (Duling 1974; Jackson, 1987). Although, the transit time for RBCs in arterioles is relatively short, meaning desaturation and ATP release would have to occur quickly. Interestingly, venules are thought to be optimally positioned for monitoring the metabolic demands of the tissue and modulating the arteriolar wall (Anciero et al., 2008; Segal, 2005). Some studies have shown that ATP injected into venules causes a conducted vasodilation response to arterioles and that ATP release from RBCs could be initiated at the arteriole level and in venules (Collins et al., 1998; Hester & Hammer, 2002; Ellsworth, 2004; Arciero et al., 2008; Segal, 2005). Mathematical model results support that conducted responses propagated to arterioles are stimulated by ATP release in venules and can account for the blood flow changes that occur in response to elevated  $[O_2]$  (Arciero et al., 2008). Experimental evidence shows that conducted responses travel 0.5-2 mm, and venular-arteriolar communication requires a travel distance of up to 1 cm (McCullough et al., 1997; Collins et al., 1998). Although, it is believed that this result is due to the limited field of view in intravital microscopy and not completely representative of the maximum distance for conducted responses. It is suggested that venules assist the overall  $O_2$  supply to larger regions of the microvascular bed in relation to their crosstalk with paired arterioles (Ellis et al., 2012; Hester & Hammer, 2002).

Although the ATP mechanism is broadly described at the arteriole level, changes in  $PO_2$  have been proposed to stimulate RBCs to release ATP downstream at the capillary level to induce a response from endothelial cells, either directly or via conversion to adenosine (Duling & Berne, 1970; Collins et al., 1998; Duza & Sarleius, 2003). It is hypothesized that capillaries signal upstream arterioles for changes in erythrocyte supply rate in an oxygen saturation ( $SO_2$ ) dependent manner through hyper-polarization of endothelial cells (Ghonaim et al., 2011; Ellis et al., 2012; Lamb et al., 2021). The capillary structure and components make it an ideal location for the transduction of  $O_2$  sensing. Erythrocytes also travel through capillaries more slowly, resulting in longer transit times when compared to arterioles. Therefore, capillaries offer a site that provides erythrocytes sufficient time for equilibrating with the surrounding tissue, using a ubiquitous mobile  $O_2$  sensor that can communicate with the surrounding vasculature via ATP release, thus producing highly localized and rapid signalling response to regulate oxygen-mediated blood flow (Figure 1.2).

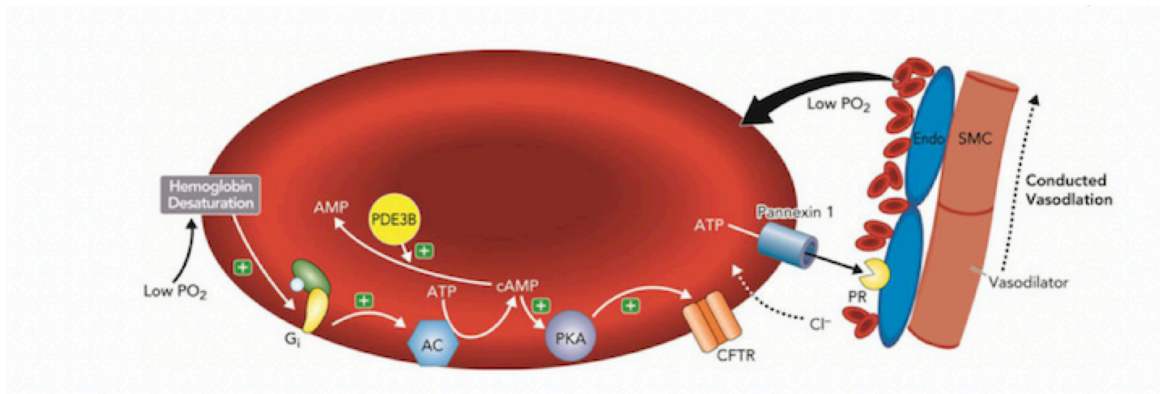


**Figure 1.2 Proposed mechanism responsible for oxygen ( $O_2$ ) mediated blood flow regulation at the capillary level.** This proposal involves a mechanism that may occur when  $[O_2]$  decreases in the tissue. It suggests that  $O_2$  released from erythrocytes causes a conformational change in hemoglobin. This activates the heterotrimeric G-protein ( $G_i$ ), which stimulates adenylyl cyclase (AC) activity and results in an increase in 3'5'-adenosine monophosphate (cAMP), activation of protein kinase A (PKA), and the cystic fibrosis transmembrane conductance regulator (CFTR). ATP is released through pannexin 1 channels and bind to purinergic receptors (PR) on the endothelium (Endo) to stimulate the production of vasodilators for local relaxation of vascular smooth muscle (SMC) and dilation that is conducted upstream (Figure obtained from Ellsworth, 2016 with permission).

## 1.6 MICROVASCULAR PREPARATIONS & MEASUREMENTS

Highly specialized techniques are necessary for studying the microvasculature due to its small scale and delicate nature. Specialized techniques are chosen for this vascular level due to the difficulty faced with the accessibility and conditions needed to maintain the physiological state of the preparation being observed. Oxygen-mediated blood flow regulatory mechanisms have been studied through various experimental methods and apparatus targeting the microvasculature (Duling, 1970, 1974; Hirai et al., 2010, 2021; Pittman, 2011; Ellsworth, 2004). Focusing on the microvascular level allows researchers to analyze blood flow responses directly at the primary exchange area, where precise regulatory processes are at play. The regulatory responses at high-level feed arteries do not entirely reflect the resulting blood flow, which could be observed in individual microvessels or the dynamic local responses in arteriolar and capillary networks. By combining specialized techniques with suitable analytics, the ability to quantify the overall tissue response and the individual responses in various vessel types can be completed.

For decades, many researchers have sought to obtain novel insights regarding O<sub>2</sub> reactivity at the microvascular level, with the tools and techniques used for measurements evolving considerably (Krogh, 1919; Duling, 1970, 1972; Hutchins et al., 1974; Jackson & Duling, 1983; Welsh & Segal, 1998; Frisbee & Lombard, 2002; Pittman & Duling, 1973; Fredricks, 1994a, 1994b; Golub & Pittman, 2008). Researchers have shifted their focus from analyzing regulatory mechanisms in large and feed arteries to targeting blood flow in arteriole and capillary microvascular preparations (Duling et al., 1972, 1973, 1981; Hutchins et al., 1974; Jackson & Duling, 1983; Busse et al., 1983; Jackson, 1987; Welsh &

Segal, 1998; Schjorring et al., 2015; Jackson, 2016). Microvascular preparations allow researchers to study local control mechanisms and observe microscale responses in exchange vessels. With the proper measurement techniques, microvascular preparations can be used to quantify tissue oxygen conditions in various tissues. In the scope of this thesis, previous studies that require oxygen tension measurements in tissues typically measure blood flow responses that co-occur, but the techniques used differ depending on the experimental preparation at hand.

Oxygen measurement techniques are commonly chosen based on the microvascular preparation used in the study. The ability to accurately measure  $[O_2]$  is critical in microvascular  $O_2$  reactivity studies that provide novel insights into the local control of microvascular blood flow. If  $O_2$  is mismeasured in experimental work that provides context for regulatory mechanisms, our understanding of the responses associated with these  $O_2$  levels may be confounded. Depending on the specific study's focus, different measurement techniques are more or less suitable. For example, the  $O_2$  microelectrode is a standard polarographic determination of oxygen tension and has been used to measure  $PO_2$  in individual microvessels such as cheek pouch arterioles (Whalen, 1967; Duling & Berne, 1970; Duling, 1972, 1974, 1979; Ivanov et al., 1982; Jackson & Duling, 1983; Beurk, 2009). The micro-electrode tip is  $<5 \mu\text{m}$  and is placed on the external surface (perivascular) of arterioles to avoid platelet aggregation that can occur from sharp object penetration (Buerk, 2004). Micro-electrodes obtain spatially specific  $O_2$  measurements, a valuable property for studying individual microvascular responses. Their use has led to novel insights into  $O_2$  reactivity in skeletal muscle arterioles (Duling & Berne, 1970; Hutchins et

al., 1974; Kimura et al., 2007). Although they require precise placement, this can be a time-consuming tool and are not an ideal option for dynamic preparations. Additionally, this tool on its own cannot simultaneously measure flow or RBC flux with  $O_2$  measurements. Therefore, two separate measurements would be required if both measurements were vital, as they are in this thesis.

Experiments requiring  $PO_2$  measurements of entire muscle tissue or for dynamic muscle preparations commonly use the phosphorescence quenching method (PQM) (Rumsey et al., 1988; Behnke et al., 2001; Poole et al., 2004; Carhalho & Pittman, 2008; Golub & Pittman, 2008; Pittman et al., 2010; Hirai et al., 2010, 2018, 2019; Colburn et al., 2020). PQM is a non-invasive tool delivered via microinjection of an oxyphor probe to the muscle of interest or through an intravascular catheter, based on the ability of  $O_2$  to quench the phosphorescence of excited phosphor molecule (Smith et al., 2002; Wilson et al., 1987; Wilson et al., 2006). PQM offers a high degree of temporal resolution but limited spatial resolution when quantifying muscle tissue  $SO_2$  and vascular  $PO_2$  gradients in skeletal muscle (Rumsey et al., 1988; Behnke et al., 2001; Poole et al., 2004; Hirai, 2018; Golub & Pittman, 2008). The phosphor is introduced intravascularly, creating a mixed signal from multiple levels of vasculature, making it impossible to only measure capillary  $O_2$ . Compared to micro-electrodes, PQM offers less spatial specificity but can obtain  $O_2$  measurements without direct tissue manipulation; except for the potential interaction of reactive oxygen species (ROS) generated by high energy excitation wavelengths (Poole et al., 1995; Colburn et al., 2020). This technique applies a principle referred to as collisional quenching, stating that a singlet  $O_2$  is created due to the excitation of phosphor and decay

by the emission of light (phosphorescence) or the transfer of energy to O<sub>2</sub> (Pittman, 2011). Collisional quenching is a limiting factor for PQM in microvascular preparations as the singlet O<sub>2</sub> can oxidize and cause tissue damage and be consumed in the tissue over-approximating the O<sub>2</sub> consumption in the vascular wall being measured (Colburn et al., 2020).

In addition to measuring O<sub>2</sub> in microvascular preparations, specialized techniques exist for quantifying microvascular O<sub>2</sub> reactivity in tissue microenvironments through measuring blood flow. A significant difference between these measurement techniques is the scale at which the measurements are taken and whether they provide a direct or indirect value for blood flow. Variations in scale include measuring superficial skin regions, arteriole diameter changes, individual capillary hemodynamics, and relative microvascular blood flow.

A few non-invasive and continuous blood flow measurement tools have been used in O<sub>2</sub> regulatory studies. One of these tools is laser doppler flowmetry (LDF), a technique that continuously measures skin microvascular blood flow, providing researchers with an understanding of tissue level activity more accurately than bulk flow (Bartlett, 2020; Pittet et al., 1992). LDF signal is the product of mean red blood cell velocity, calculated by moving RBCs in the superficial region of the skin to change the frequency of the backscattered light (Pittet et al., 1982; Nilsson et al., 1980). LDF technique has been used to determine whether the changes in DO<sub>2</sub> (oxygen delivery) and VO<sub>2</sub> (oxygen consumption) induced by vasodilators correlate with their effect on the microcirculation (Pittet et al., 1992) and to quantify microvascular hemodynamics during ischemic stimulus (Bartlett,

2020). Similarly, near-infrared spectroscopy (NIRS) is also capable of continuously and noninvasively measuring relative changes in microvascular blood flow in human organs and skeletal muscle (Bartlett, 2020; Jones, 2016). However, since NIRS is not an imaging modality, it cannot visualize the microcirculation or measure hemodynamics in individual vessels as required to study microvascular O<sub>2</sub> reactivity responses. Although LDF and NIRS can quantify microvascular flow, they cannot offer the spatial specificity to collect individual capillary responses to confirm O<sub>2</sub> regulatory responses.

Indirect indices of blood flow rate can be obtained by analyzing vessel wall diameter changes and correlating them to blood flow. Pressure myography is an ex vivo method used to study O<sub>2</sub> reactivity and vascular contractility by measuring vessel wall diameter changes in feed arteries and larger arterioles exposed to different [O<sub>2</sub>] (Pohl & Busse, 1983, 1984; Jackson, 1987; Kerkhof, 1999; Duling, 1981; Dora, 2017). This method is better suited for the interest in large vessels like feed arteries, as the technique requires discrete vessel segments for cannulation (Duling, 1981). Such cannulation requires the use of vessels with sufficient length (>2-3 mm), the ability to survive vessel isolation, and to remain undamaged between two cannulas placed for myography. For example, terminal arterioles lumen diameter (~15 μm) can handle only minimal manipulation, therefore harvesting these small vessels embedded within muscle tissue via dissection is impractical (Wenceslau et al., 2021).

A common technique to observe and manipulate the microvasculature is by visualizing live animal muscle preparations using intravital video microscopy (IVVM). IVVM is a standard imaging method that can observe the microcirculation in real-time and record

microvascular blood flow of various muscle preparations (Dietrich & Tyml, 1992; Dewhirst, 2000; Varghese, 2005; Ellis et al., 2012; Ghonaim et al., 2011, 2021; Sové et al., 2021; Russell McEvoy et al., 2021, 2021). Muscles with locomotor function are commonly chosen for studying microcirculation using IVVM as they are salient models for observing blood flow responses during exercise or hypoxia. When choosing a muscle preparation, it is essential to consider the ability for surgical isolation and externalization onto a microscope setup without damage to muscle viability. More importantly, the muscle's size and ability to separate from its surrounding structures, the preservation of nervous innervation and a continuous blood supply even when placed onto the microscope stage are factors to consider. Many muscle preparations can be used and fit the criteria to observe the microcirculation. These include, but are not limited to, the hamster cheek pouch, the cremaster, the spinotrapezius, and the extensor digitorus longus (EDL) muscles (Tyml & Budreau, 1991; Gray, 1973; Duling, 1973; Charter et al., 2018). These muscle preparations are chosen based on their physical characteristics, optical properties, and ability to be used with the available (IVVM) equipment.

The cremaster preparation has been used extensively to study the arteriolar tree and vasomotor responses to various stimuli (Hutchins, 1974; Tateishi & Faber, 1995a, 1995b; Kurjiaka & Segal, 1995; Frisbee & Lombard, 2002; Riemann et al., 2010; Murrant et al., 2014; Dora, 2017; Lamb et al., 2018; Charter et al., 2018). A considerable portion of our understanding of vascular reactivity is through work using this unique preparation. The cremaster is a thin muscle allowing easy transillumination to visualize the arteriolar tree. The cremaster can be readily externalized and pinned out flat for imaging where a

superfusion bicarbonate buffer solution continuously bathes the muscle during experimental protocols (Grant, 1964). A superfusion solution is a physiological salt solution equilibrated with specific gas concentrations dependent on each study, exposing the muscle to a mixture of fixed gas concentration and the atmospheric environment around it. Although, some common superfusion solutions contain a 95% N<sub>2</sub> and 5% CO<sub>2</sub> gas composition lacking oxygen entirely, which is a confounding factor in itself, with potential impact on local tissue oxygenation. As a result, baseline blood flow may be elevated to supply the required oxygen in these preparations. Therefore, this may affect blood flow measurements gathered from O<sub>2</sub> reactivity studies as the chosen oxygen concentrations exposed to the muscle tissue may impact them.

The cremaster muscle's unique function to maintain adequate temperature and support in the testes should be considered when discussing this preparation (Bagher & Segal, 2011). This isolated muscle can exhibit spontaneous muscle tone during experiments due to its inherent function, requiring a nerve-blocking agent to prevent spontaneous movement when visualizing and imaging blood vessels. It is difficult to know whether the O<sub>2</sub> reactivity insights gained using this muscle preparation are a good comparison for any skeletal muscle, as the cremaster may have tissue-specific responses due its highly specialized function.

The same can be said for the hamster cheek pouch, which expands to support ample food storage, a unique purpose in hamsters (Duling, 1973). The hamster cheek pouch preparation has been utilized in regulatory studies that gained novel insights into vascular smooth muscle function and conducted signalling in arterioles (Duling & Berne, 1970;

Duling, 1972; Jackson & Duling, 1983; Jackson, 1987; Lombard et al., 1999; Fox & Frame, 2002; Carvalho & Pittman, 2008). The cheek pouch is an anatomical structure that forms a sac, which is transparent, very accessible, and ideally suited for studying microcirculation (Svensjo et al., 1990). This highly vascular sac allows visualization of all microvasculature classes within a microscope field (Duling, 1973).

Interests in studying microvascular blood flow during exercise and oxygen pressure gradients prompted the development of skeletal muscle preparations as they are ideal to study movement. In addition to exercise studies, the spinotrapezius muscle has been utilized in important O<sub>2</sub> reactivity studies in combination with similar superfusion solutions as described above (Pries et al., 1995; Behnke et al., 2001; Kindig et al., 2002; Smith et al., 2004; Golub et al., 2010; Hirai et al., 2010, 2018, 2021; Gray, 1973). This muscle is relatively thin, originating in the spines of the thoracic vertebrae with a mixed fibre-type composition and citrate synthase activity that resembles the human quadriceps (Delp & Duan, 1996; Leek et al., 2001; Hirai et al., 2010). The spinotrapezius muscle is thought to be a better model for metabolic demand studies as it is a postural muscle, capable of contracting voluntarily, compared to the non-postural cremaster muscle (Xiang et al., 2008). Therefore, different muscles may exhibit variable vascular responses to the same stimuli (McAllister, 2003).

Depending on the muscle tissue's shape, size, and orientation, the experimental preparation can be combined with either a superfusion preparation or an isolated preparation that covers the muscle with an impermeable membrane. In this thesis, IVVM is used to examine the microcirculation with a skeletal muscle that does not require a

superfusion preparation, the extensor digitorum longus muscle. The EDL is a relatively thick locomotor muscle of the rat's hind limb (Tymml & Budreau, 1991). The EDL can be isolated and reflected onto an inverted microscope stage without disrupting the vasculature, blood flow, nervous innervation, or surrounding tissues (Tymml & Budreau, 1991; Fraser et al., 2012a). An impermeable film and coverslip cover the isolated muscle, protecting the preparation from the surrounding environment and allowing visualization of a large field of view (Tymml & Budreau, 1991; Ghonaim et al., 2011; Ellis et al., 2012). The isolated muscle setup eliminates the impact  $[O_2]$  deficient superfusion solutions have on tissue blood flow. Arterioles are not easily visible in this preparation like they are in the cremaster as they originate deep within the muscle, so primarily terminal arterioles, capillaries, and collecting venules are visible. Therefore, this preparation is ideal for studies focused on analyzing capillary-level responses and the spatial distribution of flow between discrete capillary units (Tymml & Budreau, 1991).

Using IVVM, microvascular blood flow and vessel diameter changes are visualized directly during tissue manipulations with various vasoactive stimuli (Duling & Berne, 1970; Duling, 1972; Dietrich & Tymml, 1992; Dewhirst, 2000; Kindig et al., 2002; Varghese, 2005; Hirai et al., 2010; Ellis et al., 2012; Ghonaim et al., 2011, 2021; Murrant et al., 2014; Lamb et al., 2021; Sové et al., 2021; Russell McEvoy et al., 2021, 2022). However, measuring hemodynamic and other microvascular measurements from IVVM data can be challenging and time-consuming. For example, a manual analysis method was used to quantify RBC hemodynamics prior to and post muscle contractions with bright field microscopy (Kindig & Poole, 2002) and to measure arteriole wall diameter changes after

altered tissue [O<sub>2</sub>] or at rest (Duling, 1970, 1972; Hutchins et al., 1974; Hirai et al., 2021). Manual analysis methods often involve comparing images taken over a period in an online software tool such as ImageJ (National Institutes of Health: <http://rsbweb.nih.gov/ij/>.) to measure the movement of cells and obtain a cell count by the distance RBCs have travelled (Kindig et al., 1999, 2002; Poole et al., 1997; Smith et al., 2004; Hirai et al., 2021; Duling, 1972). Arteriolar diameter can be measured using ImageJ at various time point images captured by IVVM to compare diameters changes during various [O<sub>2</sub>] or other vasoactive stimuli (Duling, 1970, 1972; Hutchins et al., 1974; Kindig et al., 2002; Murrant et al, 2014; Dora, 2017; Lamb et al., 2021; Hirai et al., 2021). Therefore, experimental data can be analyzed using manual frame-by-frame methods for research groups that don't have access to software packages functioning with IVVM to assist in these measurements.

In this thesis, IVVM was used to observe and measure oxygen-mediated blood flow changes in the EDL muscle by [O<sub>2</sub>] perturbations from a gas exchange chamber in contact with the muscle (Ellis et al., 2012; Ghonaim et al., 2011). This system can measure hemodynamics and oxygen saturation changes of red blood cells in selected vessel segments as shown in Figure 1.3 and 1.4 (Ellis et al., 1990, 1992, 2012; Japee et al., 2004; Fraser et al, 2012; Ghonaim et al., 2021). The intravital recordings are made using a dual-camera video microscopy system with an isosbestic wavelength (420 nm) and an oxygen-dependent wavelength (438nm). Real-time videos are later processed into functional images for use in vessel selection and determining vessel centerline for OD measurements and space-time image (STI) generation by custom MATLAB software (Ellis et al., 1990, 1992; Japee et al., 2004; Fraser et al., 2012; Ghonaim et al., 2011, 2021). Video sequences

captured at 420 nm wavelength are used to create variance functional images with a method thoroughly described by Japee et al. (Japee et al., 2004). Functional images accurately represent the borders of individual capillaries, which can be used to determine the two-dimensional coordinates of the lumen and centerline within the capillary (Japee et al., 2004; Fraser et al., 2012).

Custom computer software is used to describe the light intensity values along the centreline of selected vessels from each video frame in the captured 420 nm sequence to generate a 420 nm STI as shown in Figure 1.3 (Japee et al., 2004; Ellis et al., 1992). Functional images are used to semi-automatically determine the vessel centerline location to generate STI for both wavelengths. Changes in light intensity along the vessel centreline are used to measure the single-file flow of red blood cells travelling through capillaries in a small segment from a selected capillary. Space-time images (STIs) describe the transit of cells through the capillary and their relative positions in the capillary lumen apparent from with dark and light bands (as shown in Figure 1.3). The dark bands represent RBCs travelling through a capillary, and the light bands represent the interceding plasma gaps in vessels (Figure 1.3). The band's appearance is related to the construction of an STI image and depends on the RBC velocity in each capillary. As described thoroughly by Ellis et al., RBC velocity ( $\mu\text{m/s}$ ) and lineal density (cells/mm) are calculated using the 420 nm STI images and a spatial correlation technique on the frame-by-frame light intensity data (Ellis et al., 1990, 1992, 2012; Japee et al., 2004; Fraser et al., 2012). Using the product of RBC velocity and lineal density (LD), RBC supply rate (cells/s) can be calculated and by using LD and the 2D diameter (volume of the capillary segment being analyzed) to calculate tube

hematocrit (%) on a frame-by-frame basis (Ellis et al., 1992; Japee et al., 2004; Fraser et al., 2012).

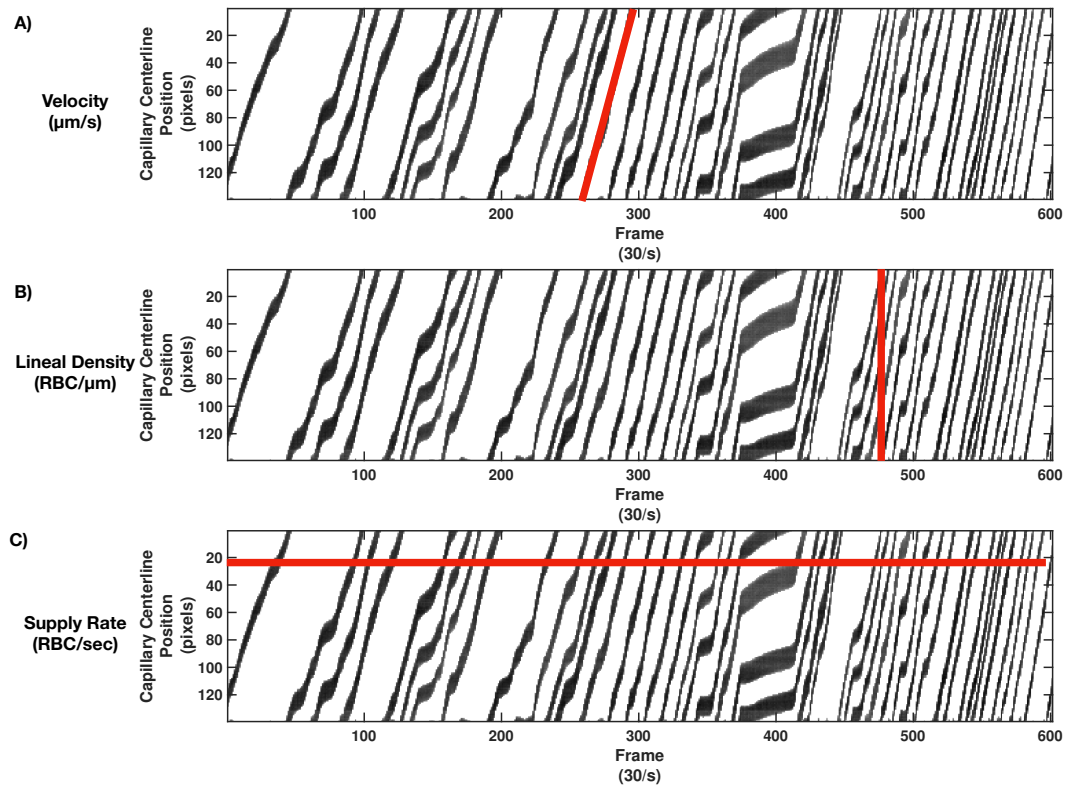


**Figure 1.3 Schematic of a space-time image with visual representation of hemodynamic parameters of a single capillary.** Each black line represents a RBC moving across the area of a selected vessel. A) Represents the determination of instantaneous velocity as the slope of the red line ( $\mu\text{m/s}$ ). B) Shows determination of lineal density as the number of RBCs present crossing the red vertical line ( $\text{RBC}/\mu\text{m}$ ). C) Shows the determination of supply rate as the number of RBCs crossing the red horizontal line ( $\text{RBC}/\text{sec}$ ). Adapted from Ellis et al. 1992.

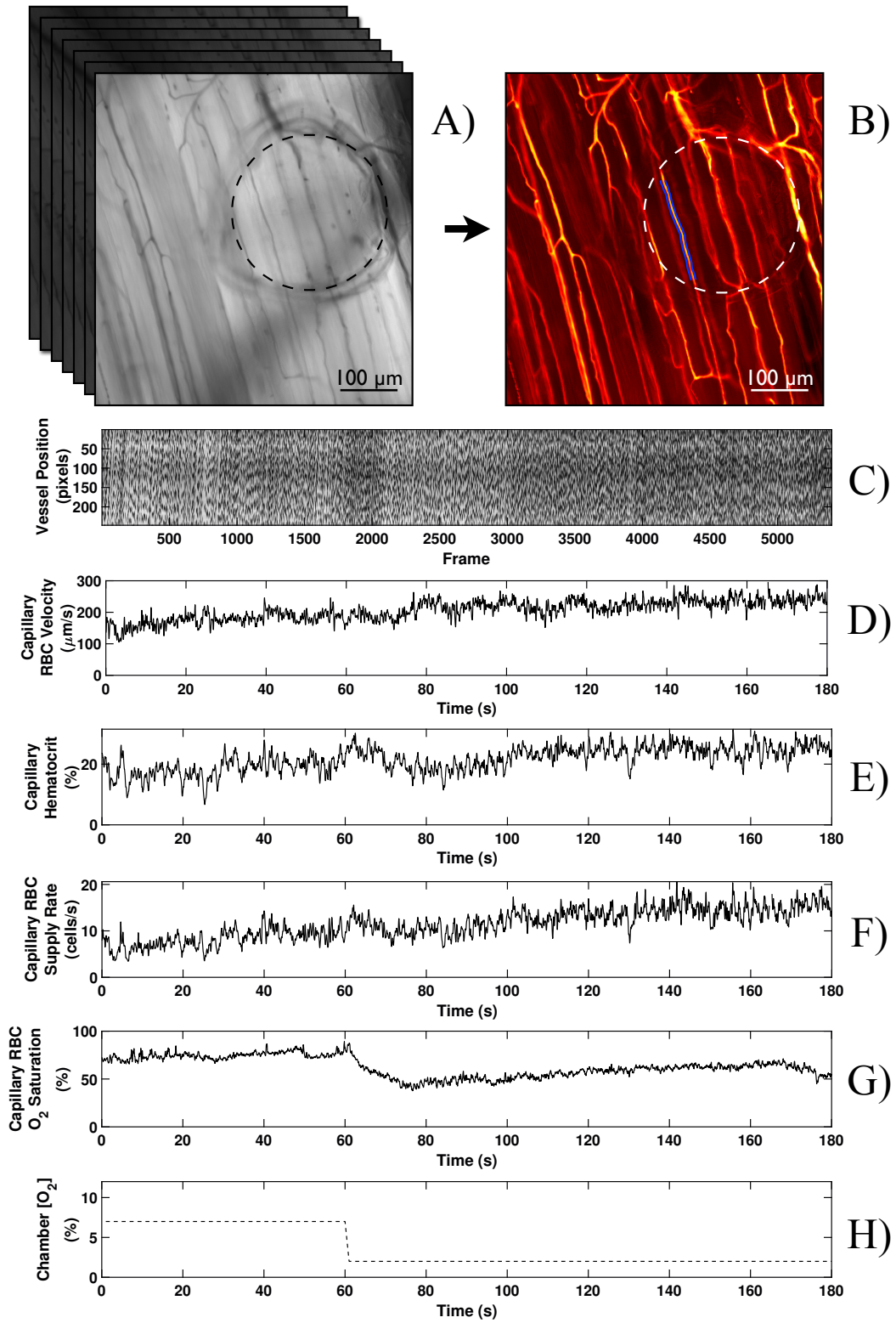


**Figure 1.4 Offline analysis completed with custom MATLAB software to measure capillary RBC oxygen saturation and hemodynamics.** Parameters were analyzed from selected capillaries during imposed oxygen oscillation and challenges in skeletal muscle tissue. A) Image representing the microcirculation from our 3-minute video sequence captured at 30 frames/sec, (5400 frames/video sequence). B) Perfused capillaries with single-file RBC flow are selected from functional images using a semi-automated process. C) Light Intensity fluctuations from plasma gaps between RBCs are used to generate space-time images (STIs), used to calculate hemodynamic parameters. D) RBC velocity of a selected capillary across the oxygen challenge recording. E) Capillary hematocrit of a selected capillary across the oxygen challenge recording. F) RBC supply rate of a selected capillary across the oxygen challenge recording. G) RBC  $SO_2$  of a selected capillary across the oxygen challenge. H) Imposed oxygen challenge from the gas exchange chamber during the 3-minute recording.

RBC oxygen saturation is measured using a spectrophotometric approach that quantifies the optical density of RBCs at two wavelengths selected based on the relative absorbance of oxy- and deoxyhemoglobin. Typically, an isosbestic and an oxygen-sensitive wavelength are established, providing a reference wavelength where both oxy- and deoxy-hemoglobin have the same molar attenuation coefficient (isosbestic) and a wavelength where there is a significant absorbance difference between oxy- and deoxy-hemoglobin (oxygen-sensitive) (Ellis et al., 1990). Both wavelengths are required to measure the oxygen saturation of RBCs in the microcirculation, calculated based on the ratio of the optical density measured from the oxygen-dependent wavelength divided by the isosbestic wavelength (Ellis et al., 1990; Ellsworth et al., 1987; Ellis et al., 1992).

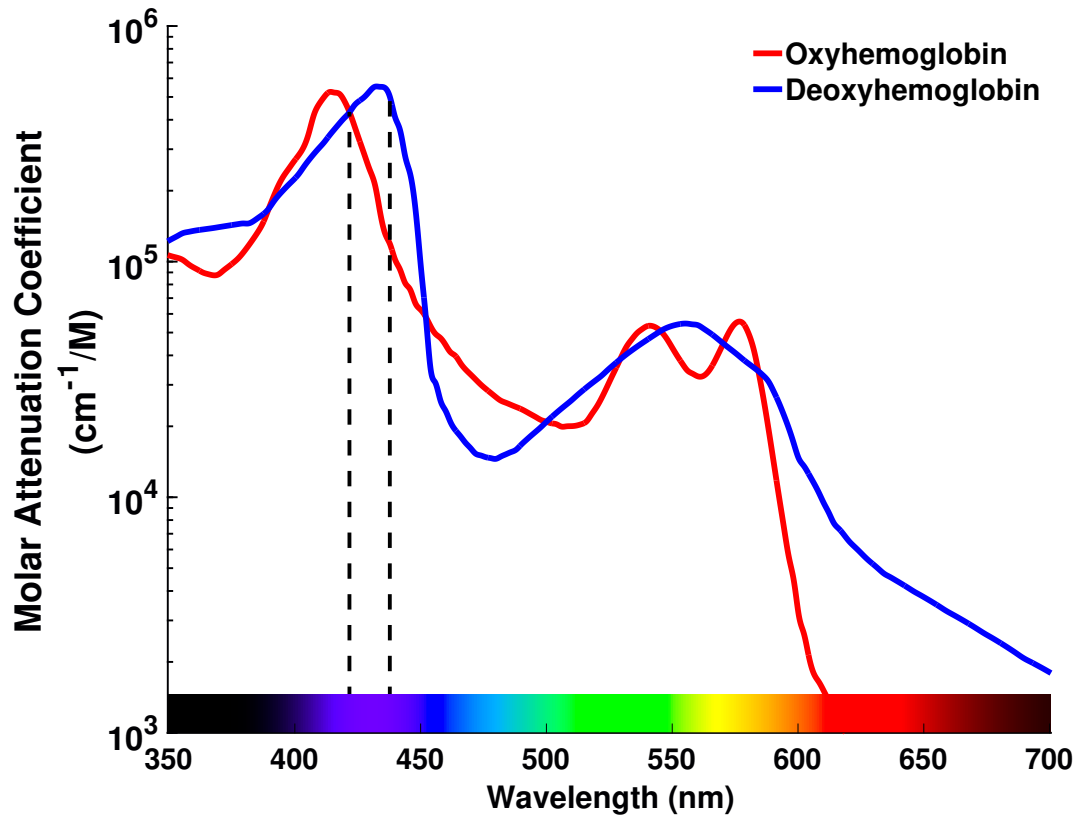


**Figure 1.5 Molar attenuation coefficients of hemoglobin.** The difference in molar attenuation coefficient for oxy- (red line) and deoxy- (blue one) hemoglobin is displayed across the visible spectrum as depicted by the horizontal colour bar. In this thesis, 420 nm and 438 nm wavelengths were used to calculate RBC oxygen saturation (Adapted from Fraser, 2012, using data from Prah, 1999).

## 1.7 MICROFLUIDIC DEVICES USED IN MICROVASCULAR STUDIES

Microfluidic devices have become popular in the biomedical field with devices finding use in clinical, industry, and bioscience research. A microfluidic device allows for the precise manipulation of fluids, usually via finely patterned microscale channels. Devices developed explicitly to study microcirculation are commonly fabricated with elastomers such as poly(dimethylsiloxane) (PDMS), an inert, inexpensive, and modular material used to mold an entire device, or components of a final prototype (McDonald et al., 2000; Ghonaim et al., 2011; Russell McEvoy et al., 2021, 2022; Sové et al., 2021).

For research purposes, these devices can be used with an IVVM setup and a muscle preparation for which the device is designed. As mentioned in the previous section, the two general preparation types for directly observing the microcirculation of a muscle by IVVM; superfusion preparations, such as the cremaster, where a solution composed of a physiological salt solution (PSS) that continuously bathes muscle, and isolated preparations, like the EDL muscle, that can be isolated from the surrounding environment (Grant, 1964; Anderson et al., 1988; Tyml & Budreau, 1991). As discussed in this chapter, a microfluidic device developed for studying O<sub>2</sub> sensing, and regulation must be custom designed to effectively work with one of these general preparations. This task requires high precision and accuracy for a suitable microfluidic device that will pair well with an in vivo preparation and fulfill the study's goals. To purposefully design a device during the conceptualization stage, mathematical modelling plays a vital role in determining likely boundary conditions, surface measurements, and other necessary criteria (Goldman et al., 2008, 2012; Ghonaim et al., 2013; Wang et al., 2013). The critical advantages of

incorporating modelling data to inform microfluidic device development will be discussed further in this section.

Before microfluidic devices were developed, studies focused on microvascular blood flow and the manipulation of skeletal muscle microenvironments employed several conventional approaches. The tissue microenvironment of muscle preparations has been manipulated by intravascular injections (Ishizaka & Kuo, 1997), micropipette delivery (Song & Tyml, 1993; Riemann et al., 2010; Charter et al., 2018), and topical application of drugs dissolved in PSS (Charter et al., 2018).

An intravascular injection involves the administration of a substance directly into venous or arterial catheters to travel through, and manipulate the circulation (Hutchins, 1974; Ishizaka and Kuo, 1997). Intravascular administration of substances will affect downstream vessels and potentially the entire systemic circulation, influencing multiple mechanisms involved with other levels of the vasculature. Micro-pipetting involves pipetting a minute volume of a solution directly onto, or nearby a vessel of interest, typically an arteriole. At the same time, the muscle surface is constantly perfused with PSS providing a means to wash away the applied agents (Duling 1974; Riemann et al., 2010; Charter et al., 2018). Although introducing substances with a micropipette is more spatially precise than an intravascular injection, the area stimulated is somewhat uncontrolled, resulting in the substance diffusing outward and being carried at lower concentrations convectively and diffusively within the solution. Researchers work to position the micropipette downstream of other vessels of interest, with the superfusion flowing away from interacting structures (Riemann et al., 2010; Charter et al., 2018). Dissolving drugs

into the buffer solution continuously bathing a muscle preparation will logically affect the entire muscle surface and the supporting vasculature. Therefore, this method is more suitable for studies targeting multiple levels of the vasculature. While these methods have been used to study microvascular blood flow regulation, they need to offer the spatial specificity and highly constrained manipulations needed to address research questions linked to specific scales of the microvasculature (Ghonaim et al., 2011; Russell McEvoy et al., 2021).

Gas and liquid-based microfluidic devices have been developed to study microvascular blood flow with a more spatially specific and dynamic approach (Ghonaim et al., 2011, 2013, 2021; Russell McEvoy et al., 2021, 2022; Sové et al., 2021). Such microfluidic devices can impose experimental perturbations on highly confined regions of tissue preparations to target the microvascular level. By combining either a gas or liquid-based microfluidic device with IVVM, researchers have simultaneously recorded changes in local capillary blood flow in response to various manipulations such as gas perturbations or vasoactive agonists and antagonists (Ghonaim et al., 2011; Russell McEvoy et al., 2021; Sové et al., 2021).

Specifically, to spatially target blood flow regulation at the microvascular level in intact tissue, a novel liquid microfluidic device (LMFD) was developed and validated for delivering vasoactive drugs to a microscale region of skeletal muscle (Russell McEvoy et al., 2021). The LMFD was composed of a laser-cut 600 x 300  $\mu\text{m}$  micro-outlet machined into a borosilicate glass coverslip, and mated to a PDMS channel, thus allowing PSS to flow underneath an isolated EDL preparation (Russell McEvoy et al., 2021). The LMFD

was a significant advancement to the technology available to study microvascular signalling mechanisms as it maintains continuous delivery to spatially specific microscale areas of the tissue surface, establishing a fixed concentration at the surface of the muscle and a distance from the micro-outlet (Russell McEvoy et al., 2021). Using a LMFD for studying O<sub>2</sub> reactivity is somewhat limited in that the PSS must be equilibrated at various O<sub>2</sub> concentrations, which hinders studying responses to dynamic changes in tissue PO<sub>2</sub>. Further, oxygen has relatively low solubility in such solutions which limits how forcefully tissue gas concentrations can be altered.

Although the ability to interrogate microvascular blood flow regulatory mechanisms has improved with liquid-based microfluidic devices, targeting specific microvascular levels remains challenging. Russell McEvoy et al.'s device constrained vasoactive drug doses to a radial diffusion distance of 500  $\mu\text{m}$  beyond the outlet's border for an area of effect around 1100 by 800  $\mu\text{m}$ , which was further supported by computational modelling, and evidenced by imaging results (Russell McEvoy et al., 2021). Therefore, the device did not target specific capillary networks as required for determining the location, and critical scale of O<sub>2</sub> sensing. Indeed, the larger area of effect may have stimulated arterioles deeper in the tissue, bypassing conducted signalling that was not quantified. Limiting factors of the LMFD, such as low solubility of oxygen in PSS, radial diffusion, the interest in underlying mechanisms of microvascular control, and the difficulty of routinely implementing LMFD, were driving forces behind our current efforts to further develop spatial specificity in gas-based microfluidic devices.

Gas-based microfluidic devices have previously been fabricated and considered in conjunction with mathematical modelling to quantify microvascular blood flow and O<sub>2</sub> reactivity responses (Goldman et al., 2008, 2012; Ghonaim et al., 2011, 2013, 2021; Sové et al., 2013, 2021). As described in section 1.4, substantial evidence supports the concept that erythrocytes play a crucial role in O<sub>2</sub> regulation, specifically through vasodilatory ATP release at the capillary level. However, it is difficult to quantify ATP release from RBCs at the capillary level in vivo. Mathematical modelling of such gas-based devices that stimulate confined tissue areas and solely target capillaries in vivo has helped conceptualise this quantification (Goldman et al., 2008, 2012; Ghonaim et al., 2013, 2021; Sové et al., 2013, 2021). Before specific mechanistic questions can be answered, the location for O<sub>2</sub> sensing must be confirmed, which is the primary goal of developing a gas-based device to target the capillary level (Ghonaim et al., 2011). Modelling results have predicted the expected tissue depth and radial diffusion distance resulting from [O<sub>2</sub>] oscillations when imposed onto an externalized skeletal muscle tissue (Goldman et al., 2008; Ghonaim et al., 2013; Sové et al., 2021). Based on these simulation results Sové et al. concluded that their devices would not stimulate higher-order vasculature deeper in the tissue or diffuse far from the device's intended area of effect. Additionally, modelling results support the ATP release hypothesis described in section 1.4 by demonstrating that gas-based microfluidic devices can produce rapid decreases in oxygen saturation of erythrocytes across various geometries of micro-outlets and analyze the dynamics of O<sub>2</sub> saturation-dependent ATP release using a mathematical model (Ghonaim et al., 2013; Sové et al., 2013). While the predicted results were not tested in vivo, they provided important insight for the design and fabrication of

gas-based devices that were later applied to study microvascular O<sub>2</sub> regulation (Sové et al., 2021).

Gas-based microfluidic devices can effectively deliver fixed gas concentrations to the surface of skeletal muscle in localized areas (Ghonaim et al., 2011, 2021; Sové et al., 2021). This device is comprised of a gas channel to direct the gas mixture from the inlet to the outlet, establishing a fixed gas concentration at the device's gas-permeable membrane, which is mated to the overlying skeletal muscle (Figure 1.6). The device is combined with an isolated muscle preparation separated from the atmosphere by an impermeable film, with the capacity to dynamically change tissue PO<sub>2</sub> within the muscle preparation (Figure 1.7). Varying levels of oxygen gas are perfused through thin glass micro-outlets to the EDL muscle to induce blood flow responses while allowing for simultaneous recording of RBC SO<sub>2</sub> resulting from changes in the tissue oxygen microenvironment (Ghoanim et al, 2011; Sové et al., 2021). Skeletal muscle tissue can be manipulated locally within seconds by flowing a 2% [O<sub>2</sub>] gas composition through the gas exchange chamber imposing hypoxic conditions and vice versa with a hyperoxic, 12-20% [O<sub>2</sub>] gas composition (Ghonaim et al., 2011; Sové et al., 2021). Such [O<sub>2</sub>] changes at the muscle surface are imposed more rapidly and precisely using a gas-based device equipped with precision mass flow meters, compared to liquid-based device that use a very low flow rate siphon or infusion pump.

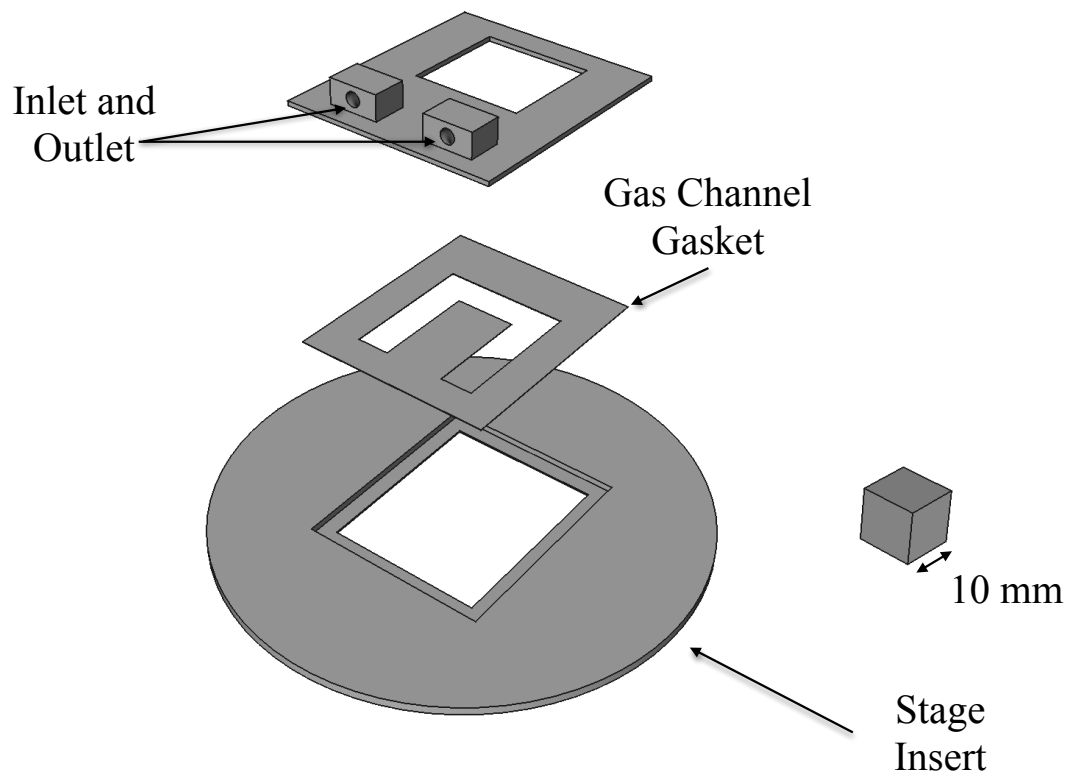


**Figure 1.6 Three-dimensional Computer Aided Design (CAD) model of a 3D printed gas exchange chamber.** The gas channel is sealed with a glass cover slide on the bottom and an ultrathin film micro-outlet layer on the top. (Figure from Sové et al., 2021, used under the Creative Commons License).

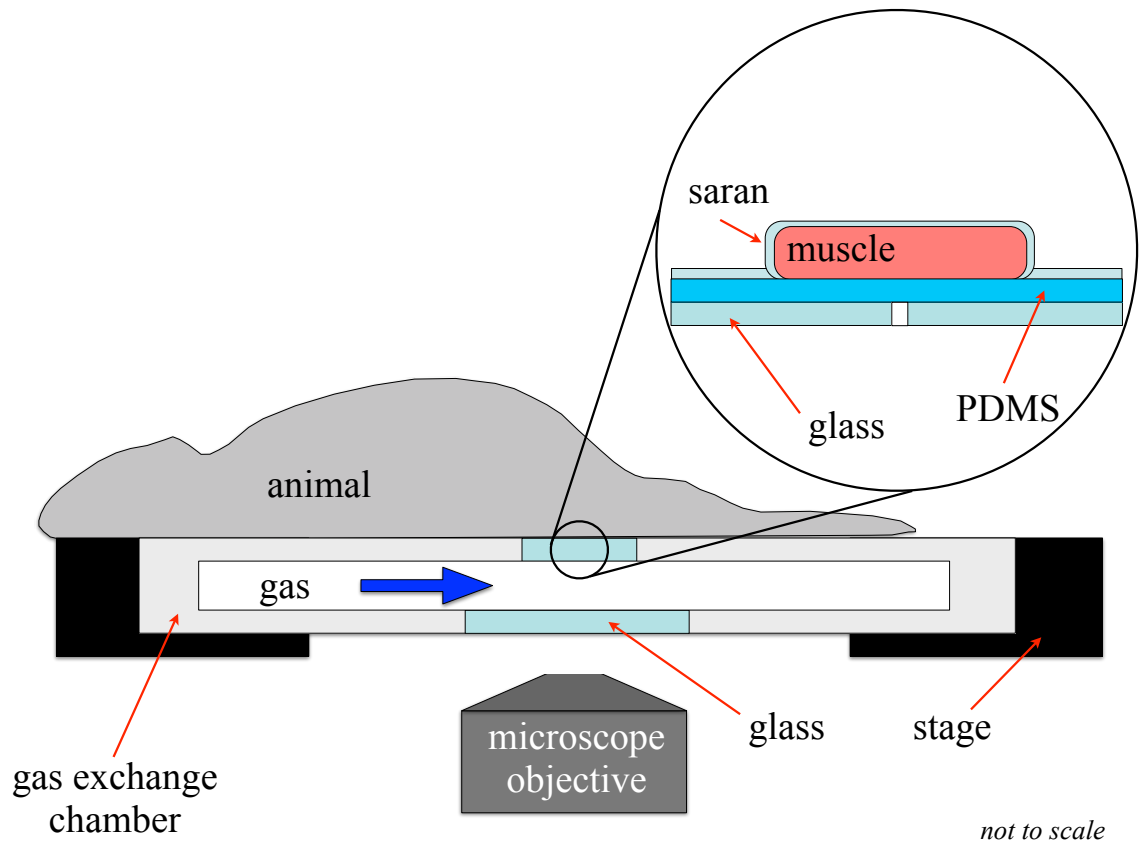


**Figure 1.7 Intravital video microscopy setup.** This experimental setup was used by Sové et al. to manipulate  $[O_2]$  locally in the tissue using micro-outlets that overly the gas exchange area. In this setup, the muscle is overlying the gas permeable layer of their micro-outlet window and is covered with a gas-impermeable polyvinylidene film for isolation of the muscle from its surrounding environment (Figure from Sové et al., 2021, used under the Creative Commons License).

Regarding the few gas-based microfluidic devices fabricated to study microvascular O<sub>2</sub> reactivity, the most significant design advancement has been the improvements in spatially constraining perturbations in the targeted tissue region (Jagger et al., 2004; Ellis et al., 2006, 2012; Ghonaim et al., 2011, 2013, 2021; Sové et al., 2021). Initially, a gas exchange chamber device was created with a 4 mm by 10 mm exchange window to alter tissue PO<sub>2</sub> in a large muscle surface area, affecting multiple microvascular networks at once by rapidly inducing flow responses (Ellis et al., 2012). This exchange window size can stimulate hundreds of capillary networks overlying it as a single microvascular unit is approximately 150 µm by 200 µm. These results represent regulatory responses at the microvascular level, but they could not be used to confirm the specific location or vessel type where O<sub>2</sub> sensing occurs (Ellis et al., 2012). Therefore, further development was essential to fabricate a gas exchange chamber device with a micrometer scale exchange window that can target specific levels of the vasculature such as an individual microvascular unit (Ghonaim et al., 2011). It is imperative to test microfluidic devices that manipulate smaller tissue regions on the scale of single microvascular units, to determine if changing [O<sub>2</sub>] in individual capillary networks is capable of provoking oxygen mediated regulatory responses.

In the pursuit of a better spatial specificity, gas-based microfluidic devices have been modelled and fabricated with micro-outlets of various sizes and shapes (Ghonaim et al., 2011, 2013, 2021; Sové et al., 2021). Such devices have been shown to significantly alter the area and volume of tissue impacted by local surface changes in gas concentrations, and the magnitude of the response to these changes in vivo (Ellis et al, 2006, 2012; Ghonaim et

al., 2011, 2013, 2021; Sové et al., 2021). Ghonaim et al. modelled the responses to  $[O_2]$  changes in different-sized glass micro-outlets over a range of  $[O_2]$  with their gas chamber setup. The three shapes and sizes of micro-outlets modelled were a square (200 X 200  $\mu\text{m}$ ), a rectangular (1000  $\mu\text{m}$  X 200  $\mu\text{m}$ ), and a circular (100  $\mu\text{m}$ ) micro-outlet (Ghonaim et al., 2011, 2013). Based on this computational model and further validation in vivo (Ghonaim et al., 2011), the 100  $\mu\text{m}$  micro-outlet was the smallest-sized outlet found to alter the  $SO_2$  in capillaries flowing directly over the micro-outlet. Although, no corresponding flow responses or supply rate changes were observed in conjunction with the  $SO_2$  changes (Ghonaim et al., 2011). The in vivo results of the capillaries overlying 100- $\mu\text{m}$  micro-outlets suggest a potential threshold for the microvasculature to sense  $O_2$  changes and respond by altering the local blood flow, which is apparently greater than stimulating 100  $\mu\text{m}$  circular area of tissue. Results for 1000 by 200  $\mu\text{m}$  rectangular micro-outlet induced  $SO_2$  changes to all exposed surface capillaries and vessels at depths up to 100  $\mu\text{m}$ s into the tissue volume, with corresponding capillary hemodynamic responses (Ghonaim et al., 2013, 2021).

Comparing the results of the two micro-outlets with support of a mathematical model, it was proposed that the signal for vasodilation is additive and depends on the number of capillaries affected (Ghonaim et al., 2013, 2021). More specifically, the model predicts that as the outlet size increases, more capillaries will be affected by  $O_2$  perturbations and that at least four vessels from a branching network need to be stimulated to elicit a regulatory flow response (Ghonaim et al., 2013). Unfortunately, limitations in their model limited the ability to verify their hypotheses for capillary level regulation (Ghonaim et al., 2011, 2013).

Furthermore, Ghonaim et al.'s model failed to consider diffusion gradients through the device's highly permeable PDMS layer that is interfaced with the muscle, which likely confounded estimates of radial oxygen distribution in the tissue surrounding the micro-outlets.

More recently, the gas-based micro-outlet device has been refined into a modular gas exchange platform with help from previous work (Sové et al., 2021; Ghonaim et al., 2011, 2013). Creating a modular device offers flexibility to change the shape and size of the exchange surface and adjust the device to work for various applications. Like previous designs, this device consists of a gas channel and gasket made from polymethylmethacrylate (PMMA), a gas-permeable PDMS membrane, and a 200 by 400  $\mu\text{m}$  glass micro-outlet (Sové et al., 2021). This micro-outlet size was designed to target single microvascular units by altering local tissue  $\text{PO}_2$  in the constrained tissue region. Sové et al.'s device contained multiple micro-outlets spaced 1 mm apart to separate the confined vascular responses associated with capillaries from distinct micro-outlets. The 1 mm micro-outlet spacing is intended to target flow responses provoked from an individual outlet, and to prevent capillaries from experiencing changes in tissue  $[\text{O}_2]$  driven from neighbouring outlets (Sové et al., 2021).

The continuation of micro-outlet device development was crucial to further understanding the mechanisms involved in oxygen-mediated blood flow regulation, which is hypothesized to be sensed at the capillary level (Collins et al., 1998; Ellsworth et al., 1995, 2004, 2009; Ghonaim et al., 2011, 2013, 2021; Sové et al., 2021). The modular device developed by Sové et al. significantly advanced the technology available for studying

capillary-level responses. Still, there were important discrepancies between in vivo measurements and predictions of the presented mathematical model (Sové et al., 2021). Their model predicted  $[O_2]$  changes in the tissue spread 117  $\mu\text{m}$  past the outlet edge, for a total area of effect of 614 by 434  $\mu\text{m}$ ; the in vivo results did not entirely agree. Measurable changes in capillary  $SO_2$  were recorded 200  $\mu\text{m}$  away from the outlet edge, approximating the total area of effect to be closer to 800 by 600  $\mu\text{m}$  (Sové et al., 2021). Consequently, the spreading effect within the PDMS layer was not previously accounted for prior to device validation experiments (Ghonaim et al., 2011, 2013, 2021; Sové et al., 2021). Oxygen has a higher diffusivity and solubility in PDMS compared to the tissue, accounting for a critical physical property to drive this spreading effect phenomenon. Therefore, positioning the PDMS layer in direct contact with the muscle surface made this device less spatially specific than previously believed (Sové et al., 2021). The results from this study emphasize a need to develop a new device with such factors in mind.

Much work has been put into developing a microfluidic device to study  $O_2$ -mediated regulation mechanisms in microcirculation. Advancements in the design of such devices continue to present themselves in the literature, and the ability of these devices to manipulate tissue microenvironments has become significantly more constrained at the micro-scale over time. Mathematical modelling has helped us understand the ability of  $O_2$  to permeate through gas-permeable layers such as PDMS and through tissues (Ghonaim et al., 2013; Sové et al., 2021). We aim to apply the findings and insights from previous studies to develop an improved device that will allow us greater spatial specificity to stimulate single capillary networks. The spatial specificity of resulting devices can be

validated by experimental studies that capture not only capillaries directly overlying a device's micro-outlets but also the oxygen saturation and hemodynamic responses from capillaries at a distance from the micro-outlets, at various distances beyond the outlet border.

## 1.8 SUMMARY

In summary, several locations and mechanisms have been suggested for O<sub>2</sub> sensing and regulation at the microvascular level. However, the scale at which these studies were completed, the experimental setup chosen, and the O<sub>2</sub> measurement techniques used varied tremendously. Therefore, the interpretability of findings related to oxygen mediated regulatory responses were potentially impacted. Still, ATP release from erythrocytes in capillaries remains the best supported concept in the literature. The experimental approaches have become highly advanced by combining IVVM, gas exchange chambers, and micro-outlet devices to manipulate and quantify capillary blood flow. This combined approach allows us to address the gap in our knowledge by directly visualizing skeletal muscle blood flow of individual capillaries as [O<sub>2</sub>] perturbations are imposed to microscale regions of tissue and gain insights into the spatial dependence of regulatory responses resulting from changes in RBC SO<sub>2</sub>. In the upcoming chapter, I will describe the fabrication and validation of a novel device that we applied to assess the minimum scale of tissue region and accompanying vessels required to stimulate an oxygen mediated blood flow response and improve our understanding to evaluate potential mechanisms associated with specific levels of the vasculature.

---

## CHAPTER 2: DEVELOPMENT OF ULTRA-THIN FILM MICRO-OUTLETS FOR SPATIALLY CONSTRAINING LOCAL O<sub>2</sub> PERTURBATIONS TO CAPILLARIES

### 2.1 INTRODUCTION

Oxygen (O<sub>2</sub>) regulation is essential for meeting the metabolic demands associated with body organs and tissues (Duling, 1970; Duling & Klitzman, 1980; Segal, 2005; Golub & Pittman, 2013). Under normal physiological conditions, energy is produced by oxidative phosphorylation in skeletal muscle to make ATP, a process that requires a constant oxygen supply. To match ever-changing local oxygen demands in tissues, the arteriolar wall will vasodilate in response to low tissue [O<sub>2</sub>] to increase flow into capillary beds or vasoconstrict in response to high tissue [O<sub>2</sub>] (Duling 1972; Pittman & Duling, 1973; Duling, 1974; Lombard & Duling, 1977; Hutchins et al., 1974; Sullivan & Johnson, 1981; Jackson, 1986, 1987; Dietrich et al., 2000; Ellis, 2005; Ngo et al., 2010).

The regulation of oxygen-mediated blood flow is highly localized and primarily driven by conditions within tissue microenvironments (Sparks, 1980; Renkin, 1985; Golub & Pittman, 2013). Regulatory mechanisms responsible for sensing flow changes to wall shear stress or vascular resistance from wall tension do not directly sense O<sub>2</sub> levels or precisely regulate O<sub>2</sub> supply (Ellis et al., 2012; Schubert & Mulvany, 1999; Pohl et al., 2000; Carlson et al., 2005). Several local mechanisms are likely responsible for the regulation, and several have been proposed (as reviewed in Jackson, 2016). However, existing evidence fails to account for the sensitivity of vascular responses across the physiological range of tissue [O<sub>2</sub>] and at different scales (Duling, 1970; Jackson & Duling,

1983; Messina et al., 1994; Pries et al., 1995; Ellsworth et al., 1995; Ellsworth, 2013; Jackson, 2016). Studies have been conducted over a very wide range of PO<sub>2</sub> conditions (10-150 mmHg) where some may not have physiological relevance at the site they are observed (e.g., 150 mmHg is not physiological in arterioles) (Coburn et al., 1979; Tateishi and Faber, 1995a, 1995b; Kerkhof et al., 1999; Jackson, 2016).

Oxygen reactivity studies have been completed on various vessels along the vascular tree using a range of experimental techniques. These varied approaches may impact the responses observed depending on the vessel of interest, as described below. Evidence exists for potential O<sub>2</sub> sensors, including the parenchymal tissue, components of the vascular wall, and the red blood cells (Duling, 1970; Pittman & Duling, 1973; Jackson & Duling, 1983; Hester, 1993; Pries et al., 1995; Pittman 1973; Ellsworth et al., 1995, 2004; Sprague, 2009; Jackson, 2016). Controversial evidence exists on their involvement in arteriolar O<sub>2</sub> regulation, but in the absence of the parenchyma in arterioles, O<sub>2</sub> responses are blunted (Jackson & Duling, 1983; Hady and Scott, 1968; Harder et al., 1996). There are ex vivo results that support vascular smooth muscle cells as the O<sub>2</sub> sensor, but when the endothelium is removed from arterioles and feed arteries, O<sub>2</sub> reactivity becomes blunted or diminished entirely (Frisbee et al., 2002; Messina et al., 1992; Tateishi & Faber, 1995a, 1995b; Kerkhof et al., 1999). Additionally, in vivo studies on hamster cheek pouches provided evidence that none of the arteriolar wall components directly sense O<sub>2</sub> changes (Jackson, 1987; Duling, 1974). However, data collected by pressure myography supports endothelial cells' participation in the O<sub>2</sub> reactivity response (Busse et al., 1983, 1984; Pohl & Busse, 1989; Jackson, 1987; Messina et al., 1992, 1994; Fredericks et al., 1994; Ward,

1999; Frisbee et al., 2001a, 2001b, 2001c, 2002). It is important to consider the differences in the vasculature used to obtain this experimental evidence. Such *ex vivo* studies focused on first-order arterioles and arteries, whereas the intravital studies used small, third-to-fifth-order arterioles. It is essential to develop appropriate experimental techniques to study microvascular blood flow regulation to confirm oxygen-associated mechanisms without interfering with higher-order vessel" responses.

Robust evidence exists in the literature to support red blood cells (RBCs) as the O<sub>2</sub> sensor (Bergfeld & Forrester, 1992; Stein & Ellsworth, 1993; Ellsworth et al., 1995, 2004, 2009; Jia et al., 1996; Stamler et al., 1997; Patel et al., 1999; Jagger et al., 2001). RBCs have the characteristics to detect O<sub>2</sub> changes and initiate regulatory mechanisms, as they are mobile carriers of O<sub>2</sub>, and they release ATP, a vasodilatory molecule capable of increasing blood flow in response to O<sub>2</sub> depletion (Delp, 1999; Olsson, 1981; Bergfeld & Forrester, 1992; Rowell, 2002; Ellsworth, 1995; Jagger, 2001; Laughlin et al., 2012; Gonzalez et al., 2012). It is proposed that RBCs regulatory actions are initiated by hemoglobin conformational changes that occur when there is a reduction in RBC SO<sub>2</sub> (Bergfeld & Forrester, 1992; Stein, 1993; Ellsworth et al., 1995; Jagger, 2001; Buehler & Alayash, 2004; Ellsworth, 2009). This allosteric alteration initiates a signal transduction pathway in RBCs, increasing ATP release and transportation through pannexin-1 channels to bind P<sub>2</sub>Y<sub>2</sub> receptors on the vascular endothelium (Sprague, 1996; McCullough et al., 1997; Collins et al., 1998; Dietrich et al., 2000). Then, an upstream conducted vasodilatory response occurs by triggering hyperpolarization via gap junctions between endothelial cells, transducing an ATP signal from capillary beds across the arteriolar tree (Jackson,

1987; Segal, 1994; Sprague et al., 1996; McCullough et al., 1997; Collins et al., 1998; Welsh & Segal, 1998; Dietrich et al., 2000).

Therefore, it is further hypothesized that  $\text{SO}_2$ -dependent ATP release from RBCs is initiated at the capillary level (Bergfeld and Forrester, 1992; Ellsworth & Stein, 1993; Ellsworth et al., 1995; McCullough et al., 1997; Stamler, 1997; Ellsworth, 2004; Gonzalez, 2012; Ellsworth, 2009; Ellis et al., 2012). Capillary beds are the most direct site for communicating tissue oxygen needs as the erythrocyte (RBC) membrane is in closest proximity to the endothelium compared to venules and arterioles (Ellis et al., 2012). This provides capillary RBCs the shortest diffusion distance and potentially a direct transfer, for ATP to diffuse and bind to  $\text{P}_2\text{Y}_2$  receptors (Ellis et al., 2012). Capillary endothelial cells are indeed electrically coupled and can communicate electrical signals to the upstream arterioles (Bagher & Segal, 2011). In support of this hypothesis, several studies have shown that conducted signalling along capillaries can occur in vivo (Lamb et al., 2021; Collins et al., 1998; Dietrich, 1989; Dietrich & Tyml, 1992; Song & Tyml, 1993).

Intravital video microscopy (IVVM), which allows for monitoring and recording of real-time blood flow hemodynamics, has been frequently used to study blood flow in relation to  $\text{O}_2$  transport and sensing in microvascular networks (Dietrich & Tyml, 1992; Duling, 1970; Potter et al., 1993; Welsh & Segal, 1998; Frisbee & Lombard, 2002; Frisbee et al., 2002). Using IVVM,  $\text{O}_2$ -mediated blood flow can be studied within an intact system with multiple levels of vasoactive control during various tissue manipulations, such as altering tissue  $[\text{O}_2]$  or locally micro-pipetting vasoactive stimuli onto an individual microvessel (Duling, 1970, 1974; Jackson and Duling 1983; Song and Tyml, 1993; Potter

et al., 1993; Welsh & Segal, 1998; Frisbee & Lombard, 2002; Riemann et al., 2010). To confirm whether O<sub>2</sub> sensing, and regulation occurs at the capillary level, related IVVM approaches were developed to gain additional insights into this vascular level (Ellis et al., 2012; Ghonaim et al., 2011, 2021; Sové et al., 2021; Russell McEvoy et al., 2022). Specifically, a gas exchange chamber setup was used to alter the PO<sub>2</sub> of an entire tissue surface, or in a microscale region of the rat extensor digitorus longus (EDL) muscle to stimulate microvascular networks and to observe their regulatory responses (Ellis et al., 2012; Ghonaim et al., 2011, 2021; Sové et al., 2021; Russell McEvoy et al., 2022).

Gas-based micro-outlet devices fabricated to visualize highly localized responses at the microvascular level have shown promising results for the proposed SO<sub>2</sub>-dependent ATP-release mechanism of O<sub>2</sub> regulation (Ellis et al., 2012; Ghonaim et al., 2011, 2013, 2021; Sové et al., 2021). Such devices aim to have the spatial specificity required to quantify individual capillary RBC hemodynamic responses to [O<sub>2</sub>] manipulations with limited interactions of nearby vasculature (Ghonaim et al., 2011, 2021; Sové et al., 2021). If the proposed mechanism is correct, this direct capillary perturbation helps assess if an ATP signal generated in individual capillary networks when O<sub>2</sub> levels are depleted and can initiate a conducted regulatory response upstream (Ghonaim et al., 2011, 2013). Micro-outlets with 100- $\mu$ m diameters have been shown to effectively alter SO<sub>2</sub> in single capillaries but not to provoke a blood flow response (Ghonaim et al., 2011). Although, larger micro-outlets that stimulated multiple capillaries obtained flow responses simultaneously with RBC SO<sub>2</sub> changes (Ghonaim et al., 2021; Sové et al., 2021). However, the mathematical models developed for these devices did not consider the diffusive spread of O<sub>2</sub> within the

device's exchange membrane, which became a novel insight in recent experimental work (Ghonaim et al., 2011, 2013, 2021; Sové et al., 2021). This limitation in the model underestimated the radial diffusion of their devices, meaning the area stimulated by  $[O_2]$  perturbations was effectively larger than expected; resulting in poorer spatial specificity than was intended (Ghonaim et al., 2011, 2021; Sové et al., 2021). Therefore, determining the location for  $O_2$  sensing using the fine spatial specificity of targeted  $O_2$  perturbations to micro-scale tissue regions remains incomplete (Ghonaim et al., 2011, 2013, 2021; Sové et al., 2016, 2021).

In this study, we aimed to develop and validate an ultra-thin film micro-outlet device with improved spatial specificity to localized oxygen perturbations to the capillary level in skeletal muscle. An improvement from previous designs, our device is designed to offer high-quality optical resolution allowing for the visualization and analysis of capillaries being manipulated. This allows for capillaries directly overlying the micro-outlet, and at a distance from the outlet edge, to be recorded with video-microscopy simultaneously (Ghonaim et al., 2011, 2013; Sové et al., 2021). We hypothesize that oxygen-mediated blood flow regulation is initiated at the capillary level through  $SO_2$ -dependent ATP release from erythrocytes. By choosing micro-outlets of different sizes coupled to a micro-fluidic gas exchange chamber to target live muscle tissue with varying  $[O_2]$  perturbations, we aim to determine the critical scale for  $O_2$  sensing and further support  $SO_2$  dependent ATP release as a major mechanism of  $O_2$ -mediated regulation.

## 2.2 METHODS

### 2.2.1 COMPUTER-AIDED DESIGN

The design of the gas exchange chamber microscope stage insert, and gasket were made using CAD software (Sové et al., 2021). Updates on the dimensions for the stage inserts used in this study were made using Tinkercad (Tinkercad.com, Accessed January 2021-September 2021). Prototypes of the micro-outlet device were created for conceptualization to model spatial setup on the muscle preparation and maximize imaging area. Using the dimensions of the gas exchange chamber window and the size of the EDL muscle, unique micro-outlet tessellations were designed specifically for each size micro-outlet device fabricated (200  $\mu\text{m}$ , 400  $\mu\text{m}$ , 600  $\mu\text{m}$ , 1000  $\mu\text{m}$ ). Micro-outlet tessellations were scaled to the exchange window dimensions, containing as many outlets as possible to maximize the number of sites for observation.

#### 2.2.2 3D PRINTING MODULAR GAS EXCHANGE CHAMBER

The gas exchange chamber (GEC) consists of a 3D printed stage insert base designed to fit the microscope, with a micro gas channel formed between a 45 x 55 mm glass coverslip, a thin 3D printed gas channel gasket, and an overlying 3D printed layer to mount the thin-film micro-outlet film coupled with an exchange membrane and connections for the gas supply. This device contains a larger 4 x 6 mm exchange window where the composite membrane micro-outlet device was positioned. The assembled device was sealed with adhesive vinyl sheets and connected by plastic tubing to a triple-inlet manifold supplied by three computer-controlled mass flow meters (SmartTrak100, Sierra Instruments, Monterey, CA, USA) for each gas channel ( $\text{CO}_2$ ,  $\text{N}_2$ ,  $\text{O}_2$ ), with a frequency response of <300 ms.

#### 2.2.3 MICRO-OUTLET DEVICE FABRICATION

### 2.2.3.1 FABRICATION OF MICRO-OUTLETS

Polyvinylidene chloride film (Saran, Dow Corning, MI, USA) was used as the gas-impermeable micro-outlet layer in a composite membrane micro-outlet device. Micro-outlet holes were laser cut into PVDC film using high-precision laser cutting (Universal Laser Systems–Model # ILS12-150D) at 100% speed and 0.1% power on a single laser using high-precision cuts and smaller cut widths. Four micro-outlet tessellations explicitly designed for each outlet diameter (section 2.2.1) were laser cut into gas impermeable PVDC film, with 1000  $\mu\text{m}$ s of solid film separating each outlet cut. Based on the 3D-printed GEC stage insert, each micro-outlet tessellation was designed to fit the 4 x 6 mm exchange window. To facilitate handling and subsequent spin coating of the PDMS membrane layer onto the PVDC film, each tessellation pattern was cut in the centre of a 25 x 75 mm laser-cut piece of PVDC film. The micro-outlets cut into the PVDC film was inspected under a stereo microscope and thoroughly cleaned using 70% isopropyl solution and distilled water. A glass microscope slide was cleaned and the 25 x 75 mm PVDC film containing the micro-outlet tessellation was carefully placed and smoothed onto the slide using 2-3 drops of distilled water and then left to dry in preparation for spin coating. The water droplets help to tightly adhere the PVDC film to the glass slide and prevent air bubbles from forming between the two layers.

### 2.2.3.2 FABRICATION OF COMPOSITE GAS EXCHANGE MEMBRANES

Gas impermeable laser-cut micro-outlet PVDC membranes were bonded to gas-permeable PDMS to create a composite device for spatially constrained gas exchange. A 10:1 (15g:1.5g) mixture of polydimethylsiloxane and curing agent (Dow Corning, Midland,

MI) was weighed and vigorously mixed for two minutes as directed by the manufacturer's instructions. The PDMS mixture was degassed in a vacuum chamber three consecutive times for 10 minutes. Once degassed, the mixture was coated on top of a glass microscope slide with a micro-outlet film and spun coat for 30 seconds at 1000 rpm. Following spin coating, the slide was transferred into a vacuum chamber for 10 minutes of degassing to ensure no bubbles were present in the PDMS covering the micro-outlet holes. The microscope slides and composite membrane were placed on a hot plate at 80 °C for 20 minutes to initiate the curing of PDMS. After heating, the slide was covered with an inverted Petri dish to prevent dust particles from adhering to the device and left for 24 hours to allow for complete curing of the PDMS. Once PDMS was cured on the PVDC film layer, the composite device was slowly peeled off the slide to ensure the delicate PDMS-filled micro-outlet holes remained intact. Once this was achieved, the composite device was placed directly over top of the 3D printed gas exchange device window to align the tessellation pattern with the 3D printed window. The extra material of the composite membrane outside of the micro-outlet tessellation was trimmed, and the membrane was secured using double-sided tape and clear adhesive vinyl to ensure the composite device was fully sealed with the GEC.

#### 2.2.4 ANIMAL PROTOCOL

##### 2.2.4.1 INSTRUMENTATION AND PHYSIOLOGICAL MONITORING

27 male 6 – 8-week-old Sprague-Dawley rats (159– 194 g) were used for device validation experiments. Rats were obtained from Charles River Laboratories and housed in Animal Care Facilities allowing them to acclimatize over a 5–7-day period before testing.

Rats were fed Teklad 2018 (Envigo, Indianapolis, IND, USA) standard rodent chow. All animal protocols were approved by Memorial University Animal Care Committee.

Animals were anesthetized using sodium pentobarbital (Euthanyl, Bimeda, Cambridge, ON, Canada) at 65 mg/kg through intraperitoneal injection. Depth of anesthesia was assessed following induction through palpebral reflex and the absence of withdrawal or reaction following firm toe pinch on the left foot. The animal was transferred to the surgical field and a rectal temperature probe was inserted to monitor body temperature. The animal's core temperature was maintained at 37°C throughout the experiment using a heating pad and/or a heat lamp as needed.

Once a surgical plane of anesthesia was established, several 0.01 ml subcutaneous injections of lidocaine (20 mg/ml) were administered along the midline of the neck between the jawline and the sternum. An incision was made between the clavicle and the jaw along the midline to allow for instrumentation as previously described (Fraser et al., 2012). Briefly, the left common carotid artery was bluntly dissected and isolated for cannulation with a 7.5 cm long, 0.58mm outside diameter polyethylene tubing mated with a 9.0 cm length of 1.19 mm outside diameter silastic tubing (Intramedic, BD, Franklin Lakes, NJ, USA). The carotid cannula was perfused with heparinized saline (1 U/ml) connected to a pressure infusion bag (C-Fusor, Smith-Medical, Minneapolis, MN, USA) and blood pressure transducer fitted with an integral momentary valve to maintain patency during the experiment. The cannula was connected to a pressure transducer (TruWave 3, Edwards Lifesciences, Irvine, CA, USA) for continuous monitoring and recording of the mean arterial blood pressure and heart rate. Blood pressure analyzer (400a, Digi-Med, Louisville,

KY, USA) data were recorded digitally using the manufacturer's software and saved to a text file. A venous catheter was fabricated using a 14 cm length of 0.119 mm internal diameter silastic tubing (Dow Corning, Midland, MI, USA). The jugular vein was bluntly dissected, isolated, and a small cut was made in the vessel to introduce the catheter. The venous cannula was connected to an infusion pump (PhD 2000, Harvard Apparatus, Holliston, MA, USA) to deliver heparinized saline (1 U/ml, 0.5 ml/kg/hour) for fluid resuscitation. Supplemental anesthetic (32.8 mg/kg) was administered periodically via a sterile T-connector hub in line with the jugular cannula as required. The depth of anesthesia was assessed frequently by checking the animal's blink response and monitoring heart rate variability and mean arterial blood pressure changes. A tracheotomy was performed for mechanical ventilation of the animal with a FiO<sub>2</sub> of 30-35 % O<sub>2</sub> balanced with N<sub>2</sub>. Ventilation rate and volume were determined based on the animal's weight per the manufacturer's instructions (Harvard Apparatus, Inspira Ventilator). Following tracheotomy, the neck incision was sutured closed using a continuous lock stitch.

#### 2.2.4.2 SURGICAL ISOLATION OF EDL MUSCLE

Following instrumentation of the animal, a small piece of skin was cut from the right lower hindlimb, and the overlying connective tissue was bluntly dissected to expose and isolate the extensor digitorum longus (EDL) muscle, as previously described (Fraser et al., 2012; Tyml & Budreau, 1991). The isolated distal tendon of the EDL was tied using silk ligature and then cut. The EDL muscle was inspected and carefully rinsed with warm saline before being reflected over the objective on the stage of an inverted microscope (Olympus IX73, Tokyo, Japan). The EDL was placed over the exchange window of the 3D-printed

stage insert. To improve optical coherence, the muscle was gently compressed using beads of vacuum grease (Dow Corning, Midland, MI, USA), a cover slip, and a microscope slide. Then, the EDL was covered with polyvinylidene chloride film for isolation from the outside environment (Saran, Dow Corning, MI, USA) and bathed in warm saline. The muscle surface overlying the microscope objective was interfaced with the GEC gas channel via the PDMS-filled micro-outlet holes within the composite device membrane.

The animal was allowed to equilibrate on the microscope stage for 30 minutes after EDL positioning and setup were complete. Following equilibration and when the animal's body temperature was between 36–37°C and mean arterial pressure (MAP) was above 80 mmHg, an arterial blood sample was collected and loaded onto a CD4+ blood gas analyzer cartridge (Abbott Point of Care Inc., Princeton, NJ, USA) and inserted into a VetScan iSTAT (Abbott Point of Care Inc., Princeton, NJ, USA). The partial pressure of oxygen (PO<sub>2</sub>) and carbon dioxide (PCO<sub>2</sub>) was maintained at physiological levels, and the ventilation rate and volume were adjusted to maintain blood gases within the normative range.

#### 2.2.5 IMPOSED OXYGEN OSCILLATIONS AND CHALLENGES

Four-minute recordings were taken in three to four different fields of view across the muscle tissue depth. Fields of view were chosen based on the placement of the micro-outlets, maximizing the number of in-focus capillaries inside and outside the micro-outlets. Oxygen oscillations were captured at the surface of the muscle from 7-12-2-7% for one minute at each oxygen concentration during four-minute recordings in each field using a gas exchange chamber (Sové et al., 2021). Similarly, oxygen challenges were imposed at

high and low oxygen levels to the surface of the muscle from 7-12% [O<sub>2</sub>] and 7-2% [O<sub>2</sub>]. High oxygen challenges consisted of three-minute recordings, with the first minute set at a baseline oxygen concentration of 7% and 2 minutes at 12%. Low oxygen challenges were three-minute recordings with the first minute at a baseline [O<sub>2</sub>] of 7% and 2 minutes at 2%. CO<sub>2</sub> was kept at 5%, with N<sub>2</sub> balancing the gas mixture. The gases were delivered to the surface of the EDL muscle via a 3D-printed gas exchange chamber, as described previously (Sové et al., 2021). Custom MATLAB software was used to dynamically control changes in gas concentrations from digital mass flow meters, providing precise timing of all changes in [O<sub>2</sub>] within the GEC.

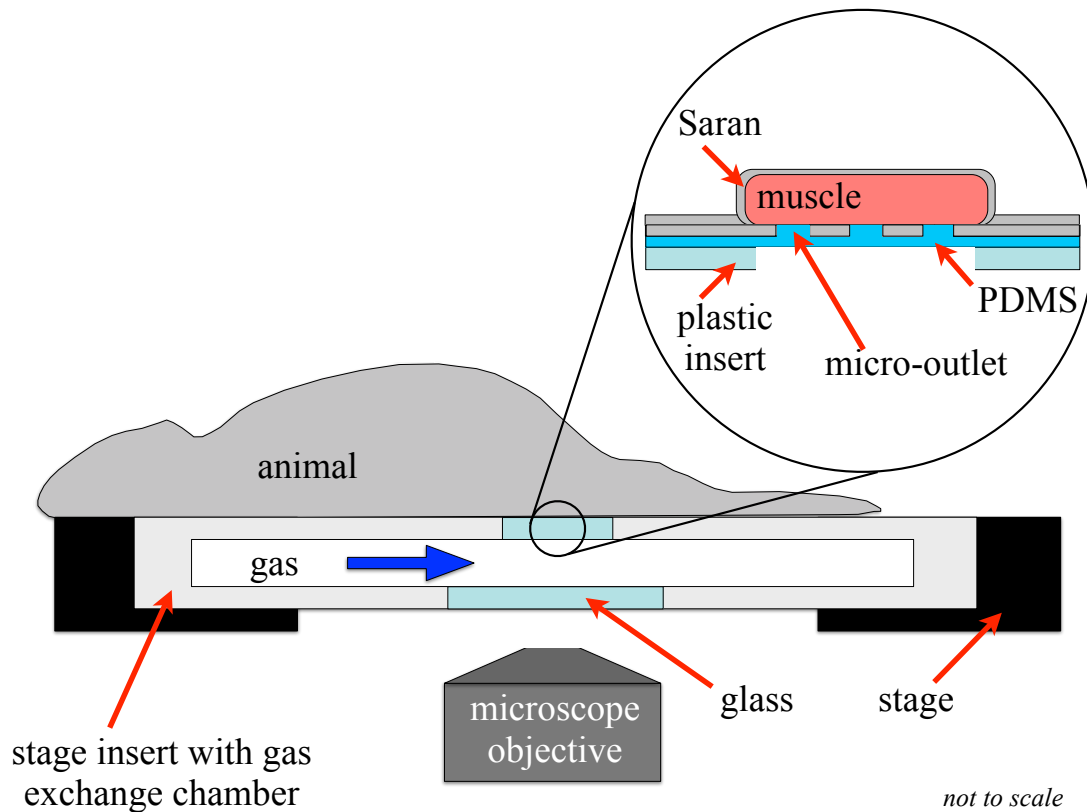


**Figure 2.1 Experimental setup of the animal placed on top of the micro-outlet and gas exchange chamber inserted into the microscope stage.** The chamber is fabricated to fit in the inverted microscope stage, with the muscle aligned directly over the ultra-thin film micro-outlet device consisting of a gas-impermeable film on top of a gas-permeable PDMS membrane and covered with a small piece of gas-impermeable polyvinylidene film (Saran, Dow Corning, Midland, MI, USA), ensuring the muscle is only affected by gases flowing through the chamber (Adapted from Sové et al., 2021, used under Creative Commons License).

## 2.2.6 OFFLINE ANALYSIS USING CUSTOM MATLAB SOFTWARE

Recorded digital video sequences were processed using a graphical user interface (GUI) driven custom program written in MATLAB (Mathworks, Natick, Mass, MA, USA). This processing software creates functional images for vessel selection and generates MP4 videos that help select in-focus vessels for analysis in the custom MATLAB software (Fraser et al., 2012; Ellis et al., 1990, 1992, 2012; Japee et al., 2004). The analysis GUI measures capillary RBC hemodynamics and capillary RBC oxygen saturation (Fraser et al., 2012; Ellis et al., 1990, 1992, 2012; Japee et al., 2004). These values are quality controlled to exclude spurious values resulting from poor vessel delineation or out-of-focus segments.

## 2.2.7 HEMODYNAMIC AND OXYGEN SATURATION MEASUREMENTS

Capillary RBC hemodynamic (velocity, supply rate, and hematocrit) and oxygen saturation ( $SO_2$ ) measurements were collected for paired capillaries during oxygen oscillations and challenges. For measurements obtained during 4-minute  $[O_2]$  oscillations, the average was taken of the first minute at 7%  $[O_2]$  and of the last 15 seconds for each one-minute oscillation following 12%, 2%, and 7%  $[O_2]$ . The data was sorted into two groups, including capillaries selected overlying the micro-outlets and capillaries selected outside the micro-outlets, to determine the efficacy of our device. Using ImageJ software and functional images, the area of effect was quantified by measuring the distance of each capillary outside the micro-outlet from the outlet edge (<https://imagej.net/ij/index.html>). Each analyzed capillary was outlined with its centre point marked on the functional image to facilitate measurement of these distances. The data were binned into three sub-categories

that assigned selected capillaries into the following distance ranges from the micro-outlet: 0-100  $\mu\text{m}$ , 100-200  $\mu\text{m}$ , and greater than 200  $\mu\text{m}$ s away from the micro-outlet edge.

Capillary RBC hemodynamic and  $\text{SO}_2$  measurements from  $\text{O}_2$  oscillation and  $\text{O}_2$  challenge experiments were sorted into groups of paired measurements. Statistical comparisons were made for each imposed oxygen concentration ( $[\text{O}_2]$ ). For  $\text{O}_2$  oscillations, normally distributed capillary data were paired with  $\text{O}_2$  perturbations, and repeated measures one-way analysis of variance (ANOVA) with Holm-Šídák's multiple comparisons test was used to identify significant differences. Non-normally distributed data were grouped by  $\text{O}_2$  perturbations, and Friedman tests with Dunn's multiple comparison post-test were used to identify significant differences. For  $\text{O}_2$  challenges, normally distributed capillary data were paired with  $\text{O}_2$  perturbations, and a paired t-test was used to identify significant differences. Non-normally distributed data were grouped by  $\text{O}_2$  perturbations, and a Wilcoxon test was used to identify significant differences. A  $p$  value of  $< 0.05$  was considered significant across all comparisons. All tests were completed using Prism 9 (GraphPad Prism Software, LLC, 9.2.0 (283)). Means and standard deviations are reported in the results section unless otherwise noted.

## 2.3 RESULTS

### 2.3.1 SYSTEMIC PHYSIOLOGICAL MEASUREMENTS

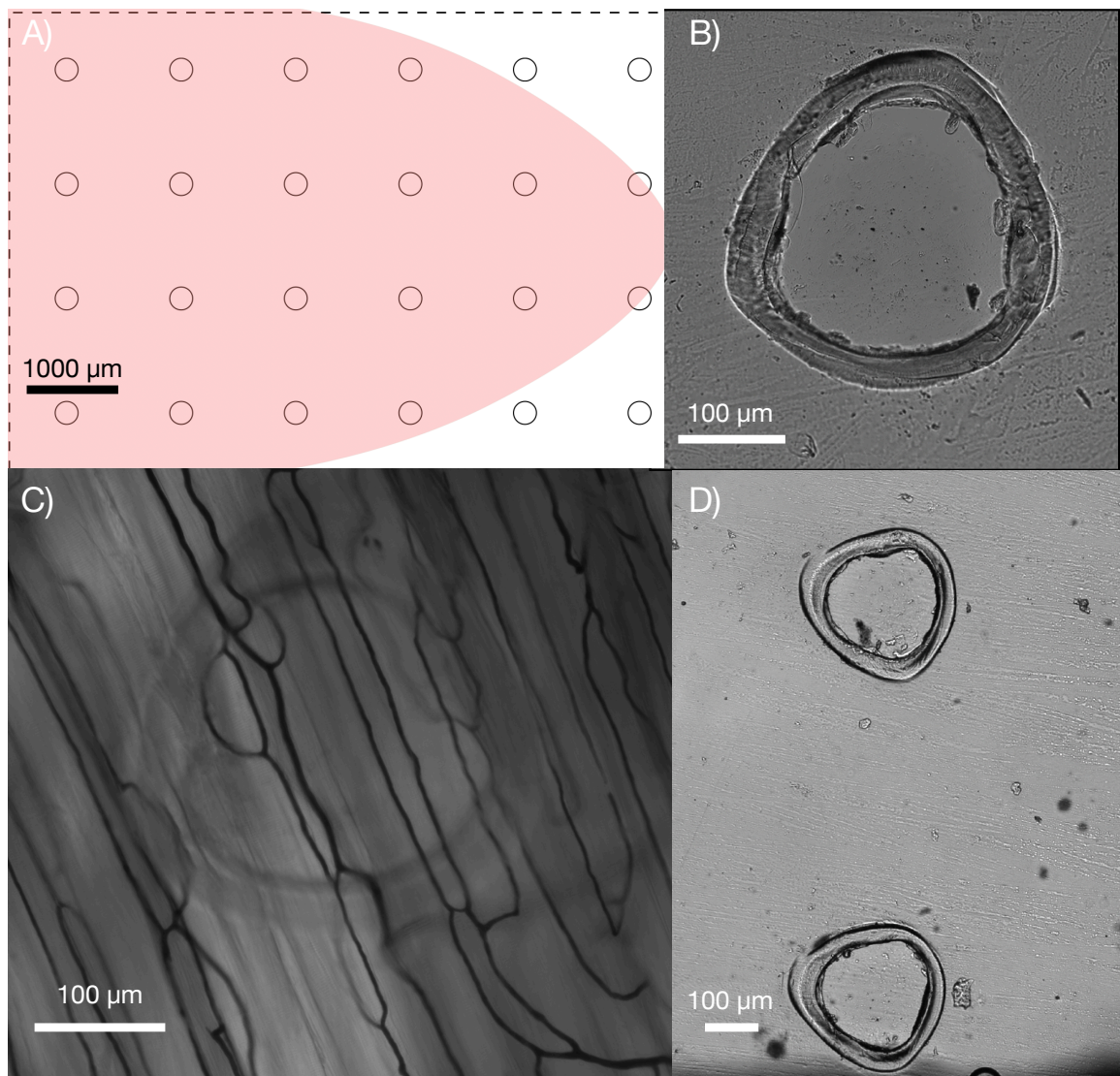
Systemic physiological measurements were taken for each animal and separated into groups based on various micro-outlet diameter sizes shown in table 2.1. Blood gas samples were collected for each animal and are displayed in table 2.2 in groups based on corresponding micro-outlet diameter sizes.

TABLE 2.1 MEAN AND STANDARD DEVIATION OF SYSTEMIC ANIMAL DATA FOR EACH EXPERIMENTAL GROUP BASED ON MICRO-OUTLET DIAMETER SIZE.

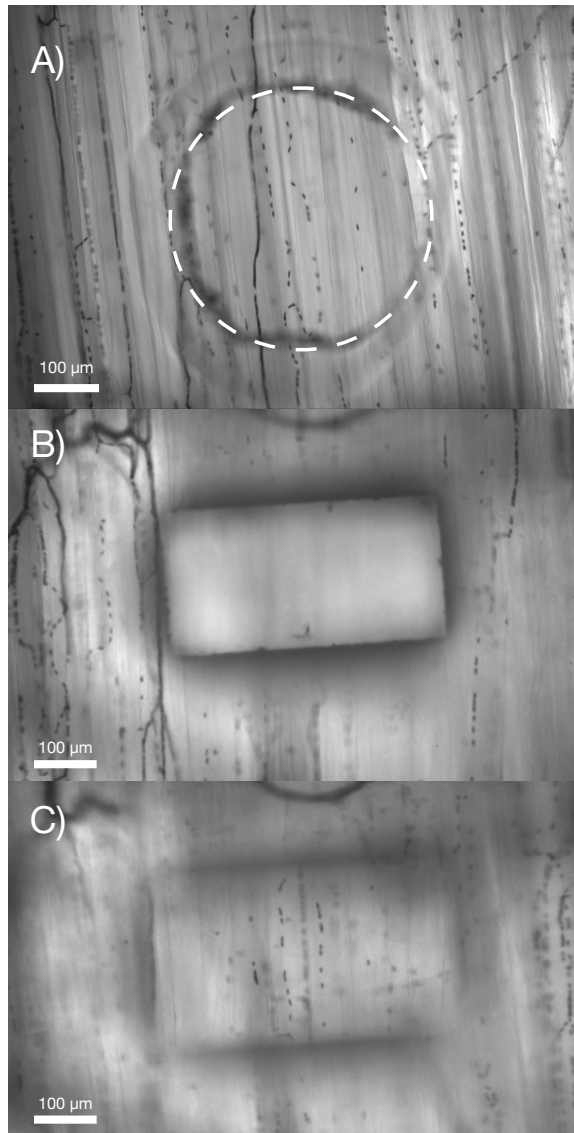
	<b>200 <math>\mu\text{m}</math></b> <b>(N= 6)</b>	<b>400 <math>\mu\text{m}</math></b> <b>(N = 6)</b>	<b>600 <math>\mu\text{m}</math></b> <b>(N = 11)</b>	<b>1000 <math>\mu\text{m}</math></b> <b>(N = 7)</b>
<b>Animal Weight (g)</b>	179.5 $\pm$ 10.7	178.5 $\pm$ 7.7	176.7 $\pm$ 7.3	187.1 $\pm$ 4.3
<b>Mean arterial pressure (mmHg)</b>	94.55 $\pm$ 6.00	94.21 +/- 8.79	94.54 $\pm$ 5.39	96.93 $\pm$ 5.47
<b>Systolic blood pressure (mmHg)</b>	99.03 $\pm$ 6.66	99.10 $\pm$ 9.04	103.04 $\pm$ 7.77	111.10 $\pm$ 5.55
<b>Diastolic blood pressure (mmHg)</b>	87.89 $\pm$ 5.42	87.17 $\pm$ 8.88	83.98 $\pm$ 6.77	81.95 $\pm$ 5.39
<b>Heart rate (beats/min)</b>	411.89 $\pm$ 21.19	402.98 $\pm$ 24.79	394.63 $\pm$ 20.65	399.21 $\pm$ 16.78.
<b>Respiratory Rate (breaths/min)</b>	83.50 $\pm$ 1.38	83.33 $\pm$ 1.21	83.81 $\pm$ 0.87	82.43 $\pm$ 0.53
<b>Respiratory volume (cc)</b>	1.18 $\pm$ 0.066	1.18 $\pm$ 0.05	1.17 $\pm$ 0.058	1.24 $\pm$ 0.028

TABLE 2.2 MEAN AND STANDARD DEVIATION OF ANIMAL BLOOD GAS DATA FOR EACH EXPERIMENTAL GROUP BASED ON MICRO-OUTLET DIAMETER SIZE USED.

	<b>200 <math>\mu\text{m}</math></b> <b>(N = 6)</b>	<b>400 <math>\mu\text{m}</math></b> <b>(N = 6)</b>	<b>600 <math>\mu\text{m}</math></b> <b>(N = 11)</b>	<b>1000 <math>\mu\text{m}</math></b> <b>(N = 7)</b>
<b>pH</b>	7.40 $\pm$ 0.030	7.42 $\pm$ 0.017	7.43 $\pm$ 0.049	7.42 $\pm$ 0.041
<b>PCO<sub>2</sub> (mmHg)</b>	49.97 $\pm$ 3.78	45.82 $\pm$ 3.51	46.35 $\pm$ 6.60	48.28 $\pm$ 5.80
<b>PO<sub>2</sub> (mmHg)</b>	113.8 $\pm$ 15.43	102.5 $\pm$ 9.20	114 $\pm$ 17.73	120.14 $\pm$ 10.25
<b>BE<sub>ecf</sub> (mmol/L)</b>	6.3 $\pm$ 1.21	5.5 $\pm$ 1.87	5.8 $\pm$ 2.32	6.86 $\pm$ 2.19
<b>HCO<sub>3</sub> (mmol/L)</b>	29.35 $\pm$ 4.41	29.82 $\pm$ 1.81	30.13 $\pm$ 2.06	31.34 $\pm$ 2.35
<b>SO<sub>2</sub> (%)</b>	98.00 $\pm$ 0.89	97.83 $\pm$ 0.75	98.18 $\pm$ 1.25	98.71 $\pm$ 0.49
<b>Lac (mmol/L)</b>	0.87 $\pm$ 0.40	0.87 $\pm$ 0.21	1.01 $\pm$ 0.68	1.01 $\pm$ 0.43



**Figure 2.2 200- $\mu\text{m}$  micro-outlet device in various forms to be coupled with IVVM.** A) Schematic of the 200- $\mu\text{m}$  laser cut micro-outlet tessellation into PVDC film overlying a 4 by 6 mm exchange window and the approximate EDL muscle position shown in pink. B) Image of a single 200- $\mu\text{m}$  micro-outlet under a 10X objective. C) Image of a 200- $\mu\text{m}$  micro-outlet with capillaries overlying in vivo. D) Image of two 200- $\mu\text{m}$  micro-outlets under a 4X magnification.

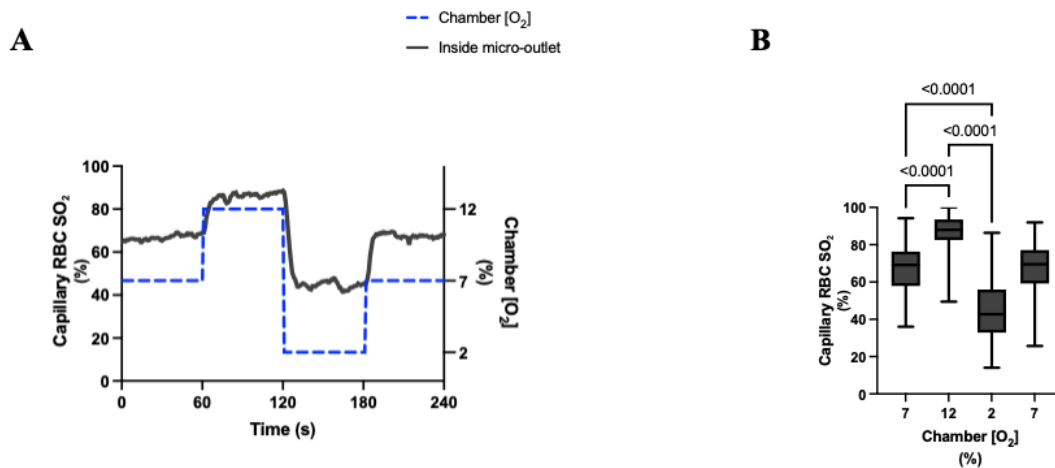


**Figure 2.3 Comparison of the optical properties obtained in our micro-outlet device with a previous device used in vivo.** A) Image of our enhanced optical resolution of the 400- $\mu\text{m}$  micro-outlet in vivo. B-C) Images of a previous micro-outlet device lacking the ability to visualize in focus vessels overlying and remote of the outlet simultaneously (Ellis et al., 2016).

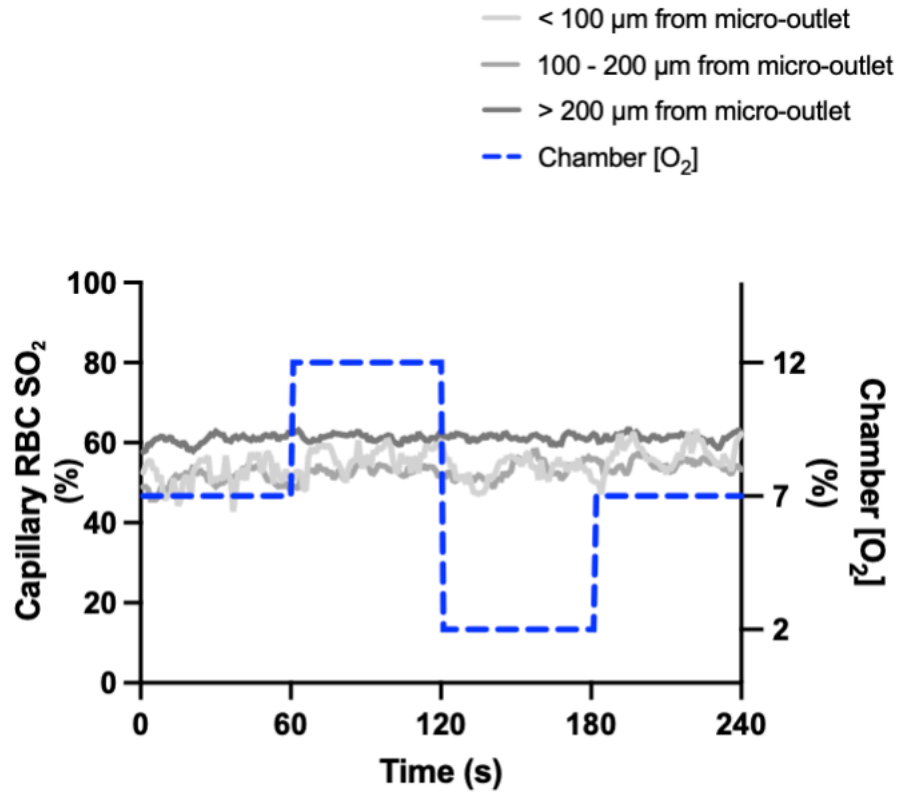
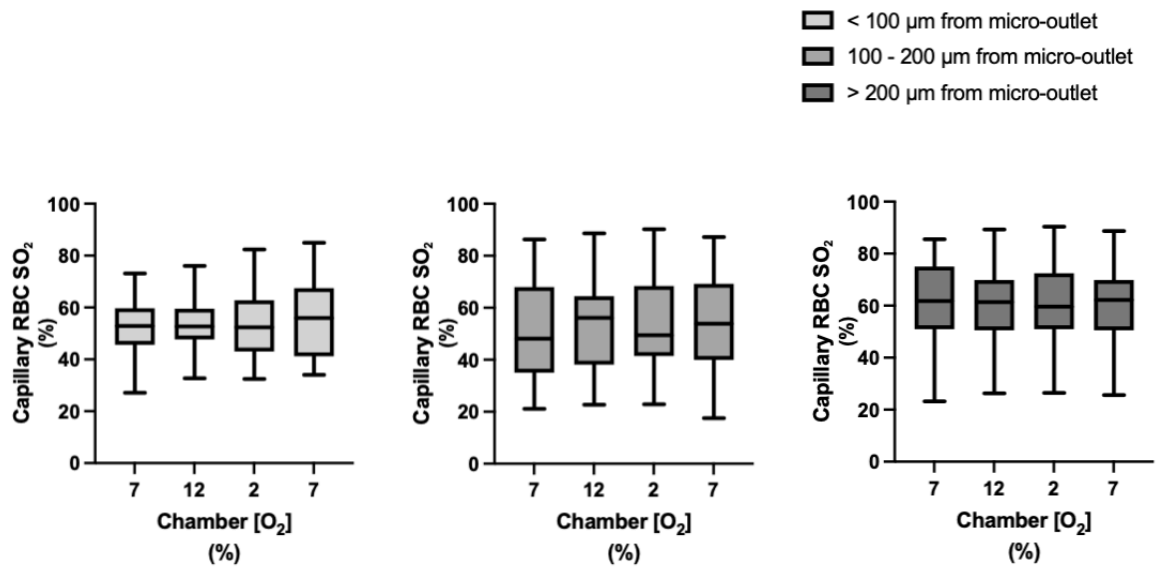
### 2.3.2 RESULTS: 400 $\mu\text{M}$ MICRO-OUTLET OXYGEN OSCILLATION DATA

Oxygen ( $\text{O}_2$ ) oscillation data utilizing 400- $\mu\text{m}$  micro-outlets for oxygen saturation ( $\text{SO}_2$ ) measurements comprised 213 capillaries across 6 animals. A total of 96 capillaries were analyzed directly overlying the window, and 117 were analyzed outside the outlet edge. Concerning capillaries measured outside the outlet edge, 10 were measured less than 100  $\mu\text{m}$ s away, 36 were between 100 – 200  $\mu\text{m}$ s away, and 71 were greater than 200  $\mu\text{m}$ s away (Figure 2.5).

$\text{O}_2$  oscillations imposed on capillaries directly overlying 400  $\mu\text{m}$  micro-outlets caused significant changes in capillary  $\text{SO}_2$  at 12% GEC [ $\text{O}_2$ ],  $86.91 \pm 9.79\%$ , and 2% GEC [ $\text{O}_2$ ],  $43.53 \pm 15.18\%$ , compared to baseline 7% GEC [ $\text{O}_2$ ],  $66.74 \pm 13.72\%$  ( $p < 0.0001$ ) (Figure 2.4).  $\text{O}_2$  oscillations imposed on capillaries directly overlying 400  $\mu\text{m}$  micro-outlets caused significant changes in capillary  $\text{SO}_2$  at 12% GEC [ $\text{O}_2$ ],  $86.91 \pm 9.786\%$ , compared to 2% GEC [ $\text{O}_2$ ],  $43.53 \pm 15.18\%$  ( $p < 0.0001$ ) (Figure 2.4).  $\text{O}_2$  oscillations imposed caused no significant changes in  $\text{SO}_2$  in capillaries outside the micro-outlet edge (Figure 2.5).



**Figure 2.4 Capillary RBC oxygen saturation in response to oxygen oscillations for capillaries directly overlying the 400  $\mu\text{m}$  micro-outlet.** A) Time series plot showing the mean capillary RBC oxygen saturation ( $\text{SO}_2$ ) in capillaries overlying the 400  $\mu\text{m}$  micro-outlet edge across the 4-minute  $\text{O}_2$  oscillation (7-12-2-7%). B) The micro-outlet gas exchange device imposes 4-minute oxygen oscillations for one minute at a baseline concentration of 7%, 12%, 2%, and 7%, respectively. Mean values are taken from the first entire minute at baseline and the last 15 seconds at 12%, 2%, and 7% ( $n = 96$  capillaries).  $p$  values are based on Tukey's multiple comparisons test after significant repeated measures ANOVA and are indicated in the figure with a  $p < 0.05$  considered to be significant. Box and whisker plots show minimum, median, maximum, and associated quartiles.

**A****B**

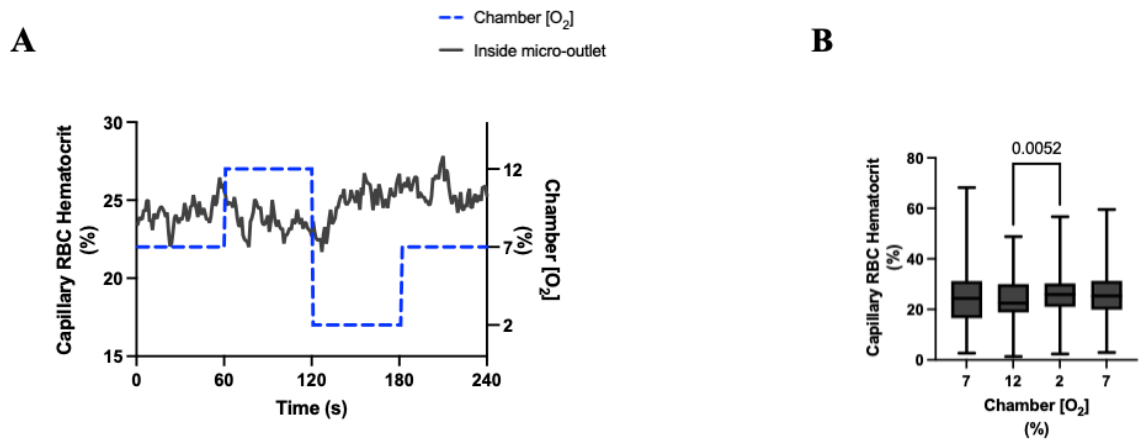
**Figure 2.5 Capillary RBC oxygen saturation responses in capillaries at various distances outside the 400  $\mu\text{m}$  micro-outlet edge.** A) Time series plot showing the mean capillary RBC oxygen saturation ( $\text{SO}_2$ ) in capillaries outside the 400  $\mu\text{m}$  micro-outlet edge across the 4-minute  $\text{O}_2$  oscillation (7-12-2-7%). B) The micro-outlet gas exchange device imposes 4-minute oxygen oscillations across 7 animals for one minute at a baseline concentration of 7%, one minute at 12%, one minute at 2%, and one minute at 7%. Panel B shows capillaries within 100  $\mu\text{m}$  from the micro-outlet edge ( $n = 10$  capillaries), capillaries between 100 – 200  $\mu\text{m}$  from the outlet edge ( $n = 36$  capillaries), and capillaries greater than 200  $\mu\text{m}$  from the outlet edge ( $n = 71$  capillaries) respectively.  $p$  values based on Tukey's multiple comparisons test after significant repeated measures ANOVA are indicated in the figure with a  $p < 0.05$  considered to be significant. Box and whisker plots show minimum, median, maximum, and associated quartiles.

Oxygen (O<sub>2</sub>) oscillation data for experiments using 400- $\mu$ m micro-outlets for hemodynamic measurements consisted of a total of 204 capillaries across 6 animals. A total of 88 capillaries were analyzed directly overlying the window, and 116 were analyzed outside the outlet edge. Concerning capillaries measured outside the outlet edge, 8 were measured less than 100  $\mu$ m away, 35 were between 100 – 200  $\mu$ m, and 73 were greater than 200  $\mu$ m away.

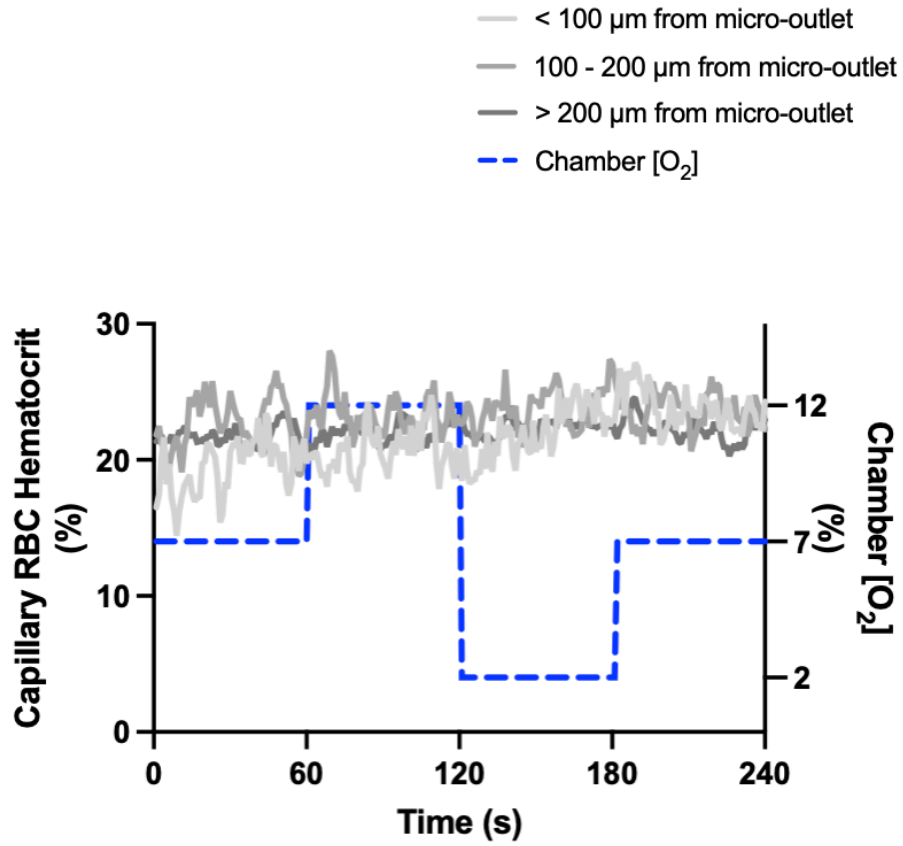
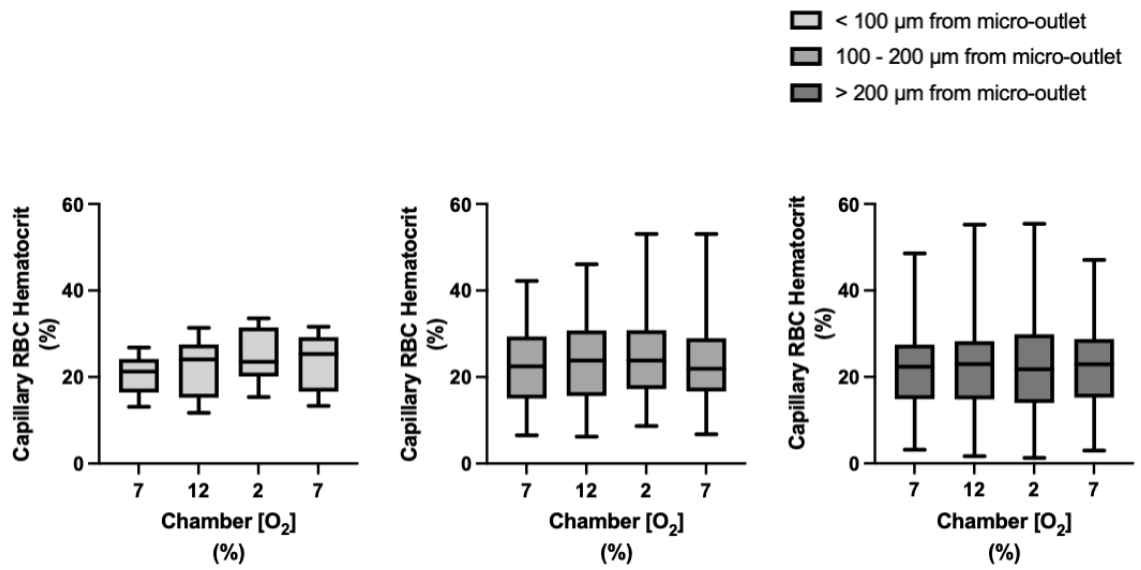
O<sub>2</sub> oscillations imposed on capillaries directly overlying 400  $\mu$ m micro-outlets caused significant changes in capillary hematocrit in capillaries overlying the outlet at 12% GEC [O<sub>2</sub>],  $23.50 \pm 10.12\%$  compared to 2% GEC [O<sub>2</sub>],  $25.39 \pm 9.70\%$ , but not in capillaries outside the outlet ( $p = 0.0052$ ) (Figure 2.6-2.7). O<sub>2</sub> oscillations imposed on capillaries directly overlying 400  $\mu$ m micro-outlets caused significant changes in capillary velocity at 2% GEC [O<sub>2</sub>],  $211.5 \pm 130.2 \mu\text{m/s}$ , compared to baseline 7% GEC [O<sub>2</sub>],  $187.4 \pm 134.2 \mu\text{m/s}$  and at 12% GEC [O<sub>2</sub>],  $185.1 \pm 122.1 \mu\text{m/s}$  compared to 2% GEC [O<sub>2</sub>],  $211.5 \pm 130.2 \mu\text{m/s}$  ( $p < 0.0001$ ) (Figure 2.8). O<sub>2</sub> oscillations imposed on capillaries directly overlying 400  $\mu$ m micro-outlets did not cause significant changes in capillary velocity in vessels outside the micro-outlet (Figure 2.9).

O<sub>2</sub> oscillations imposed on capillaries directly overlying 400  $\mu$ m micro-outlets caused significant changes in capillary supply rate at 2% GEC [O<sub>2</sub>],  $13.82 \pm 9.66 \text{ cells/s}$ , and 7% GEC [O<sub>2</sub>],  $12.75 \pm 9.33 \text{ cells/s}$  compared to baseline 7% GEC [O<sub>2</sub>]  $11.01 \pm 7.74 \text{ cells/s}$  and at 12% GEC [O<sub>2</sub>],  $10.82 \pm 7.95 \text{ cells/s}$ , compared to 2% GEC [O<sub>2</sub>],  $13.82 \pm 9.66 \text{ cells/s}$  ( $p < 0.0210$ ) (Figure 2.10). O<sub>2</sub> oscillations imposed on capillaries directly overlying

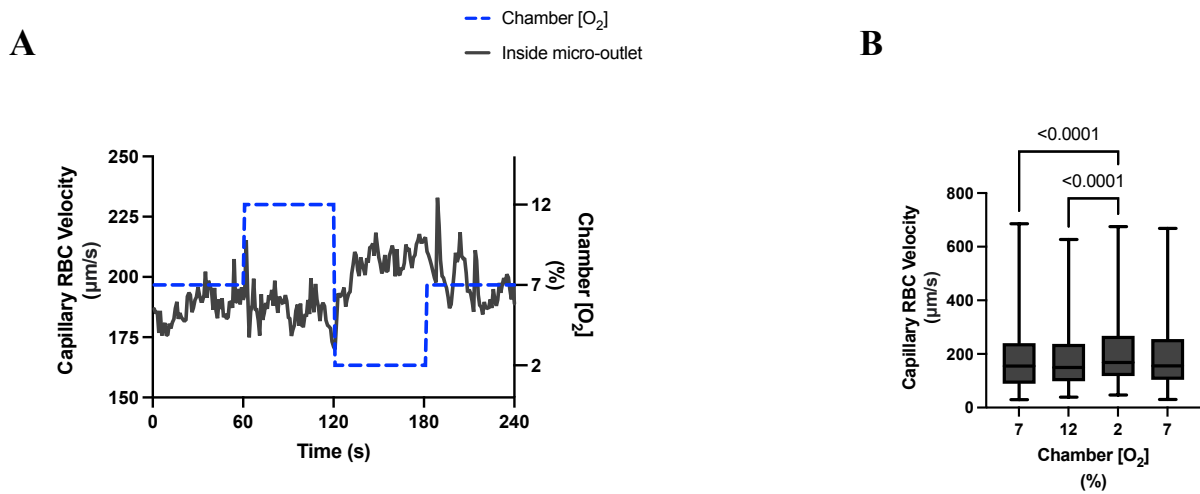
400  $\mu\text{m}$  micro-outlets did not cause significant changes in capillary supply rate in vessels outside the micro-outlet (Figure 2.11).



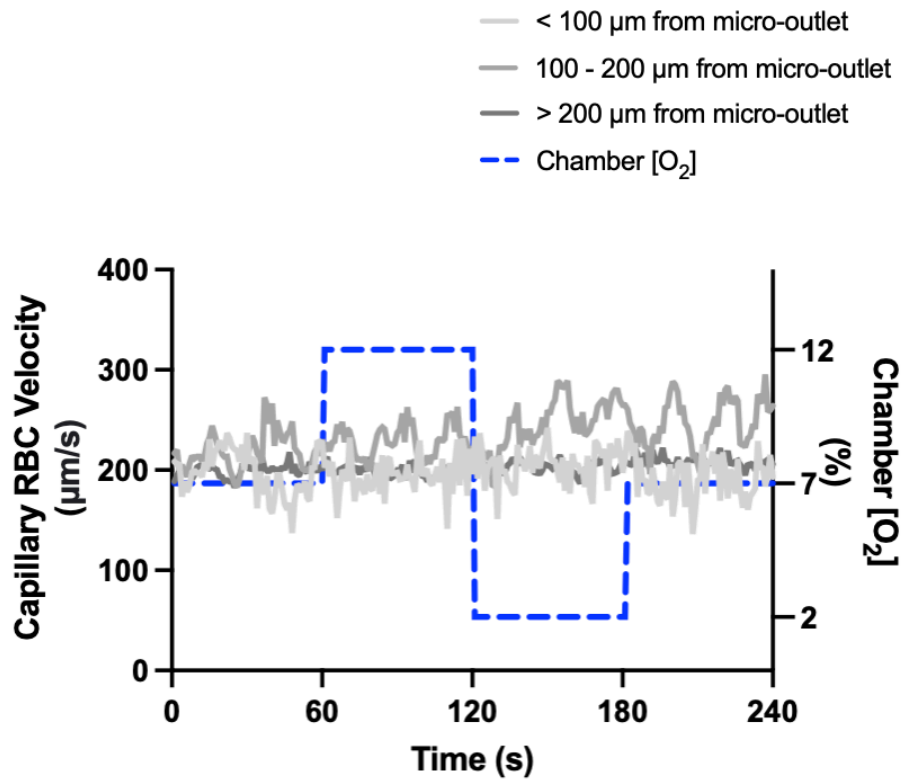
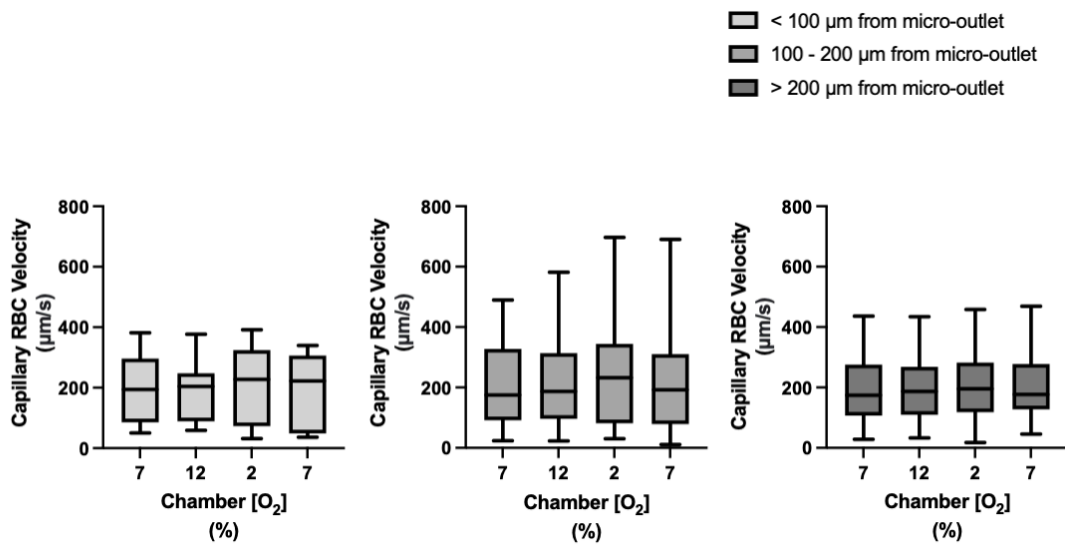
**Figure 2.6 Capillary hematocrit levels in response to oxygen oscillations for capillaries directly overlying the 400  $\mu\text{m}$  micro-outlet.** A) Time series plot showing the mean capillary hematocrit in capillaries overlying the 400  $\mu\text{m}$  micro-outlet across the 4-minute  $\text{O}_2$  oscillation (7-12-2-7%). B) The micro-outlet gas exchange device imposes 4-minute oxygen oscillations for one minute at a baseline concentration of 7%, one minute at 12%, one minute at 2%, and one minute at 7%. Mean hematocrit values are taken from the entire first minute at baseline and the last 15 seconds at 12%, 2%, and 7% ( $n = 88$  capillaries).  $p$  values based on Dunn's multiple comparisons test after significant Friedman test are indicated in the figure with a  $p < 0.05$  considered to be significant. Box and whisker plots show minimum, median, maximum, and associated quartiles.

**A****B**

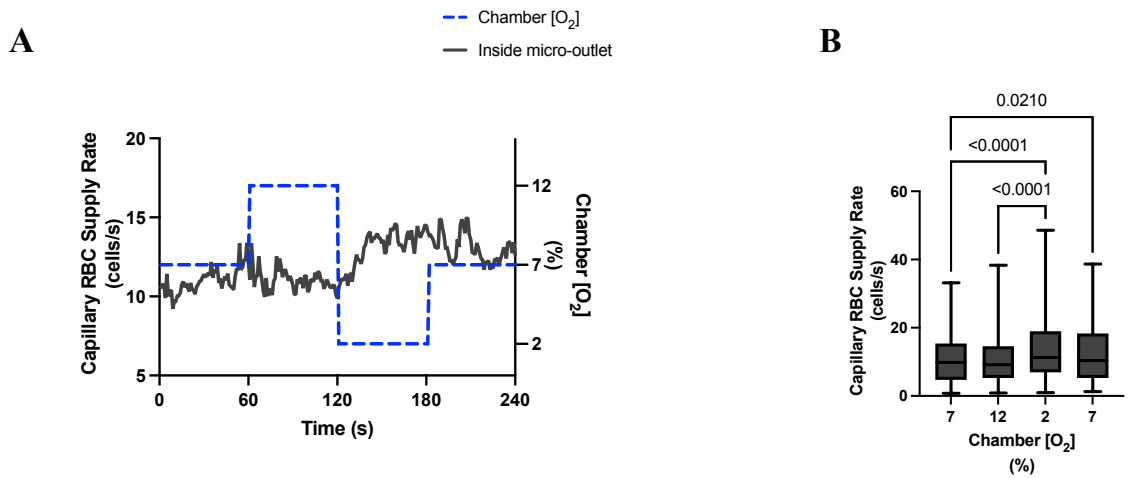
**Figure 2.7 Capillary hematocrit values in capillaries at various distances outside the 400  $\mu\text{m}$  micro-outlet edge.** A) Time series plot showing the mean capillary oxygen saturation in capillaries outside the 400  $\mu\text{m}$  micro-outlet edge across the 4-minute  $\text{O}_2$  oscillation (7-12-2-7%). B) The micro-outlet gas exchange device imposes 4-minute oxygen oscillations for one minute at a baseline concentration of 7%, one minute at 12%, one minute at 2%, and one minute at 7%. Mean hematocrit values were calculated for the first minute at baseline 7% and the last 15 seconds at 12%, 2%, and 7% ( $n = 116$  capillaries). Panel B shows capillaries within 100  $\mu\text{m}$  from the micro-outlet edge ( $n = 8$  capillaries), capillaries between 100 – 200  $\mu\text{m}$  from the outlet edge ( $n = 35$  capillaries), and capillaries greater than 200  $\mu\text{m}$  from the outlet edge ( $n = 73$  capillaries) respectively.  $p$  values based on Dunn's multiple comparisons test after significant Friedman test are indicated in the figure with a  $p < 0.05$  considered to be significant. Box and whisker plots show minimum, median, maximum, and associated quartiles.



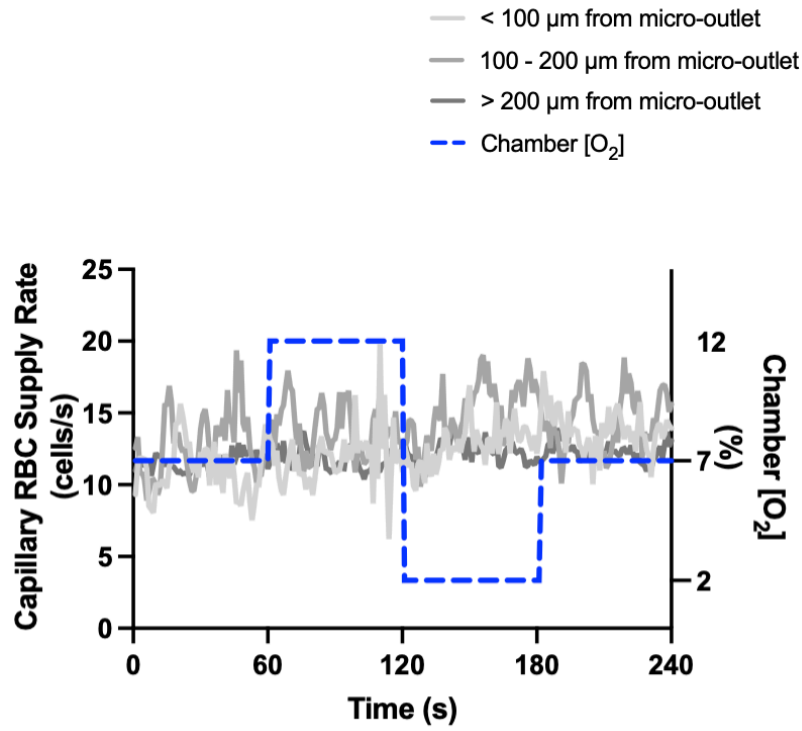
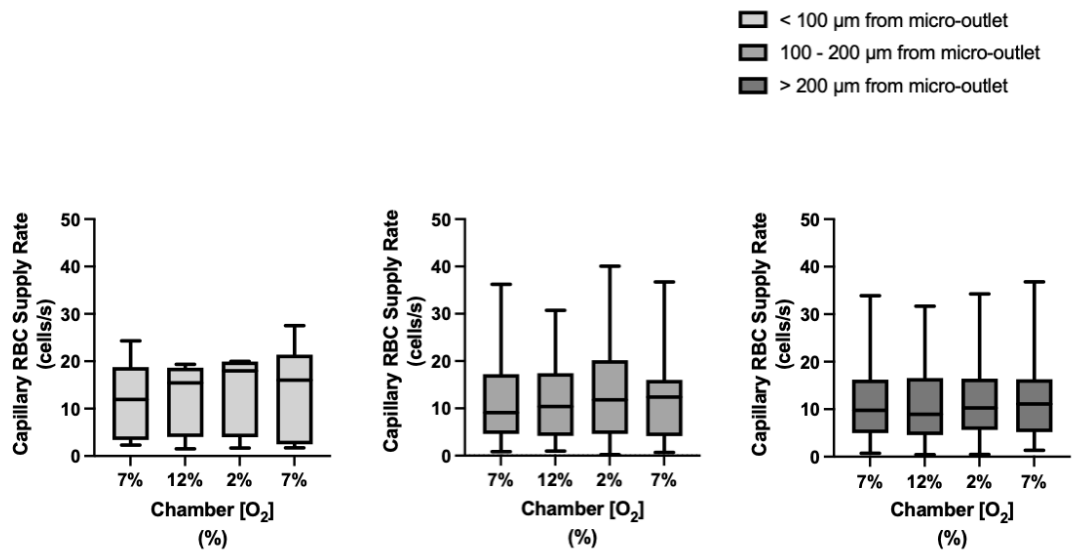
**Figure 2.8 Capillary RBC velocity for capillaries overlying the 400  $\mu\text{m}$  micro-outlet following 4-minute oxygen oscillations.** A) Time series plot showing the mean RBC velocity for capillaries overlying the 400  $\mu\text{m}$  micro-outlet across the 4-minute  $\text{O}_2$  oscillation (7-12-2-7%). B) Oxygen oscillations consisted of one minute at a baseline oxygen concentration of 7% and one minute at 12%, 2%, and 7% oxygen concentration. The mean was calculated for the first minute at a baseline 7% and the last 15 seconds of each of the following oxygen concentrations at 12%, 2%, and 7% ( $n = 88$  capillaries).  $p$  values based on Dunn's multiple comparisons test after significant Friedman test are indicated in the figure with a  $p < 0.05$  considered to be significant. Box and whisker plots show minimum, median, maximum, and associated quartiles.

**A****B**

**Figure 2.9 Capillary RBC velocity for capillaries outside the 400  $\mu\text{m}$  micro-outlet at varying distances from the outlet edge following 4-minute oxygen oscillations.** A) Time series plot showing the mean RBC velocity for capillaries outside the 400  $\mu\text{m}$  micro-outlet at varying distances across the 4-minute  $\text{O}_2$  oscillation (7-12-2-7%). B) Oscillations consisted of one minute at a baseline oxygen concentration of 7%, followed by one minute at 12%, 2%, and 7% oxygen concentration. The average was taken from the entire first minute at 7% and the last 15 seconds of the following oxygen concentrations of 12%, 2%, and 7%. Panel A shows capillaries within 100  $\mu\text{m}$  from the micro-outlet edge ( $n = 8$  capillaries), panel B shows capillaries between 100 – 200  $\mu\text{m}$  from the outlet edge ( $n = 35$  capillaries), and panel C shows capillaries greater than 200  $\mu\text{m}$  from the outlet edge ( $n = 73$  capillaries).  $p$  values based on Dunn's multiple comparisons test after significant Friedman test are indicated in the figure with a  $p < 0.05$  considered to be significant. Box and whisker plots show minimum, median, maximum, and associated quartiles.



**Figure 2.10** Capillary RBC supply rate for capillaries overlying the 400  $\mu\text{m}$  micro-outlet following 4-minute oxygen oscillations. A) Time series plot showing mean RBC supply rate for capillaries overlying the 400  $\mu\text{m}$  micro-outlet across the 4-minute  $\text{O}_2$  oscillation (7-12-2-7%). B) Oxygen oscillations consisted of one minute at a baseline oxygen concentration of 7% and one minute at 12%, 2%, and 7% oxygen concentration. The mean was calculated for the first minute at a baseline 7% and the last 15 seconds of each of the following oxygen concentrations at 12%, 2%, and 7% ( $n = 88$  capillaries).  $p$  values based on Dunn's multiple comparisons test after the significant Friedman test are indicated in the figure with a  $p < 0.05$  considered to be significant. Box and whisker plots show minimum, median, maximum, and associated quartiles.

**A****B**

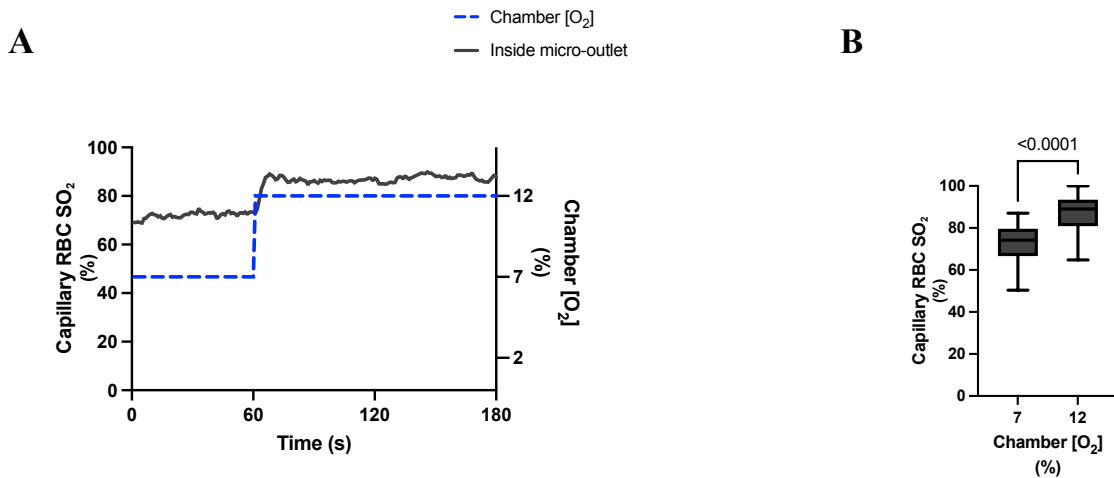
**Figure 2.11 Capillary RBC supply rate for capillaries outside the 400  $\mu\text{m}$  micro-outlet at varying distances from the outlet edge following 4-minute oxygen oscillations. A)**

Time series plot showing mean capillary RBC supply rate for capillaries outside the 400  $\mu\text{m}$  micro-outlet at varying distances across the 4-minute  $\text{O}_2$  oscillation (7-12-2-7%). B) Oscillations consisted of one minute at a baseline oxygen concentration of 7% followed by one minute at 12%, 2%, and 7% oxygen concentration. The means were calculated for the first minute at 7% and the last 15 seconds of the following oxygen concentrations of 12%, 2%, and 7%. Panel B shows capillaries within 100  $\mu\text{m}$  from the micro-outlet edge ( $n = 8$  capillaries), capillaries between 100 – 200  $\mu\text{m}$  from the outlet edge ( $n = 35$  capillaries), and capillaries greater than 200  $\mu\text{m}$  from the outlet edge respectively ( $n = 73$  capillaries).  $p$  values based on Dunn's multiple comparisons test after significant Friedman test are indicated in the figure with a  $p < 0.05$  considered to be significant. Box and whisker plots show minimum, median, maximum, and associated quartiles.

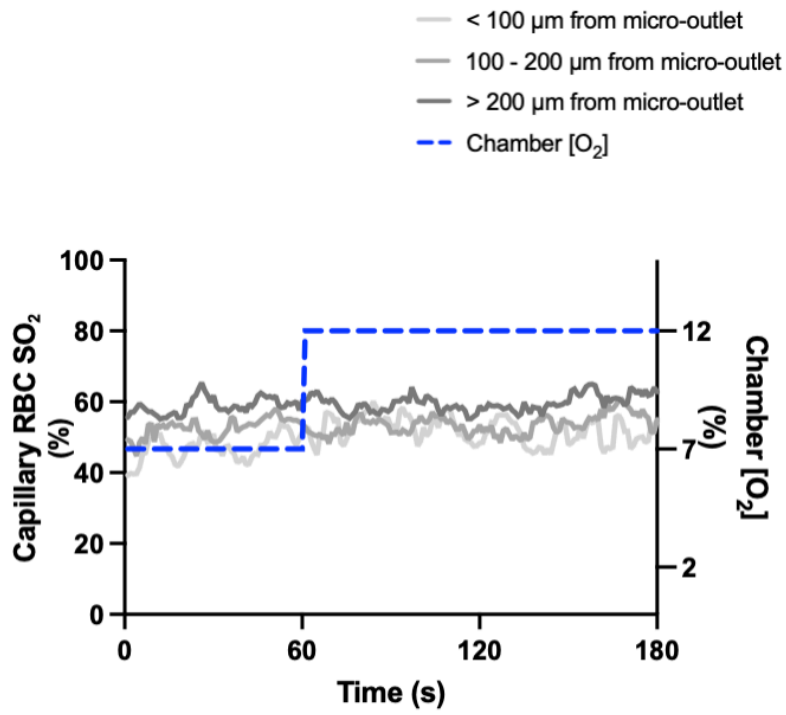
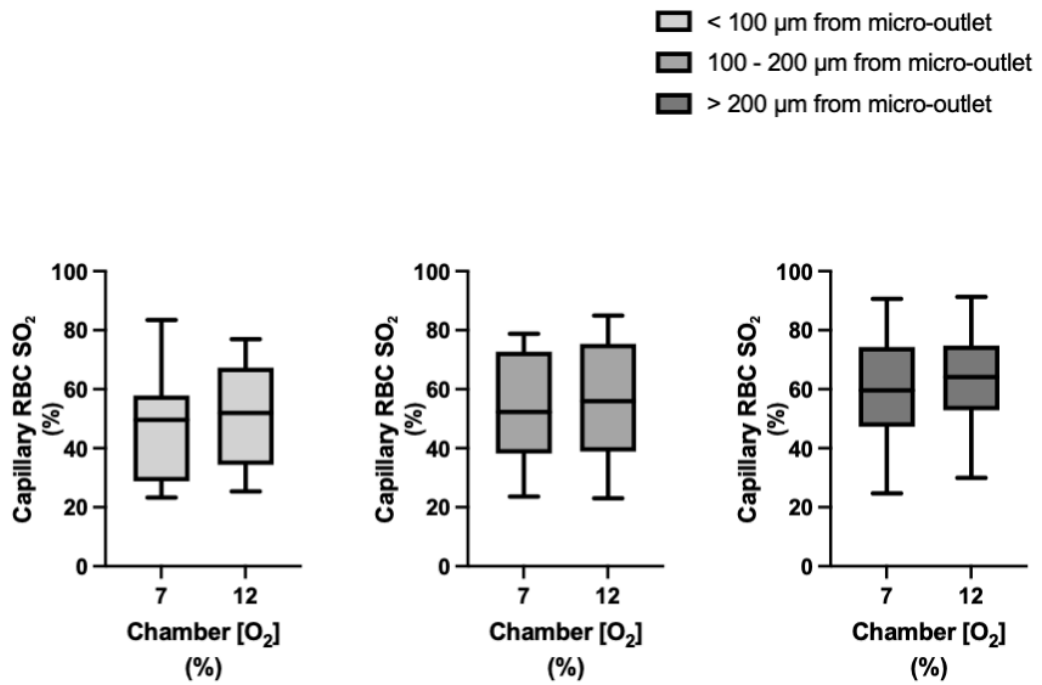
### 2.3.3 RESULTS: 400 $\mu\text{M}$ MICRO-OUTLET OXYGEN CHALLENGE DATA

Oxygen ( $\text{O}_2$ ) challenge data utilizing 400- $\mu\text{m}$  micro-outlets for oxygen saturation ( $\text{SO}_2$ ) measurements consisted of a total of 98 capillaries for high (7-12%)  $\text{O}_2$  challenges and 71 capillaries for low (7-2%)  $\text{O}_2$  challenges across 6 animals. A total of 47 capillaries in 7-12% and 36 capillaries in 7-2% were analyzed directly overlying the window. Regarding capillaries measured outside the outlet edge for high oxygen challenges, 8 were measured less than 100  $\mu\text{m}$ s away, 16 were between 100 – 200  $\mu\text{m}$ s away, and 27 were greater than 200  $\mu\text{m}$ s away (Figure 2.12). The number of capillaries measured outside the outlet edge for low oxygen challenges, 7 were measured less than 100  $\mu\text{m}$ s away, 11 were between 100 – 200  $\mu\text{m}$ s away, and 17 were greater than 200  $\mu\text{m}$ s away (Figure 2.14).

$\text{O}_2$  challenges imposed on capillaries directly overlying 400  $\mu\text{m}$  micro-outlets caused significant changes in capillary  $\text{SO}_2$  at 12% GEC [ $\text{O}_2$ ],  $87.14 \pm 8.96\%$ , compared to baseline 7% GEC [ $\text{O}_2$ ],  $72.00 \pm 9.24\%$  ( $p < 0.0001$ ) (Figure 2.12).  $\text{O}_2$  challenges imposed on capillaries directly overlying 400  $\mu\text{m}$  micro-outlets caused significant changes in capillary  $\text{SO}_2$  at 2% GEC [ $\text{O}_2$ ],  $43.07 \pm 16.76\%$ , compared to baseline 7% GEC [ $\text{O}_2$ ],  $69.11 \pm 12.14\%$  ( $p < 0.0001$ ) (Figure 2.14). Both high and low  $\text{O}_2$  challenges imposed on capillaries caused no significant change in  $\text{SO}_2$  on capillaries outside the micro-outlet edge (Figure 2.13, 2.15).



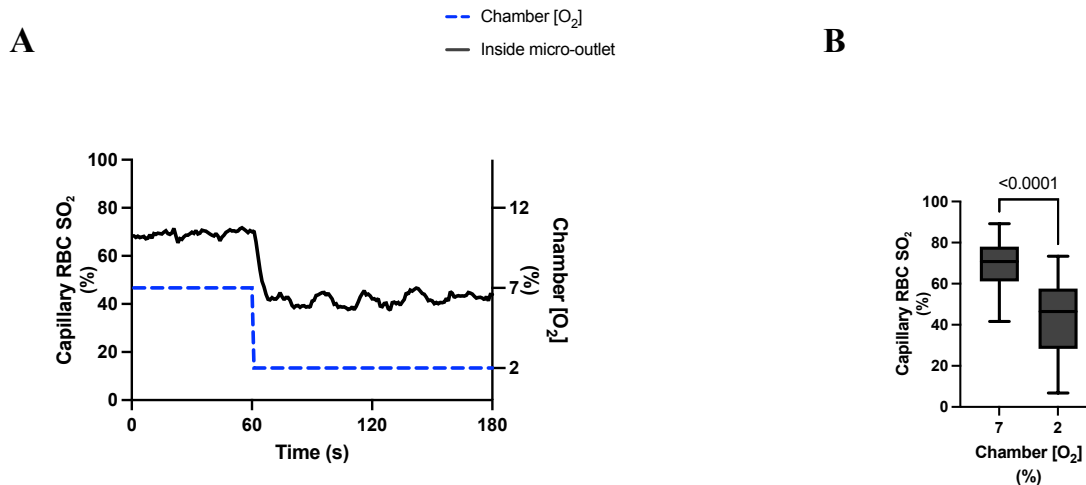
**Figure 2.12 Capillary RBC oxygen saturation in response to high oxygen challenges for capillaries directly overlying the 400  $\mu\text{m}$  micro-outlet.** A) Time series plot showing mean capillary RBC oxygen saturation ( $\text{SO}_2$ ) for capillaries overlying the micro-outlet in response to high (7-12%) oxygen challenges. B) Oxygen challenges consisted of one minute at a baseline oxygen concentration of 7% followed by two minutes at 12%. The average was taken from the entire first minute at 7% and the last 15 seconds at a 12% oxygen concentration ( $n = 47$  capillaries).  $p$  values based on paired t-tests and values indicated in the figure with a  $p < 0.05$  are considered to be significant. Box and whisker plots show minimum, median, maximum, and associated quartiles.

**A****B**

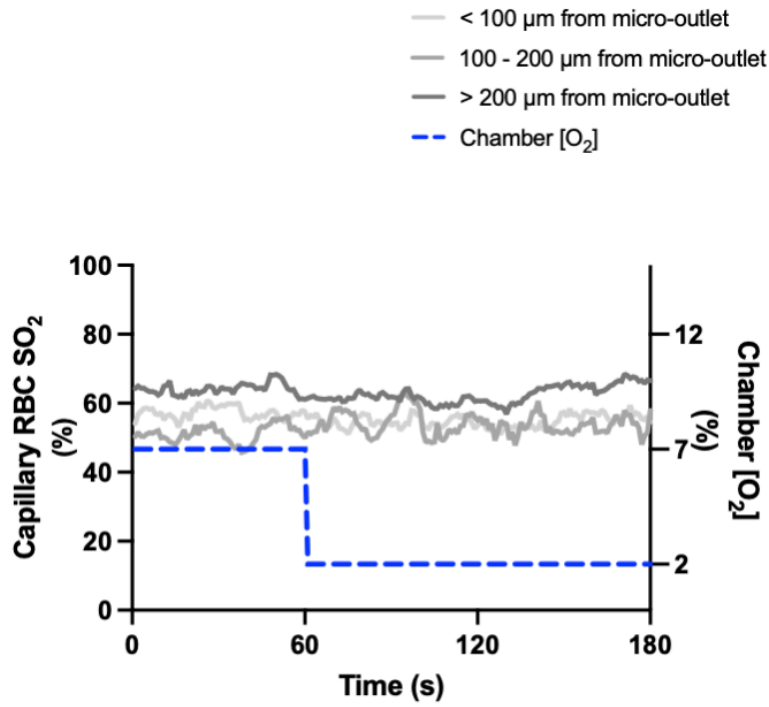
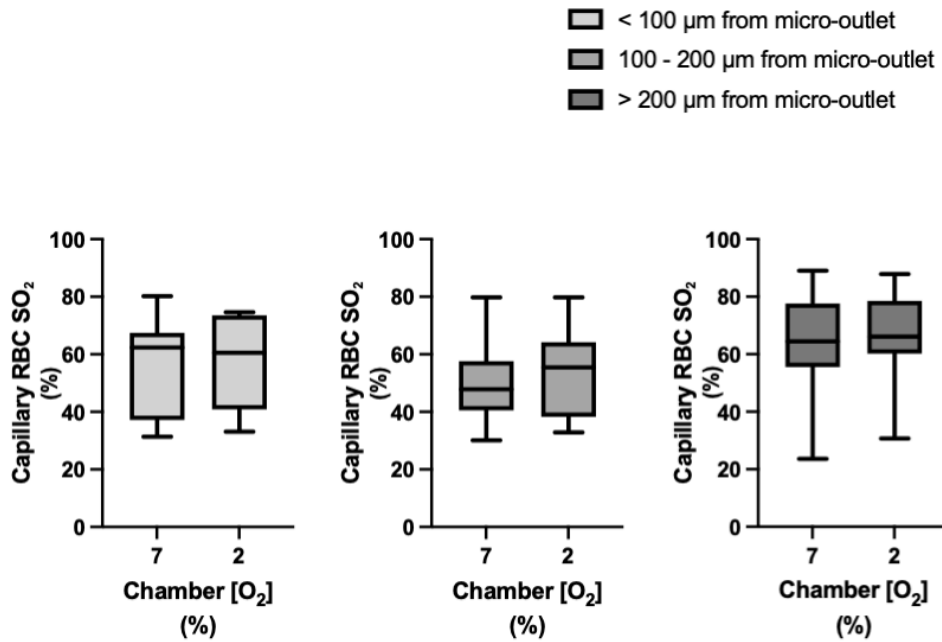
**Figure 2.13 Capillary RBC oxygen saturation responses in capillaries at various distances outside the 400  $\mu\text{m}$  micro-outlet edge in response to high oxygen challenges.**

A) Time series plot showing mean capillary RBC oxygen saturation ( $\text{SO}_2$ ) for capillaries outside the micro-outlet edge at varying distances during high (7-12%) oxygen challenges.

B) Oxygen challenges consisted of one minute at a baseline oxygen concentration of 7% followed by one minute at 12%. The mean was calculated for the first minute at 7% and the last 15 seconds at a 12% oxygen concentration. Panel B shows capillaries within 100  $\mu\text{m}$  from the micro-outlet edge ( $n = 8$  capillaries), capillaries between 100 – 200  $\mu\text{m}$  from the outlet edge ( $n = 16$  capillaries), and capillaries greater than 200  $\mu\text{m}$  from the outlet edge ( $n = 27$  capillaries) respectively.  $p$  values based on paired t tests and values indicated in the figure with a  $p < 0.05$  considered to be significant. Box and whisker plots show minimum, median, maximum, and associated quartiles.



**Figure 2.14 Capillary RBC oxygen saturation in response to low oxygen challenges for capillaries directly overlying the 400  $\mu\text{m}$  micro-outlet.** A) Time series plot showing mean capillary RBC oxygen saturation ( $\text{SO}_2$ ) for capillaries overlying the micro-outlet during low (7-2%) oxygen challenges. B) Oxygen challenges consisted of one minute at a baseline oxygen concentration of 7% followed by two minutes at 2%. The mean was calculated for the first minute at 7% and the last 15 seconds at a 2% oxygen concentration ( $n = 36$  capillaries).  $p$  values based on paired t tests and values indicated in the figure with a  $p < 0.05$  considered to be significant. Box and whisker plots show minimum, median, maximum, and associated quartiles.

**A****B**

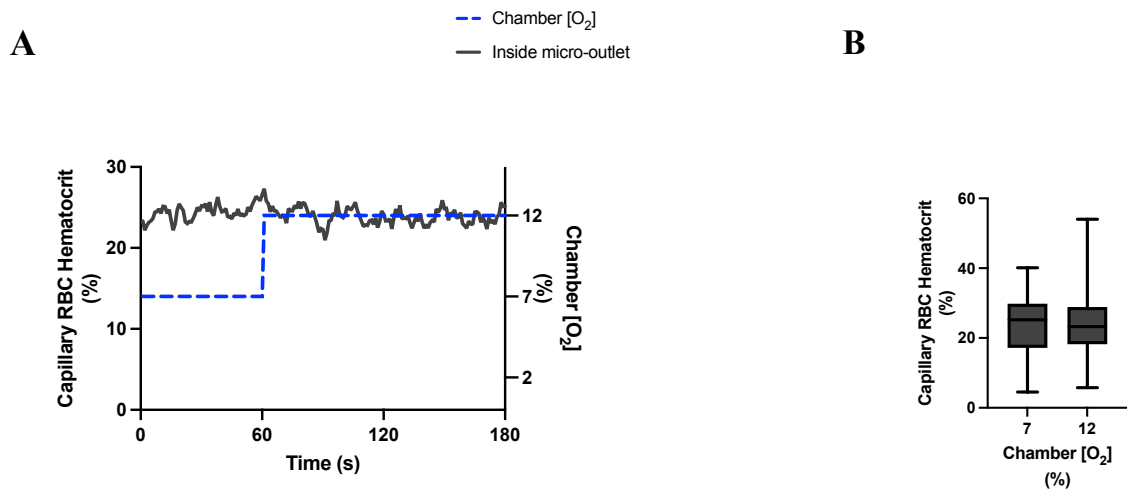
**Figure 2.15 Capillary RBC oxygen saturation responses in capillaries at various distances outside the 400  $\mu\text{m}$  micro-outlet edge in response to low oxygen challenges.**

A) Time series plot showing mean capillary RBC oxygen saturation ( $\text{SO}_2$ ) for capillaries outside the micro-outlet edge at varying distances during low (7-2%) oxygen challenges.

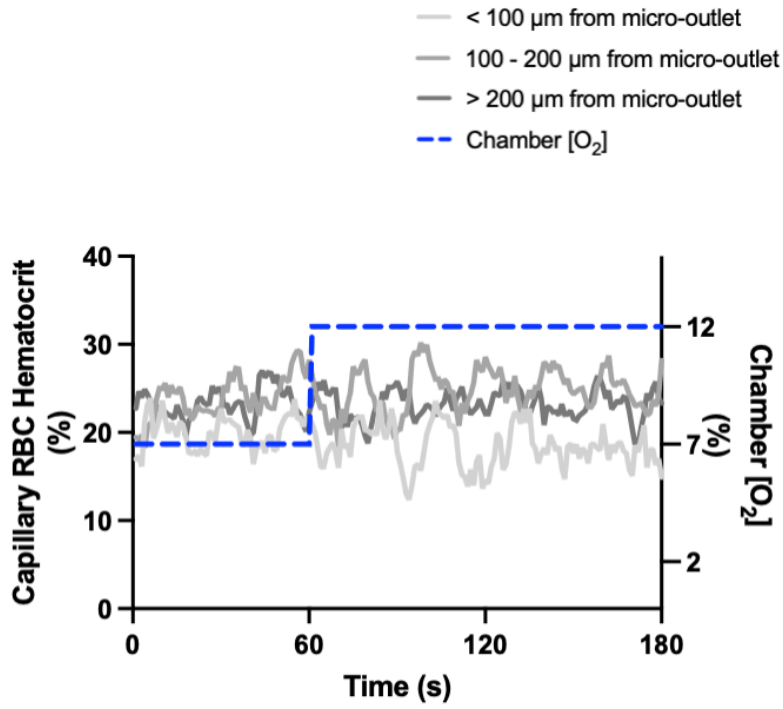
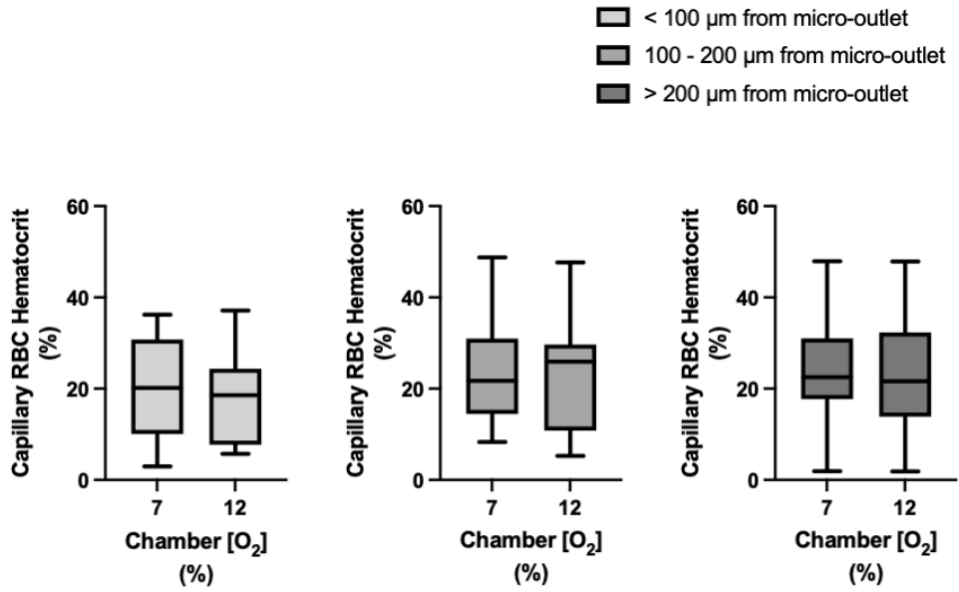
B) Oxygen challenges consisted of one minute at a baseline oxygen concentration of 7% followed by two minutes at 2%. The mean was calculated for the first minute at 7% and the last 15 seconds at a 2% oxygen concentration. Panel B shows capillaries within 100  $\mu\text{m}$  from the micro-outlet edge ( $n = 7$  capillaries), capillaries between 100 – 200  $\mu\text{m}$  from the outlet edge ( $n = 11$  capillaries), and capillaries greater than 200  $\mu\text{m}$  from the outlet edge ( $n = 17$  capillaries), respectively.  $p$  values based on paired t-tests and values indicated in the figure with a  $p < 0.05$  are considered to be significant. Box and whisker plots show minimum, median, maximum, and associated quartiles.

Oxygen (O<sub>2</sub>) challenge data utilizing 400- $\mu$ m micro-outlets for hemodynamic measurements consisted of a total of 165 capillaries across 6 animals. A total of 28 for high and 36 capillaries for low O<sub>2</sub> challenges were analyzed directly overlying the window. With respect to capillaries measured outside the outlet edge during high challenges, 9 were measured less than 100  $\mu$ m away, 14 were between 100 – 200  $\mu$ m away, and 26 were greater than 200  $\mu$ m away. With respect to capillaries measured outside the outlet edge during low challenges, 15 were measured less than 100  $\mu$ m away, 14 were between 100 – 200  $\mu$ m away, and 23 were greater than 200  $\mu$ m away.

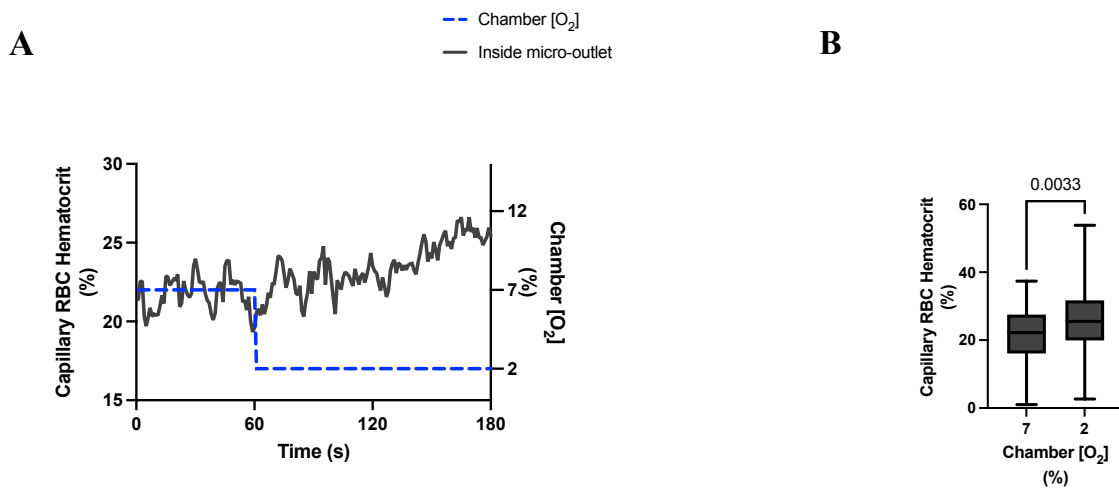
O<sub>2</sub> challenges imposed on capillaries directly overlying 400  $\mu$ m micro-outlets caused a significant change in capillary hematocrit at 2% GEC [O<sub>2</sub>],  $25.66 \pm 9.35\%$ , compared to baseline 7% GEC [O<sub>2</sub>],  $21.75 \pm 9.37\%$  ( $p < 0.0001$ ) but not at 12%,  $24.42 \pm 23.93\%$  ( $p < 0.508$ ). GEC [O<sub>2</sub>] (Figure 2.16, 2.18). High O<sub>2</sub> challenges did not cause significant changes in capillary hematocrit for vessels at various distances from the outlet edge but there was a significant change at 2% GEC [O<sub>2</sub>],  $25.35 \pm 7.00\%$ , compared to baseline 7% GEC [O<sub>2</sub>],  $22.84 \pm 7.56\%$  for vessels greater than 200  $\mu$ m away during low O<sub>2</sub> challenges ( $p = 0.0024$ ) (Figure 2.19).



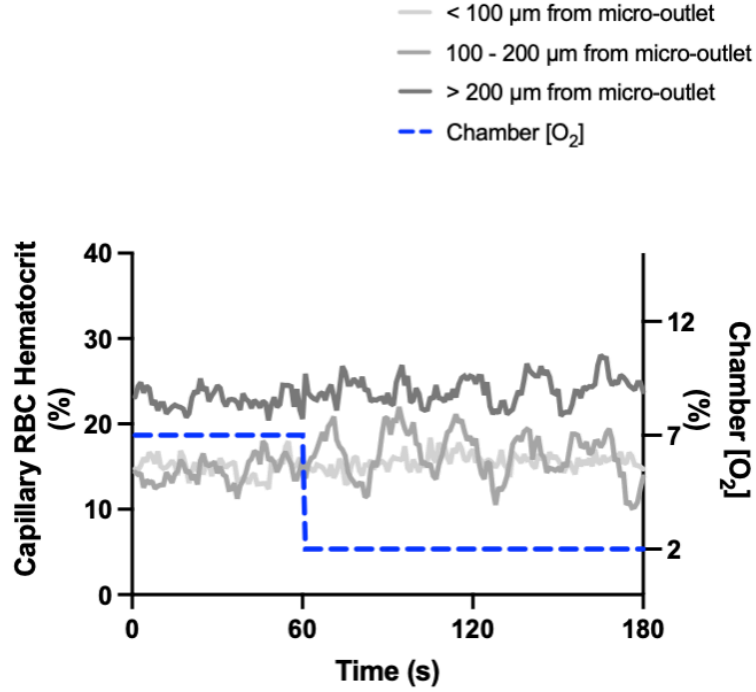
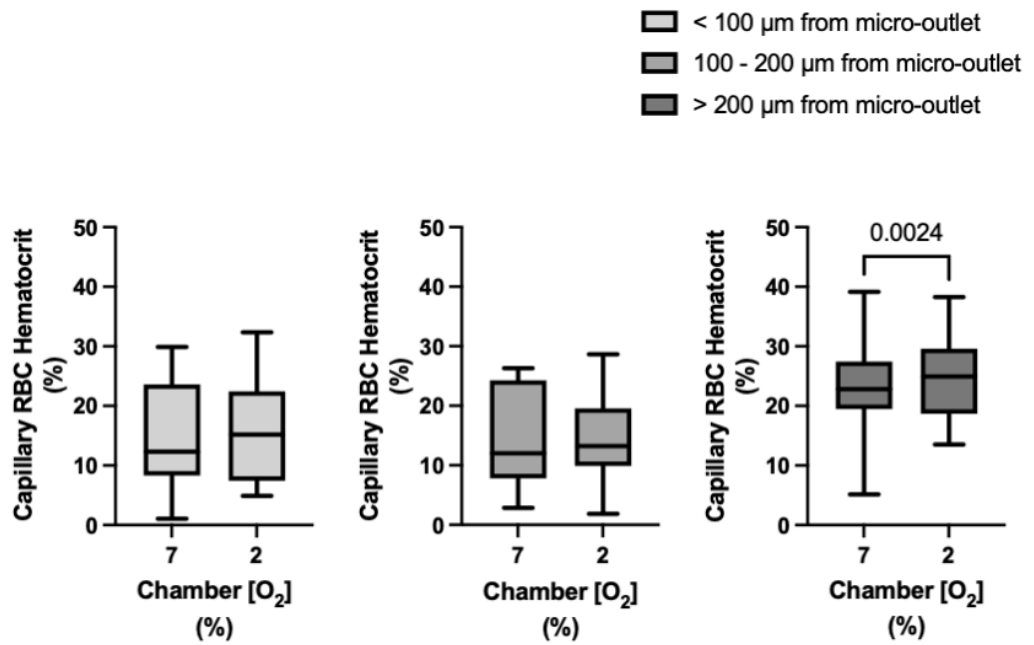
**Figure 2.16 Capillary hematocrit levels in response to high oxygen challenges for capillaries directly overlying the 400  $\mu\text{m}$  micro-outlet.** A) Time series plot showing mean capillary hematocrit levels for capillaries overlying the micro-outlet during high (7-12%) oxygen challenges. B) Oxygen challenges consisted of one minute at a baseline oxygen concentration of 7% followed by two minutes at 12%. The mean was calculated for the first minute at 7% and the last 15 seconds at a 12% oxygen concentration ( $n = 28$  capillaries).  $p$  values based on paired Wilcoxon t-test and values indicated in the figure with a  $p < 0.05$  are significant. Box and whisker plots show minimum, median, maximum, and associated quartiles.

**A****B**

**Figure 2.17 Capillary hematocrit levels in capillaries at various distances outside the 400  $\mu\text{m}$  micro-outlet edge in response to high oxygen challenges.** A) Time series plot showing mean capillary hematocrit levels for capillaries outside the micro-outlet at varying distances during high (7-12%) oxygen challenges. B) Oxygen challenges consisted of one minute at a baseline oxygen concentration of 7% followed by two minutes at 12%. The mean was calculated for the first minute at 7% and the last 15 seconds at a 12% oxygen concentration. Panel B shows capillaries within 100  $\mu\text{m}$  from the micro-outlet edge ( $n = 9$  capillaries), capillaries between 100 – 200  $\mu\text{m}$  from the outlet edge ( $n = 14$  capillaries), and capillaries greater than 200  $\mu\text{m}$  from the outlet edge ( $n = 26$  capillaries) respectively  $p$  values based on paired Wilcoxon t-test and values indicated in the figure with a  $p < 0.05$  considered to be significant. Box and whisker plots show minimum, median, maximum, and associated quartiles.



**Figure 2.18 Capillary hematocrit levels in response to low oxygen challenges for capillaries directly overlying the 400  $\mu\text{m}$  micro-outlet.** A) Time series plot showing mean capillary hematocrit levels for capillaries overlying the micro-outlet during low (7-2%) oxygen challenges. B) Oxygen challenges consisted of one minute at a baseline oxygen concentration of 7% followed by two minutes at 2%. The mean was calculated for the first minute at 7% and the last 15 seconds at a 2% oxygen concentration ( $n = 36$  capillaries).  $p$  values based on paired Wilcoxon t test and values indicated in the figure with a  $p < 0.05$  considered to be significant. Box and whisker plots show minimum, median, maximum, and associated quartiles.

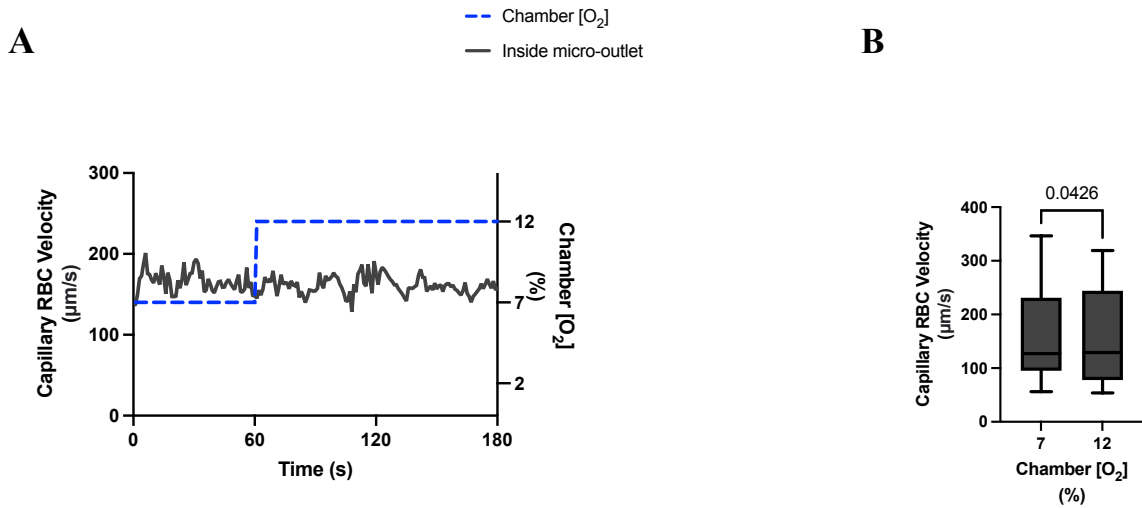
**A****B**

**Figure 2.19 Capillary hematocrit levels in capillaries at various distances outside the 400  $\mu\text{m}$  micro-outlet edge in response to low oxygen challenges.** A) Time series plot showing mean capillary hematocrit levels for capillaries outside the micro-outlet at varying distances during low (7-2%) oxygen challenges. B) Oxygen challenges consisted of one minute at a baseline oxygen concentration of 7% followed by two minutes at 2%. The mean was calculated for the first minute at 7% and the last 15 seconds at a 2% oxygen concentration. Panel B shows capillaries within 100  $\mu\text{m}$  from the micro-outlet edge ( $n = 15$  capillaries), capillaries between 100 – 200  $\mu\text{m}$  from the outlet edge ( $n = 14$  capillaries), and capillaries greater than 200  $\mu\text{m}$  from the outlet edge ( $n = 23$  capillaries) respectively  $p$  values based on paired Wilcoxon t test and values indicated in the figure with a  $p < 0.05$  considered to be significant. Box and whisker plots show minimum, median, maximum, and associated quartiles.

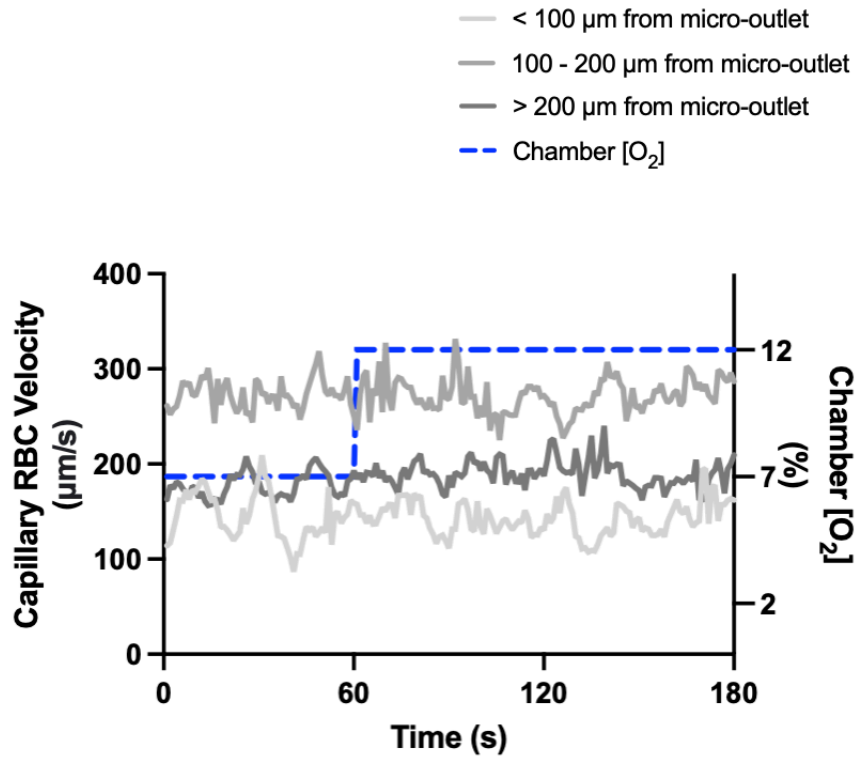
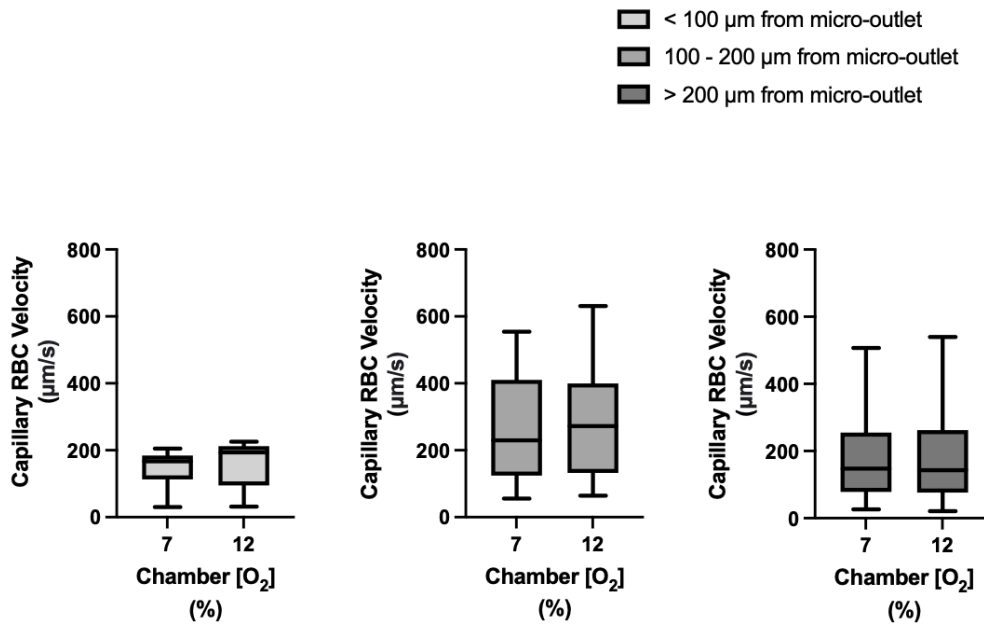
O<sub>2</sub> challenges imposed on capillaries directly overlying 400 µm micro-outlets caused significant changes in capillary velocity at 12% GEC [O<sub>2</sub>],  $157.0 \pm 84.42$  µm/s, compared to baseline 7% GEC [O<sub>2</sub>],  $165.0 \pm 89.86$  µm/s ( $p < 0.0426$ ) (Figure 2.20). O<sub>2</sub> challenges imposed on capillaries directly overlying 400 µm micro-outlets caused significant changes in capillary velocity at 2% GEC [O<sub>2</sub>],  $274.4 \pm 210.4$  µm/s, compared to baseline 7% GEC [O<sub>2</sub>],  $218.6 \pm 189.0$  µm/s ( $p < 0.0001$ ) (Figure 2.22). O<sub>2</sub> challenges imposed on capillaries directly overlying 400 µm micro-outlets caused significant changes in capillary velocity in vessels between 100 to 200 µms away from the outlet edge at 2% GEC [O<sub>2</sub>],  $385.9 \pm 237.4$  µm/s, compared to baseline 7% GEC [O<sub>2</sub>],  $355.6 \pm 244.1$  µm/s ( $p = 0.0245$ ). Vessels greater than 200 µms away from the outlet edge experienced significant changes in capillary velocity at 2% GEC [O<sub>2</sub>],  $282.0 \pm 178.9$  µm/s, compared to baseline 7% GEC [O<sub>2</sub>],  $253.9 \pm 153.0$  µm/s ( $p = 0.0277$ ) (Figure 2.23).

High O<sub>2</sub> challenges imposed on capillaries directly overlying 400 µm micro-outlets caused significant changes in capillary supply rate at 12% GEC [O<sub>2</sub>],  $9.49 \pm 5.7$  cells/s, compared to baseline 7% GEC [O<sub>2</sub>],  $10.73 \pm 7.18$  cells/s ( $p = 0.0232$ ) (Figure 2.24). Low O<sub>2</sub> challenges imposed on capillaries directly overlying 400 µm micro-outlets caused significant changes in capillary supply rate at 2% GEC [O<sub>2</sub>],  $17.70 \pm 13.39$  cells/s, compared to baseline 7% GEC [O<sub>2</sub>],  $10.70 \pm 8.13$  cells/s ( $p < 0.0001$ ) (Figure 2.26). O<sub>2</sub> challenges imposed on capillaries directly overlying 400 µm micro-outlets caused significant changes in capillary supply rate in vessels greater than 200 µms from the outlet edge at 2% GEC [O<sub>2</sub>],  $18.44 \pm 12.23$  cells/s, compared to a baseline 7% GEC [O<sub>2</sub>],  $14.70$

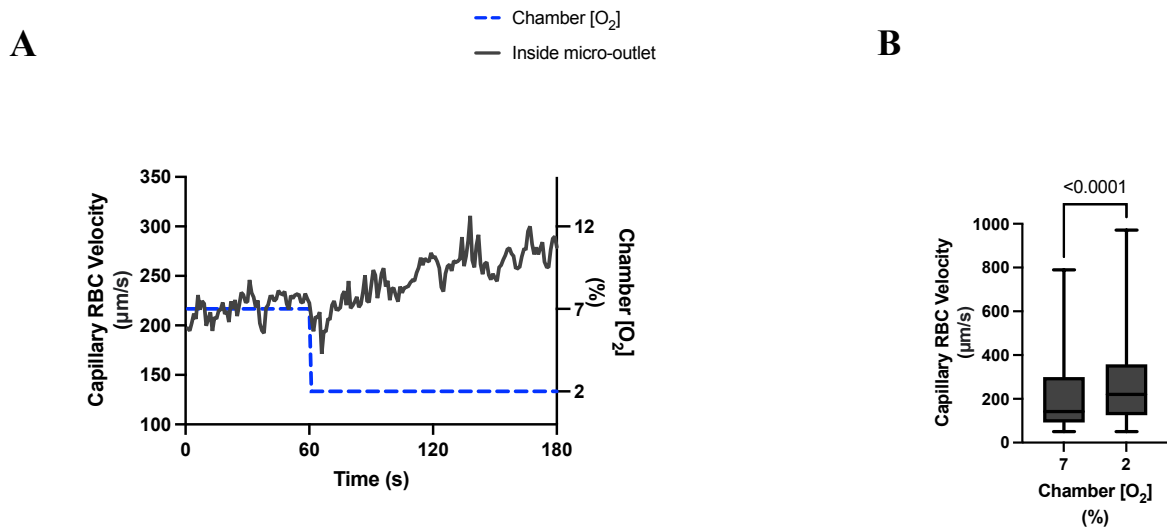
$\pm 10.52$  cells/s ( $p = 0.0004$ ) (Figure 2.27). No other outlet vessels had significant changes in capillary supply rate during high and low O<sub>2</sub> challenges.



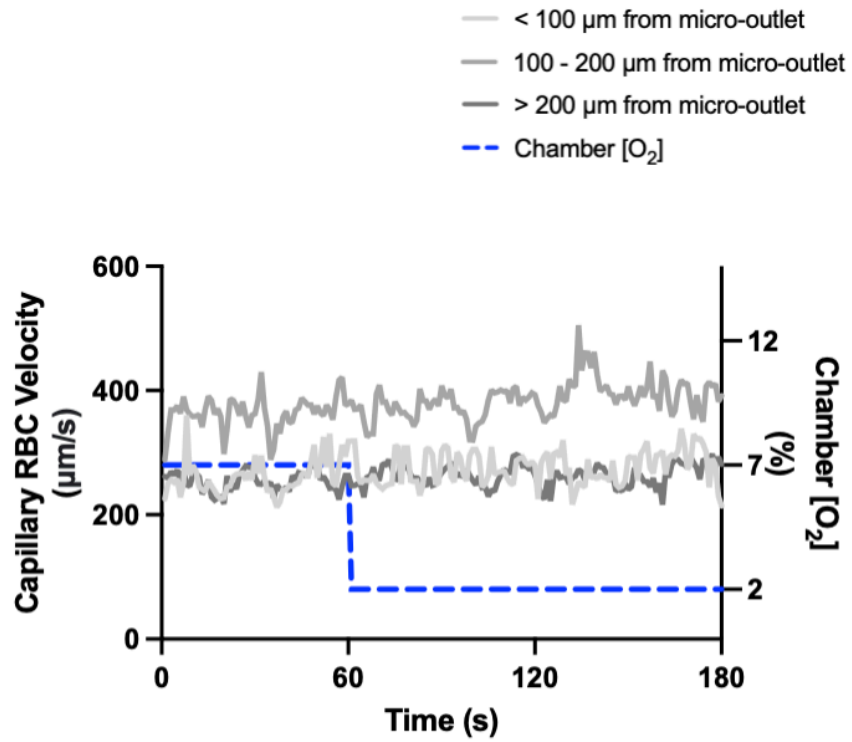
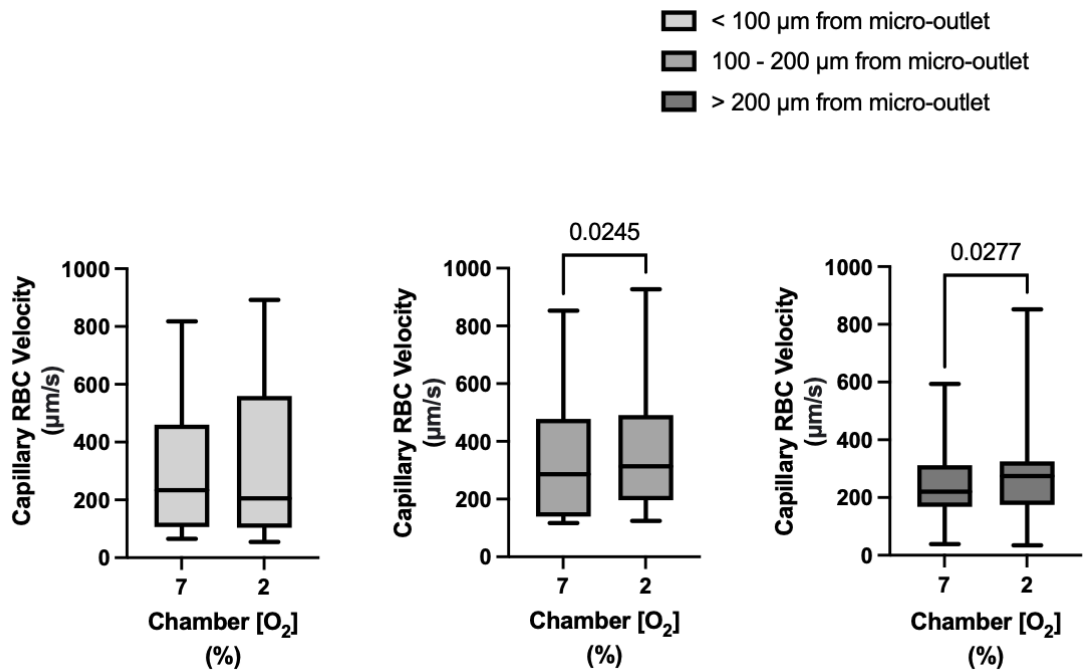
**Figure 2.20 Capillary RBC velocity response to high oxygen challenges for capillaries directly overlying the 400 µm micro-outlet.** A) Time series plot showing mean capillary RBC velocity for capillaries overlying the micro-outlet during high (7-12%) oxygen challenges. B) Oxygen challenges consisted of one minute at a baseline oxygen concentration of 7% followed by two minutes at 12%. The average was taken from the entire first minute at 7% and the last 15 seconds at a 12% oxygen concentration (n = 28 capillaries). *p* values based on paired Wilcoxon t test and values indicated in the figure with a *p* < 0.05 considered to be significant. Box and whisker plots show minimum, median, maximum, and associated quartiles.

**A****B**

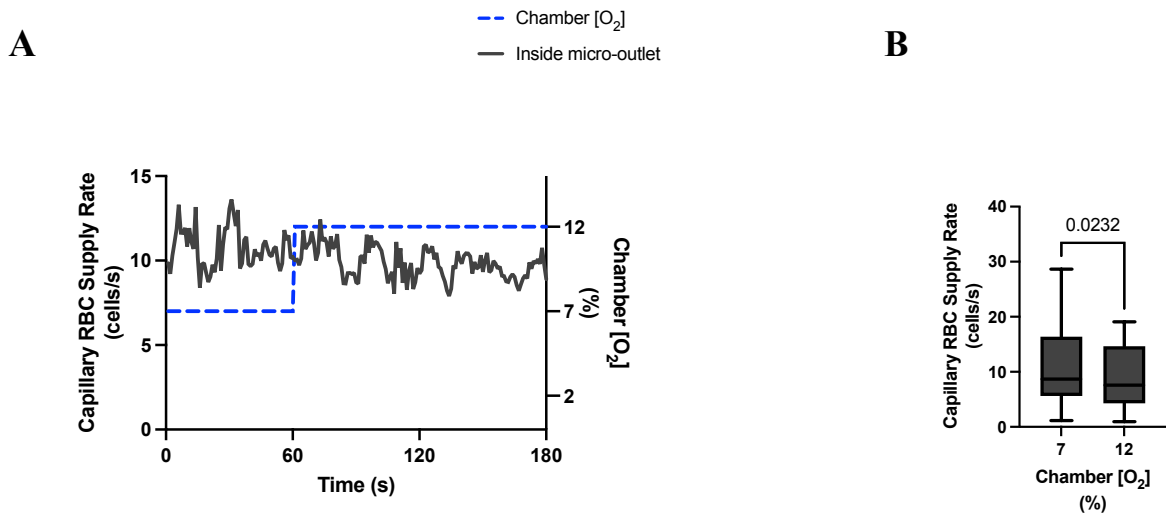
**Figure 2.21 Capillary RBC velocity levels in capillaries at various distances outside the 400  $\mu\text{m}$  micro-outlet edge in response to high oxygen challenges.** A) Time series plot showing mean capillary RBC velocity for capillaries outside the micro-outlet at varying distances during high (7-12%) oxygen challenges. B) Oxygen challenges consisted of one minute at a baseline oxygen concentration of 7% followed by two minutes at 12%. The mean was calculated for the first minute at 7% and the last 15 seconds at 12% oxygen concentration. Panel B shows capillaries within 100  $\mu\text{m}$  from the micro-outlet edge (n = 9 capillaries), capillaries between 100 – 200  $\mu\text{m}$  from the outlet edge (n = 14 capillaries), and capillaries greater than 200  $\mu\text{m}$  from the outlet edge (n = 26 capillaries) respectively. Box and whisker plots show minimum, median, maximum, and associated quartiles.



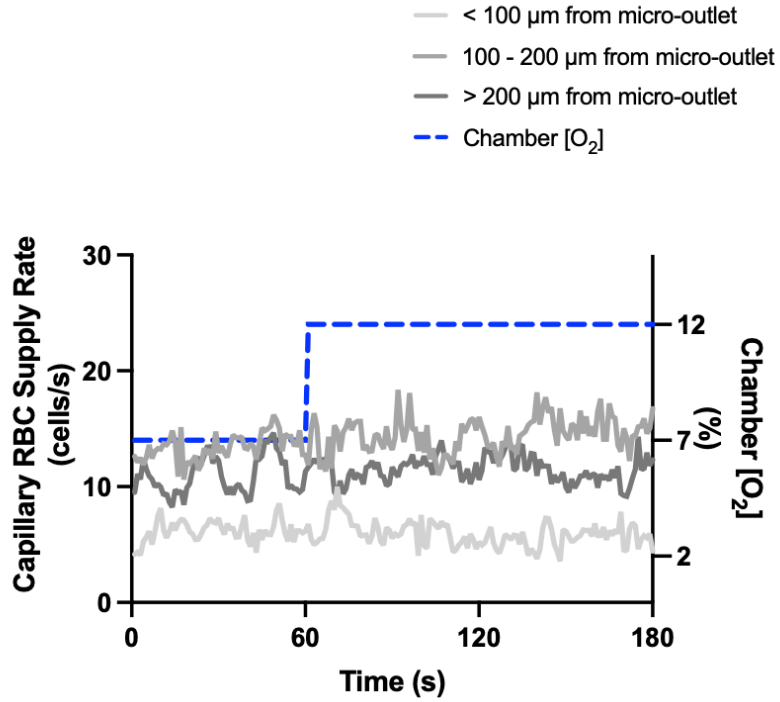
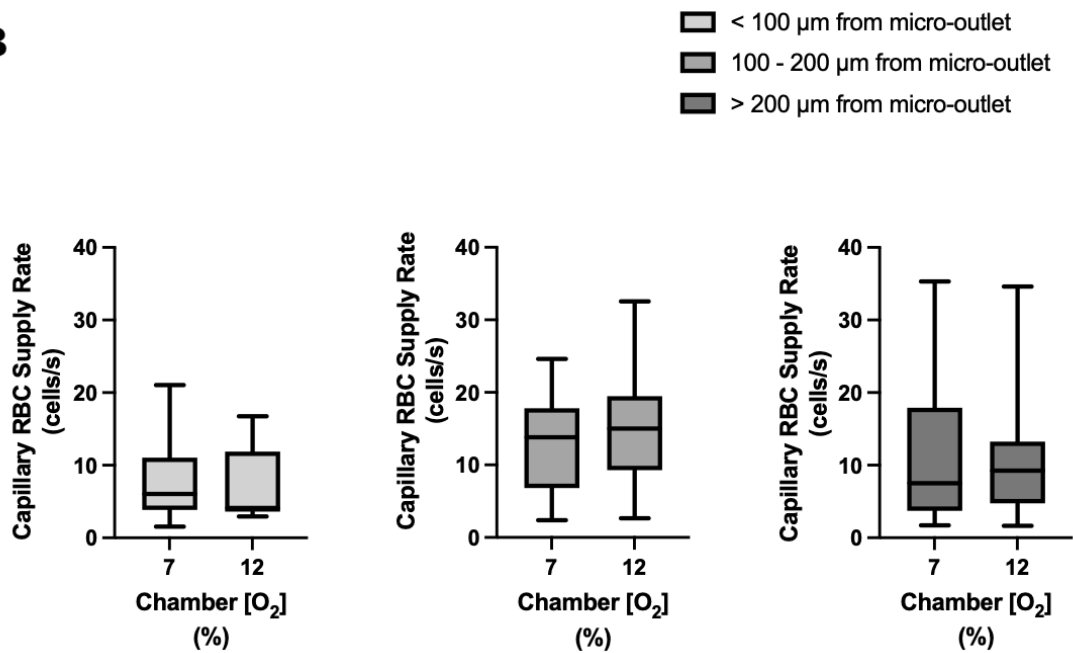
**Figure 2.22 Capillary RBC velocity response to low oxygen challenges for capillaries directly overlying the 400  $\mu\text{m}$  micro-outlet.** A) Time series plot showing mean capillary RBC velocity for capillaries overlying the micro-outlet during low (7-2%) oxygen challenges. B) Oxygen challenges consisted of one minute at a baseline oxygen concentration of 7% followed by two minutes at 2%. The mean was calculated for the first minute at 7% and the last 15 seconds at 2% oxygen concentration ( $n = 36$  capillaries).  $p$  values based on paired Wilcoxon t-test and values indicated in the figure with a  $p < 0.05$  are significant. Box and whisker plots show minimum, median, maximum, and associated quartiles.

**A****B**

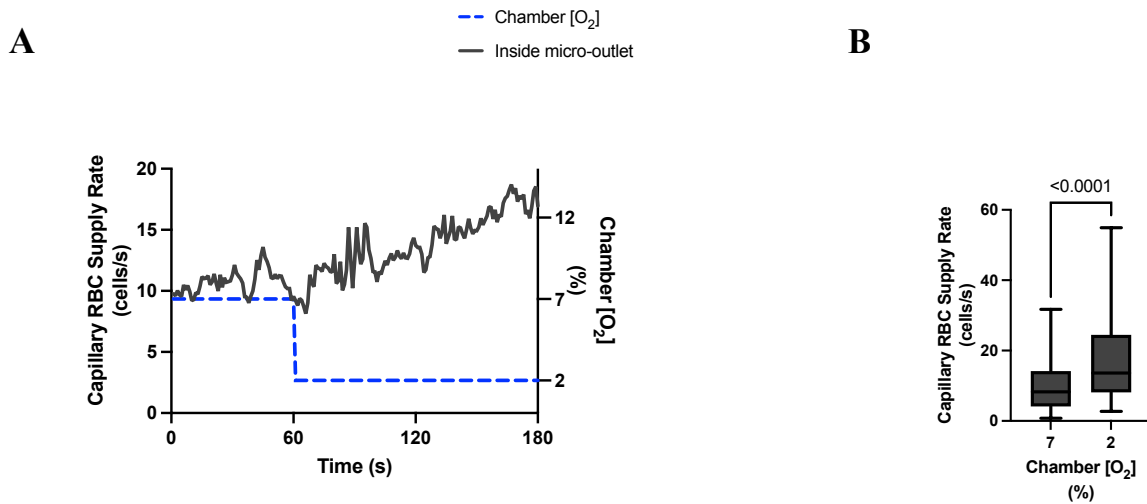
**Figure 2.23 Capillary RBC velocity in capillaries at various distances outside the 400  $\mu\text{m}$  micro-outlet edge in response to low oxygen challenges.** A) Time series plot showing mean capillary RBC velocity for capillaries outside the micro-outlet at varying distances during low (7-2%) oxygen challenges. B) Oxygen challenges consisted of one minute at a baseline oxygen concentration of 7% followed by two minutes at 2%. The mean was calculated for the first minute at 7% and the last 15 seconds at a 2% oxygen concentration. Panel B shows capillaries within 100  $\mu\text{m}$  from the micro-outlet edge (n = 15 capillaries), capillaries between 100 – 200  $\mu\text{m}$  from the outlet edge (n = 14 capillaries), and capillaries greater than 200  $\mu\text{m}$  from the outlet edge (n = 23 capillaries) respectively. *p* values based on paired Wilcoxon t-test and values indicated in the figure with a  $p < 0.05$  considered to be significant. Box and whisker plots show minimum, median, maximum, and associated quartiles.



**Figure 2.24 Capillary RBC supply rate response to high oxygen challenges for capillaries directly overlying the 400  $\mu\text{m}$  micro-outlet.** A) Time series plot showing mean capillary RBC supply rate for capillaries overlying the micro-outlet during high (7-12%) oxygen challenges. B) Oxygen challenges consisted of one minute at a baseline oxygen concentration of 7% followed by two minutes at 12%. The mean was calculated for the first minute at 7% and the last 15 seconds at a 12% oxygen concentration ( $n = 28$  capillaries).  $p$  values based on paired Wilcoxon t-test and values indicated in the figure with a  $p < 0.05$  considered to be significant. Box and whisker plots show minimum, median, maximum, and associated quartiles.

**A****B**

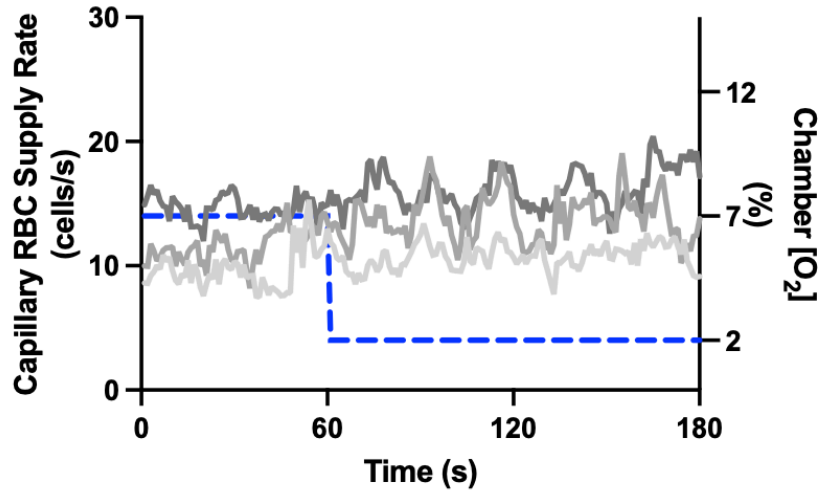
**Figure 2.25 Capillary RBC supply rate in capillaries at various distances outside the 400  $\mu\text{m}$  micro-outlet edge in response to high oxygen challenges.** A) Time series plot showing mean capillary RBC supply rate for capillaries outside the micro-outlet at varying distances during high (7-12%) oxygen challenges. B) Oxygen challenges consisted of one minute at a baseline oxygen concentration of 7% followed by two minutes at 12%. The mean was calculated for the first minute at 7% and the last 15 seconds at a 12% oxygen concentration. Panel B shows capillaries within 100  $\mu\text{m}$  from the micro-outlet edge ( $n = 9$  capillaries), capillaries between 100 – 200  $\mu\text{m}$  from the outlet edge ( $n = 14$  capillaries), and capillaries greater than 200  $\mu\text{m}$  from the outlet edge ( $n = 26$  capillaries) respectively.  $p$  values based on paired Wilcoxon t-test and values indicated in the figure with a  $p < 0.05$  are significant. Box and whisker plots show minimum, median, maximum, and associated quartiles.



**Figure 2.26 Capillary RBC supply rate in response to low oxygen challenges for capillaries directly overlying the 400  $\mu\text{m}$  micro-outlet.** A) Time series plot showing mean capillary RBC supply rate for capillaries overlying the micro-outlet during low (7-2%) oxygen challenges. B) Oxygen challenges consisted of one minute at a baseline oxygen concentration of 7% followed by two minutes at 2%. The mean was calculated for the first minute at 7% and the last 15 seconds at a 2% oxygen concentration ( $n = 36$  capillaries).  $p$  values based on paired Wilcoxon t-test and values indicated in the figure with a  $p < 0.05$  are significant. Box and whisker plots show minimum, median, maximum, and associated quartiles.

**A**

- < 100  $\mu\text{m}$  from micro-outlet
- 100 - 200  $\mu\text{m}$  from micro-outlet
- > 200  $\mu\text{m}$  from micro-outlet
- - Chamber  $[\text{O}_2]$

**B**

- < 100  $\mu\text{m}$  from micro-outlet
- ▒ 100 - 200  $\mu\text{m}$  from micro-outlet
- > 200  $\mu\text{m}$  from micro-outlet

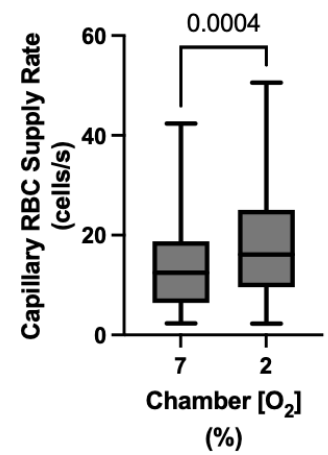
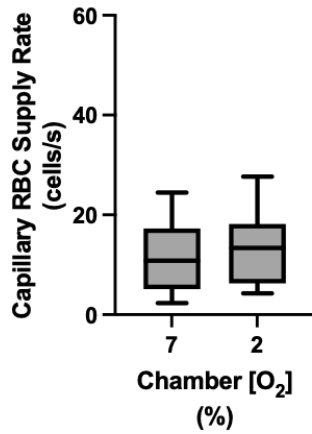
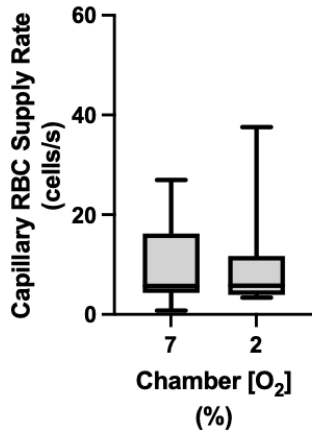


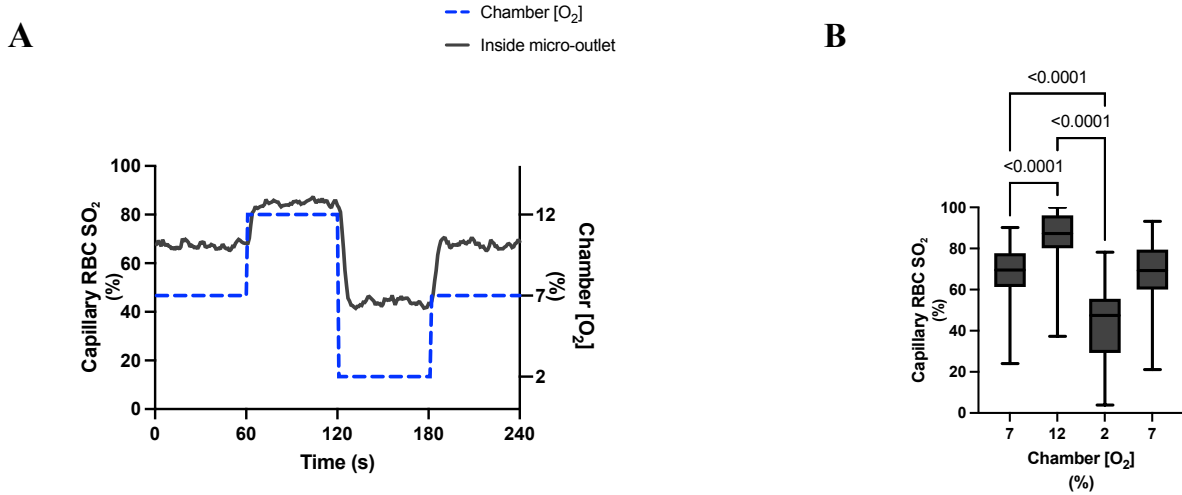
**Figure 2.27 Capillary RBC supply rate in capillaries at various distances outside the 400  $\mu\text{m}$  micro-outlet edge in response to low oxygen challenges.** A) Time series plot showing mean capillary RBC supply rate for capillaries outside the micro-outlet at varying distances during low (7-2%) oxygen challenges. B) Oxygen challenges consisted of one minute at a baseline oxygen concentration of 7% followed by two minutes at 2%. The mean was calculated for the first minute at 7% and the last 15 seconds at a 2% oxygen concentration. Panel B shows capillaries within 100  $\mu\text{m}$  from the micro-outlet edge ( $n = 15$  capillaries), capillaries between 100 – 200  $\mu\text{m}$  from the outlet edge ( $n = 14$  capillaries), and capillaries greater than 200  $\mu\text{m}$  from the outlet edge ( $n = 23$  capillaries) respectively.  $p$  values based on paired Wilcoxon t-test and values indicated in the figure with a  $p < 0.05$  are considered to be significant. Box and whisker plots show minimum, median, maximum, and associated quartiles.

#### 2.3.4 RESULTS: 200 $\mu\text{M}$ MICRO-OUTLET OXYGEN OSCILLATION DATA

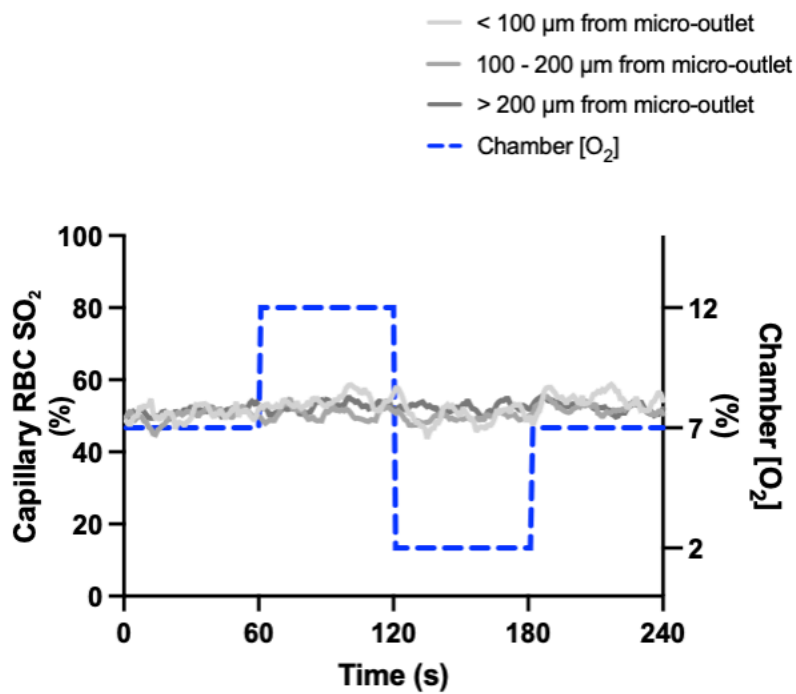
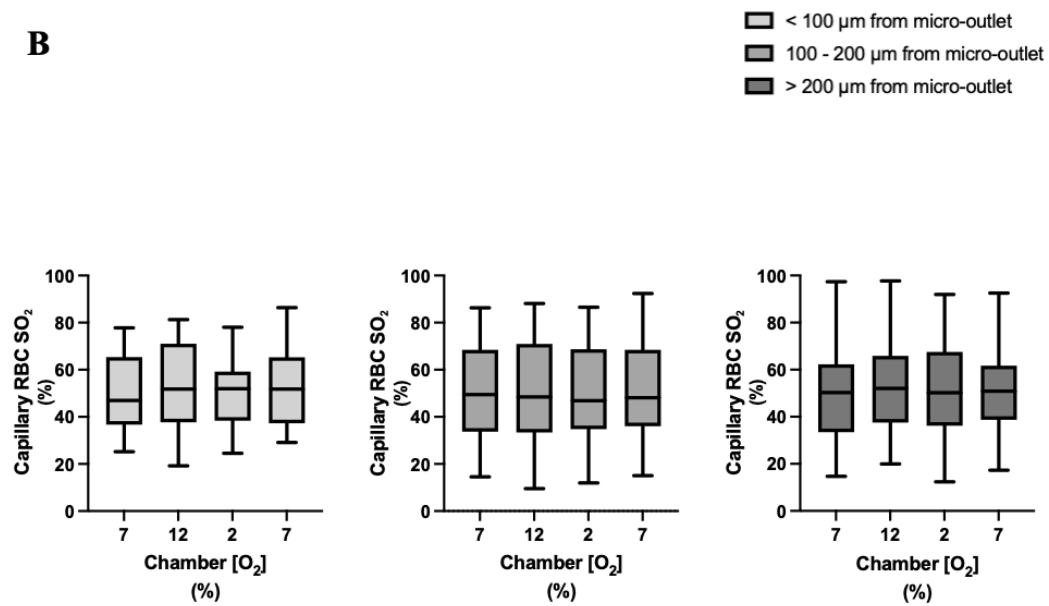
Oxygen ( $\text{O}_2$ ) oscillation data utilizing 200- $\mu\text{m}$  micro-outlets for oxygen saturation ( $\text{SO}_2$ ) measurements comprised a total of 183 capillaries across 6 animals. A total of 41 capillaries were analyzed directly overlying the window, and 142 capillaries were measured outside the outlet edge. Concerning capillaries outside the outlet edge, 33 were measured less than 100  $\mu\text{ms}$  away, 54 were between 100 – 200  $\mu\text{ms}$  away, and 55 were greater than 200  $\mu\text{ms}$  away.

$\text{O}_2$  oscillations imposed on capillaries directly overlying 200  $\mu\text{m}$  micro-outlets caused significant changes in capillary  $\text{SO}_2$  at 12% GEC [ $\text{O}_2$ ],  $84.91 \pm 13.78\%$ , and 2% GEC [ $\text{O}_2$ ],  $43.41 \pm 18.47\%$ , compared to baseline 7% GEC [ $\text{O}_2$ ],  $66.83 \pm 14.75\%$  and between 12% GEC [ $\text{O}_2$ ],  $84.91 \pm 13.78\%$  and 2% GEC [ $\text{O}_2$ ],  $43.41 \pm 18.47\%$  ( $p < 0.0001$ ) (Figure 2.28).  $\text{O}_2$  oscillations imposed on capillaries greater than 200  $\mu\text{ms}$  outside the micro-outlet edge caused a significant change in  $\text{SO}_2$  at 12% GEC [ $\text{O}_2$ ],  $52.21 \pm 19.78\%$  and at 2% GEC [ $\text{O}_2$ ],  $51.79 \pm 20.03\%$  compared to baseline 7% GEC [ $\text{O}_2$ ],  $49.75 \pm 19.79\%$  ( $p < 0.0410$ ).  $\text{O}_2$  oscillations imposed on capillaries caused no significant differences in  $\text{SO}_2$  in capillaries less than 200  $\mu\text{ms}$  from the outlet edge (Figure 2.29).

Oxygen ( $\text{O}_2$ ) oscillation data utilizing 200- $\mu\text{m}$  micro-outlets for hemodynamic measurements comprised 215 capillaries across 6 animals. A total of 46 capillaries were analyzed directly overlying the window, and 169 capillaries were measured outside the outlet edge. Concerning capillaries outside the outlet edge, 35 were measured less than 100  $\mu\text{ms}$  away, 56 were between 100 – 200  $\mu\text{ms}$  away, and 78 were greater than 200  $\mu\text{ms}$  away.



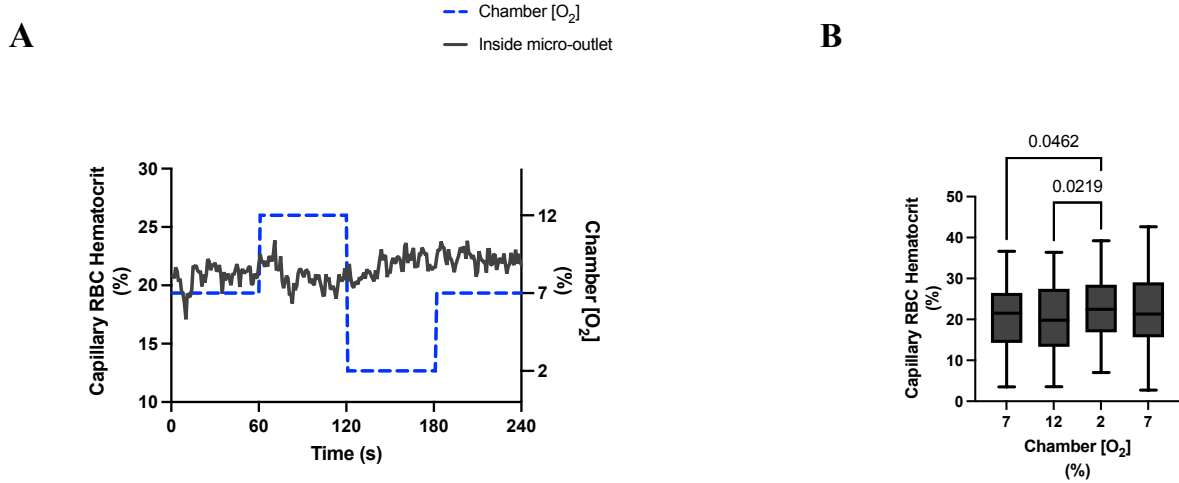
**Figure 2.28 Capillary RBC oxygen saturation in response to oxygen oscillations for capillaries directly overlying the 200  $\mu\text{m}$  micro-outlet.** A) Time series plot showing the mean capillary RBC oxygen saturation ( $\text{SO}_2$ ) in capillaries overlying the 200  $\mu\text{m}$  micro-outlet edge across the 4-minute  $\text{O}_2$  oscillation (7-12-2-7%). B) The micro-outlet gas exchange device imposes 4-minute oxygen oscillations for one minute at a baseline concentration of 7%, 12%, 2%, and 7%, respectively. Mean values are taken from the first entire minute at baseline and the last 15 seconds at 12%, 2%, and 7% ( $n = 41$  capillaries).  $p$  values are based on Tukey's multiple comparisons test after significant repeated measures ANOVA and are indicated in the figure with a  $p < 0.05$  considered to be significant. Box and whisker plots show minimum, median, maximum, and associated quartiles.

**A****B**

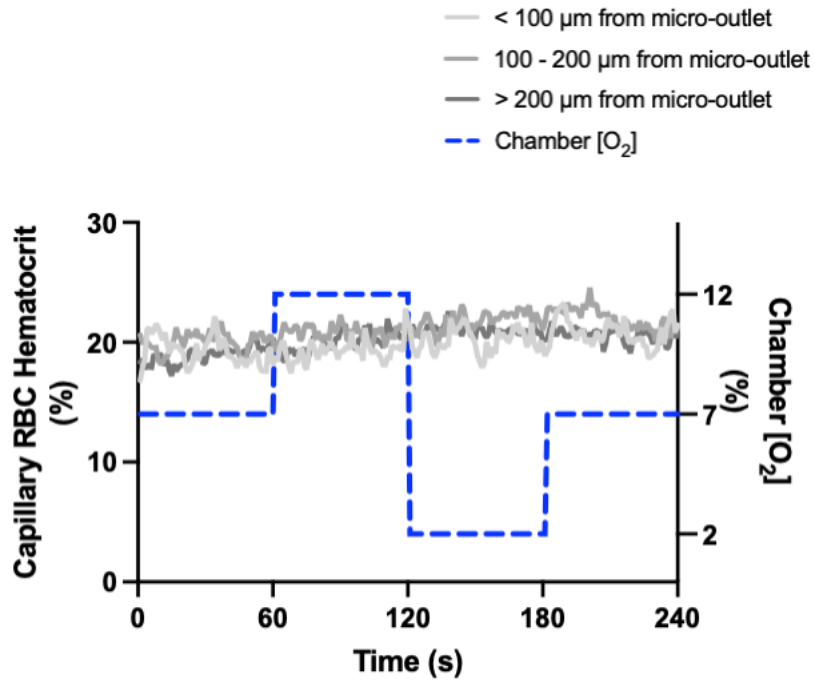
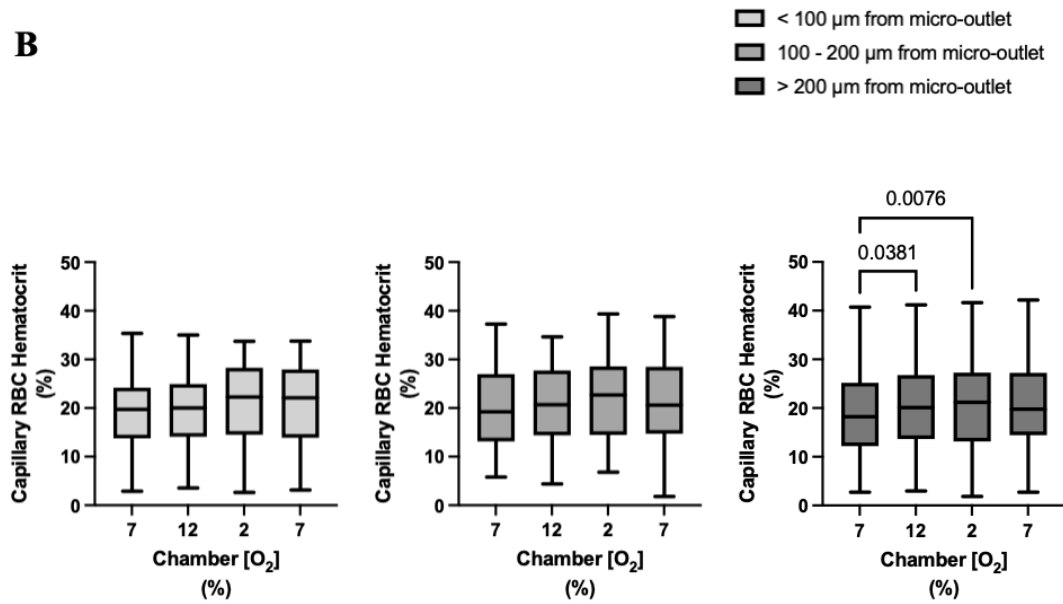
**Figure 2.29 Capillary RBC oxygen saturation responses in capillaries at various distances outside the 200  $\mu\text{m}$  micro-outlet edge.** A) Time series plot showing the mean capillary RBC oxygen saturation ( $\text{SO}_2$ ) in capillaries outside the 200  $\mu\text{m}$  micro-outlet edge across the 4-minute  $\text{O}_2$  oscillation (7-12-2-7%). B) The micro-outlet gas exchange device imposes 4-minute oxygen oscillations across 4 animals for one minute at a baseline concentration of 7%, one minute at 12%, one minute at 2%, and one minute at 7%. Panel B shows capillaries within 100  $\mu\text{m}$  from the micro-outlet edge ( $n = 33$  capillaries), capillaries between 100 – 200  $\mu\text{m}$  from the outlet edge ( $n = 54$  capillaries), and capillaries greater than 200  $\mu\text{m}$  from the outlet edge ( $n = 55$  capillaries) respectively.  $p$  values based on Tukey's multiple comparisons test after significant repeated measures ANOVA are indicated in the figure with a  $p < 0.05$  considered to be significant. Box and whisker plots show minimum, median, maximum, and associated quartiles.

O<sub>2</sub> oscillations imposed on capillaries directly overlying 200 μm micro-outlets caused significant changes in capillary hematocrit in capillaries overlying the outlets at 2% GEC [O<sub>2</sub>], 22.20 ± 8.50%, compared to baseline 7% GEC [O<sub>2</sub>], 20.77 ± 7.98% and at 12% GEC [O<sub>2</sub>], 20.20 ± 8.67% compared to 2% GEC [O<sub>2</sub>], 22.20 ± 8.50% ( $p < 0.0462$ ) (Figure 2.30). O<sub>2</sub> oscillations imposed on capillaries directly overlying 200 μm micro-outlets caused significant changes in capillary hematocrit in capillaries greater than 200 μms away from the outlet at 12% GEC [O<sub>2</sub>], 20.52 ± 8.90%, and 2% GEC [O<sub>2</sub>], 20.91 ± 9.12%, compared to baseline 7% GEC [O<sub>2</sub>], 18.92 ± 8.61% ( $p < 0.0381$ ) (Figure 2.31).

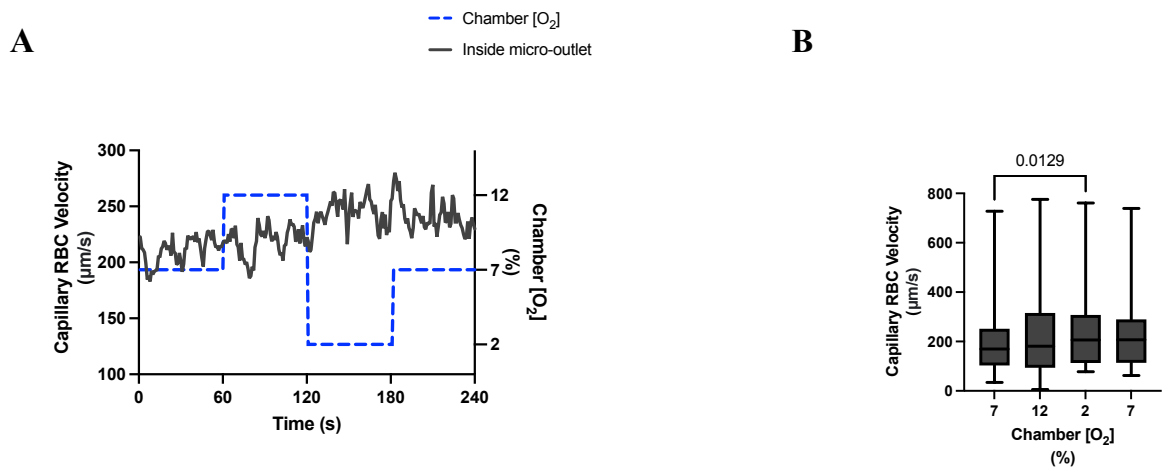
O<sub>2</sub> oscillations imposed on capillaries directly overlying 200 μm micro-outlets did cause a significant change in capillary velocity in capillaries inside the micro-outlet at 2% GEC [O<sub>2</sub>], 239.0 ± 161.5 μm/s, compared to baseline 7% GEC [O<sub>2</sub>], 208.6 ± 144.1 μm/s, ( $p = 0.0129$ ) (Figure 2.32). O<sub>2</sub> oscillations imposed on capillaries directly overlying 200 μm micro-outlets did not cause significant changes in capillary velocity in vessels less than 200 μms away from the outlet edge but did in capillaries greater than 200 μms. In vessels greater than 200 μms away from the outlet edge, there were significant changes in capillary velocity at 2% GEC [O<sub>2</sub>], 192.5 ± 108.5 μm/s, and at 7% GEC [O<sub>2</sub>], 185.4 ± 99.51 μm/s, compared to baseline 7% GEC [O<sub>2</sub>], 177.4 ± 92.14 μm/s ( $p = 0.0315$ ). O<sub>2</sub> oscillations imposed on capillaries directly overlying 200 μm micro-outlets caused significant changes in capillary velocity in vessels greater than 200 μms away from the outlet edge between 12% GEC [O<sub>2</sub>], 170.2 ± 89.00 μm/s, and 2% GEC [O<sub>2</sub>], 192.5 ± 108.5 μm/s ( $p < 0.0001$ ) (Figure 2.33).



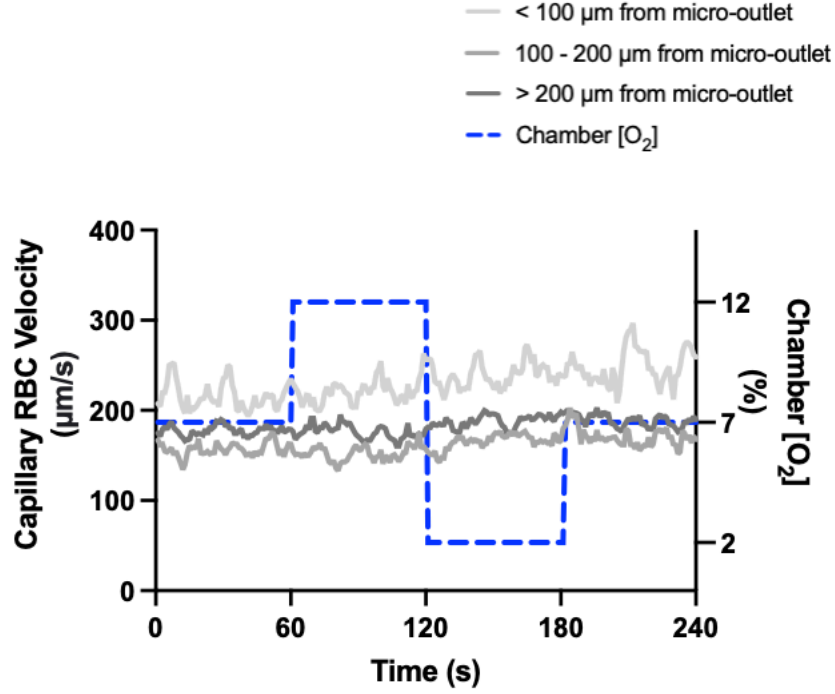
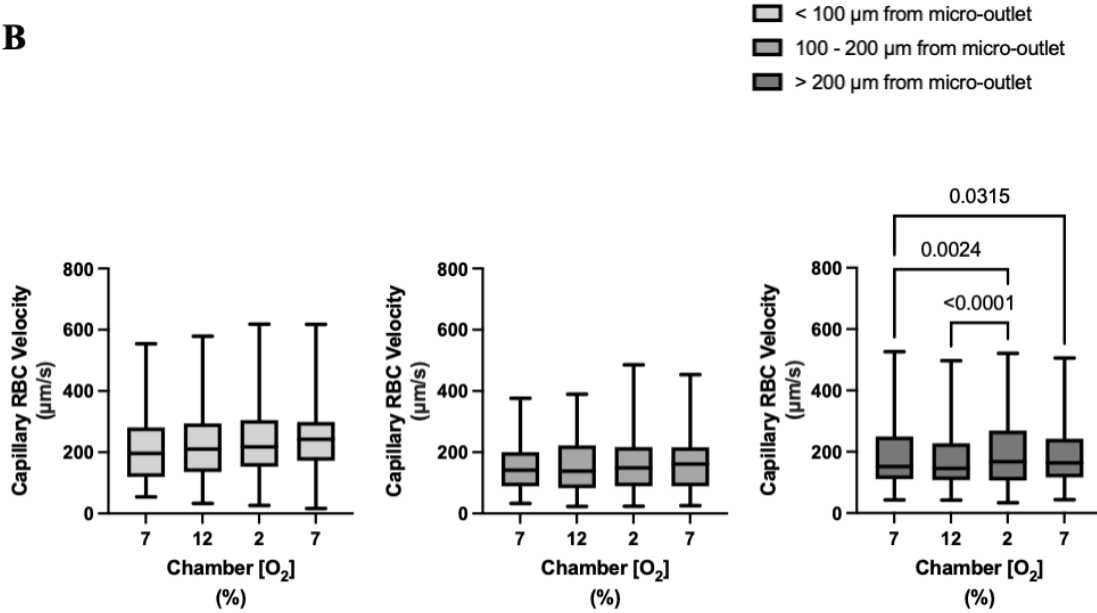
**Figure 2.30 Capillary hematocrit levels in response to oxygen oscillations for capillaries directly overlying the 200  $\mu\text{m}$  micro-outlet.** A) Time series plot showing the mean capillary hematocrit in capillaries overlying the 200  $\mu\text{m}$  micro-outlet across the 4-minute  $\text{O}_2$  oscillation (7-12-2-7%). B) The micro-outlet gas exchange device imposes 4-minute oxygen oscillations for one minute at a baseline concentration of 7%, one minute at 12%, one minute at 2%, and one minute at 7%. Mean hematocrit values are taken from the first entire minute at baseline and the last 15 seconds at 12%, 2%, and 7% ( $n = 46$  capillaries).  $p$  values based on Dunn's multiple comparisons test after significant Friedman test are indicated in the figure with a  $p < 0.05$  considered to be significant.

**A****B**

**Figure 2.31 Capillary hematocrit values in capillaries at various distances outside the 200  $\mu\text{m}$  micro-outlet edge.** A) Time series plot showing the mean capillary hematocrit levels in capillaries outside the 200  $\mu\text{m}$  micro-outlet edge across the 4-minute  $\text{O}_2$  oscillation (7-12-2-7%). B) The micro-outlet gas exchange device imposes 4-minute oxygen oscillations for one minute at a baseline concentration of 7%, one minute at 12%, one minute at 2%, and one minute at 7%. Mean hematocrit values are taken from the first entire minute at baseline and the last 15 seconds at 12%, 2%, and 7%. Panel B shows capillaries within 100  $\mu\text{m}$  from the micro-outlet edge ( $n = 35$  capillaries), capillaries between 100 – 200  $\mu\text{m}$  from the outlet edge ( $n = 56$  capillaries), and capillaries greater than 200  $\mu\text{m}$  from the outlet edge ( $n = 78$  capillaries) respectively.  $p$  values based on Dunn's multiple comparisons test after significant Friedman test are indicated in the figure with a  $p < 0.05$  considered to be significant.



**Figure 2.32 Capillary RBC velocity for capillaries overlying the 200  $\mu\text{m}$  micro-outlet following 4-minute oxygen oscillations.** A) Time series plot showing the mean RBC velocity for capillaries overlying the 200  $\mu\text{m}$  micro-outlet across the 4-minute  $\text{O}_2$  oscillation (7-12-2-7%). B) Oxygen oscillations consisted of one minute at a baseline oxygen concentration of 7% and one minute at 12%, 2%, and 7% oxygen concentration. The average was taken from the entire first minute at a baseline 7% and the last 15 seconds of each of the following oxygen concentrations at 12%, 2%, and 7% ( $n = 46$  capillaries).  $p$  values based on Dunn's multiple comparisons test after significant Friedman test are indicated in the figure with a  $p < 0.05$  considered to be significant. Box and whisker plots show minimum, median, maximum, and associated quartiles.

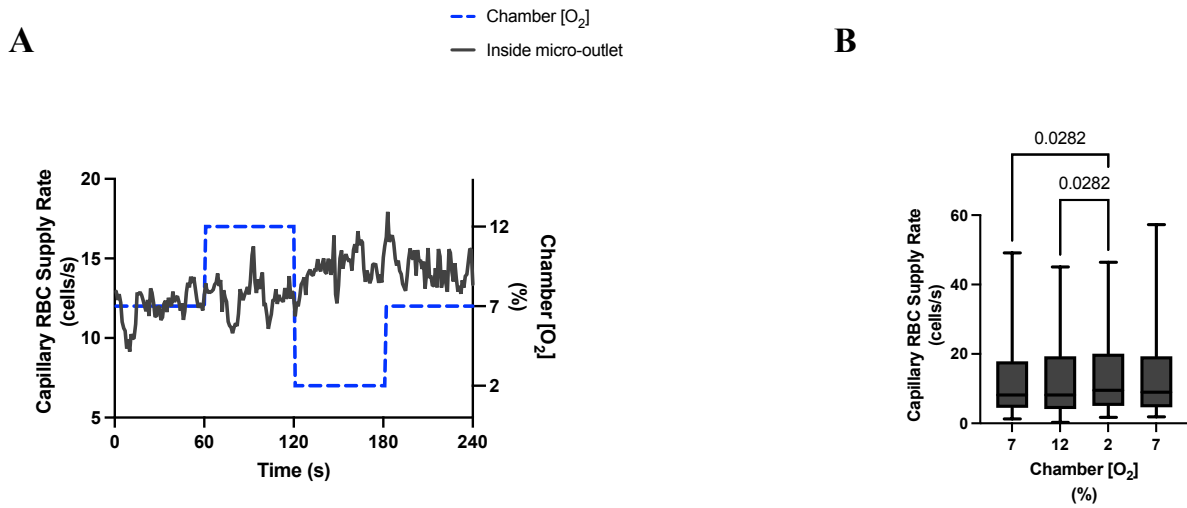
**A****B**

**Figure 2.33 Capillary RBC velocity for capillaries outside the 200  $\mu\text{m}$  micro-outlet at varying distances from the outlet edge following 4-minute oxygen oscillations.** A) Time series plot showing the mean RBC velocity for capillaries outside the 200  $\mu\text{m}$  micro-outlet at varying distances across the 4-minute  $\text{O}_2$  oscillation (7-12-2-7%). B) Oscillations consisted of one minute at a baseline oxygen concentration of 7% followed by one minute at 12%, 2%, and 7% oxygen concentration. The mean was calculated for the first minute at 7% and the last 15 seconds of the following oxygen concentrations of 12%, 2%, and 7%. Panel A shows capillaries within 100  $\mu\text{m}$  from the micro-outlet edge ( $n = 35$  capillaries), panel B shows capillaries between 100 – 200  $\mu\text{m}$  from the outlet edge ( $n = 56$  capillaries), and panel C shows capillaries greater than 200  $\mu\text{m}$  from the outlet edge ( $n = 78$  capillaries).  $p$  values based on Dunn's multiple comparisons test after significant Friedman test are indicated in the figure with a  $p < 0.05$  considered to be significant. Box and whisker plots show minimum, median, maximum, and associated quartiles.

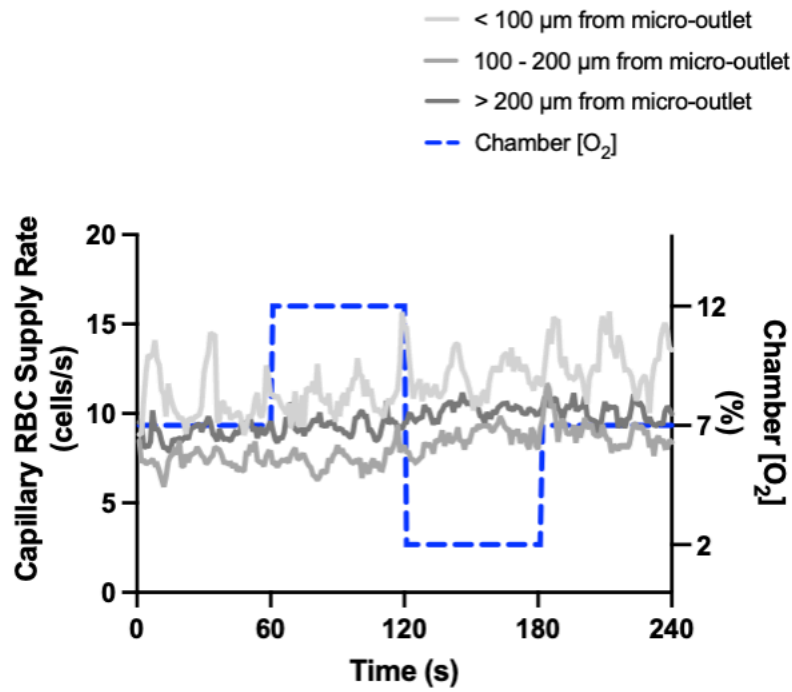
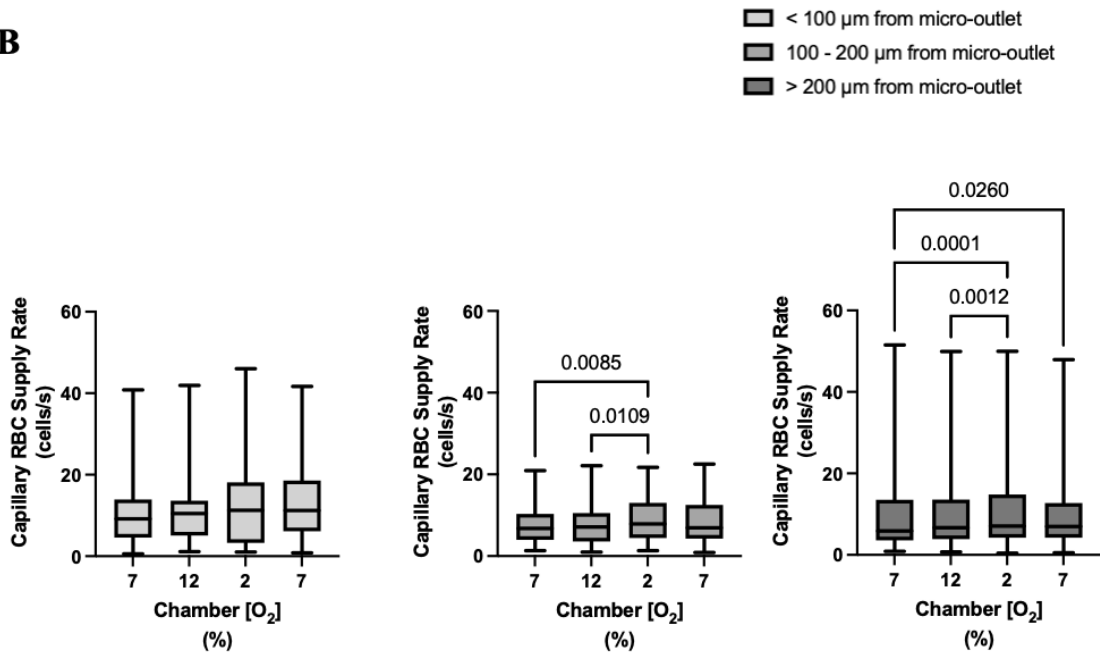
O<sub>2</sub> oscillations imposed on capillaries directly overlying 200 μm micro-outlets caused significant changes in capillary supply rate in the capillaries overlying the micro-outlet at 2% GEC [O<sub>2</sub>], 14.35 ± 12.87 cells/s, compared to baseline 7% GEC [O<sub>2</sub>], 12.00 ± 11.10 cells/s, and between 12% GEC [O<sub>2</sub>], 12.60 ± 12.30 cells/s, and 2% GEC [O<sub>2</sub>], 14.35 ± 12.87 cells/s ( $p = 0.0282$ ) (Figure 2.34).

O<sub>2</sub> oscillations imposed on capillaries directly overlying 200 μm micro-outlets caused no significant changes in the capillary supply rate in the capillaries less than 100 μms away. There were significant changes in capillary supply rate in vessels between 100 to 200 μms away at 2% GEC [O<sub>2</sub>], 8.75 ± 5.44 cells/s compared to baseline 7% GEC [O<sub>2</sub>], 7.43 ± 4.56 cells/s as well as at 12% GEC [O<sub>2</sub>], 7.78 ± 4.88 cells/s, compared to 2% GEC [O<sub>2</sub>], 8.75 ± 5.44 cells/s ( $p < 0.0109$ ) (Figure 2.35).

In vessels greater than 200 μms away at 2% GEC [O<sub>2</sub>], 10.23 ± 8.59 cells/s, and 7% GEC [O<sub>2</sub>], 9.82 ± 8.35 cells/s, compared to baseline 7% GEC [O<sub>2</sub>] 8.98 ± 8.29 cells/s and at 12% GEC [O<sub>2</sub>], 9.27 ± 8.25 cells/s, compared to 2% GEC [O<sub>2</sub>], 10.23 ± 8.59 cells/s ( $p < 0.0061$ ) (Figure 2.35).



**Figure 2.34 Capillary RBC supply rate for capillaries overlying the 200  $\mu\text{m}$  micro-outlet following 4-minute oxygen oscillations.** A) Time series plot showing mean RBC supply rate for capillaries overlying the 200  $\mu\text{m}$  micro-outlet across the 4-minute  $\text{O}_2$  oscillation (7-12-2-7%). B) Oxygen oscillations consisted of one minute at a baseline oxygen concentration of 7% and one minute at 12%, 2%, and 7% oxygen concentration. The mean was calculated for the first minute at a baseline 7% and the last 15 seconds of each of the following oxygen concentrations at 12%, 2%, and 7% ( $n = 46$  capillaries).  $p$  values based on Dunn's multiple comparisons test after the significant Friedman test are indicated in the figure with a  $p < 0.05$  considered to be significant. Box and whisker plots show minimum, median, maximum, and associated quartiles.

**A****B**

**Figure 2.35 Capillary RBC supply rate for capillaries outside the 200  $\mu\text{m}$  micro-outlet at varying distances from the outlet edge following 4-minute oxygen oscillations. A)**

Time series plot showing mean RBC supply rate for capillaries outside the 200  $\mu\text{m}$  micro-outlet at varying distances across the 4-minute  $\text{O}_2$  oscillation (7-12-2-7%). B) Oscillations consisted of one minute at a baseline oxygen concentration of 7% followed by one minute at 12%, 2%, and 7% oxygen concentration. The mean was calculated for the first minute at 7% and the last 15 seconds of the following oxygen concentrations of 12%, 2%, and 7%. Panel B shows capillaries within 100  $\mu\text{m}$  from the micro-outlet edge ( $n = 35$  capillaries), capillaries between 100 – 200  $\mu\text{m}$  from the outlet edge ( $n = 56$  capillaries), and capillaries greater than 200  $\mu\text{m}$  from the outlet edge respectively ( $n = 78$  capillaries).  $p$  values based on Dunn's multiple comparisons test after significant Friedman test are indicated in the figure with a  $p < 0.05$  considered to be significant. Box and whisker plots show minimum, median, maximum, and associated quartiles.

### 2.3.5 RESULTS: 200 $\mu$ M MICRO-OUTLET OXYGEN CHALLENGE DATA

Oxygen ( $O_2$ ) challenge data utilizing 200- $\mu$ m micro-outlets for oxygen saturation ( $SO_2$ ) measurements consisted of 167 capillaries for 7-12% and 175 capillaries for 7-2% across 5 animals. A total of 44 capillaries were sampled in high  $O_2$  challenges (7-12%) and 43 in low  $O_2$  challenges (7-2%) capillaries were analyzed directly overlying the window. Concerning capillaries measured outside the outlet edge for high oxygen challenges, 37 were measured less than 100  $\mu$ ms away, 38 were between 100 – 200  $\mu$ ms away, and 48 were greater than 200  $\mu$ ms away. Concerning capillaries measured outside the outlet edge for low oxygen challenges, 41 were measured less than 100  $\mu$ ms away, 34 were between 100 – 200  $\mu$ ms away, and 57 were greater than 200  $\mu$ ms away.

$O_2$  challenges imposed on capillaries directly overlying 200  $\mu$ m micro-outlets caused significant changes in capillary  $SO_2$  at 12% GEC [ $O_2$ ],  $80.00 \pm 13.93\%$ , compared to baseline 7% GEC [ $O_2$ ],  $60.74 \pm 16.74\%$  ( $p < 0.0001$ ) (Figure 2.36).  $O_2$  challenges imposed on capillaries directly overlying 200  $\mu$ m micro-outlets caused significant changes in capillary  $SO_2$  at 2% GEC [ $O_2$ ],  $43.73 \pm 18.65\%$ , compared to baseline 7% GEC [ $O_2$ ],  $65.26 \pm 13.03\%$  ( $p < 0.0001$ ) (Figure 2.38).

$O_2$  challenges imposed on capillaries directly overlying 200  $\mu$ m micro-outlets caused significant changes in capillary  $SO_2$  at 12% GEC [ $O_2$ ],  $47.21 \pm 20.56\%$ , compared to baseline 7% GEC [ $O_2$ ],  $42.24 \pm 17.57\%$  in capillaries less than 100  $\mu$ ms away from the outlet edge ( $p = 0.0008$ ) (Figure 2.37). There were no significant changes in capillary  $SO_2$  at 2% GEC [ $O_2$ ], compared to baseline 7% GEC [ $O_2$ ], in capillaries outside the micro-outlet at any distance from edge (Figure 2.39).

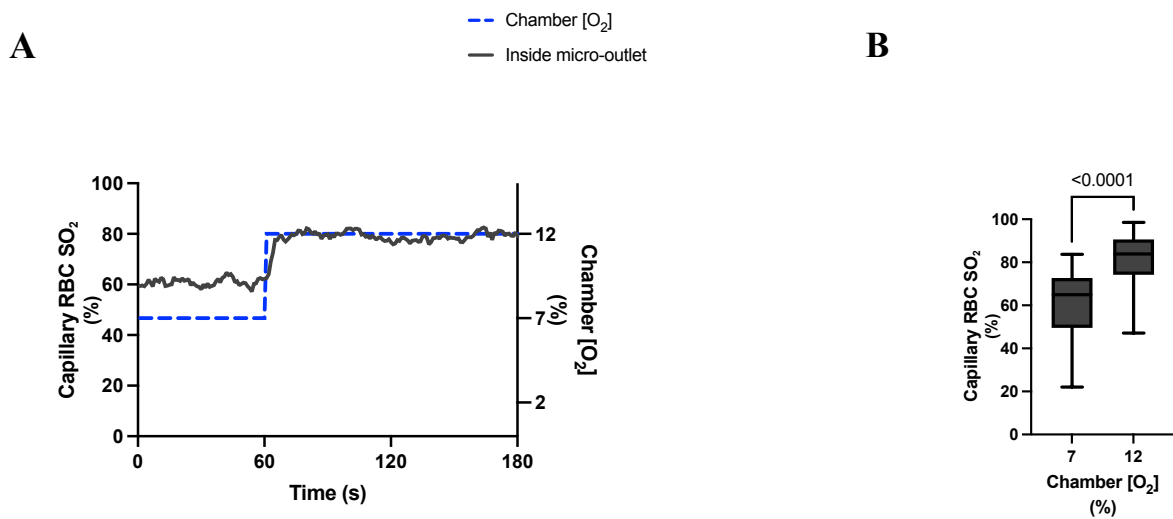
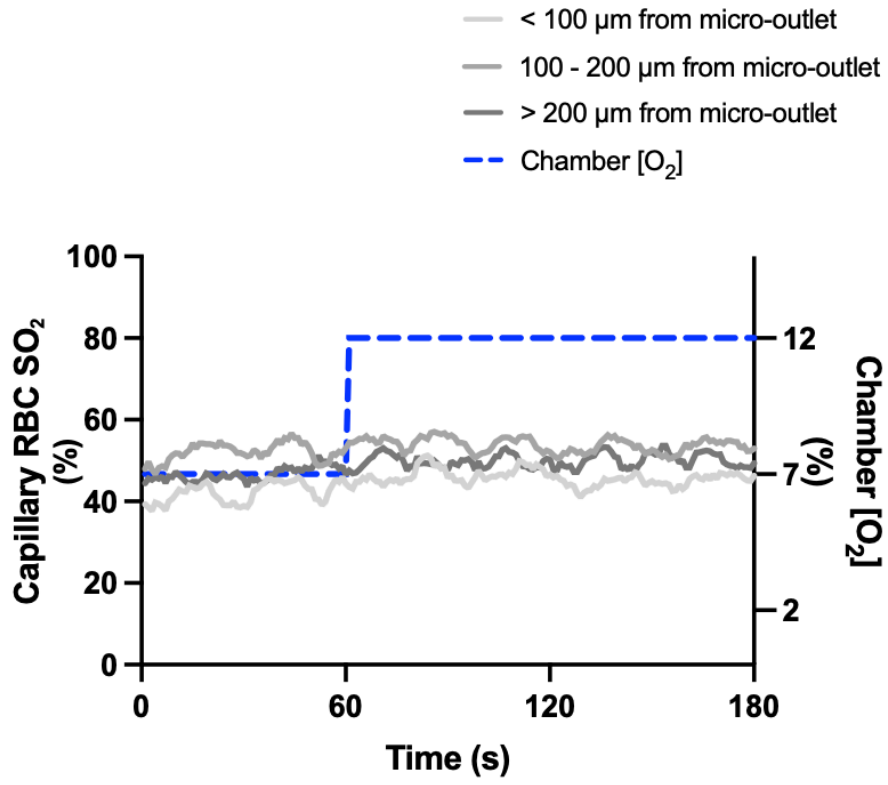
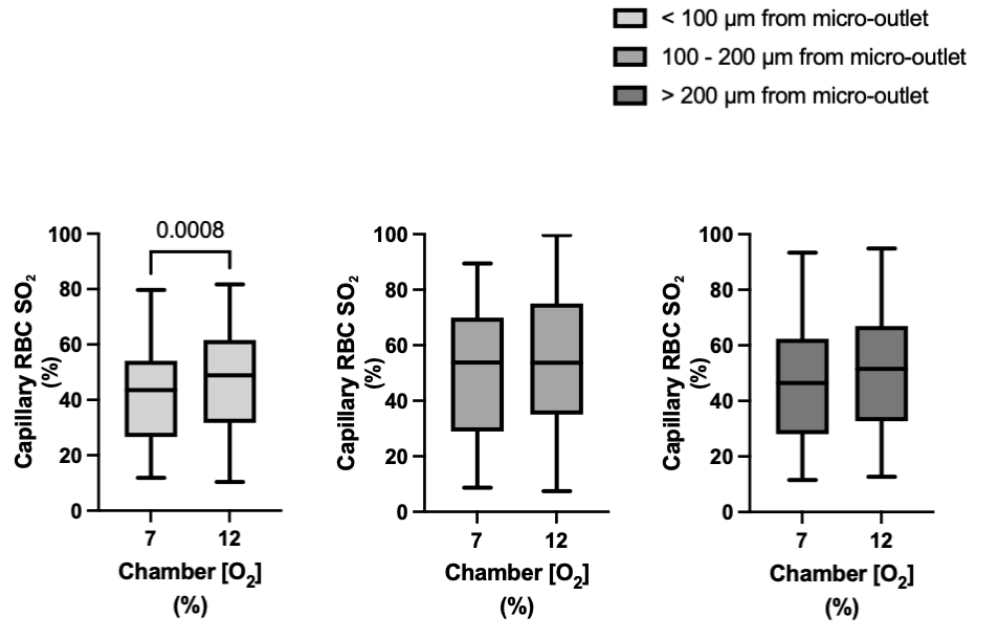


**Figure 2.36 Capillary RBC oxygen saturation in response to high oxygen challenges for capillaries directly overlying the 200  $\mu\text{m}$  micro-outlet.** A) Time series plot showing mean capillary RBC oxygen saturation ( $\text{SO}_2$ ) for capillaries overlying the micro-outlet in response to high (7-12%) oxygen challenges. B) Oxygen challenges consisted of one minute at a baseline oxygen concentration of 7% followed by two minutes at 12%. The mean was calculated for the first minute at 7% and the last 15 seconds at a 12% oxygen concentration ( $n = 44$  capillaries).  $p$  values based on paired t-tests and values indicated in the figure with a  $p < 0.05$  are considered significant. Box and whisker plots show minimum, median, maximum, and associated quartiles.

**A**



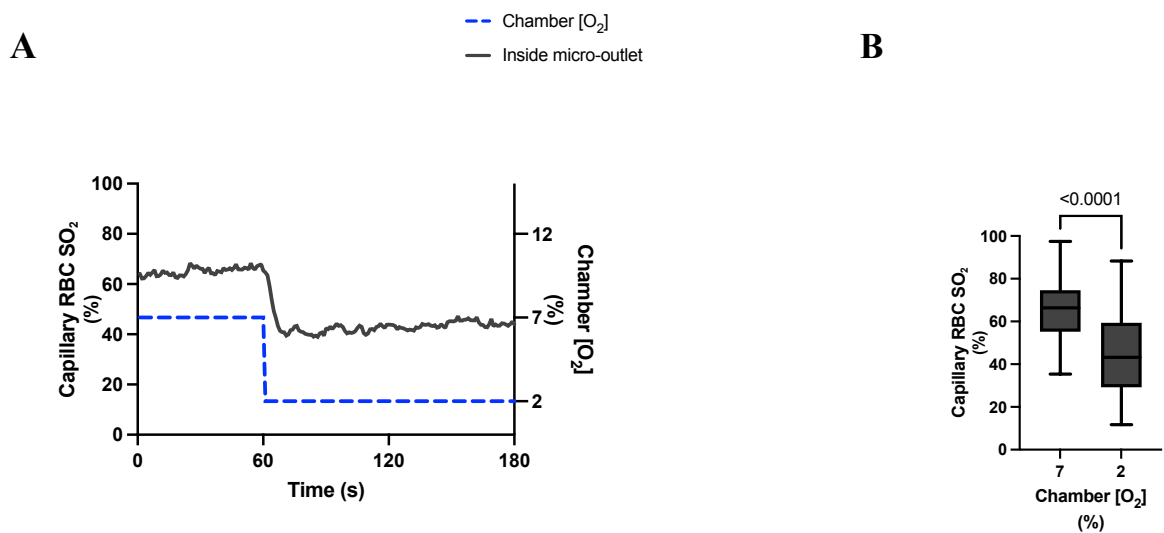
**B**



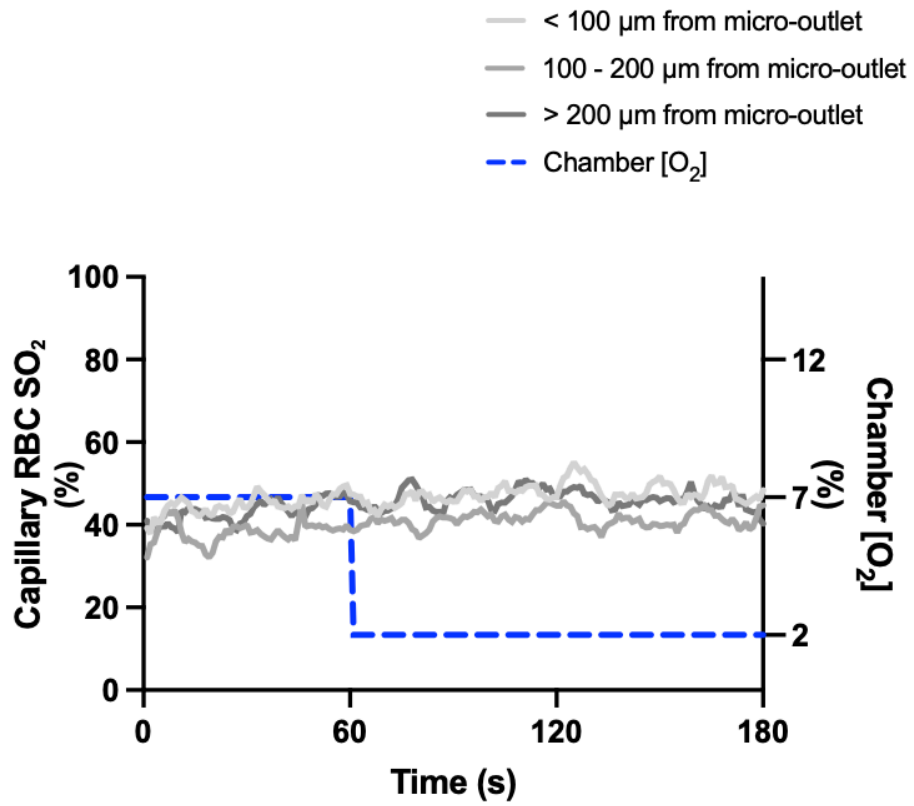
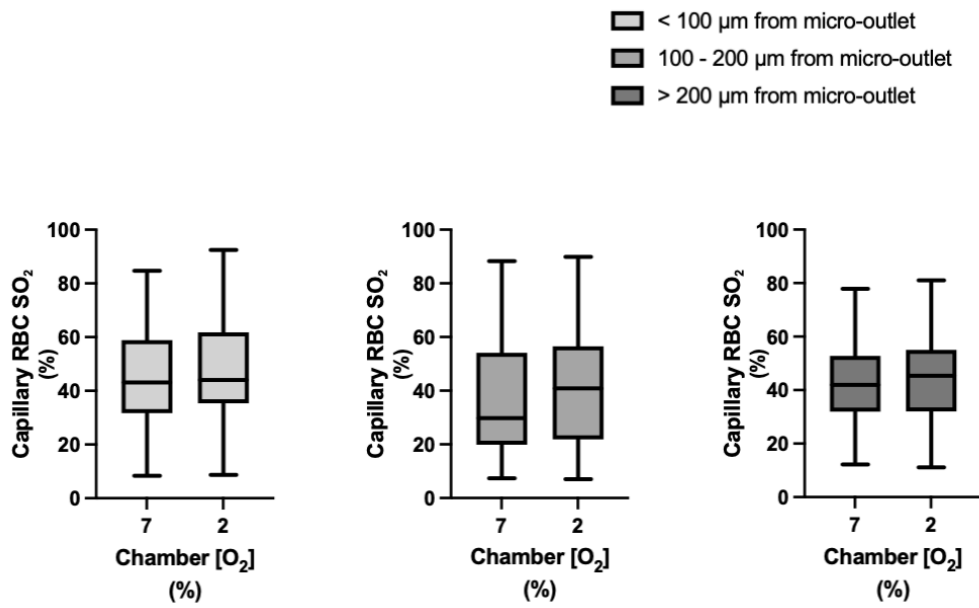
**Figure 2.37 Capillary RBC oxygen saturation responses in capillaries at various distances outside the 200  $\mu\text{m}$  micro-outlet edge in response to high oxygen challenges.**

A) Time series plot showing mean capillary RBC oxygen saturation ( $\text{SO}_2$ ) for capillaries outside the micro-outlet edge at varying distances during high (7-12%) oxygen challenges.

B) Oxygen challenges consisted of one minute at a baseline oxygen concentration of 7% followed by one minute at 12%. The mean was calculated for the first minute at 7% and the last 15 seconds at a 12% oxygen concentration. Panel B shows capillaries within 100  $\mu\text{m}$  from the micro-outlet edge ( $n = 37$  capillaries), capillaries between 100 – 200  $\mu\text{m}$  from the outlet edge ( $n = 38$  capillaries), and capillaries greater than 200  $\mu\text{m}$  from the outlet edge ( $n = 48$  capillaries) respectively.  $p$  values based on paired t-tests and values indicated in the figure with a  $p < 0.05$  considered significant. Box and whisker plots show minimum, median, maximum, and associated quartiles.



**Figure 2.38 Capillary RBC oxygen saturation in response to low oxygen challenges for capillaries directly overlying the 200  $\mu\text{m}$  micro-outlet.** A) Time series plot showing mean capillary RBC oxygen saturation (SO<sub>2</sub>) for capillaries overlying the micro-outlet during low (7-2%) oxygen challenges. B) Oxygen challenges consisted of one minute at a baseline oxygen concentration of 7% followed by two minutes at 2%. The mean was calculated for the first minute at 7% and the last 15 seconds at a 2% oxygen concentration (n = 43 capillaries). *p* values based on paired t-tests and values indicated in the figure with a *p* < 0.05 are significant. Box and whisker plots show minimum, median, maximum, and associated quartiles.

**A****B**

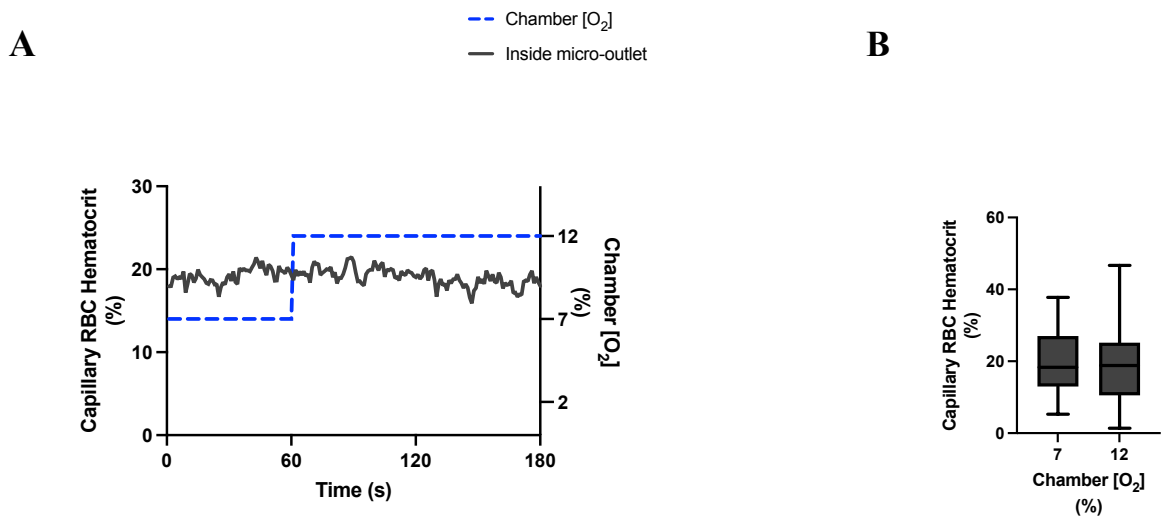
**Figure 2.39 Capillary RBC oxygen saturation responses in capillaries at various distances outside the 200  $\mu\text{m}$  micro-outlet edge in response to low oxygen challenges.**

A) Time series plot showing mean capillary RBC oxygen saturation ( $\text{SO}_2$ ) for capillaries outside the micro-outlet edge at varying distances during low (7-2%) oxygen challenges.

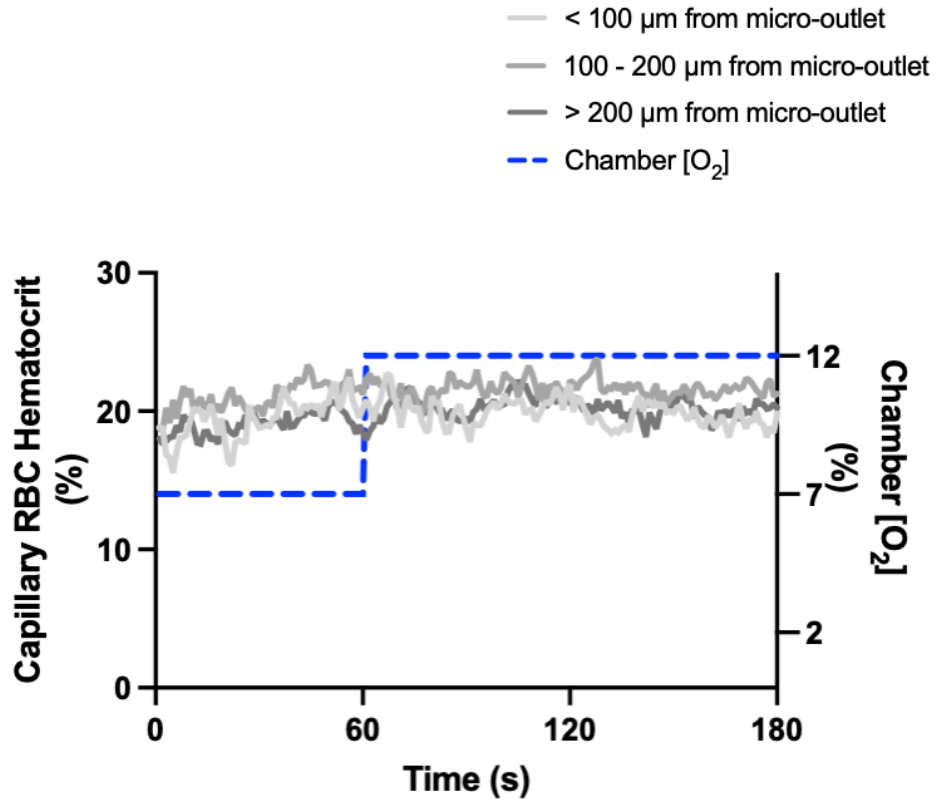
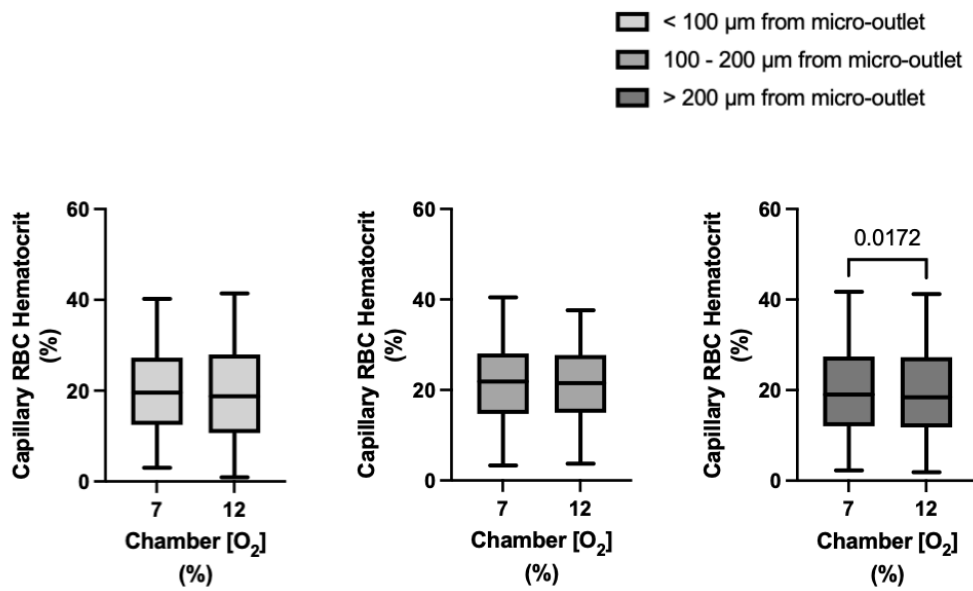
B) Oxygen challenges consisted of one minute at a baseline oxygen concentration of 7% followed by two minutes at 2%. The average was taken from the entire first minute at 7% and the last 15 seconds at a 2% oxygen concentration. Panel B shows capillaries within 100  $\mu\text{m}$  from the micro-outlet edge ( $n = 41$  capillaries), capillaries between 100 – 200  $\mu\text{m}$  from the outlet edge ( $n = 34$  capillaries), and capillaries greater than 200  $\mu\text{m}$  from the outlet edge ( $n = 57$  capillaries), respectively.  $p$  values based on paired t-tests and values indicated in the figure with a  $p < 0.05$  are considered significant. Box and whisker plots show minimum, median, maximum, and associated quartiles.

Oxygen (O<sub>2</sub>) challenge data utilizing 200- $\mu$ m micro-outlets for hemodynamic measurements consisted of a total of 388 capillaries across 5 animals. A total of 42 for high and 53 capillaries for low O<sub>2</sub> challenges were analyzed directly overlying the window. Concerning capillaries measured outside the outlet edge during high challenges, 31 were measured less than 100  $\mu$ m away, 54 were between 100 – 200  $\mu$ m away, and 68 were greater than 200  $\mu$ m away. Concerning capillaries measured outside the outlet edge during low challenges, 30 were measured less than 100  $\mu$ m away, 38 were between 100 – 200  $\mu$ m away, and 72 were greater than 200  $\mu$ m away.

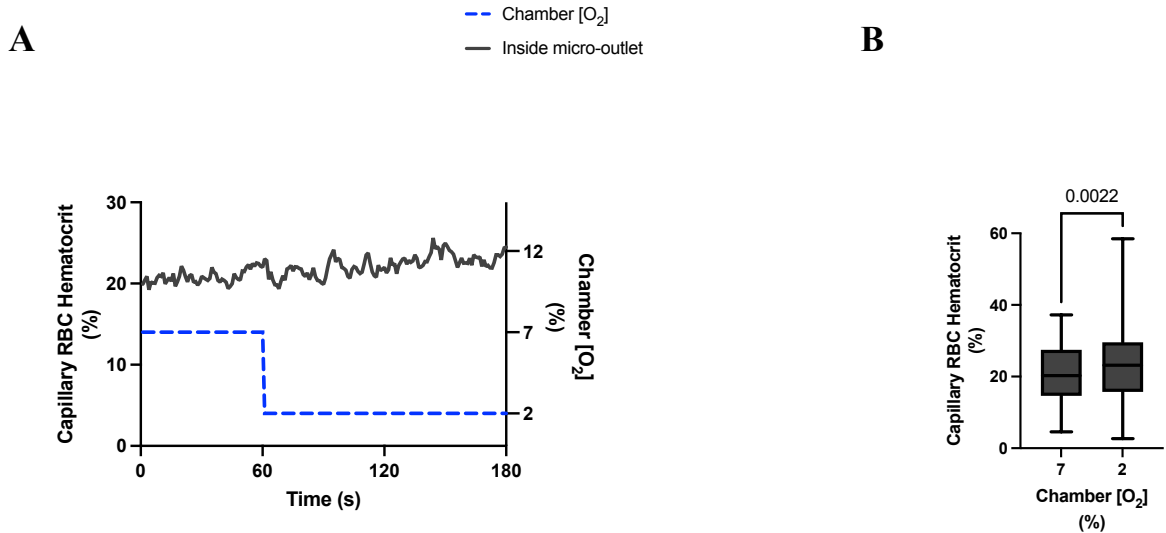
O<sub>2</sub> challenges imposed on capillaries directly overlying 200  $\mu$ m micro-outlets caused significant changes in capillary hematocrit in vessels greater than 200  $\mu$ m away at 12% GEC [O<sub>2</sub>],  $20.13 \pm 9.55\%$ , compared to baseline 7% GEC [O<sub>2</sub>],  $19.13 \pm 9.49\%$  ( $p = 0.0172$ ) (Figure 2.41). O<sub>2</sub> challenges imposed on capillaries directly overlying 200  $\mu$ m micro-outlets caused significant changes in capillary hematocrit at 2% GEC [O<sub>2</sub>],  $22.88 \pm 10.18\%$ , compared to baseline 7% GEC [O<sub>2</sub>],  $20.69 \pm 8.53\%$  ( $p = 0.0022$ ) (Figure 2.42). O<sub>2</sub> challenges imposed on capillaries directly overlying 200  $\mu$ m micro-outlets caused significant changes in capillary hematocrit in vessels less than 100  $\mu$ m away from the outlet at 2% GEC [O<sub>2</sub>],  $18.93 \pm 10.68\%$ , compared to baseline 7% GEC [O<sub>2</sub>],  $17.77 \pm 10.37\%$  ( $p = 0.0348$ ) (Figure 2.43).



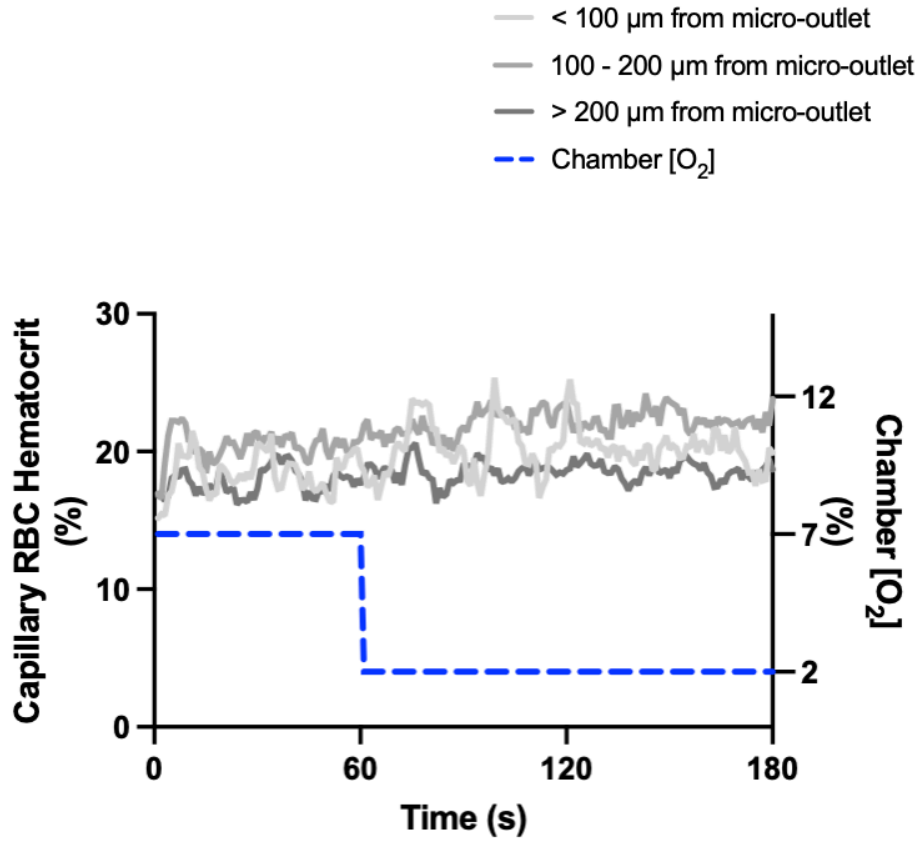
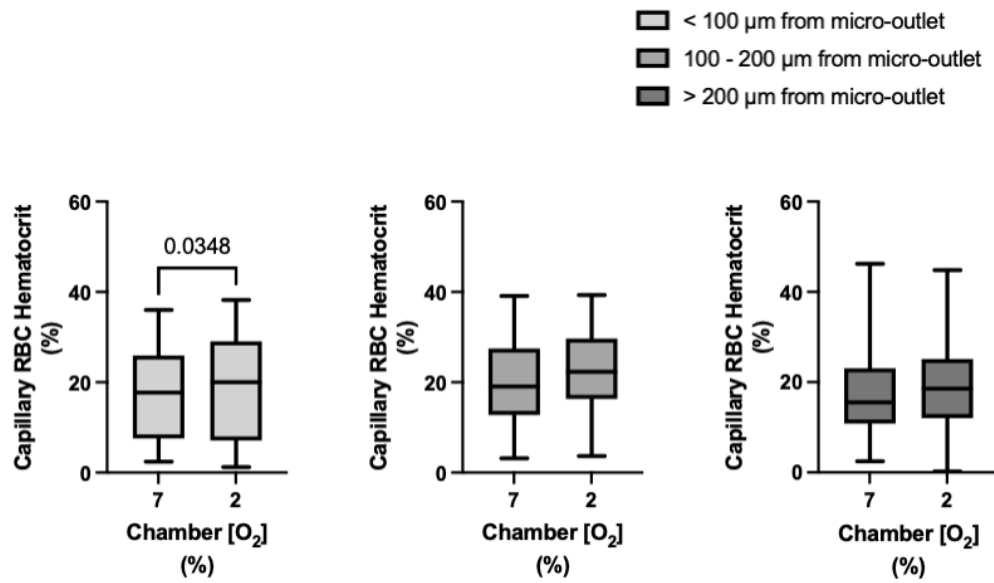
**Figure 2.40 Capillary hematocrit levels in response to high oxygen challenges for capillaries directly overlying the 200  $\mu\text{m}$  micro-outlet.** A) Time series plot showing mean capillary hematocrit levels for capillaries overlying the micro-outlet during high (7-12%) oxygen challenges. B) Oxygen challenges consisted of one minute at a baseline oxygen concentration of 7% followed by two minutes at 12%. The mean was calculated for the first minute at 7% and the last 15 seconds at a 12% oxygen concentration ( $n = 42$  capillaries). Box and whisker plots show minimum, median, maximum, and associated quartiles.

**A****B**

**Figure 2.41 Capillary hematocrit levels in capillaries at various distances outside the 200  $\mu\text{m}$  micro-outlet edge in response to high oxygen challenges.** A) Time series plot showing mean capillary hematocrit levels for capillaries outside the micro-outlet at varying distances during high (7-12%) oxygen challenges. B) Oxygen challenges consisted of one minute at a baseline oxygen concentration of 7% followed by two minutes at 12%. The mean was calculated for the first minute at 7% and the last 15 seconds at a 12% oxygen concentration. Panel B shows capillaries within 100  $\mu\text{m}$  from the micro-outlet edge (n = 31 capillaries), capillaries between 100 – 200  $\mu\text{m}$  from the outlet edge (n = 54 capillaries), and capillaries greater than 200  $\mu\text{m}$  from the outlet edge (n = 68 capillaries) respectively. *p* values based on paired Wilcoxon t-test and values indicated in the figure with a *p* < 0.05 considered to be significant. Box and whisker plots show minimum, median, maximum, and associated quartiles.



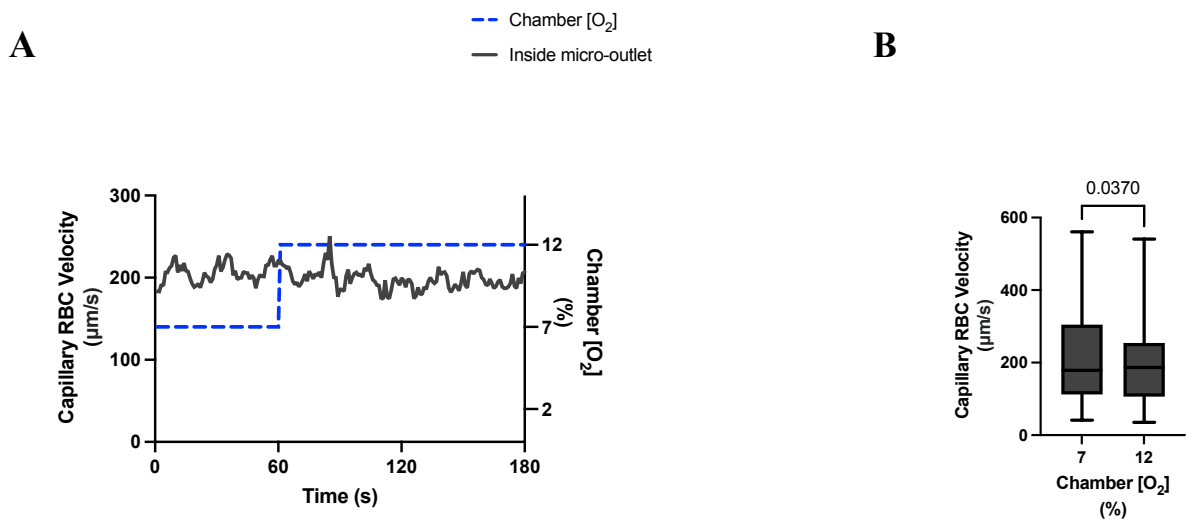
**Figure 2.42 Capillary hematocrit levels in response to low oxygen challenges for capillaries directly overlying the 200  $\mu\text{m}$  micro-outlet.** A) Time series plot showing mean capillary hematocrit levels for capillaries overlying the micro-outlet during low (7-2%) oxygen challenges. B) Oxygen challenges consisted of one minute at a baseline oxygen concentration of 7% followed by two minutes at 2%. The mean was calculated for the first minute at 7% and the last 15 seconds at a 2% oxygen concentration ( $n = 53$  capillaries).  $p$  values based on paired Wilcoxon t-test and values indicated in the figure with a  $p < 0.05$  considered to be significant. Box and whisker plots show minimum, median, maximum, and associated quartiles.

**A****B**

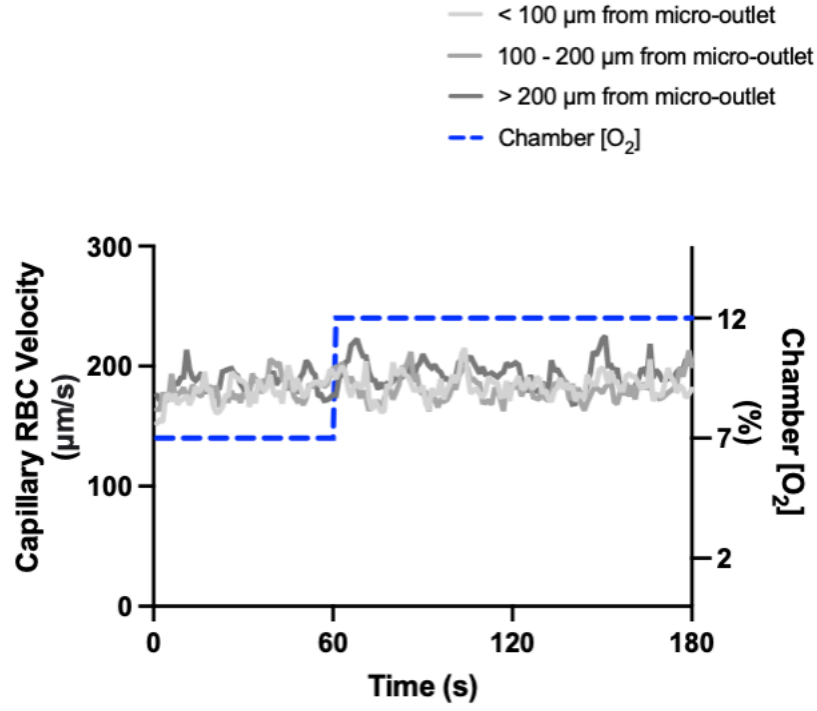
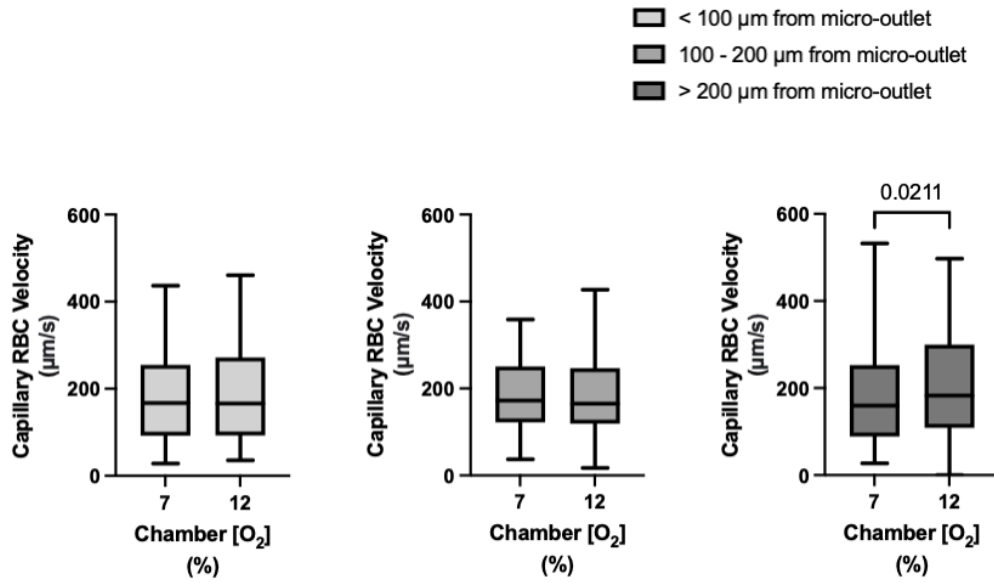
**Figure 2.43 Capillary hematocrit levels in capillaries at various distances outside the 200  $\mu\text{m}$  micro-outlet edge in response to low oxygen challenges.** A) Time series plot showing mean capillary hematocrit levels for capillaries outside the micro-outlet at varying distances during low (7-2%) oxygen challenges. B) Oxygen challenges consisted of one minute at a baseline oxygen concentration of 7% followed by two minutes at 2%. The mean was calculated for the first minute at 7% and the last 15 seconds at a 2% oxygen concentration. Panel B shows capillaries within 100  $\mu\text{m}$  from the micro-outlet edge ( $n = 30$  capillaries), capillaries between 100 – 200  $\mu\text{m}$  from the outlet edge ( $n = 38$  capillaries), and capillaries greater than 200  $\mu\text{m}$  from the outlet edge ( $n = 72$  capillaries) respectively.  $p$  values based on paired Wilcoxon t-test and values indicated in the figure with a  $p < 0.05$  considered to be significant. Box and whisker plots show minimum, median, maximum, and associated quartiles.

O<sub>2</sub> challenges imposed on capillaries directly overlying 200 μm micro-outlets caused significant changes in capillary velocity at 12% GEC [O<sub>2</sub>], 192.7 ± 107.5 μm/s, compared to baseline 7% GEC [O<sub>2</sub>], 207.5 ± 123.7 μm/s ( $p = 0.0370$ ) (Figure 2.44). O<sub>2</sub> challenges imposed on capillaries directly overlying 200 μm micro-outlets caused significant changes in capillary velocity at 2% GEC [O<sub>2</sub>], 293.1 ± 175.6 μm/s, compared to baseline 7% GEC [O<sub>2</sub>], 230.2 ± 141.0 μm/s ( $p < 0.0001$ ) (Figure 2.46)

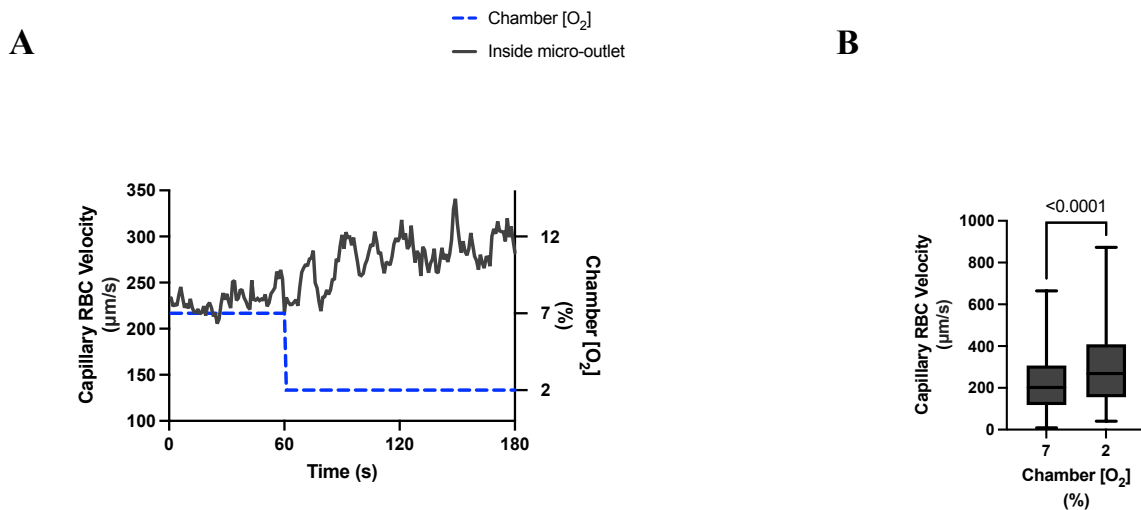
O<sub>2</sub> challenges imposed on 200 μm micro-outlets caused significant changes in capillary velocity in vessels greater than 200 μms away from the outlet at 12% GEC [O<sub>2</sub>], 197.2 ± 117.8 μm/s compared to baseline 7% GEC [O<sub>2</sub>], 183.5 ± 116.5 μm/s ( $p = 0.0211$ ) (Figure 2.45). O<sub>2</sub> challenges imposed on 200 μm micro-outlets caused significant changes in capillary velocity in vessels less than 100 μms away from the outlet at 2% GEC [O<sub>2</sub>], 207.8 ± 123.6 μm/s compared to baseline 7% GEC [O<sub>2</sub>], 182.0 ± 118.9 μm/s, in vessels between 100 – 200 μms away at 2% GEC [O<sub>2</sub>], 223.8 ± 122.3 μm/s, compared to baseline 7% GEC [O<sub>2</sub>], 189.1 ± 95.1 μm/s, and in vessels greater than 200 μms away from the outlet at 2% GEC [O<sub>2</sub>], 225.9 ± 143.8 μm/s compared to baseline 7% GEC [O<sub>2</sub>], 210.1 ± 119.8 μm/s ( $p < 0.0161$ ) (Figure 2.47).



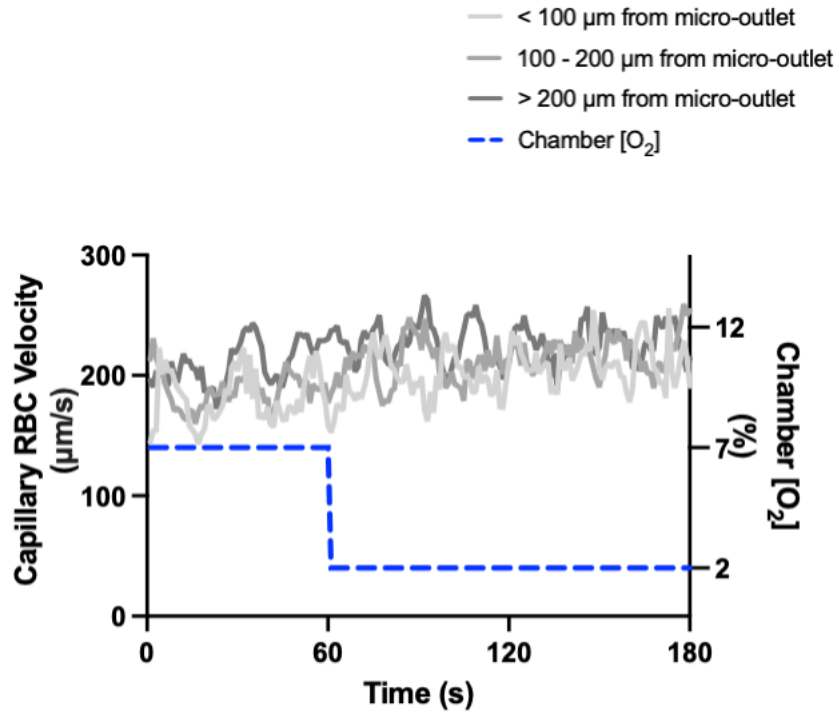
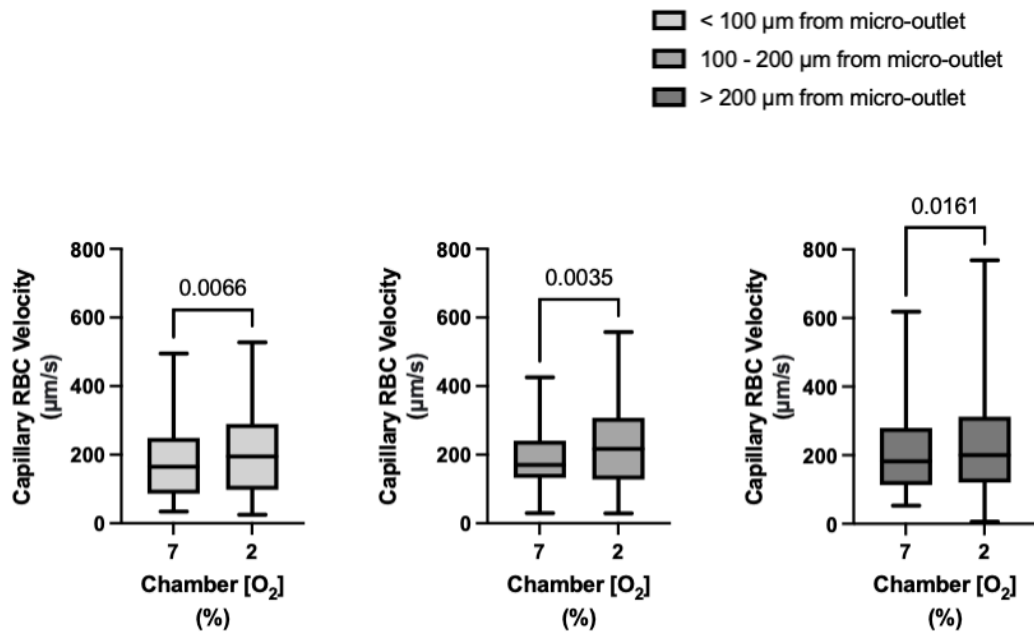
**Figure 2.44 Capillary RBC velocity response to high oxygen challenges for capillaries directly overlying the 200 µm micro-outlet.** A) Time series plot showing mean capillary RBC velocity for capillaries overlying the micro-outlet during high (7-12%) oxygen challenges. B) Oxygen challenges consisted of one minute at a baseline oxygen concentration of 7% followed by two minutes at 12%. The mean was calculated for the first minute at 7% and the last 15 seconds at a 12% oxygen concentration (n = 42 capillaries). *p* values based on paired Wilcoxon t test and values indicated in the figure with a *p* < 0.05 considered to be significant. Box and whisker plots show minimum, median, maximum, and associated quartiles.

**A****B**

**Figure 2.45: Capillary RBC velocity levels in capillaries at various distances outside the 200  $\mu\text{m}$  micro-outlet edge in response to high oxygen challenges.** A) Time series plot showing mean capillary RBC velocity for capillaries outside the micro-outlet at varying distances during high (7-12%) oxygen challenges. B) Oxygen challenges consisted of one minute at a baseline oxygen concentration of 7% followed by two minutes at 12%. The mean was calculated for the first minute at 7% and the last 15 seconds at 12% oxygen concentration. Panel B shows capillaries within 100  $\mu\text{m}$  from the micro-outlet edge ( $n = 31$  capillaries), capillaries between 100 – 200  $\mu\text{m}$  from the outlet edge ( $n = 54$  capillaries), and capillaries greater than 200  $\mu\text{m}$  from the outlet edge ( $n = 68$  capillaries) respectively.  $p$  values based on paired Wilcoxon t test and values indicated in the figure with a  $p < 0.05$  considered to be significant. Box and whisker plots show minimum, median, maximum, and associated quartiles.

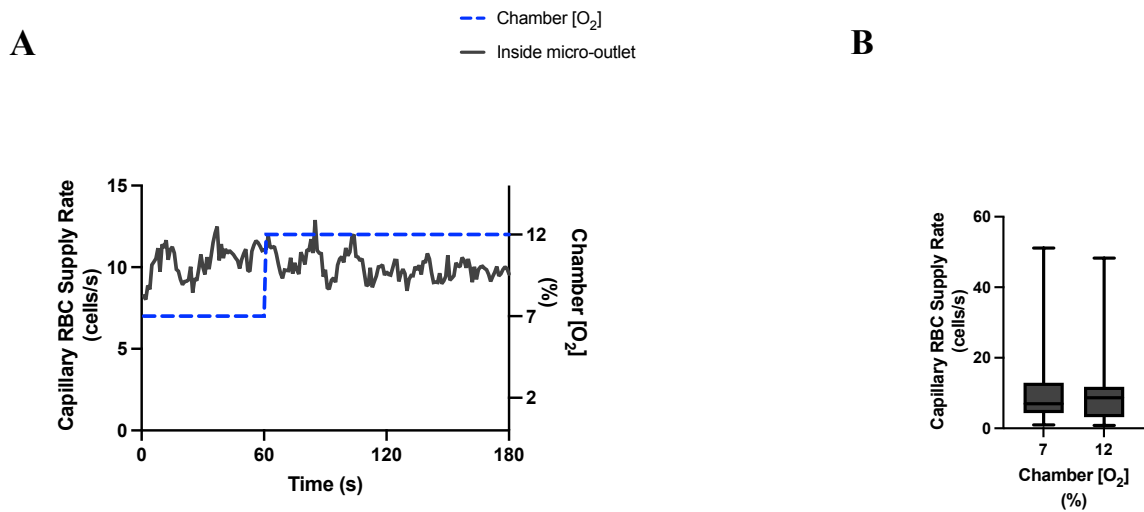


**Figure 2.46 Capillary RBC velocity response to low oxygen challenges for capillaries directly overlying the 200 µm micro-outlet.** A) Time series plot showing mean capillary RBC velocity for capillaries overlying the micro-outlet during low (7-2%) oxygen challenges. B) Oxygen challenges consisted of one minute at a baseline oxygen concentration of 7% followed by two minutes at 2%. The average was calculated for the first minute at 7% and the last 15 seconds at 2% oxygen concentration (n = 53 capillaries). *p* values based on paired Wilcoxon t-test and values indicated in the figure with a *p* < 0.05 considered to be significant. Box and whisker plots show minimum, median, maximum, and associated quartiles.

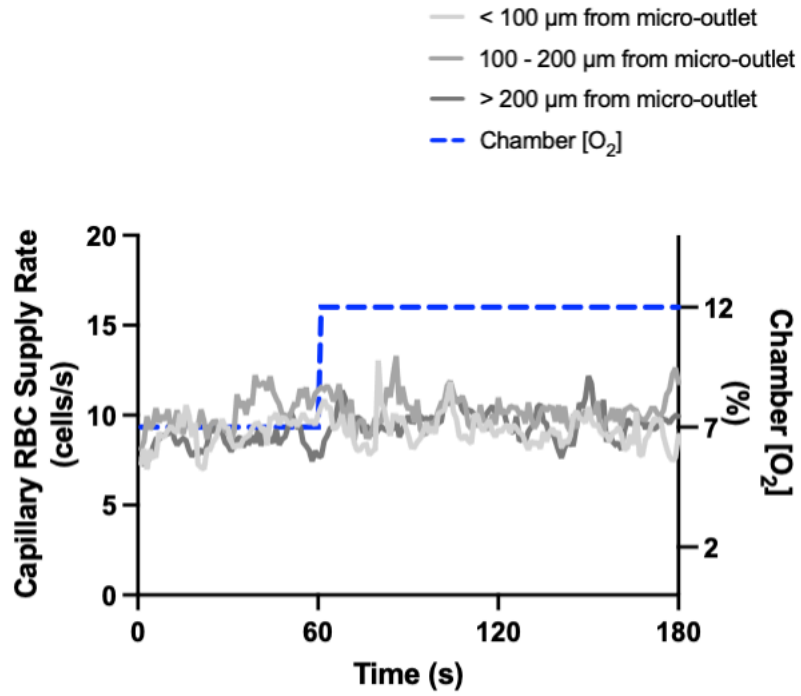
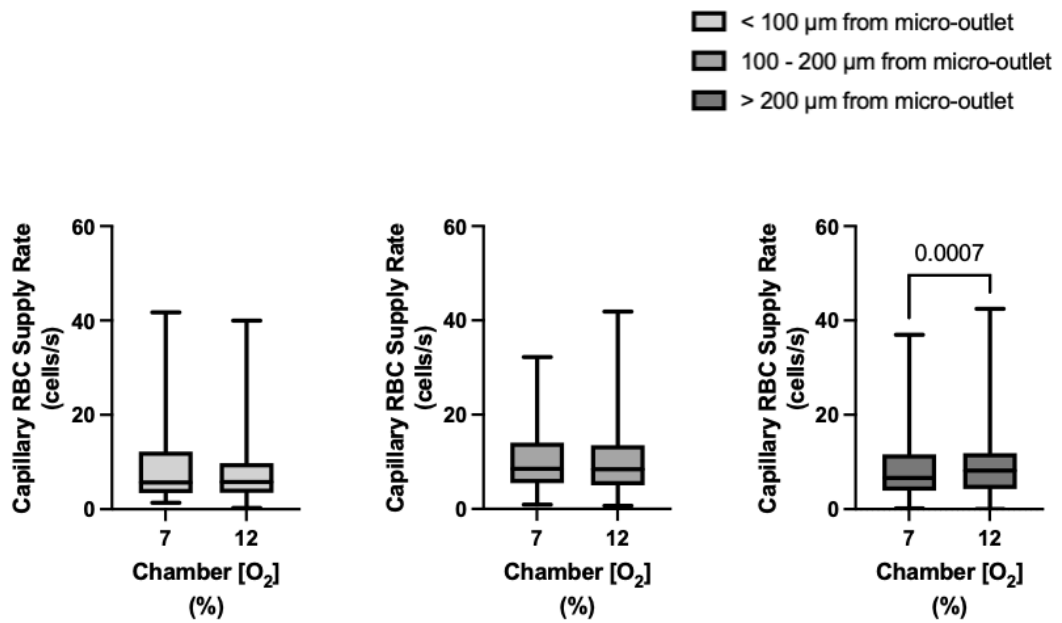
**A****B**

**Figure 2.47 Capillary RBC velocity in capillaries at various distances outside the 200  $\mu\text{m}$  micro-outlet edge in response to low oxygen challenges.** A) Time series plot showing mean capillary RBC velocity for capillaries outside the micro-outlet at varying distances during low (7-2%) oxygen challenges. B) Oxygen challenges consisted of one minute at a baseline oxygen concentration of 7% followed by two minutes at 2%. The mean was calculated for the first minute at 7% and the last 15 seconds at a 2% oxygen concentration. Panel B shows capillaries within 100  $\mu\text{m}$  from the micro-outlet edge ( $n = 30$  capillaries), capillaries between 100 – 200  $\mu\text{m}$  from the outlet edge ( $n = 38$  capillaries), and capillaries greater than 200  $\mu\text{m}$  from the outlet edge ( $n = 72$  capillaries) respectively.  $p$  values based on paired Wilcoxon t-test and values indicated in the figure with a  $p < 0.05$  considered to be significant. Box and whisker plots show minimum, median, maximum, and associated quartiles.

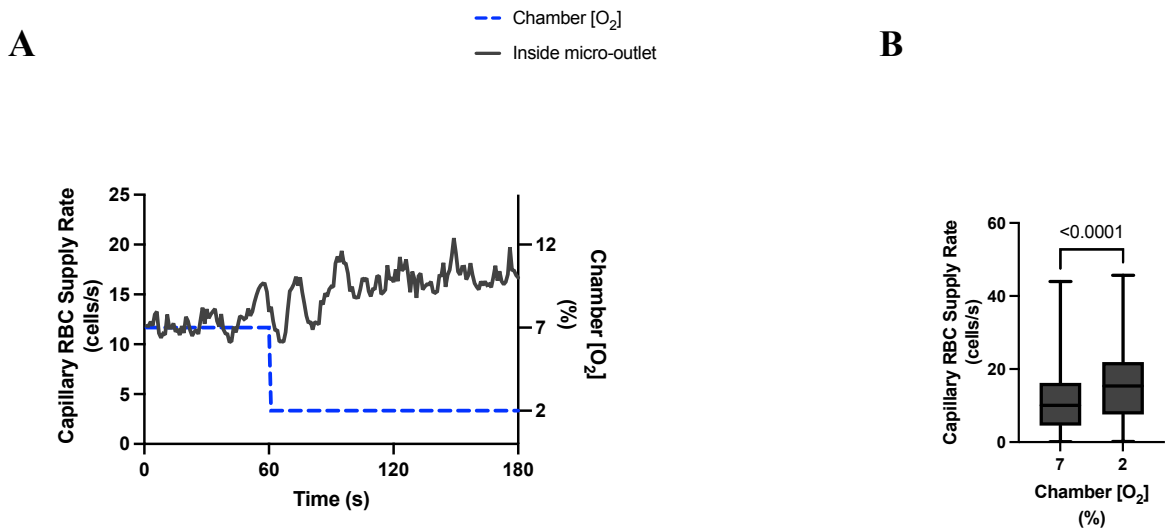
O<sub>2</sub> challenges imposed on capillaries directly overlying 200 μm micro-outlets caused significant changes in capillary supply rate at 2% GEC [O<sub>2</sub>], 17.28 ± 12.29 cells/s, compared to baseline 7% GEC [O<sub>2</sub>], 12.57 ± 10.21 cells/s ( $p < 0.0001$ ) but not at 12% GEC [O<sub>2</sub>] (Figure 2.48, 2.50). O<sub>2</sub> challenges imposed on 200 μm micro-outlets caused significant changes in capillary supply rate for vessels 200 μms away from the outlet edge at 12% GEC [O<sub>2</sub>], 9.62 ± 7.81 cells/s, compared to baseline 7% GEC [O<sub>2</sub>], 8.51 ± 6.93 cells/s ( $p = 0.0007$ ) (Figure 2.49). O<sub>2</sub> challenges imposed on capillaries directly overlying 200 μm micro-outlets caused significant changes in capillary supply rate for outside vessels less than 100 μms away at 2% GEC [O<sub>2</sub>], 11.02 ± 9.26 cells/s, compared to baseline 7% GEC [O<sub>2</sub>], 9.03 ± 8.72 cells/s, in vessels in the 100 to 200 μms range from the outlet edge at 2% GEC [O<sub>2</sub>], 12.19 ± 8.66 cells/s, compared to baseline 7% GEC [O<sub>2</sub>], 9.07 ± 6.84 cells/s, and in vessels greater than 200 μms away at 2% GEC [O<sub>2</sub>], 11.20 ± 11.28 cells/s compared to baseline 7% GEC [O<sub>2</sub>], 9.49 ± 8.68 cells/s ( $p < 0.0248$ ) (Figure 2.51).



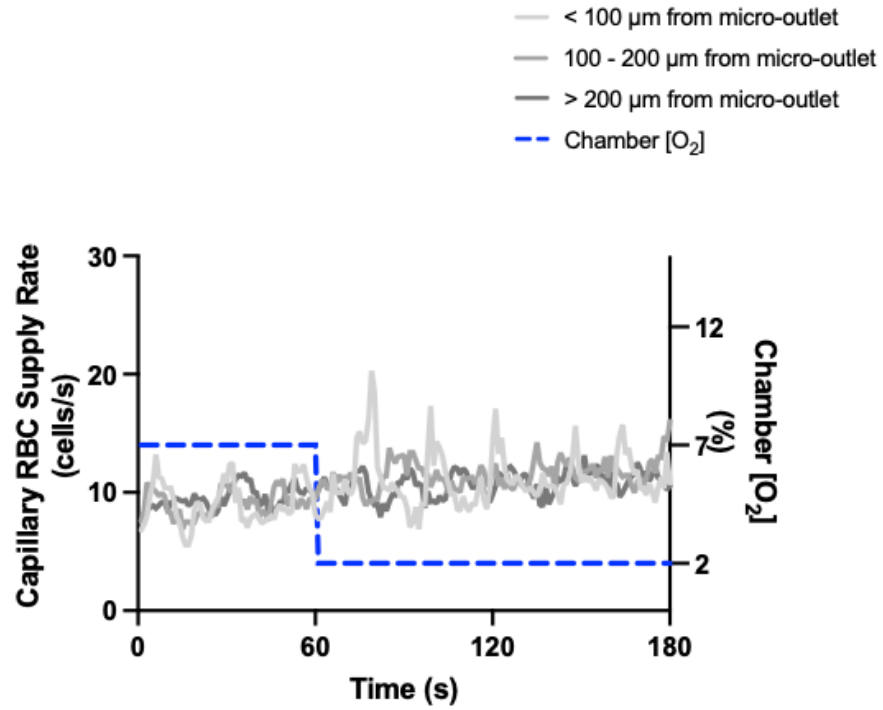
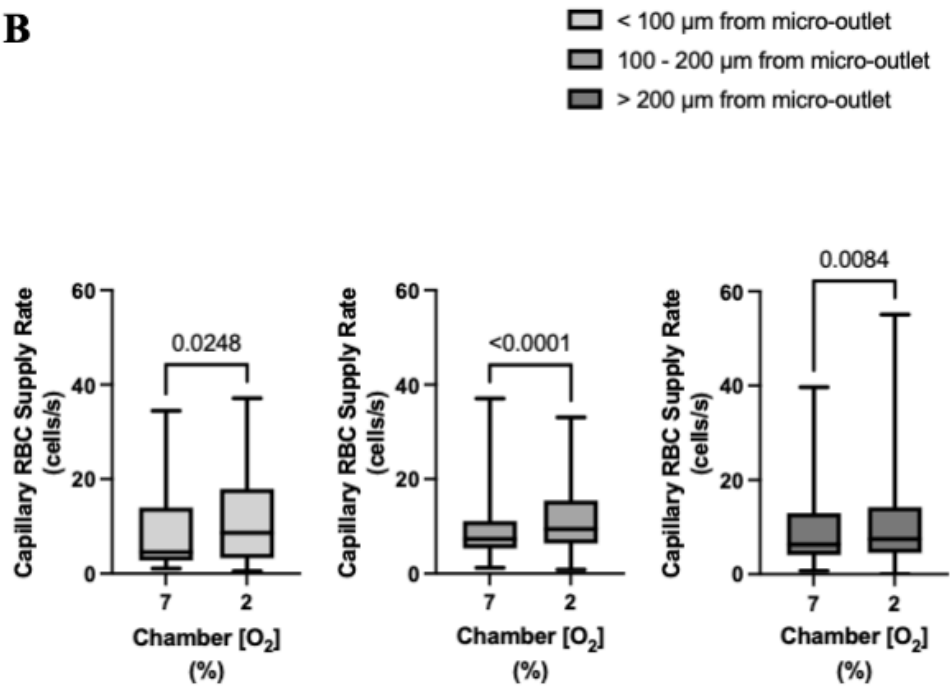
**Figure 2.48 Capillary RBC supply rate response to high oxygen challenges for capillaries directly overlying the 200  $\mu\text{m}$  micro-outlet.** A) Time series plot showing mean capillary RBC supply rate for capillaries overlying the micro-outlet during high (7-12%) oxygen challenges. B) Oxygen challenges consisted of one minute at a baseline oxygen concentration of 7% followed by two minutes at 12%. The mean was calculated for the first minute at 7% and the last 15 seconds at a 12% oxygen concentration ( $n = 42$  capillaries). Box and whisker plots show minimum, median, maximum, and associated quartiles.

**A****B**

**Figure 2.49 Capillary RBC supply rate in capillaries at various distances outside the 200  $\mu\text{m}$  micro-outlet edge in response to high oxygen challenges.** A) Time series plot showing mean capillary RBC supply rate for capillaries outside the micro-outlet at varying distances during high (7-12%) oxygen challenges. B) Oxygen challenges consisted of one minute at a baseline oxygen concentration of 7% followed by two minutes at 12%. The mean was calculated for the first minute at 7% and the last 15 seconds at a 12% oxygen concentration. Panel B shows capillaries within 100  $\mu\text{m}$  from the micro-outlet edge ( $n = 31$  capillaries), capillaries between 100 – 200  $\mu\text{m}$  from the outlet edge ( $n = 54$  capillaries), and capillaries greater than 200  $\mu\text{m}$  from the outlet edge ( $n = 68$  capillaries) respectively.  $p$  values based on paired Wilcoxon t test and values indicated in the figure with a  $p < 0.05$  considered to be significant. Box and whisker plots show minimum, median, maximum, and associated quartiles.



**Figure 2.50 Capillary RBC supply rate in response to low oxygen challenges for capillaries directly overlying the 200  $\mu\text{m}$  micro-outlet.** A) Time series plot showing mean capillary RBC supply rate for capillaries overlying the micro-outlet during low (7-2%) oxygen challenges. B) Oxygen challenges consisted of one minute at a baseline oxygen concentration of 7% followed by two minutes at 2%. The mean was calculated for the first minute at 7% and the last 15 seconds at a 2% oxygen concentration ( $n = 53$  capillaries).  $p$  values based on paired Wilcoxon t test and values indicated in the figure with a  $p < 0.05$  considered to be significant. Box and whisker plots show minimum, median, maximum, and associated quartiles.

**A****B**

**Figure 2.51 Capillary RBC supply rate in capillaries at various distances outside the 200  $\mu\text{m}$  micro-outlet edge in response to low oxygen challenges.** A) Time series plot showing mean capillary RBC supply rate for capillaries outside the micro-outlet at varying distances during low (7-2%) oxygen challenges. B) Oxygen challenges consisted of one minute at a baseline oxygen concentration of 7% followed by two minutes at 2%. The mean was calculated from the entire first minute at 7% and the last 15 seconds at a 2% oxygen concentration. Panel B shows capillaries within 100  $\mu\text{m}$  from the micro-outlet edge ( $n = 30$  capillaries), capillaries between 100 – 200  $\mu\text{m}$  from the outlet edge ( $n = 38$  capillaries), and capillaries greater than 200  $\mu\text{m}$  from the outlet edge ( $n = 72$  capillaries) respectively.  $p$  values based on paired Wilcoxon t test and values indicated in the figure with a  $p < 0.05$  considered to be significant. Box and whisker plots show minimum, median, maximum, and associated quartiles.

### 2.3.6 RESULTS: 1000 AND 600 $\mu\text{M}$ MICRO-OUTLET OSCILLATION AND CHALLENGE DATA

The results obtained using our 600 and 1000  $\mu\text{m}$  micro-outlet devices are displayed in the appendix as there is limited space to discuss these results. However, they support the overall findings presented from the 200 and 400  $\mu\text{m}$  outlets as detailed below.

## 2.4 DISCUSSION

In this study, we developed and validated a novel ultra-thin film micro-outlet device to deliver highly localized oxygen perturbations to regions of skeletal muscle tissue with simultaneous quantification of blood flow responses using intravital video microscopy. The knowledge obtained from previous designs, in vivo experiments, and the size of a single microvascular unit in rodents ( $\sim 150 \times 200 \mu\text{m}$ ), aided our device development process (Ghonaim et al., 2011, 2013, 2021; Sové et al., 2021; Ellis et al., 2012). Polyvinylidene chloride (PVDC) gas-impermeable film was used to pattern thin-film micro-outlets onto our device to deliver oxygen perturbations into tissue regions. The device was coupled with computer-controlled mass flow meters connected to a gas exchange chamber for transporting oxygen perturbations to the surface of the extensor digitorum longus (EDL) muscle overlying an inverted microscope setup. To validate the ability of our device to deliver various oxygen concentrations from the gas exchange chamber to the muscle, RBC  $\text{SO}_2$  was analyzed in capillaries overlying the outlet and at various distances away from the outlet edge using IVVM and offline MATLAB software (Ellis et al., 1990, 1992, 2012; Japee, 2004, 2005; Fraser et al., 2012; Ghonaim et al., 2021).

Other groups have obtained the sensitivity level required to alter blood flow through induced microvascular RBC  $\text{SO}_2$  changes in vivo (Frisbee & Lombard, 2002; Frisbee et al.,

2002; Ghonaim et al., 2011, 2021; Sové et al., 2021). Superfusion solutions of varying O<sub>2</sub> levels have stimulated arterioles to either vasoconstrict or vasodilate, depending on the [O<sub>2</sub>] bathing the tissue surface (Duling, 1970; Frisbee & Lombard, 2002; Frisbee et al., 2002; Riemann et al., 2010; Charter et al., 2018). Compared to a micro-outlet device coupled to a gas exchange chamber that directly stimulates individual microvascular networks of an isolated muscle, this stimulated area in a bathed muscle preparation is much larger, affecting approximately 40-fold the microvascular surface area (Ghonaim et al., 2011; Frisbee & Lombard, 2002; Duling, 1970). When the whole muscle is targeted in this type of preparation, multiple levels of the vasculature and their regulatory mechanisms may be affected (Duling, 1970; Frisbee & Lombard, 2002; Charter, 2018; Russel McEvoy et al., 2022). Additionally, superfusion solution preparations are unsuitable for constraining a stimulus to a specific vessel unless administered through micropipettes (Riemann et al., 2010; Frisbee & Lombard, 2002; Duling, 1970). Therefore, micro-outlet devices offer more spatially constrained tissue manipulations at precise concentrations that can be manipulated transiently or maintained for extended durations.

Unlike isolated muscle preparations, superfusion setups do not isolate the muscle from the environment (Tymml & Budreau, 1991; Riemann et al., 2010). Instead, a fixed gas concentration is maintained within the solution that bathes it (Riemann et al., 2010; Charter et al., 2018). This solution typically has a 0% [O<sub>2</sub>] which may interfere with the interpretation of muscle blood flow, as regardless of other stimuli, the regulatory system will adjust to facilitate matching O<sub>2</sub> supply and demand (Kindig et al., 2002). Due to the superfusate being continuously washed away and replenished, other regulatory molecules,

such as nitric oxide, may also be continuously washed away, affecting physiological pathways and basal tone (Jackson, 2016). This may lead to confounding results in O<sub>2</sub> reactivity studies (Jackson, 2016). In general, oxygen has a low solubility in water, thus, superfusion solutions have a limited carrying capacity. Using gas exchange chambers to stimulate the overlying muscle mitigates the consideration of oxygen's solubility properties as O<sub>2</sub> flows readily through the chamber (Ellis et al., 2012; Ghonaim et al., 2011, 2021; Sové et al., 2021; Russell McEvoy et al., 2022). These limitations support the use of gas-based micro-fluidic approaches for studying microvascular oxygen regulation.

Through studies focused on O<sub>2</sub> reactivity at the microvascular level, it has been shown that when enough tissue surface is stimulated, an appropriate blood flow response will occur; a further insight on the location for O<sub>2</sub> sensing (Ellis et al., 2012; Ghonaim et al., 2011, 2013, 2021; Sové et al., 2021; Russell McEvoy et al., 2022). In this study, we aimed to quantify blood flow responses in individual capillary networks to gain novel insights into O<sub>2</sub> sensing at the capillary level. Previously, a 100 µm diameter circular outlet was shown to change RBC SO<sub>2</sub> in the 1- 2 capillaries overlying it but could not stimulate a blood flow response (Ghonaim et al., 2011). RBC SO<sub>2</sub> manipulations in capillary networks overlying 1000 by 200 µm micro-outlet elicited a blood flow response, suggesting O<sub>2</sub> sensing, and control is localized in capillaries (Ghonaim et al., 2021). Subsequently a similar microvascular preparation with a 400 by 200 µm micro-outlet was shown to elicit a substantial RBC SO<sub>2</sub> change in capillaries overlying their micro-outlets to elicit a blood flow response by activating O<sub>2</sub> mediated response (Sové et al., 2021). An important finding, as previous studies used a smaller micro-outlet that stimulated about half the area of

capillary networks compared to previous designs, providing us further insights into the scale for O<sub>2</sub> sensing (Ghonaim et al., 2011, 2021; Sové et al., 2021). A better characterization of the minimum scale for sensing will improve our understanding of potential regulatory mechanisms, and the relative contribution from different vessel types. By quantifying the minimum-sized micro-outlet that can initiate an O<sub>2</sub> sensing and control mechanism to changing tissue O<sub>2</sub> levels, it will help specify the exact spatial location that regulatory mechanisms are activated (Sové et al., 2021). In addition to the previous studies, we tested multiple micro-outlet diameter sizes and compared the hemodynamic responses measured to determine the critical area of O<sub>2</sub> sensing, as discussed in detail below.

Radial diffusion is an important characteristic of gas-based micro-outlet devices as it relates to their achievable spatial specificity. Importantly, the distance a stimulus propagates in the tissue will affect how well constrained imposed oxygen perturbations are. Mathematical modelling and empirical studies have been used to describe the distribution of PO<sub>2</sub> in tissue overlying the micro-outlets (Ghonaim et al., 2013). The results from Ghonaim et al. suggested that imposed PO<sub>2</sub> changes from the gas exchange chamber diffused to capillaries overlying the outlet and to capillaries up to 100 µm away. Still, logically this change in PO<sub>2</sub> declined over distance as the tissue returned to the mean background tissue PO<sub>2</sub> (Ghonaim et al., 2013). Unfortunately, this mathematical model did not consider the gas permeable PDMS layer directly interfaced with the muscle of interest (Ghonaim et al., 2013; Sové et al., 2021). Therefore, O<sub>2</sub> perturbations were propagated more readily through the PDMS layer (due to the higher diffusivity and solubility of oxygen in PDMS), and into the muscle tissue, but the perturbation spread further to capillaries at

significant distances away from the outlet (Markov et al., 2014). Therefore, this led to an underestimated radial diffusion, PO<sub>2</sub> distribution, and spatial specificity of the micro-outlets in the tissue (Ghonaim et al., 2011, 2013). Further in vivo studies were performed, and a new model that incorporated the PDMS layer was created to interpret the results from Sové et al.'s 400 by 200 µm rectangular micro-outlet device (Sové et al., 2021). This new model and its associated in vivo RBC SO<sub>2</sub> data from capillaries at various distances away from the micro-outlets provided novel insights on the extent of O<sub>2</sub> spread within the PDMS layer in their device (Sové et al., 2021). The spreading effect increased this previous outlets' area of effect to greater than 614 by 434 µms, meaning tissue and capillaries greater than 200 µms from the outlet were experiencing significant O<sub>2</sub> changes (Sové et al., 2021). Therefore, the O<sub>2</sub> perturbations coming through this device were stimulating a larger area of tissue and vasculature than originally proposed. This observation suggests more than a 400 by 200 µm of tissue was stimulated and additional, non-capillary-based mechanisms may have been activated, leading to a flow response.

To determine if similar control responses would occur in a device that more precisely stimulated regions of muscle tissue, device modifications and further experiments were deemed necessary (Sové et al., 2021). With these insights in mind, our design for circular micro-outlets with diameters of 200 and 400 µm were fabricated to further our knowledge on the minimum scale of O<sub>2</sub> sensing and control. One of the critical device modifications that was made in the present study was changing the position of the gas permeable layer to be in contact with the gas exchange chamber, and only interfaced with the muscle at the surface of the patterned micro-outlets (Ghonaim et al., 2011, 2013, 2021;

Sové et al., 2021). The purpose of this design modification was to eliminate or mitigate the effects O<sub>2</sub> spreading within the PDMS that exacerbates remote changes to tissue [O<sub>2</sub>] that confounded previous studies (Sové et al., 2021).

In addition to providing greater spatial specificity, our thin film micro-outlet devices provide superior optical properties compared to previous devices, which allowed us to observe and analyze capillary responses inside and outside the outlets simultaneously (Figure 2.2) (Sové et al., 2021). Our micro-outlet device was designed with a thin polyvinylidene chloride film for the gas impermeable layer, whereas previous groups used thin glass substrates of different thicknesses ranging from 80 – 180 µm (Ghonaim et al., 2011, 2013, 2021; Sové et al., 2021). When using glass substrates with air filled micro-outlets, the disparity in refractive index causes capillaries overlying the outlets to resolve at a different focal plane than those outside, even though they are at the same tissue depth (Sové et al., 2021). This is also a disadvantage for quantifying capillary responses overlying and outside the outlets, as the recordings must be captured separately and results in temporally unpaired measurements. The PVDC film employed in our device produces a much thinner exchange membrane, provides excellent optical clarity, and as a result the ability to analyze responses of capillaries overlying and outside the outlets simultaneously during oxygen oscillations and challenges.

#### 2.4.1 OXYGEN OSCILLATIONS

In our study, we altered muscle oxygen concentrations using a gas based micro-outlet device and gas exchange chamber that was directly interfaced with the EDL muscle. As expected, the four-minute oxygen oscillations in the GEC were able to induce rapid and

profound alterations in capillary RBC  $\text{SO}_2$  in capillaries overlying the 400- $\mu\text{m}$  micro-outlets without affecting the  $\text{SO}_2$  in capillaries outside the outlets. The  $\text{SO}_2$  measurements validated our device's ability to impose rapid localized gas-based perturbations without altering the tissue microenvironment in neighbouring vessels outside the micro-outlet. Capillary RBC  $\text{SO}_2$  changes in the tissue occurred rapidly reaching their mean peak responses within 12 seconds at 12%  $\text{O}_2$  (86.91%) and 11 seconds at 2%  $\text{O}_2$  (43.53%) (Figure 2.4).

Significant flow responses in capillaries directly overlying the 400- $\mu\text{m}$  micro-outlets occurred without affecting neighbouring vessels adjacent to the micro-outlet during  $\text{O}_2$  oscillations (Figure 2.6 - 2.11). Specifically, significant differences were observed for RBC supply rate, velocity, and hematocrit levels between 12% and 2% [ $\text{O}_2$ ] oscillations (Figure 2.6, 2.8, 2.10). Interestingly, there was a significant difference in mean RBC supply rate between the first, baseline 7% [ $\text{O}_2$ ] and the last 7%, where we expected to see similar flow states as both time periods were collected at the same baseline [ $\text{O}_2$ ]. This data suggests that one minute at baseline 7% may not be enough time for the flow to normalize after it undergoes high and low one-minute  $\text{O}_2$  oscillations; this is interpreted further below.

During  $\text{O}_2$  oscillations, hematocrit levels were only significantly different between 12% and 2% GEC [ $\text{O}_2$ ] (Figure 2.6), suggesting hematocrit levels do not modulate readily to  $\text{O}_2$  perturbations slightly above or below baseline conditions. It was presented in the literature by Kindig et al. and supported by Russell McEvoy et al. that transient changes in hematocrit are a result of diameter changes in higher order arterioles altering hematocrit levels of downstream vessels based on the Fåhræus-Lindqvist effect (Fåhræus and

Lindqvist, 1931; Barbee and Cokelet, 1971; Pries et al., 1986; Kindig et al., 2002; Russell McEvoy et al., 2022). Since the microvascular region affected is highly confined in our 200- and 400- $\mu\text{m}$  micro-outlets, it is unlikely that higher order arterioles are stimulated; thus, they do not readily change hematocrit levels during  $\text{O}_2$  oscillations. Therefore, the number of capillaries stimulated by  $\text{O}_2$  perturbations was enough to elicit a flow increase in response to low  $\text{O}_2$  conditions but not a consistent decrease at high  $\text{O}_2$  conditions.

$\text{O}_2$  perturbations stimulating capillaries overlying 200  $\mu\text{m}$  micro-outlets induced rapid and profound alterations in capillary RBC  $\text{SO}_2$  (as shown in Figure 2.28). Capillary RBC  $\text{SO}_2$  changes in the tissue occurred rapidly reaching their mean peak responses in 12 seconds at 12%  $\text{O}_2$  (84.91%) and 9 seconds at 2%  $\text{O}_2$  (43.41%) (Figure 2.28). Our 200  $\mu\text{m}$  outlet devices were able to elicit profound flow responses in capillaries overlying the outlet with some minor responses in capillaries outside the outlets at various distances. For all three hemodynamic channels measured, there is a significant difference at baseline 7% compared to 2%  $\text{O}_2$  (Figure 2.30, 2.32, 2.34). Significant differences exist between 12% and 2%  $\text{O}_2$  in hematocrit and supply rate, but not velocity. Depending on the magnitude of the flow response, it may be more difficult to obtain a significant change when imposing high oxygen challenges (Ghonaim et al., 2011). Supply rate is the product of velocity and lineal density; thus, supply rate provides a more sensitive measure when velocity and hematocrit both changes, but not significantly in and of themselves.

For capillaries 100 to 200  $\mu\text{m}$  away from the outlet, there were significant differences in supply rate between 7-2% and 12-2% [ $\text{O}_2$ ] during the oscillations (see Figure 2.35). Although they were significant changes, they are comparatively small gradual

increases in supply rate over time during the 4-minute oscillation. As detailed below, these results support a role for conducted signalling at the capillary level to O<sub>2</sub> changes (Collins et al., 1998; Ghonaim et al., 2011, 2021; Sové et al., 2021).

For capillaries greater than 200 µms away from the outlet, significant hematocrit differences were observed at 12% and 2% compared to baseline 7% (Figure 2.30). The significant change at 12% was a slight increase in hematocrit, an unexpected local response to high [O<sub>2</sub>] (Ghonaim et al., 2011, 2021; Sové et al., 2021; Russell McEvoy et al., 2022). Based on the mean RBC hematocrit levels, we interpret that hematocrit levels increased from baseline to 12% and remained at the same level for the remainder of the oscillation (Figure 2.35). Considering there were no significant differences between 7 and 12% in capillaries overlying the outlet during oscillations in either size outlet, we suspect this result is due to the natural periodic variability of blood flow and vasomotion (Goldman & Popel, 2001). There is spatial heterogeneity in the microcirculation's geometry, blood flow, and oxygen delivery, which may influence observations of this type (Goldman & Popel, 2001).

There were significant differences in velocity and supply rate between the first 7% and the last one minute 7% baseline oscillation, which suggests flow did not return to baseline after increasing during the 2% [O<sub>2</sub>]. A study published by our group using full tissue surface perturbations described time transients during 2-7% O<sub>2</sub> challenges with their associated mean peak responses in capillary RBC velocity ( $t = 77$  s), hematocrit, ( $t = 105$  s), and supply rate ( $t = 76$  s) (Russell McEvoy et al., 2022). Such results suggest that after a one-minute oscillation at 2%, the hemodynamic responses at 7% did not have enough time to reach their mean peak response in the one-minute oscillation; affecting the system's

ability to return blood flow back to baseline. Therefore, this may explain why we found significant differences between our first and last baseline 7% minute. The longer oscillation time may have influenced the hemodynamic results obtained from this study and allowed capillaries to reach their peak response and regulate back to normal conditions at baseline [O<sub>2</sub>].

Although some flow responses did occur in vessels outside the 200- $\mu\text{m}$  outlets, there were no corresponding RBC SO<sub>2</sub> changes in these vessels. The changes in flow outside the 200  $\mu\text{m}$  diameter micro-outlets may be a result of conducted signalling from vasculature overlying the micro-outlets, directly connected with vessels at a distance (Collins, 1998; McCullough et al., 1997; Bagher & Segal, 2011). If stimulating a capillary network overlying the micro-outlet affected capillary networks connected to the same feed arteriole situated outside the outlet, it would support the role of conducted signalling in the response (Collins, 1998; Ellsworth, 2004, 2009; Ellis et al., 2012; Ghonaim et al., 2011). In comparison, Sové et al., did not obtain robust hemodynamic changes in capillaries outside their outlets, though details regarding this data were not reported. Still, they provide data showing profound changes in RBC SO<sub>2</sub> in capillaries measured at three distances reaching farther than 200  $\mu\text{m}$ s from the outlet edge. Based on the significant SO<sub>2</sub> changes found, it is surprising that they did not observe corresponding flow changes in these capillaries as they did in capillaries overlying outlets. However, this might result from relatively few remote capillaries sampled (Sové et al., 2021).

Neither capillaries analyzed in our 400 nor our 200  $\mu\text{m}$  diameter micro-outlets experienced significant differences in hemodynamic values between baseline 7% and 12%

[O<sub>2</sub>] during oscillations. There are a few potential reasons for this result. Compared to previous studies, our results suggest the chosen outlet sizes could not perturb the vasculature sufficiently to initiate O<sub>2</sub> sensing mechanisms to react when [O<sub>2</sub>] was increased to 12% (Ghonaim et al., 2011, 2013; Sové et al., 2021; Russel McEvoy et al., 2022). Russel McEvoy et al., provided evidence to show that 7-12% and 7-2% [O<sub>2</sub>] changes obtain regulatory responses that are asymmetric and that when O<sub>2</sub> is increased from baseline, the hemodynamic regulatory response is not as profound as it is when O<sub>2</sub> is decreased to 2%. This is due to a more considerable change in SO<sub>2</sub> between 7-2% GEC [O<sub>2</sub>] in RBCs compared to between 7-12% (Russell McEvoy et al., 2022). Thus, the more profound the RBC SO<sub>2</sub> change, the greater the flow response will be elicited. Our oscillation data provides supports for this conclusion as we obtained significant hemodynamic changes consistently during low 2% [O<sub>2</sub>] oscillations compared to baseline 7%. Furthermore, in some previous micro-outlet studies, the baseline GEC [O<sub>2</sub>] used was 5% (Ghonaim et al., 2011, 2021; Sové et al., 2021). The high [O<sub>2</sub>] used was 12% and 20%, creating a considerably more forceful step change in [O<sub>2</sub>] compared to the present study, which may also influence the magnitude and robustness of their resulting decrease in flow (Ghonaim et al., 2011, 2021; Sové et al., 2021). Furthermore, this creates a more symmetrical SO<sub>2</sub> change when comparing high and low step changes from a baseline of 5% and 7% O<sub>2</sub>. Depending on the peak response time of specific hemodynamics during high O<sub>2</sub> conditions, it may require more than 1-minute to obtain a robust significant response (Russell McEvoy et al., 2022). Significant hemodynamic differences were found during similar high O<sub>2</sub> conditions in previous studies, but their oscillations were longer than in our current work, with high and low step changes occurring for two minutes each (Sové et al., 2021; Ghonaim

et al., 2021). Therefore, inducing serial O<sub>2</sub> perturbations sequentially may interfere with the ability of the control system to reach a peak hemodynamic response over the observation period. Lastly, the location of terminal arterioles supplying the network of interest and their distance from an outlet may influence the ability to modulate blood flow. Studies that stimulated larger areas of muscle tissue are more likely to interact with terminal arterioles, or higher vasculature (Ghonaim et al., 2021; Sové et al., 2021; Russell McEvoy et al., 2022). Modulating tissue [O<sub>2</sub>] both at a terminal arteriole and its downstream capillary network may result in a more robust or rapid regulatory response.

#### 2.4.2 OXYGEN CHALLENGES

As expected, high (7-12%) and low (7-2%) oxygen challenges from the gas exchange chamber caused rapid and profound alterations in capillary RBC SO<sub>2</sub> in capillaries overlying the 400 μm micro-outlets without causing significant changes in capillary RBC SO<sub>2</sub> outside the outlets (Figure 2.12-215). The RBC SO<sub>2</sub> changes objectively demonstrate the ability of our micro-outlets to impose changes to the tissue microenvironment at this scale and validate the intended approach. Similarly, capillaries overlying 200 μm micro-outlets experienced profound and rapid changes in RBC SO<sub>2</sub> during both oxygen challenges (Figure 2.36, 2.38). Additionally, capillaries less than 100 μm away from the 200 μm outlets experienced significant but comparatively small RBC SO<sub>2</sub> changes during high O<sub>2</sub> challenges (Figure 2.37). Compared to the RBC SO<sub>2</sub> change experienced by capillaries directly overlying the micro-outlet, capillaries less than 100 μm away from the outlet edge changed from 42.24% to 47.21%, whereas the capillaries inside experienced an increase from 60.74% to 80.00% RBC SO<sub>2</sub> (Figure 2.36-2.37). Our data

shows that the area of effect for our 200  $\mu\text{m}$  diameter micro-outlets is within 100  $\mu\text{m}$  of the micro-outlet edge when imposing 2-minute  $\text{O}_2$  challenges.

Our 7-2 %  $[\text{O}_2]$  challenges induced significant flow responses in capillaries directly overlying 400  $\mu\text{m}$  micro-outlets, as determined by increased mean RBC supply rate and velocity (Figure 2.22, 2.26). Profound flow decreases were observed during high oxygen challenges in capillaries overlying the 400  $\mu\text{m}$  diameter outlets. This is an exciting finding as we did not observe significant responses between 7% and 12% during our 4-minute oscillations. This finding supports our interpretation of a time-dependent effect related to stimulating  $\text{O}_2$  regulatory mechanisms in high  $[\text{O}_2]$  areas in small muscle tissue regions. Significant hematocrit changes occurred during low  $\text{O}_2$  challenges but not during high  $\text{O}_2$  challenges.

Hemodynamic responses were observed in capillaries outside the 400  $\mu\text{m}$  diameter outlets at distances farther than 100  $\mu\text{m}$  away but not in vessels less than 100  $\mu\text{m}$  away during low  $\text{O}_2$  challenges. This observation showed a 25% SR increase in capillaries 200  $\mu\text{m}$  away from the outlet compared to a 65% mean SR increase in vessels directly crossing the outlets (Figure 2.26-2.27). These hemodynamic changes remote to the micro-outlets may be due to conducted signalling, as mentioned above. In our devices and in previous devices, multiple micro-outlets are in contact with the muscle within a relatively small region of the tissue surface (Sové et al., 2021). In our devices, adjacent micro-outlets are separated by 1000  $\mu\text{m}$ . Since the microcirculation is highly interconnected, vessels overlying the micro-outlets that experience a SR change may also induce a SR change in vessels at a distance from the outlet; one that may be unrelated to the local tissue micro-

environment in these remote vessels. Multiple micro-outlets may stimulate responses remote to the confined stimulated region, which is more likely to cause significant SR changes in outside vessels.

Our novel 200  $\mu\text{m}$  diameter micro-outlet device similarly provoked profound flow responses during high and low oxygen challenges. RBC velocity significantly decreased during high  $\text{O}_2$  challenges but the change in supply rate and hematocrit were not significant (Figure 2.40, 2.44, 2.48). Profound flow responses occurred during 7-2%  $\text{O}_2$  challenges in capillaries outside the 200- $\mu\text{m}$  outlets, but capillary blood flow responses experienced by capillaries overlying the outlets were larger. Specifically, mean RBC SR increased by 37.5% in capillaries overlying the outlets, while the capillaries outside the outlet edge experienced an 18% mean RBC SR increase (Figure 2.50 - 2.51).

It has been hypothesized that the magnitude of the flow responses observed in relation to oxygen perturbations is proportional to the number of capillaries and endothelial cells stimulated within a network (Ellis et al., 2012; Ghonaim et al., 2013, 2021; Sové et al., 2021). Our results support this hypothesis in low  $\text{O}_2$  challenges for different outlet sizes, as we observed a 38% increase in SR in the 200  $\mu\text{m}$  diameter outlets and a 65% increase in SR in the 400  $\mu\text{m}$  outlets resulting from a 7-2% GEC [ $\text{O}_2$ ] challenge in overlying capillaries. During high  $\text{O}_2$  challenges, our 200  $\mu\text{m}$  diameter micro-outlets did not provoke a significant change in RBC SR, but in 400- $\mu\text{m}$  micro-outlets SR responses were significant with a 12% decrease in mean RBC SR. During oscillations, capillaries experienced a more moderate mean SR increase in the transition from 12% to 2%  $\text{O}_2$  with the 200  $\mu\text{m}$  micro-outlets (13.9%) compared to 400  $\mu\text{m}$  outlets where the increase was 27.7% (Figure 2.10, 2.34).

Endothelial cells in skeletal muscle are approximately 104  $\mu\text{m}$  long, and microvascular units are typically 150 x 200  $\mu\text{m}$  in rodents (Adamson, 1993; Yuan et al., 2011), so larger outlet would be expected to stimulate more endothelial cells to hyperpolarize and contribute to a conducted response from  $[\text{O}_2]$  changes. Therefore, the larger the micro-outlet device and muscle tissue size stimulated by  $\text{O}_2$  perturbations, the greater the flow response should be. This may be due to the integration of conducted signals reaching arterioles reflecting hyperpolarization of the capillary endothelium from multiple vessels that the arteriole supplies (McCullough et al., 1997; Collins et al., 1998; Lidington et al., 2002; Dietrich et al., 2009; Ellis et al., 2012; Dora, 2016). Therefore, the magnitude of the flow response should be at least in part reflected by the number of endothelial cells and individual capillaries influenced by the micro-outlet perturbation (Ghonaim et al., 2011, 2013). Furthermore, a 100  $\mu\text{m}$  outlet affecting 1-2 capillaries overlying it through oxygen perturbations did not elicit a flow response, but our 200- $\mu\text{m}$  micro-outlet affecting approximately double the capillaries and endothelial cells did yield a hemodynamic response. Therefore, our results support the concept of spatially summative responses and provide evidence for capillary level  $\text{O}_2$  sensing.

It has been proposed many times in the literature that capillaries are involved in oxygen-mediated blood flow regulation (Ellsworth, 1995, 2009, 2013; Ellis et al., 2012; Dietrich et al., 1992; Song & Tyml, 1993; Ghoniam et al., 2011, 2013, 2021; Sové et al., 2021; Lamb et al., 2021). Capillaries are suggested to play a role in mediating conducted signalling to arterioles through  $\text{SO}_2$ -dependent ATP release from erythrocytes (Collins, 1998; Dietrich et al., 2009; Arciero et al., 2008; Ellsworth, 2009; Dora, 2017). Our

significant capillary hemodynamic responses from 200  $\mu\text{m}$  diameter micro-outlets represent a promising means to manipulate blood flow via  $[\text{O}_2]$  at the capillary level without directly stimulating higher levels of the vasculature. The profound flow responses we observed in our small, circular 200  $\mu\text{m}$  diameter micro-outlets suggest individual capillary networks can sense  $\text{O}_2$  and modulate blood flow in response. In previous studies, micro-outlet devices could not achieve a blood flow response to a stimulus of this small size, therefore, our findings provide novel insights into the scale of  $\text{O}_2$  sensing.

In conclusion, we have developed and validated an ultra-thin film micro-outlet device that can elicit  $\text{O}_2$  perturbations onto highly confined regions of skeletal muscle tissue, effectively modulating local RBC  $\text{SO}_2$  with corresponding flow changes. Compared to previous devices, design modifications have assisted in improving the spatial specificity and constraining the radial diffusion properties of our device (Ghonaim et al., 2011, 2013; Sové et al., 2021). RBC  $\text{SO}_2$  changes elicited in 200- $\mu\text{m}$  diameter micro-outlets induced corresponding RBC hemodynamic changes, by stimulating a confined region of capillaries. Therefore, we collected novel insights on the minimum scale for inducing significant capillary RBC hemodynamic changes to tissue  $\text{O}_2$  modulations. Our micro-outlet device has high-quality optical properties with the most precise spatial specificity yet in which direct, temporally matched comparisons were made between capillaries directly experiencing imposed  $[\text{O}_2]$  stimulated and vessels at a distance from the stimulus.

In future studies, our device can be used to obtain the high level of spatial specificity necessary to interrogate capillary level regulation mechanisms using multi-modal approaches, such as intravascular pharmacological studies. Our modular device can easily

be modified to address a wide range of research questions and is suitable for future studies to target various levels of microcirculation and specific mechanisms responsible for oxygen-mediated blood flow regulation.

## 2.5 ACKNOWLEDGEMENTS

We would like to thank NSERC for funding this project. Special thanks to MUN MED 3D printing services for the printing of our gas exchange chamber microscope components. Also, we could not have fabricated our devices without the high precision laser cutting work of mechanical technologists Matthew Fudge and Evan Kearley from Engineering Technical Services of Memorial University.

---

## CHAPTER 3: SUMMARY

### 3.1 SUMMARY AND DISCUSSION OF RESULTS

In this thesis, we describe the development and fabrication of an ultra-thin film micro-outlet device of various diameter sizes (200, 400, 600, and 1000  $\mu\text{m}$ ) capable of imposing local oxygen perturbations to skeletal muscle tissue. To stimulate capillaries via modulation of RBC  $\text{SO}_2$ , our device was interfaced with a modular gas exchange chamber to deliver  $[\text{O}_2]$  oscillations and challenges to muscle tissue. The validation of our device is described in chapter 2, which was completed using IVVM to assess our device's ability to deliver  $[\text{O}_2]$  to capillaries overlying the outlet. Offline MATLAB software was used to analyze the spatial region for the diffusion of  $[\text{O}_2]$  perturbations into capillaries overlying and at various distances remote to our outlets. Our novel devices provide superior optical properties compared to other recent micro-fluidic platforms designed for similar purposes. The improved optical properties allowed us to observe and capture capillary RBC  $\text{SO}_2$  and hemodynamic measurements in vessels directly overlying the stimulated area, and in regions remote to the stimulus, simultaneously, which was not possible with previously published approaches.

Our micro-outlets successfully manipulated capillary RBC  $\text{SO}_2$  in vessels overlying and, in some capillaries, less than 200  $\mu\text{m}$ s away from our 200- and 400- $\mu\text{m}$  micro-outlets. As described in Chapter 2, our results demonstrated that capillaries overlying our 200  $\mu\text{m}$  diameter micro-outlets experienced profound changes in RBC  $\text{SO}_2$  via manipulations to the gas exchange chamber  $\text{O}_2$  concentration and were able to elicit significant capillary blood

flow changes in response. This is the first study to demonstrate that oxygen mediated stimulation of muscle regions as small as  $\sim 200 \mu\text{m}$  in diameter can provoke significant localized changes in blood flow, providing novel insights on regulation at the capillary level (Ghonaim et al., 2011, 2013, 2021; Sové et al., 2021) and lending further support for the role of  $\text{O}_2$  sensing in capillaries.

### 3.2 LIMITATIONS

Although our device was highly effective at manipulating  $[\text{O}_2]$  in spatially constrained areas of skeletal muscle tissue, new technologies can be fraught with some limitations. Our device was explicitly designed to align with the following: the thesis objectives stated in Chapter 1, the dimensions of a rat EDL muscle, and the working distance of our microscope's objectives. If a different muscle preparation or microscope were chosen for a future study, our device would require minor modifications to align with the specific tissue and the optical limitations of the optics chosen.

All measurements and assessments were carried out in the muscle at rest. We acknowledge that though  $\text{O}_2$  levels were increased and decreased in our experimental protocol, the energy expenditure of the muscle likely did not change. Although a decrease in  $[\text{O}_2]$  would typically occur during exercise and not in resting state, this was an advantage for our study's focus as it limited the additional interacting mechanisms at play during exercise.

Positioning the muscle on top of the micro-outlets was a challenge during experimental work. Concerning the sensitivity of the muscle preparation, our data was captured from the

initial position chosen. This task was difficult and required precise placement. The main goal in selecting the muscle position was to collect a representative sample of capillary data with vessels visible both overlying and remote to the micro-outlets while maintaining the muscle at *in situ* length and position. In an attempt to mitigate the difficulty with positioning, we chose a close tessellation pattern for device fabrication. This device design included many outlets where data could be collected during a single experiment. Compared to past devices, each device had 1-5 micro-outlets for analysis whereas ours had 12-24 micro-outlets, depending on the outlet size (Ghonaim et al., 2011, 2013, 2021; Sové et al., 2021). This tessellation design helped us obtain sufficient data. However, due to the variable topology of microvascular networks, some sites provided more capillaries suitable for sampling within the microvascular field than others. Therefore, the spatial location of the outlet concerning local and adjacent vasculature could have impacted the responses observed.

Heterogeneity in blood flow states was encountered throughout our data collection, a characteristic of our results that made obtaining statistical significance more difficult. Intravital muscle preparations are subject to heterogeneity in blood flow states across the muscle tissue. This can impact results as the responses observed during [O<sub>2</sub>] challenges and oscillations may vary respectively. Our [O<sub>2</sub>] challenges and oscillations may act as an additional stimulus to variable blood flow. In addition, our experimental data was captured in a timed fashion. The combination of these factors may act as a confounder to our results.

### 3.3 FUTURE DIRECTIONS

Our study has provided us with essential findings from various aspects of the research questions at hand. However, a logical next step for our study is to develop a mathematical model specific to our device's geometry, design, and materials used, to determine traits such as PO<sub>2</sub> distribution, depth of tissue penetration, and radial diffusion. As mentioned in chapter 2, previous studies using micro-outlet devices developed their own model and gained new insights, providing them with a greater understanding of microvascular O<sub>2</sub> regulation, as well as micro-outlet device abilities (Ghonaim et al., 2011, 2013, 2021; Sové et al., 2021). Importantly, our device is a direct result of utilizing modelling to interpret experimental data (Sové et al., 2021). Hence, implementing existing models to address the current design of our device is a critical future direction in our research.

In the future, our outlets can function as a tool to address mechanistic questions related to O<sub>2</sub>-mediated blood flow regulation. More specifically, to address the regulatory hypothesis, the site where sensing takes place must be confirmed. As previously mentioned, multiple locations have been proposed as regulators for O<sub>2</sub> sensing, including the extravascular space, arterioles, and RBCs at the capillary level. Our current study focused on the capillary level, where we observed flow responses at various O<sub>2</sub> conditions in confined tissue regions using our micro-outlet device. In the future, this device could be used on a different location, such as the extravascular space, to focus on avascular tissue. A study like this provides us with an opportunity to obtain evidence to either support or eliminate the idea of O<sub>2</sub> sensing in extravascular spaces such as in parenchymal cells. By

manipulating the tissue microenvironment in avascular areas with  $[O_2]$ , it can be determined if such alterations can regulate blood flow from afar.

Since our modular micro-outlet devices can be fabricated with different tessellations and outlet geometries, future devices could be developed to target spatial specificity at one end of the microvascular unit. This would allow us to determine if a flow response is initiated at a specific vascular level under observation or if it is part of a conducted response travelling from a different area of vasculature. We could evaluate this by analyzing flow responses from a stimulus at either the venular end or directly at a terminal arteriole. Additionally, an outlet could be placed overlying multiple capillaries feeding from the same arteriole to determine if their flow rates are constant and similar in response to  $[O_2]$  changes. This would provide evidence on if stimulating one arteriole-venular unit of capillaries will affect all units connected to the same feed arteriole. Additionally, this type of device could help to provide further evidence for oxygen mediated conducted signalling at the capillary level, if combined with appropriate pharmacological interventions.

### 3.4 FINAL SUMMARY

In summary, this thesis provides novel insights into the sensitivity and scale of  $O_2$  sensing in microvascular networks and proves our ability to spatially constrain  $[O_2]$  perturbations to specified microscale areas using novel micro-outlet devices. We improved upon previous device designs to enhance the optical properties of a micro-outlet device to simultaneously measure RBC saturation and hemodynamics in capillaries directly overlying the stimulated area and in vessels at a distance from the micro-outlet device. We

successfully manipulated the  $[O_2]$  conditions of capillaries directly overlying all our micro-outlets as evidenced by capillary RBC  $SO_2$  changes that occurred simultaneously with capillary RBC hemodynamic responses. Most importantly, we obtained this result in our 200- $\mu\text{m}$  micro-outlet device, the smallest micro-outlet device to both successfully impose changes in capillary RBC  $SO_2$  and provoke an accompanying blood flow response, firmly establishing the scale of oxygen sensing in the microvasculature to regions 200  $\mu\text{m}$  in diameter or smaller.

## REFERENCES

- Adamson R. H. (1993). Microvascular endothelial cell shape and size in situ. *Microvascular research*, 46(1), 77–88.  
<https://doi.org/10.1006/mvre.1993.1036>
- Ahmed, M. H., Ghatge, M. S., & Safo, M. K. (2020). Hemoglobin: Structure, Function and Allostery. *Sub-cellular biochemistry*, 94, 345–382.  
[https://doi.org/10.1007/978-3-030-41769-7\\_14](https://doi.org/10.1007/978-3-030-41769-7_14)
- Aiello, E. A., Malcolm, A. T., Walsh, M. P., & Cole, W. C. (1998). Beta-adrenoceptor activation and PKA regulate delayed rectifier K<sup>+</sup> channels of vascular smooth muscle cells. *The American journal of physiology*, 275(2), H448–H459.  
<https://doi.org/10.1152/ajpheart.1998.275.2.H448>
- Akerstrom, T., Goldman, D., Nilsson, F., Milkovich, S. L., Fraser, G. M., Brand, C. L., et al. (2019). Hyperinsulinemia does not cause de novo capillary recruitment in rat skeletal muscle. *Microcirculation*, 1985(104), 889.  
<http://doi.org/10.1111/micc.12593>
- Albertini, M., Vanelli, G., & Clement, M. G. (1996). PGI<sub>2</sub> and nitric oxide involvement in the regulation of systemic and pulmonary basal vascular tone in the pig. *Prostaglandins, leukotrienes, and essential fatty acids*, 54(4), 273–278.  
[https://doi.org/10.1016/s0952-3278\(96\)90058-7](https://doi.org/10.1016/s0952-3278(96)90058-7)
- Alberts B, Johnson A, Lewis J, et al. (2002). Blood vessels and endothelial cells. *Molecular biology of the Cell*. 4<sup>th</sup> Edition. Doi:  
<https://www.ncbi.nlm.nih.gov/books/NBK26848/>
- Anderson, G. L., Acland, R. D., Siemionow, M., & McCabe, S. J. (1988). Vascular isolation of the rat cremaster muscle. *Microvascular research*, 36(1), 56–63.  
[https://doi.org/10.1016/0026-2862\(88\)90038-6](https://doi.org/10.1016/0026-2862(88)90038-6)
- Anderson, D. R., Pochettino, A., Hammond, R. L., & Stephenson, L. W. (1991). Skeletal muscle as a myocardial substitute. *Proceedings of the Society for Experimental Biology and Medicine. Society for Experimental Biology and Medicine (New York, N.Y.)*, 197(2), 109–118. <https://doi.org/10.3181/00379727-197-43232>
- Ando, J., & Yamamoto, K. (2013). Flow detection and calcium signalling in vascular endothelial cells. *Cardiovascular research*, 99(2), 260–268.  
<https://doi.org/10.1093/cvr/cvt084>
- Augustin, H. G., & Koh, G. Y. (2017). Organotypic vasculature: From descriptive heterogeneity to functional pathophysiology. *Science (American Association for the Advancement of Science)*, 357(6353).  
<https://doi.org/10.1126/science.aal2379>

- Arciero, J. C., Carlson, B. E., & Secomb, T. W. (2008). Theoretical model of metabolic blood flow regulation: roles of ATP release by red blood cells and conducted responses. *American journal of physiology. Heart and circulatory physiology*, 295(4), H1562–H1571. <https://doi.org/10.1152/ajpheart.00261.2008>
- Arnold, W. P., Mittal, C. K., Katsuki, S., & Murad, F. (1977). Nitric oxide activates guanylate cyclase and increases guanosine 3':5'-cyclic monophosphate levels in various tissue preparations. *Proceedings of the National Academy of Sciences of the United States of America*, 74(8), 3203–3207. <https://doi.org/10.1073/pnas.74.8.3203>
- Aroesty, J., & Gross, J. F. (1970). Convection and diffusion in the microcirculation. *Microvascular research*, 2(3), 247–267.
- Attrill, E., Ramsay, C., Ross, R., Richards, S., Sutherland, B. A., Keske, M. A., Eringa, E., & Premilovac, D. (2020). Metabolic-vascular coupling in skeletal muscle: A potential role for capillary pericytes? *Clinical and experimental pharmacology & physiology*, 47(3), 520–528. <https://doi.org/10.1111/1440-681.13208>  
[https://doi.org/10.1016/0026-2862\(70\)90016-6](https://doi.org/10.1016/0026-2862(70)90016-6)
- Baba, K., Kawamura, T., Shibata, M., Sohirad, M., & Kamiya, A. (1995). Capillary-tissue arrangement in the skeletal muscle optimized for oxygen transport in all mammals. *Microvascular research*, 49(2), 163–179. <https://doi.org/10.1006/mvre.1995.1013>
- Bailey, J. K., Kindig, C. A., Behnke, B. J., Musch, T. I., Schmid-Schoenbein, G. W. & Poole, D. C. (2000). Spinotrapezius muscle microcirculatory function: effects of surgical exteriorization. *Am J Physiol Heart Circ Physiol*, 279, 3131-3137. <https://doi.org/10.1152/ajpheart.2000.279.6.h3131>
- Bagher P, Segal SS. The Mouse cremaster muscle preparation for intravital imaging of the microcirculation. *J Vis Exp*. 2011; 52:2874
- Bagher, P., & Segal, S. S. (2011). Regulation of blood flow in the microcirculation: role of conducted vasodilation. *Acta physiologica (Oxford, England)*, 202(3), 271–284. <https://doi.org/10.1111/j.1748-1716.2010.02244.x>
- Barbee, J. H., & Cokelet, G. R. (1971). The Fahraeus effect. *Microvascular research*, 3(1), 6–16. [https://doi.org/10.1016/0026-2862\(71\)90002-1](https://doi.org/10.1016/0026-2862(71)90002-1)
- Bartlett, M. F., Oneglia, A., Jaffery, M., Maniowabi-Huebner, S., Hueber, D. M., & Nelson, M. D. (2020). Kinetic differences between macro- and microvascular measures of reactive hyperemia. *Journal of applied physiology (Bethesda, Md.: 1985)*, 129(5), 1183–1192. <https://doi.org/10.1152/jappphysiol.00481.2020>

- Bayliss W. M. (1902). On the local reactions of the arterial wall to changes of internal pressure. *The Journal of physiology*, 28(3), 220–231. <https://doi.org/10.1113/jphysiol.1902.sp000911>
- Beach, J. M., McGahren, E. D., & Duling, B. R. (1998). Capillaries and arterioles are electrically coupled in hamster cheek pouch. *The American journal of physiology*, 275(4), H1489–H1496. <https://doi.org/10.1152/ajpheart.1998.275.4.H1489>
- Behnke, B. J., Kindig, C. A., Musch, T. I., Koga, S., & Poole, D. C. (2001). Dynamics of microvascular oxygen pressure across the rest-exercise transition in rat skeletal muscle. *Respiration physiology*, 126(1), 53–63. [https://doi.org/10.1016/s0034-5687\(01\)00195-5](https://doi.org/10.1016/s0034-5687(01)00195-5)
- Berg, B. R., & Sarelius, I. H. (1995). Functional capillary organization in striated muscle. *The American journal of physiology*, 268(3 Pt 2), H1215–H1222. <https://doi.org/10.1152/ajpheart.1995.268.3.H1215>
- Bergfeld G, Forrester T, (1992). Release of ATP from human erythrocytes in response to a brief period of hypoxia and hypercapnia. *Cardiovascular Research*, vol. 26, no. 1, pp. 40-47.
- Blinder, P., Tsai, P. S., Kaufhold, J. P., Knutsen, P. M., Suhl, H., & Kleinfeld, D. (2013). The cortical angiome: an interconnected vascular network with noncolumnar patterns of blood flow. *Nature neuroscience*, 16(7), 889–897. <https://doi.org/10.1038/nn.3426>
- Bloch, E. H., & Iberall, A. S. (1982). Toward a concept of the functional unit of mammalian skeletal muscle. *The American journal of physiology*, 242(5), R411–R420. <https://doi.org/10.1152/ajpregu.1982.242.5.R411>
- Brayden J. E. (1996). Potassium channels in vascular smooth muscle. *Clinical and experimental pharmacology & physiology*, 23(12), 1069–1076. <https://doi.org/10.1111/j.1440-1681.1996.tb01172.x>
- Brekke, J. F., Jackson, W. F., & Segal, S. S. (2006). Arteriolar smooth muscle Ca<sup>2+</sup> dynamics during blood flow control in hamster cheek pouch. *Journal of applied physiology (Bethesda, Md.: 1985)*, 101(1), 307–315. <https://doi.org/10.1152/jappphysiol.01634.2005>
- Budel, S., Bartlett, I. S., & Segal, S. S. (2003). Homocellular conduction along endothelium and smooth muscle of arterioles in hamster cheek pouch: unmasking an NO wave. *Circulation Research*, 93(1), 61-68. doi: 10.1161/01.RES.0000080318.81205.FD
- Buehler, P. W., & Alayash, A. I. (2004). Oxygen sensing in the circulation: "cross talk" between red blood cells and the vasculature. *Antioxidants & redox signaling*, 6(6), 1000–1010. <https://doi.org/10.1089/ars.2004.6.1000>

- Buerk D. G. (2004). Measuring tissue PO<sub>2</sub> with microelectrodes. *Methods in enzymology*, 381, 665–690. [https://doi.org/10.1016/S0076-6879\(04\)81043-7](https://doi.org/10.1016/S0076-6879(04)81043-7)
- Buerk D. G. (2009). Mathematical modeling of the interaction between oxygen, nitric oxide and superoxide. *Advances in experimental medicine and biology*, 645, 7–12. [https://doi.org/10.1007/978-0-387-85998-9\\_2](https://doi.org/10.1007/978-0-387-85998-9_2)
- Busse, R., Edwards, G., F.I.tou, M., Fleming, I., Vanhoutte, P. M., & Weston, A. H. (2002). EDHF: bringing the concepts together. *Trends in Pharmacological Sciences*, 23(8), 374-380. doi:10.1016/s0165-6147(02)02050-3
- Busse, R., Pohl, U., Kellner, C., & Klemm, U. (1983). Endothelial cells are involved in the vasodilatory response to hypoxia. *Pflugers Archiv : European journal of physiology*, 397(1), 78–80. <https://doi.org/10.1007/BF00585175>
- Busse, R., Förstermann, U., Matsuda, H., & Pohl, U. (1984). The role of prostaglandins in the endothelium-mediated vasodilatory response to hypoxia. *Pflugers Archiv: European journal of physiology*, 401(1), 77–83. <https://doi.org/10.1007/BF00581536>
- Campbell, W. B., Gebremedhin, D., Pratt, P. F., & Harder, D. R. (1996). Identification of epoxyeicosatrienoic acids as endothelium-derived hyperpolarizing factors. *Circulation research*, 78(3), 415–423. <https://doi.org/10.1161/01.res.78.3.415>
- Cassot, F., Lauwers, F., Fouard, C., Prohaska, S., & Lauwers-Cances, V. (2006). A novel three-dimensional computer-assisted method for a quantitative study of microvascular networks of the human cerebral cortex. *Microcirculation (New York, N.Y.: 1994)*, 13(1), 1–18. <https://doi.org/10.1080/10739680500383407>
- Carlson, B. E., & Secomb, T. W. (2005). A theoretical model for the myogenic response based on the length-tension characteristics of vascular smooth muscle. *Microcirculation (New York, N.Y.: 1994)*, 12(4), 327–338. <https://doi.org/10.1080/10739680590934745>
- Carvalho, H., & Pittman, R. N. (2008). Longitudinal and radial gradients of PO<sub>2</sub> in the hamster cheek pouch microcirculation. *Microcirculation (New York, N.Y.: 1994)*, 15(3), 215–224. <https://doi.org/10.1080/10739680701616175>
- Charter, M. E., Lamb, I. R., & Murrant, C. L. (2018). Arteriolar and capillary responses to CO<sub>2</sub> and H<sup>+</sup> in hamster skeletal muscle microvasculature: Implications for active hyperemia. *Microcirculation (New York, N.Y.: 1994)*, 25(7), e12494. doi:10.1111/micc.12494
- Chauhan, S., Rahman, A., Nilsson, H., Clapp, L., MacAllister, R., & Ahluwalia, A. (2003). NO contributes to EDHF-like responses in rat small arteries: a role for NO

- stores. *Cardiovascular research*, 57(1), 207–216.  
[https://doi.org/10.1016/s0008-6363\(02\)00611-9](https://doi.org/10.1016/s0008-6363(02)00611-9)
- Coburn, R. F., Grubb, B., & Aronson, R. D. (1979). Effect of cyanide on oxygen tension-dependent mechanical tension in rabbit aorta. *Circulation research*, 44(3), 368–378. <https://doi.org/10.1161/01.res.44.3.368>
- Colburn, T. D., Holdsworth, C. T., Craig, J. C., Hirai, D. M., Montgomery, S., Poole, D. C., Musch, T. I., & Kenney, M. J. (2020). ATP-sensitive K<sup>+</sup> channel inhibition in rats decreases kidney and skeletal muscle blood flow without increasing sympathetic nerve discharge. *Respiratory physiology & neurobiology*, 278, 103444. <https://doi.org/10.1016/j.resp.2020.103444>
- Collins, D. M., McCullough, W. T. & Ellsworth, M. L. (1998). Conducted vascular responses: communication across the capillary bed. *Microvasc. Res*, 56, 43–53. <https://doi.org/10.1006/mvre.1998.2076>
- Cosby, K., Partovi, K. S., Crawford, J. H., Patel, R. P., Reiter, C. D., Martyr, S., Yang, B. K., Waclawiw, M. A., Zalos, G., Xu, X., Huang, K. T., Shields, H., Kim-Shapiro, D. B., Schechter, A. N., Cannon, R. O., 3rd, & Gladwin, M. T. (2003). Nitrite reduction to nitric oxide by deoxyhemoglobin vasodilates the human circulation. *Nature medicine*, 9(12), 1498–1505. <https://doi.org/10.1038/nm954>
- Crystal, G. J., & Pagel, P. S. (2020). The Physiology of Oxygen Transport by the Cardiovascular System: Evolution of Knowledge. *Journal of cardiothoracic and vascular anesthesia*, 34(5), 1142–1151. <https://doi.org/10.1053/j.jvca.2019.12.029>
- Davis M. J. (1993). Myogenic response gradient in an arteriolar network. *The American journal of physiology*, 264(6 Pt 2), H2168–H2179. <https://doi.org/10.1152/ajpheart.1993.264.6.H2168>
- Davis, M. J., & Hill, M. A. (1999). Signaling mechanisms underlying the vascular myogenic response. *Physiological reviews*, 79(2), 387–423. <https://doi.org/10.1152/physrev.1999.79.2.387>
- Davis, M. J., Hill, M. A., and Kuo, L. (2008). “Local regulation of microvascular perfusion,” in *Handbook of Physiology: Microcirculation*, Second edition, eds R. F. Tuma, W. N. Duran, and K. Ley (San Diego, CA: Academic Press), 161–284. <http://dx.doi.org/10.1002/cphy.cp020406>
- Delp M. D. (1999). Control of skeletal muscle perfusion at the onset of dynamic exercise. *Medicine and science in sports and exercise*, 31(7), 1011–1018. <https://doi.org/10.1097/00005768-199907000-00014>
- Denninger, J. W., & Marletta, M. A. (1999). Guanylate cyclase and the .NO/cGMP signaling pathway. *Biochimica et biophysica acta*, 1411(2-3), 334–350. [https://doi.org/10.1016/s0005-2728\(99\)00024-9](https://doi.org/10.1016/s0005-2728(99)00024-9)

- Dewhirst, M. W., Klitzman, B., Braun, R. D., Brizel, D. M., Haroon, Z. A., & Secomb, T. W. (2000). Review of methods used to study oxygen transport at the microcirculatory level. *International journal of cancer*, *90*(5), 237–255.
- Diep, H. K., Vigmond, E. J., Segal, S. S., & Welsh, D. G. (2005). Defining electrical communication in skeletal muscle resistance arteries: a computational approach. *The Journal of physiology*, *568*(Pt 1), 267–281. <https://doi.org/10.1113/jphysiol.2005.090233>
- Dietrich H. H. (1989). Effect of locally applied epinephrine and norepinephrine on blood flow and diameter in capillaries of rat mesentery. *Microvascular research*, *38*(2), 125–135. [https://doi.org/10.1016/0026-2862\(89\)90021-6](https://doi.org/10.1016/0026-2862(89)90021-6)
- Dietrich, H. H., Ellsworth, M. L., Sprague, R. S., & Dacey, R. G., Jr (2000). Red blood cell regulation of microvascular tone through adenosine triphosphate. *American journal of physiology. Heart and circulatory physiology*, *278*(4), H1294–H1298. <https://doi.org/10.1152/ajpheart.2000.278.4.H1294>
- Dietrich, H. H., Horiuchi, T., Xiang, C., Hongo, K., Falck, J. R., & Dacey, R. G., Jr (2009). Mechanism of ATP-induced local and conducted vasomotor responses in isolated rat cerebral penetrating arterioles. *Journal of vascular research*, *46*(3), 253–264. <https://doi.org/10.1159/000167273>
- Dietrich, H. H., & Tynl, K. (1992). Capillary as a communicating medium in the microvasculature. *Microvascular research*, *43*(1), 87–99. [https://doi.org/10.1016/0026-2862\(92\)90008-d](https://doi.org/10.1016/0026-2862(92)90008-d)
- Ding, H., Kubes, P., & Triggle, C. (2000). Potassium- and acetylcholine-induced vasorelaxation in mice lacking endothelial nitric oxide synthase. *British journal of pharmacology*, *129*(6), 1194–1200. <https://doi.org/10.1038/sj.bjp.0703144>
- Dora K. A. (2017). Conducted dilatation to ATP and K<sup>+</sup> in rat skeletal muscle arterioles. *Acta physiologica (Oxford, England)*, *219*(1), 202–218. <https://doi.org/10.1111/apha.12656>
- Dora K. A. (2016). Endothelial-smooth muscle cell interactions in the regulation of vascular tone in skeletal muscle. *Microcirculation (New York, N.Y.: 1994)*, *23*(8), 626–630. <https://doi.org/10.1111/micc.12322>
- Dora K. A. (2010). Coordination of vasomotor responses by the endothelium. *Circulation journal : official journal of the Japanese Circulation Society*, *74*(2), 226–232. <https://doi.org/10.1253/circj.cj-09-0879>
- Doyle, M. P., & Duling, B. R. (1997). Acetylcholine induces conducted vasodilation by nitric oxide-dependent and -independent mechanisms. *The American journal of physiology*, *272*(3 Pt 2), H1364–H1371. <https://doi.org/10.1152/ajpheart.1997.272.3.H1364>

- Duling B. R. (1972). Microvascular responses to alterations in oxygen tension. *Circulation research*, 31(4), 481–489.  
<https://doi.org/10.1161/01.res.31.4.481>
- Duling B. R. (1973). The preparation and use of the hamster cheek pouch for studies of the microcirculation. *Microvascular research*, 5(3), 423–429.  
[https://doi.org/10.1016/0026-2862\(73\)90059-9](https://doi.org/10.1016/0026-2862(73)90059-9)
- Duling B. R. (1974). Oxygen sensitivity of vascular smooth muscle. II. In vivo studies. *The American journal of physiology*, 227(1), 42–49.  
<https://doi.org/10.1152/ajplegacy.1974.227.1.42>
- Duling, B. R., & Berne, R. M. (1970). Longitudinal gradients in periarteriolar oxygen tension. A possible mechanism for the participation of oxygen in local regulation of blood flow. *Circulation research*, 27(5), 669–678.  
<https://doi.org/10.1161/01.res.27.5.669>
- Duling, B. R., & Berne, R. M. (1970). Propagated vasodilation in the microcirculation of the hamster cheek pouch. *Circulation research*, 26(2), 163–170.  
<https://doi.org/10.1161/01.res.26.2.163>
- Duling, B. R., Gore, R. W., Dacey, R. G., Jr, & Damon, D. N. (1981). Methods for isolation, cannulation, and in vitro study of single microvessels. *The American journal of physiology*, 241(1), H108–H116.  
<https://doi.org/10.1152/ajpheart.1981.241.1.H108>
- Duling, B. R., & Klitzman, B. (1980). Local control of microvascular function: role in tissue oxygen supply. *Annual review of physiology*, 42, 373–382.  
<https://doi.org/10.1146/annurev.ph.42.030180.002105>
- Duling, B. R., Kuschinsky, W., & Wahl, M. (1979). Measurements of the perivascular PO<sub>2</sub> in the vicinity of the pial vessels of the cat. *Pflugers Archiv : European journal of physiology*, 383(1), 29–34. <https://doi.org/10.1007/BF00584471>
- Dunn, J. O., Mythen, M.G., Grocott, M.P., (2016). Physiology of oxygen transport, *BJA Education*, Volume 16, Issue 10, October 2016, Pages 341–348, <https://doi.org/10.1093/bjaed/mkw012>
- Duza, T., & Sarelius, I. H. (2003). Conducted dilations initiated by purines in arterioles are endothelium dependent and require endothelial Ca<sup>2+</sup>. *American journal of physiology. Heart and circulatory physiology*, 285(1), H26–H37.  
<https://doi.org/10.1152/ajpheart.00788.2002>
- Ellis, C. G., Ellsworth, M. L., & Pittman, R. N. (1990). Determination of red blood cell oxygenation in vivo by dual video densitometric image analysis. *The American journal of physiology*, 258(4 Pt 2), H1216–H1223.  
<https://doi.org/10.1152/ajpheart.1990.258.4.H1216>

- Ellis, C. G., Ellsworth, M. L., Pittman, R. N., & Burgess, W. L. (1992). Application of image analysis for evaluation of red blood cell dynamics in capillaries. *Microvascular research*, 44(2), 214–225. [https://doi.org/10.1016/0026-2862\(92\)90081-y](https://doi.org/10.1016/0026-2862(92)90081-y)
- Ellis, C. G., Jagger, J., & Sharpe, M. (2005). The microcirculation as a functional system. *Critical care (London, England)*, 9 Suppl 4(Suppl 4), S3–S8. <https://doi.org/10.1186/cc3751>
- Ellis C., Milkovich S., Goldman D. (2006). Experimental protocol investigating local regulation of oxygen supply in rat skeletal muscle in vivo. *J. Vasc. Res.* 43:45. 10.1159/000094939
- Ellis, C. G., Milkovich, S., & Goldman, D. (2012). What is the efficiency of ATP signaling from erythrocytes to regulate distribution of O<sub>2</sub> supply within the microvasculature?. *Microcirculation (New York, N.Y.: 1994)*, 19(5), 440–450. <https://doi.org/10.1111/j.1549-8719.2012.00196.x>
- Ellsworth M. L. (2000). The red blood cell as an oxygen sensor: what is the evidence?. *Acta physiologica Scandinavica*, 168(4), 551–559. <https://doi.org/10.1046/j.1365-201x.2000.00708.x>
- Ellsworth M. L. (2004). Red blood cell-derived ATP as a regulator of skeletal muscle perfusion. *Medicine and science in sports and exercise*, 36(1), 35–41. <https://doi.org/10.1249/01.MSS.0000106284.80300.B2>
- Ellsworth, M. L., Ellis, C. G., Popel, A. S., & Pittman, R. N. (1994). Role of Microvessels in Oxygen Supply to Tissue. *News in physiological sciences: an international journal of physiology produced jointly by the International Union of Physiological Sciences and the American Physiological Society*, 9(3), 119–123. <https://doi.org/10.1152/physiologyonline.1994.9.3.119>
- Ellsworth, M. L., Ellis, C. G., Goldman, D., Stephenson, A. H., Dietrich, H. H., & Sprague, R. S. (2009). Erythrocytes: oxygen sensors and modulators of vascular tone. *Physiology (Bethesda, Md.)*, 24, 107–116. <https://doi.org/10.1152/physiol.00038.2008>
- Ellsworth, M. L., Ellis, C. G., & Sprague, R. S. (2016). Role of erythrocyte-released ATP in the regulation of microvascular oxygen supply in skeletal muscle. *Acta physiological (Oxford,England)*, 216(3),265276. <https://doi.org/10.1111/apha.12596>
- Ellsworth, M. L., Forrester, T., Ellis, C. G., & Dietrich, H. H. (1995). The erythrocyte as a regulator of vascular tone. *The American journal of physiology*, 269(6 Pt 2), H2155–H2161. <https://doi.org/10.1152/ajpheart.1995.269.6.H2155>

- Ellsworth, M. L., Pittman, R. N., & Ellis, C. G. (1987). Measurement of hemoglobin oxygen saturation in capillaries. *The American journal of physiology*, 252(5 Pt 2), H1031–H1040. <https://doi.org/10.1152/ajpheart.1987.252.5.H1031>
- Emerson, G. G., & Segal, S. S. (1997). Alignment of microvascular units along skeletal muscle fibers of hamster retractor. *Journal of applied physiology (Bethesda, Md.: 1985)*, 82(1), 42–48. <https://doi.org/10.1152/jappl.1997.82.1.42>
- Emerson, G. G., & Segal, S. S. (2000). Electrical coupling between endothelial cells and smooth muscle cells in hamster feed arteries: role in vasomotor control. *Circulation research*, 87(6), 474–479. <https://doi.org/10.1161/01.res.87.6.474>
- Eriksson, E., & Myrhage, R. (1972). Microvascular dimensions and blood flow in skeletal muscle. *Acta physiologica Scandinavica*, 86(2), 211–222. <https://doi.org/10.1111/j.1748-1716.1972.tb05327.x>
- Faber J. E. (1988). In situ analysis of alpha-adrenoceptors on arteriolar and venular smooth muscle in rat skeletal muscle microcirculation. *Circulation research*, 62(1), 37–50. <https://doi.org/10.1161/01.res.62.1.37>
- Fahraeus R., Lindqvist T. (1931). The viscosity of the blood in narrow capillary tubes. *Am. J. Physiology-Legacy Content* 96 (3), 562–568. <https://doi.org/10.1152/ajplegacy.1931.96.3.562>
- Falcone, J. C., Kuo, L., & Meininger, G. A. (1993). Endothelial cell calcium increases during flow-induced dilation in isolated arterioles. *The American journal of physiology*, 264(2 Pt 2), H653–H659. <https://doi.org/10.1152/ajpheart.1993.264.2.H653>
- Federspiel, W. J., & Popel, A. S. (1986). A theoretical analysis of the effect of the particulate nature of blood on oxygen release in capillaries. *Microvascular research*, 32(2), 164–189. [https://doi.org/10.1016/0026-2862\(86\)90052-x](https://doi.org/10.1016/0026-2862(86)90052-x)
- Félétou, M., & Vanhoutte, P. M. (2009). EDHF: an update. *Clinical science (London, England: 1979)*, 117(4), 139–155. <https://doi.org/10.1042/CS20090096>
- Fox, R. J., & Frame, M. D. (2002). Regulation of flow and wall shear stress in arteriolar networks of the hamster cheek pouch. *Journal of applied physiology (Bethesda, Md.: 1985)*, 92(5), 2080–2088. <https://doi.org/10.1152/japplphysiol.00984.2001>
- Fournier, S., Keulards, D. C. J., van 't Veer, M., Colaiori, I., Di Gioia, G., Zimmermann, F. M., Mizukami, T., Nagumo, S., Kodeboina, M., El Farissi, M., Zelis, J. M., Sonck, J., Collet, C., Pijls, N. H. J., & De Bruyne, B. (2021). Normal values of thermodilution-derived absolute coronary blood flow and microvascular resistance in humans. *EuroIntervention: journal of EuroPCR in collaboration with*

*the Working Group on Interventional Cardiology of the European Society of Cardiology*, 17(4), e309–e316. <https://doi.org/10.4244/EIJ-D-20-00684>

- Fraser, G. M. (2012). Modeling Oxygen Transport in Three-Dimensional Capillary Networks. Electronic Thesis and Dissertation Repository. 500. <https://ir.lib.uwo.ca/etd/500>
- Fraser, G. M., Goldman, D., & Ellis, C. G. (2012a). Microvascular flow modeling using in vivo hemodynamic measurements in reconstructed 3D capillary networks. *Microcirculation (New York, N.Y.: 1994)*, 19(6), 510–520. <https://doi.org/10.1111/j.1549-8719.2012.00178.x>
- Fraser, G. M., Milkovich, S., Goldman, D., & Ellis, C. G. (2012b). Mapping 3-D functional capillary geometry in rat skeletal muscle in vivo. *American journal of physiology. Heart and circulatory physiology*, 302(3), H654–H664. <https://doi.org/10.1152/ajpheart.01185.2010>
- Fredricks, K. T., Liu, Y., & Lombard, J. H. (1994a). Response of extra parenchymal resistance arteries of rat skeletal muscle to reduced PO<sub>2</sub>. *The American journal of physiology*, 267(2 Pt 2), H706–H715. <https://doi.org/10.1152/ajpheart.1994.267.2.H706>
- Fredricks, K. T., Liu, Y., Rusch, N. J., & Lombard, J. H. (1994b). Role of endothelium and arterial K<sup>+</sup> channels in mediating hypoxic dilation of middle cerebral arteries. *The American journal of physiology*, 267(2 Pt 2), H580–H586. <https://doi.org/10.1152/ajpheart.1994.267.2.H580>
- Friedman J. M. (1985). Structure, dynamics, and reactivity in hemoglobin. *Science (New York, N.Y.)*, 228(4705), 1273–1280. <https://doi.org/10.1126/science.4001941>
- Frisbee J. C. (2001). Impaired dilation of skeletal muscle microvessels to reduced oxygen tension in diabetic obese Zucker rats. *American journal of physiology. Heart and circulatory physiology*, 281(4), H1568–H1574. <https://doi.org/10.1152/ajpheart.2001.281.4.H1568>
- Frisbee, J. C., & Stepp, D. W. (2001). Impaired NO-dependent dilation of skeletal muscle arterioles in hypertensive diabetic obese Zucker rats. *American journal of physiology. Heart and circulatory physiology*, 281(3), H1304–H1311. <https://doi.org/10.1152/ajpheart.2001.281.3.H1304>
- Frisbee, J. C., Roman, R. J., Krishna, U. M., Falck, J. R., & Lombard, J. H. (2001). Relative contributions of cyclooxygenase- and cytochrome P450 omega-hydroxylase-dependent pathways to hypoxic dilation of skeletal muscle resistance arteries. *Journal of vascular research*, 38(4), 305–314. <https://doi.org/10.1159/000051061>

- Frisbee JC, Lombard JH. (2002). Parenchymal tissue cytochrome P450 4A enzymes contribute to oxygen-induced alterations in skeletal muscle arteriolar tone. *Microvascular Research*, vol. 63, no. 3, pp. 340-343. <https://doi.org/10.1006/mvre.2002.2409>
- Frisbee J. C., Maier K. G., Falck J. R., Roman R. J., Lombard J. H. (2002). Integration of hypoxic dilation signaling pathways for skeletal muscle resistance arteries. *Am. J. Physiol. Regul. Integr. Compar. Physiol.* 283, R309–R319. [10.1152/ajpregu.00741.2001](https://doi.org/10.1152/ajpregu.00741.2001)
- Furchgott, R. F., & Zawadzki, J. V. (1980). The obligatory role of endothelial cells in the relaxation of arterial smooth muscle by acetylcholine. *Nature*, 288(5789), 373–376. <https://doi.org/10.1038/288373a0>
- Ghonaim, N. W., Lau, L. W., Goldman, D., Ellis, C. G., & Yang, J. (2011). A micro-delivery approach for studying microvascular responses to localized oxygen delivery. *Microcirculation (New York, N.Y.:1994)*, 18(8),646–654. <https://doi.org/10.1111/j.1549-8719.2011.00132.x>
- Ghonaim, N. W., Fraser, G. M., Ellis, C. G., Yang, J., & Goldman, D. (2013). Modeling steady state SO<sub>2</sub>-dependent changes in capillary ATP concentration using novel O<sub>2</sub> micro-delivery methods. *Frontiers in physiology*, 4, 260. <https://doi.org/10.3389/fphys.2013.00260>
- Ghonaim, N. W., Fraser, G. M., Goldman, D., Milkovich, S., Yang, J., & Ellis, C. G. (2021). Evidence for role of capillaries in regulation of skeletal muscle oxygen supply. *Microcirculation (New York, N.Y.:1994)*, 28(6), e12699. <https://doi.org/10.1111/micc.12699>
- Gladwin, M. T., Lancaster, J. R., Jr, Freeman, B. A., & Schechter, A. N. (2003). Nitric oxide's reactions with hemoglobin: a view through the SNO-storm. *Nature medicine*, 9(5), 496–500. <https://doi.org/10.1038/nm0503-496>
- Gladwin, M. T., Crawford, J. H., & Patel, R. P. (2004). The biochemistry of nitric oxide, nitrite, and hemoglobin: role in blood flow regulation. *Free radical biology & medicine*, 36(6), 707–717. <https://doi.org/10.1016/j.freeradbiomed.2003.11.032>
- Goldman D. (2008). A mathematical model of oxygen transport in intact muscle with imposed surface oscillations. *Mathematical biosciences*, 213(1), 18–28. <https://doi.org/10.1016/j.mbs.2008.01.010>
- Goldman, D., Fraser, G. M., Ellis, C. G., Sprague, R. S., Ellsworth, M. L., & Stephenson, A. H. (2012). Toward a multiscale description of microvascular flow regulation: o(2)-dependent release of ATP from human erythrocytes and the distribution of ATP in capillary networks. *Frontiers in physiology*, 3, 246. <https://doi.org/10.3389/fphys.2012.00246>

- Goldman, D., & Popel, A. S. (2000). A computational study of the effect of capillary network anastomoses and tortuosity on oxygen transport. *Journal of theoretical biology*, 206(2), 181–194. <https://doi.org/10.1006/jtbi.2000.2113>
- Goldman, D., & Popel, A. S. (2001). A computational study of the effect of vasomotion on oxygen transport from capillary networks. *Journal of theoretical biology*, 209(2), 189–199. <https://doi.org/10.1006/jtbi.2000.2254>
- Golub, A. S., & Pittman, R. N. (2013). Bang-bang model for regulation of local blood flow. *Microcirculation (New York, N.Y. : 1994)*, 20(6), 455–483. <https://doi.org/10.1111/micc.12051>
- Golub, A. S., Tevald, M. A., & Pittman, R. N. (2011). Phosphorescence quenching microrespirometry of skeletal muscle in situ. *American journal of physiology. Heart and circulatory physiology*, 300(1), H135–H143. <https://doi.org/10.1152/ajpheart.00626.2010>
- González-Alonso J. (2012). ATP as a mediator of erythrocyte-dependent regulation of skeletal muscle blood flow and oxygen delivery in humans. *The Journal of physiology*, 590(20), 5001–5013. <https://doi.org/10.1113/jphysiol.2012.235002>
- González-Alonso, J., Mortensen, S. P., Dawson, E. A., Secher, N. H., & Damsgaard, R. (2006). Erythrocytes and the regulation of human skeletal muscle blood flow and oxygen delivery: role of erythrocyte count and oxygenation state of haemoglobin. *The Journal of physiology*, 572(Pt 1), 295–305. <https://doi.org/10.1113/jphysiol.2005.101121>
- González-Alonso, J., Olsen, D. B., & Saltin, B. (2002). Erythrocyte and the regulation of human skeletal muscle blood flow and oxygen delivery: role of circulating ATP. *Circulation research*, 91(11), 1046–1055. <https://doi.org/10.1161/01.res.0000044939.73286.e2>
- Grant R.T. (1964). Direct observation of skeletal muscle blood vessels (rat cremaster). *The Journal of physiology*, 172(1), 123–137. <https://doi.org/10.1113/jphysiol.1964.sp007407>
- Gray S. D. (1973). Rat spinotrapezius muscle preparation for microscopic observation of the terminal vascular bed. *Microvascular research*, 5(3), 395–400. [https://doi.org/10.1016/0026-2862\(73\)90055-1](https://doi.org/10.1016/0026-2862(73)90055-1)
- Griffith, T. M., Edwards, D. H., Davies, R. L., & Henderson, A. H. (1989). The role of EDRF in flow distribution: a microangiographic study of the rabbit isolated ear. *Microvascular research*, 37(2), 162–177. [https://doi.org/10.1016/0026-2862\(89\)90035-6](https://doi.org/10.1016/0026-2862(89)90035-6)

- Groebe, K., & Thews, G. (1990). Calculated intra- and extracellular PO<sub>2</sub> gradients in heavily working red muscle. *The American journal of physiology*, 259(1 Pt 2), H84–H92. <https://doi.org/10.1152/ajpheart.1990.259.1.H84>
- Haddy, F. J., & Scott, J. B. (1968). Metabolically linked vasoactive chemicals in local regulation of blood flow. *Physiological reviews*, 48(4), 688–707. <https://doi.org/10.1152/physrev.1968.48.4.688>
- Hanson, M. S., Ellsworth, M. L., Achilleus, D., Stephenson, A. H., Bowles, E. A., Sridharan, M., Adderley, S., & Sprague, R. S. (2009). Insulin inhibits low oxygen-induced ATP release from human erythrocytes: implication for vascular control. *Microcirculation (New York, N.Y.: 1994)*, 16(5), 424–433. <https://doi.org/10.1080/10739680902855218>
- Harder, D. R., Narayanan, J., Birks, E. K., Liard, J. F., Imig, J. D., Lombard, J. H., Lange, A. R., & Roman, R. J. (1996). Identification of a putative microvascular oxygen sensor. *Circulation research*, 79(1), 54–61. <https://doi.org/10.1161/01.res.79.1.54>
- Hearon, C. M., Jr, Richards, J. C., Racine, M. L., Luckasen, G. J., Larson, D. G., & Dinunno, F. A. (2020). Augmentation of endothelium-dependent vasodilatory signalling improves functional sympatholysis in contracting muscle of older adults. *The Journal of physiology*, 598(12), 2323–2336. <https://doi.org/10.1113/JP279462>
- Hellsten, Y., Nyberg, M., Jensen, L. G., & Mortensen, S. P. (2012). Vasodilator interactions in skeletal muscle blood flow regulation. *The Journal of physiology*, 590(24), 6297–6305. <https://doi.org/10.1113/jphysiol.2012.240762>
- Hepple R. T. (1997). A new measurement of tissue capillarity: the capillary-to-fibre perimeter exchange index. *Canadian journal of applied physiology = Revue canadienne de physiologie appliquee*, 22(1), 11–22. <https://doi.org/10.1139/h97-002>
- Hester R. L. (1993). Uptake of metabolites by postcapillary venules: mechanism for the control of arteriolar diameter. *Microvascular research*, 46(2), 254–261. <https://doi.org/10.1006/mvre.1993.1050>
- Hester, R. L., & Hammer, L. W. (2002). Venular-arteriolar communication in the regulation of blood flow. *American journal of physiology. Regulatory, integrative and comparative physiology*, 282(5), R1280–R1285. <https://doi.org/10.1152/ajpregu.00744.2001>
- Hirai, D. M., Copp, S. W., Ferreira, L. F., Musch, T. I., & Poole, D. C. (2010). Nitric oxide bioavailability modulates the dynamics of microvascular oxygen exchange during recovery from contractions. *Acta physiologica (Oxford, England)*, 200(2), 159–169. <https://doi.org/10.1111/j.1748-1716.2010.02137.x>

- Hirai, D. M., Craig, J. C., Colburn, T. D., Eshima, H., Kano, Y., Sexton, W. L., Musch, T. I., & Poole, D. C. (2018). Skeletal muscle microvascular and interstitial PO<sub>2</sub> from rest to contractions. *The Journal of physiology*, *596*(5), 869–883. <https://doi.org/10.1113/JP275170>
- Hirai, D. M., Colburn, T. D., Craig, J. C., Hotta, K., Kano, Y., Musch, T. I., & Poole, D. C. (2019). Skeletal muscle interstitial O<sub>2</sub> pressures: bridging the gap between the capillary and myocyte. *Microcirculation (New York, N.Y.: 1994)*, *26*(5), e12497. <https://doi.org/10.1111/micc.12497>
- Hirai, D. M., Tabuchi, A., Craig, J. C., Colburn, T. D., Musch, T. I., & Poole, D. C. (2021). Regulation of capillary hemodynamics by K<sub>ATP</sub> channels in resting skeletal muscle. *Physiological reports*, *9*(8), e14803. <https://doi.org/10.14814/phy2.14803>
- Hirsch, S., Reichold, J., Schneider, M., Székely, G., & Weber, B. (2012). Topology and hemodynamics of the cortical cerebrovascular system. *Journal of cerebral blood flow and metabolism: official journal of the International Society of Cerebral Blood Flow and Metabolism*, *32*(6), 952–967. <https://doi.org/10.1038/jcbfm.2012.39>
- Hu, S. L., Kim, H. S., & Jeng, A. Y. (1991). Dual action of endothelin-1 on the Ca<sup>2+</sup>(+)-activated K<sup>+</sup> channel in smooth muscle cells of porcine coronary artery. *European journal of pharmacology*, *194*(1), 31–36. [https://doi.org/10.1016/0014-2999\(91\)90120-f](https://doi.org/10.1016/0014-2999(91)90120-f)
- Hull, S. S., Jr, Kaiser, L., Jaffe, M. D., & Sparks, H. V., Jr (1986). Endothelium-dependent flow-induced dilation of canine femoral and saphenous arteries. *Blood vessels*, *23*(4-5), 183–198. <https://doi.org/10.1159/000158641>
- Hudlicka, O., & Brown, M. D. (2009). Adaptation of skeletal muscle microvasculature to increased or decreased blood flow: role of shear stress, nitric oxide and vascular endothelial growth factor. *Journal of vascular research*, *46*(5), 504–512. <https://doi.org/10.1159/000226127>
- Hudlicka O. (2011). Microcirculation in skeletal muscle. *Muscles, ligaments and tendons journal*, *1*(1), 3–11.
- Hungerford, J. E., Sessa, W. C., & Segal, S. S. (2000). Vasomotor control in arterioles of the mouse cremaster muscle. *FASEB journal: official publication of the Federation of American Societies for Experimental Biology*, *14*(1), 197–207. <https://doi.org/10.1096/fasebj.14.1.197>
- Hutchins, P.M., Bond R.F., and Green H.D. Participation of oxygen in the local control of skeletal muscle microvasculature. (1974). *Circulation Research*, vol. 34, no. 1, pp. 85-93.

- Injarabian, L., Scherlinger, M., Devin, A., Ransac, S., Lykkesfeldt, J., & Marteyn, B. S. (2020). Ascorbate maintains a low plasma oxygen level. *Scientific reports*, *10*(1), 10659. <https://doi.org/10.1038/s41598-020-67778-w>
- Ishizaka, H., & Kuo, L. (1997). Endothelial ATP-sensitive potassium channels mediate coronary microvascular dilation to hyperosmolarity. *The American journal of physiology*, *273*(1 Pt 2), H104–H112. <https://doi.org/10.1152/ajpheart.1997.273.1.H104>
- Ivanov, K. P., Derry, A. N., Vovenko, E. P., Samoilov, M. O., & Semionov, D. G. (1982). Direct measurements of oxygen tension at the surface of arterioles, capillaries and venules of the cerebral cortex. *Pflugers Archiv : European journal of physiology*, *393*(1), 118–120. <https://doi.org/10.1007/BF00582403>
- Jackson W. F. (1986). Prostaglandins do not mediate arteriolar oxygen reactivity. *The American journal of physiology*, *250*(6 Pt 2), H1102–H1108. <https://doi.org/10.1152/ajpheart.1986.250.6.H1102>
- Jackson W. F. (2005). Potassium channels in the peripheral microcirculation. *Microcirculation (New York, N.Y.: 1994)*, *12*(1), 113–127. <https://doi.org/10.1080/10739680590896072>
- Jackson, W. F. (2016). Arteriolar oxygen reactivity: where is the sensor and what is the mechanism of action? *J. Physiol*, *594*(18): 5055–5077. doi: 10.1113/JP270192.
- Jackson W. F. (2021). Calcium-Dependent Ion Channels and the Regulation of Arteriolar Myogenic Tone. *Frontiers in physiology*, *12*, 770450. <https://doi.org/10.3389/fphys.2021.770450>
- Jackson W. F. (2020). Ion channels and the regulation of myogenic tone in peripheral arterioles. *Current topics in membranes*, *85*, 19–58. <https://doi.org/10.1016/bs.ctm.2020.01.002>
- Jackson, W. F., & Duling, B. R. (1983). The oxygen sensitivity of hamster cheek pouch arterioles. In vitro and in situ studies. *Circulation research*, *53*(4), 515–525. <https://doi.org/10.1161/01.res.53.4.515>
- Jackson, W. F., Mülsch, A., & Busse, R. (1991). Rhythmic smooth muscle activity in hamster aortas is mediated by continuous release of NO from the endothelium. *The American journal of physiology*, *260*(1 Pt 2), H248–H253. <https://doi.org/10.1152/ajpheart.1991.260.1.H248>
- Jackson WF, Pohl U & Busse R (1987). Endothelium-dependent oxygen reactivity in hamster carotid arteries. *Federation Proceedings*, *46*, 1530.
- Jacob, M., Chappell, D., & Becker, B. F. (2016). Regulation of blood flow and volume exchange across the microcirculation. *Critical care (London, England)*, *20*(1), 319. <https://doi.org/10.1186/s13054-016-1485-0>

- Jagger, J. E., Bateman, R. M., Ellsworth, M. L., & Ellis, C. G. (2001). Role of erythrocyte in regulating local O<sub>2</sub> delivery mediated by hemoglobin oxygenation. *American journal of physiology. Heart and circulatory physiology*, 280(6), H2833–H2839. <https://doi.org/10.1152/ajpheart.2001.280.6.H2833>
- Jagger J., McCullen S., Yun C., Ellis C. (2004). Erythrocyte hemodynamics as a function of the local o<sub>2</sub> environment in the edl muscle of the rat. *FASEB J.* 18: A632.
- Japee, S. A., Ellis, C. G., & Pittman, R. N. (2004). Flow visualization tools for image analysis of capillary networks. *Microcirculation (New York, N.Y.: 1994)*, 11(1), 39–54. <https://doi.org/10.1080/10739680490266171>
- Japee, S. A., Pittman, R. N., & Ellis, C. G. (2005). A new video image analysis system to study red blood cell dynamics and oxygenation in capillary networks. *Microcirculation (New York, N.Y.: 1994)*, 12(6), 489–506. <https://doi.org/10.1080/10739680591003332>
- Jensen F. B. (2004). Red blood cell pH, the Bohr effect, and other oxygenation-linked phenomena in blood O<sub>2</sub> and CO<sub>2</sub> transport. *Acta physiologica Scandinavica*, 182(3), 215–227. <https://doi.org/10.1111/j.1365-201X.2004.01361.x>
- Jia, L., Bonaventura, C., Bonaven- tura, J. & Stamler, J. S. (1996). S-nitrosohaemoglobin: a dynamic activity of blood involved in vascular control. *Nature*, 380, 221–226. <https://doi.org/10.1038/380221a0>
- Jimenez, A. H., Tanner, M. A., Caldwell, W. M., & Myers, P. R. (1996). Effects of oxygen tension on flow-induced vasodilation in porcine coronary resistance arterioles. *Microvascular research*, 51(3), 365–377. <https://doi.org/10.1006/mvre.1996.0033>
- Joyner, M. J., & Casey, D. P. (2014). Muscle blood flow, hypoxia, and hypoperfusion. *Journal of applied physiology (Bethesda, Md.: 1985)*, 116(7), 852–857. <https://doi.org/10.1152/jappphysiol.00620.2013>
- Kaley, G., Rodenburg, J. M., Messina, E. J., & Wolin, M. S. (1989). Endothelium-associated vasodilators in rat skeletal muscle microcirculation. *The American journal of physiology*, 256(3 Pt 2), H720–H725. <https://doi.org/10.1152/ajpheart.1989.256.3.H720>
- Kawanabe, Y., & Nauli, S. M. (2011). Endothelin. *Cellular and molecular life sciences: CMLS*, 68(2), 195–203. <https://doi.org/10.1007/s00018-010-0518-0>
- Kerkhof, C. J., Bakker, E. N., & Sipkema, P. (1999). Role of cytochrome P-450 4A in oxygen sensing and NO production in rat cremaster resistance arteries. *The*

- American journal of physiology*, 277(4), H1546–H1552.  
<https://doi.org/10.1152/ajpheart.1999.277.4.H1546>
- Kimura, S., Matsumoto, K., Mineura, K., & Itoh, T. (2007). A new technique for the mapping of oxygen tension on the brain surface. *Journal of the neurological sciences*, 258(1-2), 60–68. <https://doi.org/10.1016/j.jns.2007.02.032>
- Kindig, C. A., Musch, T. I., Basaraba, R. J., & Poole, D. C. (1999). Impaired capillary hemodynamics in skeletal muscle of rats in chronic heart failure. *Journal of applied physiology (Bethesda, Md.: 1985)*, 87(2), 652–660.  
<https://doi.org/10.1152/jappl.1999.87.2.652>
- Kindig, C. A., Richardson, T. E., & Poole, D. C. (2002). Skeletal muscle capillary hemodynamics from rest to contractions: implications for oxygen transfer. *Journal of applied physiology (Bethesda, Md.: 1985)*, 92(6), 2513–2520.  
<https://doi.org/10.1152/japplphysiol.01222.2001>
- Koller, A., & Kaley, G. (1991). Endothelial regulation of wall shear stress and blood flow in skeletal muscle microcirculation. *The American journal of physiology*, 260(3 Pt 2), H862–H868.  
<https://doi.org/10.1152/ajpheart.1991.260.3.H862>
- Korthuis, R. J. (2011). *Skeletal Muscle Circulation*. Morgan & Claypool Life Sciences. <https://doi.org/10.4199/c00035ed1v01y201106isp023>
- Kotecha, N., & Hill, M. A. (2005). Myogenic contraction in rat skeletal muscle arterioles: smooth muscle membrane potential and Ca (2+) signaling. *American journal of physiology. Heart and circulatory physiology*, 289(4), H1326–H1334.  
<https://doi.org/10.1152/ajpheart.00323.2005>
- Krogh A. (1919). The supply of oxygen to the tissues and the regulation of the capillary circulation. *The Journal of physiology*, 52(6), 457–474.  
<https://doi.org/10.1113/jphysiol.1919.sp001844>
- Krüger-Genge, A., Blocki, A., Franke, R. P., & Jung, F. (2019). Vascular Endothelial Cell Biology: An Update. *International journal of molecular sciences*, 20(18), 4411.  
<https://doi.org/10.3390/ijms20184411>
- Kuo, L., Davis, M. J., & Chilian, W. M. (1990). Endothelium-dependent, flow-induced dilation of isolated coronary arterioles. *The American journal of physiology*, 259(4 Pt 2), H1063–H1070. <https://doi.org/10.1152/ajpheart.1990.259.4.H1063>
- Kurjiaka, D. T., & Segal, S. S. (1995). Interaction between conducted vasodilation and sympathetic nerve activation in arterioles of hamster striated muscle. *Circulation research*, 76(5), 885–891. <https://doi.org/10.1161/01.res.76.5.885>

- Lai, A., & Frishman, W. H. (2005). Rho-kinase inhibition in the therapy of cardiovascular disease. *Cardiology in review*, 13(6), 285–292. <https://doi.org/10.1097/01.crd.0000138079.91392.37>
- Lamb, I. R., Novielli, N. M., & Murrant, C. L. (2018). Capillary response to skeletal muscle contraction: evidence that redundancy between vasodilators is physiologically relevant during active hyperaemia. *The Journal of physiology*, 596(8), 1357–1372. <https://doi.org/10.1113/JP275467>
- Lamb, I. R., Novielli-Kuntz, N. M., & Murrant, C. L. (2021). Capillaries communicate with the arteriolar microvascular network by a pannexin/purinergic-dependent pathway in hamster skeletal muscle. *American journal of physiology. Heart and circulatory physiology*, 320(4), H1699–H1711. <https://doi.org/10.1152/ajpheart.00493.2020>
- Latroche, C., Gitiaux, C., Chrétien, F., Desguerre, I., Mounier, R., & Chazaud, B. (2015). Skeletal Muscle Microvasculature: A Highly Dynamic Lifeline. *Physiology (Bethesda, Md.)*, 30(6), 417–427. <https://doi.org/10.1152/physiol.00026.2015>
- Laughlin, M. H., Davis, M. J., Secher, N. H., van Lieshout, J. J., Arce-Esquivel, A. A., Simmons, G. H., Bender, S. B., Padilla, J., Bache, R. J., Merkus, D., & Duncker, D. J. (2012). Peripheral circulation. *Comprehensive Physiology*, 2(1), 321–447. <https://doi.org/10.1002/cphy.c100048>
- Leach, R. M., & Treacher, D. F. (1992). The pulmonary physician and critical care. 6. Oxygen transport: the relation between oxygen delivery and consumption. *Thorax*, 47(11), 971–978. <https://doi.org/10.1136/thx.47.11.971>
- Ledoux, J., Werner, M. E., Brayden, J. E., & Nelson, M. T. (2006). Calcium-activated potassium channels and the regulation of vascular tone. *Physiology (Bethesda, Md.)*, 21, 69–78. <https://doi.org/10.1152/physiol.00040.2005>
- Leek, B. T., Mudaliar, S. R., Henry, R., Mathieu-Costello, O., & Richardson, R. S. (2001). Effect of acute exercise on citrate synthase activity in untrained and trained human skeletal muscle. *American journal of physiology. Regulatory, integrative, and comparative physiology*, 280(2), R441–R447. <https://doi.org/10.1152/ajpregu.2001.280.2.R441>
- Lehoux, S., Castier, Y., & Tedgui, A. (2006). Molecular mechanisms of the vascular responses to haemodynamic forces. *Journal of internal medicine*, 259(4), 381–392. <https://doi.org/10.1111/j.1365-2796.2006.01624.x>
- Li, N., Tourovskaia, A., & Folch, A. (2003). Biology on a chip: microfabrication for studying the behavior of cultured cells. *Critical reviews in biomedical engineering*, 31(5-6), 423–488. <https://doi.org/10.1615/critrevbiomedeng.v31.i56.20>

- Li, J., King, N. C., & Sinoway, L. I. (2005). Interstitial ATP and norepinephrine concentrations in active muscle. *Circulation*, *111*(21), 2748–2751. <https://doi.org/10.1161/CIRCULATIONAHA.104.510669>
- Lidington, D., Ouellette, Y., & Tyml, K. (2002). Communication of agonist-induced electrical responses along 'capillaries' in vitro can be modulated by lipopolysaccharide, but not nitric oxide. *Journal of vascular research*, *39*(5), 405–413. <https://doi.org/10.1159/000064519>
- Li, C., & Xu, Q. (2007). Mechanical stress-initiated signal transduction in vascular smooth muscle cells in vitro and in vivo. *Cellular signalling*, *19*(5), 881–891. <https://doi.org/10.1016/j.cellsig.2007.01.004>
- Lo, A., Fuglevand, A. J., & Secomb, T. W. (2003). Oxygen delivery to skeletal muscle fibers: effects of microvascular unit structure and control mechanisms. *American journal of physiology. Heart and circulatory physiology*, *285*(3), H955–H963. <https://doi.org/10.1152/ajpheart.00278.2003>
- Lombard, J. H., & Duling, B. R. (1977). Relative importance of tissue oxygenation and vascular smooth muscle hypoxia in determining arteriolar responses to occlusion in the hamster cheek pouch. *Circulation research*, *41*(4), 546–551. <https://doi.org/10.1161/01.res.41.4.546>
- Lombard, J. H., Kunert, M. P., Roman, R. J., Falck, J. R., Harder, D. R., & Jackson, W. F. (1999). Cytochrome P-450 omega-hydroxylase senses O<sub>2</sub> in hamster muscle, but not cheek pouch epithelium, microcirculation. *The American journal of physiology*, *276*(2), H503–H508. <https://doi.org/10.1152/ajpheart.1999.276.2.H503>
- Lüscher, T. F., Aarhus, L. L., & Vanhoutte, P. M. (1990). Indomethacin improves the impaired endothelium-dependent relaxations in small mesenteric arteries of the spontaneously hypertensive rat. *American journal of hypertension*, *3*(1), 55–58. <https://doi.org/10.1093/ajh/3.1.55>
- Malmsjö, M., Erlinge, D., Högestätt, E. D., & Zygmunt, P. M. (1999). Endothelial P2Y receptors induce hyperpolarisation of vascular smooth muscle by release of endothelium-derived hyperpolarising factor. *European journal of pharmacology*, *364*(2-3), 169–173. [https://doi.org/10.1016/s0014-2999\(98\)00848-6](https://doi.org/10.1016/s0014-2999(98)00848-6)
- Malte, H., Lykkeboe, G., & Wang, T. (2021). The magnitude of the Bohr effect profoundly influences the shape and position of the blood oxygen equilibrium curve. *Comparative biochemistry and physiology. Part A, Molecular & integrative physiology*, *254*, 110880. <https://doi.org/10.1016/j.cbpa.2020.110880>
- Marden, M. C., Griffon, N., & Poyart, C. (1995). Oxygen delivery and autoxidation of hemoglobin. *Transfusion clinique et biologique: journal de la Societe francaise*

*de transfusion sanguine*, 2(6), 473–480. [https://doi.org/10.1016/s1246-7820\(05\)80074-6](https://doi.org/10.1016/s1246-7820(05)80074-6)

Markov, D. A., Lillie, E. M., Garbett, S. P., & McCawley, L. J. (2014). Variation in diffusion of gases through PDMS due to plasma surface treatment and storage conditions. *Biomedical microdevices*, 16(1), 91–96. <https://doi.org/10.1007/s10544-013-9808-2>

Marvar, P. J., Hammer, L. W., & Boegehold, M. A. (2007). Hydrogen peroxide-dependent arteriolar dilation in contracting muscle of rats fed normal and high salt diets. *Microcirculation (New York, N.Y.: 1994)*, 14(8), 779–791. <https://doi.org/10.1080/10739680701444057>

Marshall J. M. (1982). The influence of the sympathetic nervous system on individual vessels of the microcirculation of skeletal muscle of the rat. *The Journal of physiology*, 332, 169–186. <https://doi.org/10.1113/jphysiol.1982.sp014408>

Martinez-Lemus L. A. (2012). The dynamic structure of arterioles. *Basic & clinical pharmacology & toxicology*, 110(1), 5–11. <https://doi.org/10.1111/j.1742-7843.2011.00813.x>

Mathewson, A. M., & Dunn, W. R. (2014). A comparison of responses to raised extracellular potassium and endothelium-derived hyperpolarizing factor (EDHF) in rat pressurised mesenteric arteries. *PloS one*, 9(11), e111977. <https://doi.org/10.1371/journal.pone.0111977>

Max, M., Kuhlen, R., Dembinski, R., & Rossaint, R. (1999). Effect of aerosolized prostacyclin and inhaled nitric oxide on experimental hypoxic pulmonary hypertension. *Intensive care medicine*, 25(10), 1147–1154. <https://doi.org/10.1007/s001340051027>

Messina, L. M., Podrazik, R. M., Whitehill, T. A., Ekhterae, D., Brothers, T. E., Wilson, J. M., Burkel, W. E., & Stanley, J. C. (1992). Adhesion and incorporation of lacZ-transduced endothelial cells into the intact capillary wall in the rat. *Proceedings of the National Academy of Sciences of the United States of America*, 89(24), 12018–12022 <https://doi.org/10.1073/pnas.89.24.12018>

Messina, L. M., Ekhterae, D., Whitehill, T. A., Podrazik, R. M., Burkel, W. E., Ford, J., Gardner, A. K., & Stanley, J. C. (1994). Transplantation of lac-Z-transduced microvascular endothelial cells into the skeletal muscle capillary bed of the rat hindlimb occurs independent of the duration of femoral artery occlusion after injection of cells. *The Journal of surgical research*, 57(6), 661–666. <https://doi.org/10.1006/jsre.1994.1197>

McClatchey, P., Wu, F., Olfert, I. M., Ellis, C. G., Goldman, D., Reusch, J. E. B., & Frisbee, J. C. (2017). Impaired Tissue Oxygenation in Metabolic Syndrome

- Requires Increased Microvascular Perfusion Heterogeneity. *Journal of cardiovascular translational research*, 10(1), 69–81.  
<https://doi.org/10.1007/s12265-017-9732-6>
- McCullough, W. T., Collins, D. M. & Ellsworth, M. L. (1997). Arteriolar responses to extracellular ATP in striated muscle. *Am. J. Physiol*, 272, H1886–H1891.  
<https://doi.org/10.1152/ajpheart.1997.272.4.h1886>
- McDonald, J. C., Duffy, D. C., Anderson, J. R., Chiu, D. T., Wu, H., Schueller, O. J., & Whitesides, G. M. (2000). Fabrication of microfluidic systems in poly(dimethylsiloxane). *Electrophoresis*, 21(1), 27–40.  
[https://doi.org/10.1002/\(SICI\)1522-2683\(20000101\)21:1<27::AID-ELPS27>3.0.CO;2-C](https://doi.org/10.1002/(SICI)1522-2683(20000101)21:1<27::AID-ELPS27>3.0.CO;2-C)
- Minami, Y., Kono, T., Miyazaki, T., & Taniguchi, T. (1993). The IL-2 receptor complex: its structure, function, and target genes. *Annual review of immunology*, 11, 245–268. <https://doi.org/10.1146/annurev.iy.11.040193.001333>
- Mishra, R. C., Rahman, M. M., Davis, M. J., Wulff, H., Hill, M. A., & Braun, A. P. (2018). Alpha<sub>1</sub>-adrenergic stimulation selectively enhances endothelium-mediated vasodilation in rat cremaster arteries. *Physiological reports*, 6(9), e13703. <https://doi.org/10.14814/phy2.13703>
- Murrant, C. L., Dodd, J. D., Foster, A. J., Inch, K. A., Muckle, F. R., Ruiz, D. A., Simpson, J. A., & Scholl, J. H. (2014). Prostaglandins induce vasodilatation of the microvasculature during muscle contraction and induce vasodilatation independent of adenosine. *The Journal of physiology*, 592(6), 1267–1281.  
<https://doi.org/10.1113/jphysiol.2013.264259>
- Murrant, C. L., & Fletcher, N. M. (2022). Capillary communication: the role of capillaries in sensing the tissue environment, coordinating the microvascular, and controlling blood flow. *American journal of physiology. Heart and circulatory physiology*, 323(5), H1019–H1036. <https://doi.org/10.1152/ajpheart.00088.2022>
- Murrant, C. L., Lamb, I. R., & Novielli, N. M. (2017). Capillary endothelial cells as coordinators of skeletal muscle blood flow during active hyperemia. *Microcirculation (New York, N.Y.: 1994)*, 24(3), 10.1111/micc.12348. <https://doi.org/10.1111/micc.12348>
- Nase, G. P., Tuttle, J., & Bohlen, H. G. (2003). Reduced perivascular PO<sub>2</sub> increases nitric oxide release from endothelial cells. *American journal of physiology. Heart and circulatory physiology*, 285(2), H507–H515.  
<https://doi.org/10.1152/ajpheart.00759.2002>
- Needham, L., Cusack, N. J., Pearson, J. D., & Gordon, J. L. (1987). Characteristics of the P<sub>2</sub> purinoceptor that mediates prostacyclin production by pig aortic endothelial

- cells. *European journal of pharmacology*, 134(2), 199–209.  
[https://doi.org/10.1016/0014-2999\(87\)90166-x](https://doi.org/10.1016/0014-2999(87)90166-x)
- Ngo, A. T., Jensen, L. J., Riemann, M., Holstein-Rathlou, N. H., & Torp-Pedersen, C. (2010). Oxygen sensing and conducted vasomotor responses in mouse cremaster arterioles in situ. *Pflugers Archiv: European journal of physiology*, 460(1), 41–53. <https://doi.org/10.1007/s00424-010-0837-x>
- Ngo, A. T., Riemann, M., Holstein-Rathlou, N. H., Torp-Pedersen, C., & Jensen, L. J. (2013). Significance of K(ATP) channels, L-type Ca<sup>2+</sup> channels and CYP450-4A enzymes in oxygen sensing in mouse cremaster muscle arterioles in vivo. *BMC physiology*, 13, 8. <https://doi.org/10.1186/1472-6793-13-8>
- Nilsson, G. E., Tenland, T., & Oberg, P. A. (1980). Evaluation of a laser Doppler flowmeter for measurement of tissue blood flow. *IEEE transactions on bio-medical engineering*, 27(10), 597–604.  
<https://doi.org/10.1109/TBME.1980.326582>
- Nourbakhsh, N., & Singh, P. (2014). Role of renal oxygenation and mitochondrial function in the pathophysiology of acute kidney injury. *Nephron. Clinical practice*, 127(1-4), 149–152. <https://doi.org/10.1159/000363545>
- Norel X. (2007). Prostanoid receptors in the human vascular wall. *The Scientific World Journal*, 7, 1359–1374. <https://doi.org/10.1100/tsw.2007.184>
- Olsson R. A. (1981). Local factors regulating cardiac and skeletal muscle blood flow. *Annual review of physiology*, 43, 385–395.  
<https://doi.org/10.1146/annurev.ph.43.030181.002125>
- Palmer, R. M., Ferrige, A. G., & Moncada, S. (1987). Nitric oxide release accounts for the biological activity of endothelium-derived relaxing factor. *Nature*, 327(6122), 524–526. <https://doi.org/10.1038/327524a0>
- Patel, S., Joseph, S. K., & Thomas, A. P. (1999). Molecular properties of inositol 1,4,5-trisphosphate receptors. *Cell calcium*, 25(3), 247–264.  
<https://doi.org/10.1054/ceca.1999.0021>
- Perutz M. F. (1992). What are enzyme structures telling us? *Faraday discussions*, (93), 1–11. <https://doi.org/10.1039/fd9929300001>
- Perutz, M. F., Wilkinson, A. J., Paoli, M., & Dodson, G. G. (1998). The stereochemical mechanism of the cooperative effects in hemoglobin revisited. *Annual review of biophysics and biomolecular structure*, 27, 1–34.  
<https://doi.org/10.1146/annurev.biophys.27.1.1>
- Pfister G. (2001). Invited review: regulation of myosin phosphorylation in smooth muscle. *Journal of applied physiology (Bethesda, Md.: 1985)*, 91(1), 497–503.  
<https://doi.org/10.1152/jappl.2001.91.1.497>

- Pias S. C. (2021). How does oxygen diffuse from capillaries to tissue mitochondria? Barriers and pathways. *The Journal of physiology*, 599(6), 1769–1782. <https://doi.org/10.1113/JP278815>
- Pittet, J. F., Lacroix, J. S., Gunning, K., Déom, A., Neidhart, P., Morel, D. R., & Suter, P. M. (1992). Different effects of prostacyclin and phentolamine on delivery-dependent O<sub>2</sub> consumption and skin microcirculation after cardiac surgery. *Canadian journal of anaesthesia = Journal canadien d'anesthésie*, 39(10), 1023–1029. <https://doi.org/10.1007/BF03008369>
- Pittman, R. N., & Duling, B. R. (1973). Oxygen sensitivity of vascular smooth muscle. I. In vitro studies. *Microvascular research*, 6(2), 202–211. [https://doi.org/10.1016/0026-2862\(73\)90020-4](https://doi.org/10.1016/0026-2862(73)90020-4)
- Pittman R. N. (2000). Oxygen supply to contracting skeletal muscle at the microcirculatory level: diffusion vs. convection. *Acta physiologica Scandinavica*, 168(4), 593–602. <https://doi.org/10.1046/j.1365-201x.2000.00710.x>
- Pittman R. N. (2005). Oxygen transport and exchange in the microcirculation. *Microcirculation (New York, N.Y.: 1994)*, 12(1), 59–70. <https://doi.org/10.1080/10739680590895064>
- Pittman R. N. (2011). Oxygen gradients in the microcirculation. *Acta physiologica (Oxford, England)*, 202(3), 311–322. <https://doi.org/10.1111/j.1748-1716.2010.02232.x>
- Pittman R. N. (2013). Oxygen transport in the microcirculation and its regulation. *Microcirculation (New York, N.Y.: 1994)*, 20(2), 117–137. <https://doi.org/10.1111/micc.12017>
- Pohl, U., De Wit, C., & Gloe, T. (2000). Large arterioles in the control of blood flow: role of endothelium-dependent dilation. *Acta physiologica Scandinavica*, 168(4), 505–510. <https://doi.org/10.1046/j.1365-201x.2000.00702.x>
- Pohl, U., & Busse, R. (1989). Hypoxia stimulates release of endothelium-derived relaxant factor. *The American journal of physiology*, 256(6 Pt 2), H1595–H1600. <https://doi.org/10.1152/ajpheart.1989.256.6.H1595>
- Poole, D. C., Behnke, B. J., McDonough, P., McAllister, R. M., & Wilson, D. F. (2004). Measurement of muscle microvascular oxygen pressures: compartmentalization of phosphorescent probe. *Microcirculation (New York, N.Y.: 1994)*, 11(4), 317–326. <https://doi.org/10.1080/10739680490437487>
- Poole, D. C., Wagner, P. D., & Wilson, D. F. (1995). Diaphragm microvascular plasma PO<sub>2</sub> measured in vivo. *Journal of applied physiology (Bethesda, Md.: 1985)*, 79(6), 2050–2057. <https://doi.org/10.1152/jappl.1995.79.6.2050>

- Poiseuille JLM. Recherches expérimentales sur le mouvement des liquids dans les tubes de très petits diamètres. *Mem Acad Sci (Paris)* 1846; 9:433–544.
- Popel A. S. (1989). Theory of oxygen transport to tissue. *Critical reviews in biomedical engineering*, 17(3), 257–321.
- Potter, R. F., Dietrich, H. H., Tyml, K., Ellis, C. G., Cronkwright, J., & Groom, A. C. (1993). Ischemia-reperfusion induced microvascular dysfunction in skeletal muscle: application of intravital video microscopy. *International journal of microcirculation, clinical and experimental*, 13(3), 173–186.
- Prahl, S. (1999). Optical absorption of hemoglobin. Retrieved from <https://omlc.org/spectra/hemoglobin/>.
- Pries, A. R., Ley, K., & Gaehtgens, P. (1986). Generalization of the Fahraeus principle for microvessel networks. *The American journal of physiology*, 251(6 Pt 2), H1324–H1332. <https://doi.org/10.1152/ajpheart.1986.251.6.H1324>
- Pries, A. R., Secomb, T. W., Gessner, T., Sperandio, M. B., Gross, J. F., & Gaehtgens, P. (1994). Resistance to blood flow in microvessels in vivo. *Circulation research*, 75(5), 904–915. <https://doi.org/10.1161/01.res.75.5.904>
- Pries, A. R., Secomb, T. W., & Gaehtgens, P. (1995). Structure and hemodynamics of microvascular networks: heterogeneity and correlations. *The American journal of physiology*, 269(5 Pt 2), H1713–H1722. <https://doi.org/10.1152/ajpheart.1995.269.5.H1713>
- Pugsley, M. K., & Tabrizchi, R. (2000). The vascular system. An overview of structure and function. *Journal of pharmacological and toxicological methods*, 44(2), 333–340. [https://doi.org/10.1016/s1056-8719\(00\)00125-8](https://doi.org/10.1016/s1056-8719(00)00125-8)
- Quayle, J. M., Nelson, M. T., & Standen, N. B. (1997). ATP-sensitive and inwardly rectifying potassium channels in smooth muscle. *Physiological reviews*, 77(4), 1165–1232. <https://doi.org/10.1152/physrev.1997.77.4.1165>
- Reglin, B., Secomb, T. W., & Pries, A. R. (2009). Structural adaptation of microvessel diameters in response to metabolic stimuli: where are the oxygen sensors? *American journal of physiology. Heart and circulatory physiology*, 297(6), H2206–H2219. <https://doi.org/10.1152/ajpheart.00348.2009>
- Renkin E. M. (1985). B. W. Zweifach Award lecture. Regulation of the microcirculation. *Microvascular research*, 30(3), 251–263. [https://doi.org/10.1016/0026-2862\(85\)90057-3](https://doi.org/10.1016/0026-2862(85)90057-3)
- Riemann, M., Rai, A., Ngo, A. T., Dziegiel, M. H., Holstein-Rathlou, N. H., & Torp-Pedersen, C. (2011). Oxygen-dependent vasomotor responses are conducted upstream in the mouse cremaster microcirculation. *Journal of vascular research*, 48(1), 79–89. <https://doi.org/10.1159/000318777>

- Rowell L. B. (2004). Ideas about control of skeletal and cardiac muscle blood flow (1876-2003): cycles of revision and new vision. *Journal of applied physiology (Bethesda, Md.: 1985)*, 97(1), 384–392.  
<https://doi.org/10.1152/jappphysiol.01220.2003>
- Roy, T. K., Pries, A. R., & Secomb, T. W. (2012). Theoretical comparison of wall-derived and erythrocyte-derived mechanisms for metabolic flow regulation in heterogeneous microvascular networks. *American journal of physiology. Heart and circulatory physiology*, 302(10), H1945–H1952.  
<https://doi.org/10.1152/ajpheart.01176.2011>
- Roy, T. K. & Secomb, T. W. (2014). Functional sympatholysis and sympathetic escape in a theoretical model for blood flow regulation. *Frontiers in Physiology*, 5, 192.  
<https://doi.org/10.3389/fphys.2014.00192>
- Rubanyi, G. M., & Polokoff, M. A. (1994). Endothelins: molecular biology, biochemistry, pharmacology, physiology, and pathophysiology. *Pharmacological reviews*, 46(3), 325–415
- Rubino, A., Ralevic, V., & Burnstock, G. (1995). Contribution of P1-(A2b subtype) and P2-purinoreceptors to the control of vascular tone in the rat isolated mesenteric arterial bed. *British journal of pharmacology*, 115(4), 648–652.  
<https://doi.org/10.1111/j.1476-5381.1995.tb14981.x>
- Rumsey, W. L., Vanderkooi, J. M., & Wilson, D. F. (1988). Imaging of phosphorescence: a novel method for measuring oxygen distribution in perfused tissue. *Science (New York, N.Y.)*, 241(4873), 1649–1651.  
<https://doi.org/10.1126/science.241.4873.1649>
- Russell McEvoy, G. M., Shogan, H., Sové, R. J., & Fraser, G. M. (2021). Development and validation of a novel microfluidic device for the manipulation of skeletal muscle microvascular blood flow in vivo. *Microcirculation (New York, N.Y.: 1994)*, 28(5), e12698. <https://doi.org/10.1111/micc.12698>
- Russell McEvoy, G. M., Wells, B. N., Kiley, M. E., Kaur, K. K., & Fraser, G. M. (2022). Dynamics of capillary blood flow responses to acute local changes in oxygen and carbon dioxide concentrations. *Frontiers in physiology*, 13, 1052449.  
<https://doi.org/10.3389/fphys.2022.1052449>
- Safo, M.K. & Bruno, S. (2011). Allosteric effectors of hemoglobin: past, present, and future. In: *Chemistry and biochemistry of oxygen therapeutics*. Wiley, Ltd, pp 285–300.
- Saltin B. (2007). Exercise hyperaemia: magnitude and aspects on regulation in humans. *The Journal of physiology*, 583(Pt 3), 819–823.  
<https://doi.org/10.1113/jphysiol.2007.136309>

- Samora, J. B., Frisbee, J. C., & Boegehold, M. A. (2008). Increased myogenic responsiveness of skeletal muscle arterioles with juvenile growth. *American journal of physiology. Heart and circulatory physiology*, 294(5), H2344–H2351. <https://doi.org/10.1152/ajpheart.00053.2008>
- Schifffrin, E. L., & Touyz, R. M. (1998). Vascular biology of endothelin. *Journal of cardiovascular pharmacology*, 32 Suppl 3, S2–S13.
- Schjørring, O. L., Carlsson, R., & Simonsen, U. (2015). Pressure Myography to Study the Function and Structure of Isolated Small Arteries. *Methods in molecular biology (Clifton, N.J.)*, 1339, 277–295. [https://doi.org/10.1007/978-1-4939-2929-0\\_19](https://doi.org/10.1007/978-1-4939-2929-0_19)
- Schubert, R., & Mulvany, M. J. (1999). The myogenic response: established facts and attractive hypotheses. *Clinical science (London, England: 1979)*, 96(4), 313–326.
- Secomb T. W. (2008). Theoretical models for regulation of blood flow. *Microcirculation (New York, N.Y.: 1994)*, 15(8), 765–775. <https://doi.org/10.1080/10739680802350112>
- Secomb, T. W., & Pries, A. R. (2011). The microcirculation: physiology at the mesoscale. *The Journal of physiology*, 589(Pt 5), 1047–1052. <https://doi.org/10.1113/jphysiol.2010.201541>
- Secomb, T. W., & Pries, A. R. (2016). Microvascular Plasticity: Angiogenesis in Health and Disease--Preface. *Microcirculation (New York, N.Y.: 1994)*, 23(2), 93–94. <https://doi.org/10.1111/micc.12262>
- Segal S. S. (1994). Cell-to-cell communication coordinates blood flow control. *Hypertension (Dallas, Tex.: 1979)*, 23(6 Pt 2), 1113–1120. <https://doi.org/10.1161/01.hyp.23.6.1113>
- Segal S. S. (2000). Integration of blood flow control to skeletal muscle: key role of feed arteries. *Acta physiologica Scandinavica*, 168(4), 511–518. <https://doi.org/10.1046/j.1365-201x.2000.00703.x>
- Segal S. S. (1991). Microvascular recruitment in hamster striated muscle: role for conducted vasodilation. *The American journal of physiology*, 261(1 Pt 2), H181–H189. <https://doi.org/10.1152/ajpheart.1991.261.1.H181>
- Segal S. S. (2005). Regulation of blood flow in the microcirculation. *Microcirculation (New York, N.Y.:1994)*, 12, 33–45. <https://doi.org/10.1080/10739680590895028>
- Segal, S. S., Damon, D. N., & Duling, B. R. (1989). Propagation of vasomotor responses coordinates arteriolar resistances. *The American journal of physiology*, 256(3 Pt 2), H832–H837. <https://doi.org/10.1152/ajpheart.1989.256.3.H832>

- Segal, S. S., & Duling, B. R. (1986). Communication between feed arteries and microvessels in hamster striated muscle: segmental vascular responses are functionally coordinated. *Circulation research*, *59*(3), 283–290. <https://doi.org/10.1161/01.res.59.3.283>
- Segal, S. S., & Duling, B. R. (1987). Propagation of vasodilation in resistance vessels of the hamster: development and review of a working hypothesis. *Circulation research*, *61*(5 Pt 2), II20–II25.
- Segal, S. S., & Kurjiaka, D. T. (1995). Coordination of blood flow control in the resistance vasculature of skeletal muscle. *Medicine and science in sports and exercise*, *27*(8), 1158–1164.
- Sessa W. C. (2004). eNOS at a glance. *Journal of cell science*, *117*(Pt 12), 2427–2429. <https://doi.org/10.1242/jcs.01165>
- Shi, Z. D., & Tarbell, J. M. (2011). Fluid flow mechanotransduction in vascular smooth muscle cells and fibroblasts. *Annals of biomedical engineering*, *39*(6), 1608–1619. <https://doi.org/10.1007/s10439-011-0309-2>
- Si, H., Heyken, W. T., Wölfle, S. E., Tysiac, M., Schubert, R., Grgic, I., Vilianovich, L., Giebing, G., Maier, T., Gross, V., Bader, M., de Wit, C., Hoyer, J., & Köhler, R. (2006). Impaired endothelium-derived hyperpolarizing factor-mediated dilations and increased blood pressure in mice deficient of the intermediate-conductance Ca<sup>2+</sup>-activated K<sup>+</sup> channel. *Circulation research*, *99*(5), 537–544. <https://doi.org/10.1161/01.RES.0000238377.08219.0c>
- Sindler, A. L., Delp, M. D., Reyes, R., Wu, G., & Muller-Delp, J. M. (2009). Effects of ageing and exercise training on eNOS uncoupling in skeletal muscle resistance arterioles. *The Journal of physiology*, *587*(Pt 15), 3885–3897. <https://doi.org/10.1113/jphysiol.2009.172221>
- Smith, L. M., Golub, A. S., & Pittman, R. N. (2002). Interstitial PO<sub>2</sub> determination by phosphorescence quenching microscopy. *Microcirculation (New York, N.Y.: 1994)*, *9*(5), 389–395. <https://doi.org/10.1038/sj.mn.7800147>
- Somlyo, A. V., Khromov, A. S., Webb, M. R., Ferenczi, M. A., Trentham, D. R., He, Z. H., Sheng, S., Shao, Z., & Somlyo, A. P. (2004). Smooth muscle myosin: regulation and properties. *Philosophical transactions of the Royal Society of London. Series B, Biological sciences*, *359*(1452), 1921–1930. <https://doi.org/10.1098/rstb.2004.1562>
- Somlyo, A. P., & Somlyo, A. V. (1994). Smooth muscle: excitation-contraction coupling contractile regulation, and the cross-bridge cycle. *Alcoholism, clinical and experimental research*, *18*(1), 138–143. <https://doi.org/10.1111/j.1530-0277.1994.tb00893.x>

- Song, H., & Tyml, K. (1993). Evidence for sensing and integration of biological signals by the capillary network. *The American journal of physiology*, 265(4 Pt 2), H1235–H1242. <https://doi.org/10.1152/ajpheart.1993.265.4.H1235>
- Sove, R. J., Ghonaim, N., Goldman, D., & Ellis, C. G. (2013). A computational model of a microfluidic device to measure the dynamics of oxygen-dependent ATP release from erythrocytes. *PloS one*, 8(11), e81537. <https://doi.org/10.1371/journal.pone.0081537>
- Sové, R. J., Fraser, G. M., Goldman, D., & Ellis, C. G. (2016). Finite Element Model of Oxygen Transport for the Design of Geometrically Complex Microfluidic Device Used in Biological Studies. *PloS one*, 11(11), e0166289. <https://doi.org/10.1371/journal.pone.0166289>
- Sové, R. J., Milkovich, S., Nikolov, H. N., Holdsworth, D. W., Ellis, C. G., & Fraser, G. M. (2021). Localized Oxygen Exchange Platform for Intravital Video Microscopy Investigations of Microvascular Oxygen Regulation. *Frontiers in physiology*, 12, 654928. <https://doi.org/10.3389/fphys.2021.654928>
- Sorriento, D., Trimarco, B., & Iaccarino, G. (2011). Adrenergic mechanism in the control of endothelial function. *Translational medicine @ UniSa*, 1, 213–228.
- Sparks H. V. (1980). Mechanism of vasodilation during and after ischemic exercise. *Federation proceedings*, 39(5), 1487–1490.
- Spires, J., Gladden, L. B., Grassi, B., Goodwin, M. L., Saidel, G. M., & Lai, N. (2013). Distinguishing the effects of convective and diffusive O<sub>2</sub> delivery on VO<sub>2</sub> on-kinetics in skeletal muscle contracting at moderate intensity. *American journal of physiology. Regulatory, integrative, and comparative physiology*, 305(5), R512–R521. <https://doi.org/10.1152/ajpregu.00136.2013>
- Sprague, R. S., & Ellsworth, M. L. (2012). Erythrocyte-derived ATP and perfusion distribution: role of intracellular and intercellular communication. *Microcirculation (New York, N.Y.:1994)*, 19(5), 430–439. <https://doi.org/10.1111/j.1549-8719.2011.00158.x>
- Sprague, R. S., Ellsworth, M. L., Stephenson, A. H., & Lonigro, A. J. (1996). ATP: the red blood cell link to NO and local control of the pulmonary circulation. *The American journal of physiology*, 271(6 Pt 2), H2717–H2722. <https://doi.org/10.1152/ajpheart.1996.271.6.H2717>
- Sprague, R. S., Ellsworth, M. L., Stephenson, A. H., Kleinhenz, M. E., & Lonigro, A. J. (1998). Deformation-induced ATP release from red blood cells requires CFTR activity. *The American journal of physiology*, 275(5), H1726–H1732. <https://doi.org/10.1152/ajpheart.1998.275.5.H1726>

- Sprague, R. S., Hanson, M. S., Achilleus, D., Bowles, E. A., Stephenson, A. H., Sridharan, M., Adderley, S., Procknow, J., & Ellsworth, M. L. (2009). Rabbit erythrocytes release ATP and dilate skeletal muscle arterioles in the presence of reduced oxygen tension. *Pharmacological reports: PR*, *61*(1), 183–190. [https://doi.org/10.1016/s1734-1140\(09\)70020-9](https://doi.org/10.1016/s1734-1140(09)70020-9)
- Sprague, R. S., Goldman, D., Bowles, E. A., Achilleus, D., Stephenson, A. H., Ellis, C. G., & Ellsworth, M. L. (2010). Divergent effects of low-O<sub>2</sub> tension and iloprost on ATP release from erythrocytes of humans with type 2 diabetes: implications for O<sub>2</sub> supply to skeletal muscle. *American journal of physiology. Heart and circulatory physiology*, *299*(2), H566–H573. <https://doi.org/10.1152/ajpheart.00430.2010>
- Sridharan, M., Sprague, R. S., Adderley, S. P., Bowles, E. A., Ellsworth, M. L., & Stephenson, A. H. (2010). Diamide decreases deformability of rabbit erythrocytes and attenuates low oxygen tension-induced ATP release. *Experimental biology and medicine (Maywood, N.J.)*, *235*(9), 1142–1148. <https://doi.org/10.1258/ebm.2010.010118>
- Sridharan, M., Adderley, S. P., Bowles, E. A., Egan, T. M., Stephenson, A. H., Ellsworth, M. L., Sprague, R. S. (2010). Pannexin 1 is the conduit for low oxygen tension-induced ATP release from human erythrocytes. *American journal of physiology. Heart and circulatory physiology*, *299*(4), H1146–H1152. <https://doi.org/10.1152/ajpheart.00301.2010>
- Stamler, J. S., Jia, L., Eu, J. P., McMahon, T. J., Demchenko, I. T., Bonaventura, J., Gernert, K., & Piantadosi, C. A. (1997). Blood flow regulation by S-nitrosohemoglobin in the physiological oxygen gradient. *Science (New York, N.Y.)*, *276*(5321), 2034–2037. <https://doi.org/10.1126/science.276.5321.2034>
- Stein, J. C., Ellis, C. G., & Ellsworth, M. L. (1993). Relationship between capillary and systemic venous PO<sub>2</sub> during nonhypoxic and hypoxic ventilation. *The American journal of physiology*, *265*(2 Pt 2), H537–H542. <https://doi.org/10.1152/ajpheart.1993.265.2.H537>
- Stein, J. C., & Ellsworth, M. L. (1993). Capillary oxygen transport during severe hypoxia: role of hemoglobin oxygen affinity. *Journal of applied physiology (Bethesda, Md.: 1985)*, *75*(4), 1601–1607. <https://doi.org/10.1152/jappl.1993.75.4.1601>
- Storch, U., Blodow, S., Gudermann, T., & Mederos Y Schnitzler, M. (2015). Cysteinyl leukotriene 1 receptors as novel mechanosensors mediating myogenic tone together with angiotensin II type 1 receptors-brief report. *Arteriosclerosis, thrombosis, and vascular biology*, *35*(1), 121–126. <https://doi.org/10.1161/ATVBAHA.114.304844>

- Sullivan, S. M., & Johnson, P. C. (1981). Effect of oxygen on blood flow autoregulation in cat sartorius muscle. *The American journal of physiology*, 241(6), H807–H815. <https://doi.org/10.1152/ajpheart.1981.241.6.H807>
- Sutera, S P., & Skalak, R. (1993). The History of Poiseuille's Law. *Annual Review of Fluid Mechanics*. 25: 19. 1993. doi:10.1146/annurev.fl.25.010193.000245
- Swain, D. P., & Pittman, R. N. (1989). Oxygen exchange in the microcirculation of hamster retractor muscle. *The American journal of physiology*, 256(1 Pt 2), H247–H255. <https://doi.org/10.1152/ajpheart.1989.256.1.H247>
- Takano, H., Dora, K. A., & Garland, C. J. (2005). Spreading vasodilatation in resistance arteries. *Journal of smooth muscle research = Nihon Heikatsukin Gakkai kikanishi*, 41(6), 303–311. <https://doi.org/10.1540/jsmr.41.303>
- Tateishi, J., & Faber, J. E. (1995a). ATP-sensitive K<sup>+</sup> channels mediate alpha 2D-adrenergic receptor contraction of arteriolar smooth muscle and reversal of contraction by hypoxia. *Circulation research*, 76(1), 53–63. <https://doi.org/10.1161/01.res.76.1.53>
- Tateishi, J., & Faber, J. E. (1995b). Inhibition of arteriole alpha 2- but not alpha 1-adrenoceptor constriction by acidosis and hypoxia in vitro. *The American journal of physiology*, 268(5 Pt 2), H2068–H2076. <https://doi.org/10.1152/ajpheart.1995.268.5.H2068>
- Tykocki, N. R., Boerman, E. M., & Jackson, W. F. (2017). Smooth Muscle Ion Channels and Regulation of Vascular Tone in Resistance Arteries and Arterioles. *Comprehensive Physiology*, 7(2), 485–581. <https://doi.org/10.1002/cphy.c160011>
- Tyml, K., & Budreau, C. H. (1991). A new preparation of rat extensor digitorum longus muscle for intravital investigation of the microcirculation. *International journal of microcirculation, clinical and experimental*, 10(4), 335–343.
- Vanhoutte P. M. (2001). Endothelial adrenoceptors. *Journal of cardiovascular pharmacology*, 38(5), 796–808. <https://doi.org/10.1097/00005344-200111000-00016>
- Varghese, H. J., Mackenzie, L. T., Groom, A. C., Ellis, C. G., Ryan, A., MacDonald, I. C., & Chambers, A. F. (2004). In vivo video microscopy reveals differential effects of the vascular-targeting agent ZD6126 and the anti-angiogenic agent ZD6474 on vascular function in a liver metastasis model. *Angiogenesis*, 7(2), 157–164. <https://doi.org/10.1007/s10456-004-1941-3>
- Wan, J., Forsyth, A. M., & Stone, H. A. (2011). Red blood cell dynamics: from cell deformation to ATP release. *Integrative biology: quantitative biosciences from nano to macro*, 3(10), 972–981. <https://doi.org/10.1039/c1ib00044f>

- Wan, J., Ristenpart, W. D., & Stone, H. A. (2008). Dynamics of shear-induced ATP release from red blood cells. *Proceedings of the National Academy of Sciences of the United States of America*, *105*(43), 16432–16437. <https://doi.org/10.1073/pnas.0805779105>
- Wang, X. Y., Pichl, C., Gabor, F., & Wirth, M. (2013). A novel cell-based microfluidic multichannel setup-impact of hydrodynamics and surface characteristics on the bio adhesion of polystyrene microspheres. *Colloids and surfaces. B, Biointerfaces*, *102*, 849–856. <https://doi.org/10.1016/j.colsurfb.2012.09.012>
- Ward M. E. (1999). Dilation of rat diaphragmatic arterioles by flow and hypoxia: roles of nitric oxide and prostaglandins. *Journal of applied physiology (Bethesda, Md: 1985)*, *86*(5), 1644–1650. <https://doi.org/10.1152/jappl.1999.86.5.1644>
- Webb, D. J., & Haynes, W. G. (1995). The role of endothelin-1 in cardiovascular physiology and pathophysiology. *Scottish medical journal*, *40*(3), 69–1. <https://doi.org/10.1177/003693309504000302>
- Weibel ER. The Pathway for Oxygen Structure and Function in the Mammalian Respiratory System. Cambridge, MA: Harvard University Press; 1984. p.425.
- Welsh, D. G., Jackson, W. F., & Segal, S. S. (1998). Oxygen induces electromechanical coupling in arteriolar smooth muscle cells: a role for L-type Ca<sup>2+</sup> channels. *The American journal of physiology*, *274*(6), H2018–H2024. <https://doi.org/10.1152/ajpheart.1998.274.6.H2018>
- Welsh, D. G., & Segal, S. S. (1998). Endothelial and smooth muscle cell conduction in arterioles controlling blood flow. *The American journal of physiology*, *274*(1), H178–H186. <https://doi.org/10.1152/ajpheart.1998.274.1.H178>
- Welsh, D. G., & Segal, S. S. (2000). Role of EDHF in conduction of vasodilation along hamster cheek pouch arterioles in vivo. *American journal of physiology. Heart and circulatory physiology*, *278*(6), H1832–H1839. <https://doi.org/10.1152/ajpheart.2000.278.6.H1832>
- Wenceslau, C. F., McCarthy, C. G., Earley, S., England, S. K., Filosa, J. A., Goulopoulou, S., Gutterman, D. D., Isakson, B. E., Kanagy, N. L., Martinez-Lemus, L. A., Sonkusare, S. K., Thakore, P., Trask, A. J., Watts, S. W., & Webb, R. C. (2021). Guidelines for the measurement of vascular function and structure in isolated arteries and veins. *American journal of physiology. Heart and circulatory physiology*, *321*(1), H77–H111. <https://doi.org/10.1152/ajpheart.01021.2020>
- Whalen, W. J., Riley, J., & Nair, P. (1967). A microelectrode for measuring intracellular PO<sub>2</sub>. *Journal of applied physiology*, *23*(5), 798–801. <https://doi.org/10.1152/jappl.1967.23.5.798>

- Whiteley, J. P., Gavaghan, D. J., & Hahn, C. E. (2002). Mathematical modelling of oxygen transport to tissue. *Journal of mathematical biology*, 44(6), 503–522. <https://doi.org/10.1007/s002850200135>
- Whiteley, J. P., Gavaghan, D. J., & Hahn, C. E. (2003). Mathematical modelling of pulmonary gas transport. *Journal of mathematical biology*, 47(1), 79–99. <https://doi.org/10.1007/s00285-003-0196-8>
- Wihlborg, A. K., Malmjö, M., Eyjolfsson, A., Gustafsson, R., Jacobson, K., & Erlinge, D. (2003). Extracellular nucleotides induce vasodilatation in human arteries via prostaglandins, nitric oxide and endothelium-derived hyperpolarising factor. *British journal of pharmacology*, 138(8), 1451–1458. <https://doi.org/10.1038/sj.bjp.0705186>
- Wilson D. F. (1990). Contribution of diffusion to the oxygen dependence of energy metabolism in cells. *Experientia*, 46(11-12), 1160–1162. <https://doi.org/10.1007/BF01936927>
- Wilson, D. F., Erecińska, M., Drown, C., & Silver, I. A. (1979). The oxygen dependence of cellular energy metabolism. *Archives of biochemistry and biophysics*, 195(2), 485–493. [https://doi.org/10.1016/0003-9861\(79\)90375-8](https://doi.org/10.1016/0003-9861(79)90375-8)
- Wilson, D. F., Lee, W. M., Makonnen, S., Finikova, O., Apreleva, S., & Vinogradov, S. A. (2006). Oxygen pressures in the interstitial space and their relationship to those in the blood plasma in resting skeletal muscle. *Journal of applied physiology (Bethesda, Md.: 1985)*, 101(6), 1648–1656. <https://doi.org/10.1152/japplphysiol.00394.2006>
- Wilson, D. F., Vanderkooi, J. M., Green, T. J., Maniara, G., DeFeo, S. P., & Bloomgarden, D. C. (1987). A versatile and sensitive method for measuring oxygen. *Advances in experimental medicine and biology*, 215, 71–77. <https://doi.org/10.1007/978-1-4684-7433-69>
- Wynne, B. M., Chiao, C. W., & Webb, R. C. (2009). Vascular Smooth Muscle Cell Signaling Mechanisms for Contraction to Angiotensin II and Endothelin-1. *Journal of the American Society of Hypertension: JASH*, 3(2), 84–95. <https://doi.org/10.1016/j.jash.2008.09.002>
- Xiang, L., Naik, J. S., & Hester, R. L. (2008). Functional vasodilation in the rat spinotrapezius muscle: role of nitric oxide, prostanoids and epoxyeicosatrienoic acids. *Clinical and experimental pharmacology & physiology*, 35(5-6), 617–624. <https://doi.org/10.1111/j.1440-1681.200704864.x>
- Yonetani, T., & Laberge, M. (2008). Protein dynamics explain the allosteric behaviors of hemoglobin. *Biochimica et biophysica acta*, 1784(9), 1146–1158. <https://doi.org/10.1016/j.bbapap.2008.04.025>
- Yuan, S. Y., & Rigor, R. R. (2010). Regulation of Endothelial Barrier Function. Morgan & Claypool Life Sciences. <https://doi.org/10.4199/c00025ed1v01y201101isp013>

Zweifach, B.W. and Lipowsky, H.H. (1984) Pressure-Flow Relations in Blood and Lymph Microcirculation. In: Handbook of Physiology, Sect. 2 (The Cardiovascular System), American Physiological Society, Bethesda, Chapter 7, 231-307.

## APPENDIX 1

### 1000 $\mu\text{m}$ Micro-Outlet Oxygen Oscillation Data

Oxygen ( $\text{O}_2$ ) oscillation data utilizing 1000  $\mu\text{m}$  micro-outlets for oxygen saturation ( $\text{SO}_2$ ) measurements consisted of a total of 266 capillaries across 7 animals (Figures AI.1-AI.4). A total of 150 capillaries were analyzed directly overlying the window and 116 capillaries were measured outside the outlet edge. With respect to capillaries measured outside the outlet edge, 26 were measured less than 100  $\mu\text{ms}$  away, 33 were between 100 – 200  $\mu\text{ms}$  away, and 57 were greater than 200  $\mu\text{ms}$  away.

$\text{O}_2$  oscillations imposed on capillaries directly overlying 1000  $\mu\text{m}$  diameter micro-outlets caused significant changes in capillary  $\text{SO}_2$  at 12% GEC [ $\text{O}_2$ ],  $87.38 \pm 9.04\%$ , and 2% GEC [ $\text{O}_2$ ],  $35.36 \pm 15.47\%$ , compared to baseline 7% GEC [ $\text{O}_2$ ],  $64.55 \pm 12.72\%$  and at 12% GEC [ $\text{O}_2$ ],  $87.38 \pm 9.04\%$ , compared to 2% GEC [ $\text{O}_2$ ],  $35.36 \pm 15.47\%$  (Figure AI.1) ( $p < 0.0001$ ).  $\text{O}_2$  oscillations imposed on capillaries less than 100  $\mu\text{ms}$  outside the micro-outlet edge caused a significant change in  $\text{SO}_2$  at 12% GEC [ $\text{O}_2$ ],  $63.54 \pm 15.59\%$  compared to baseline 7% GEC [ $\text{O}_2$ ],  $56.74 \pm 16.96\%$  ( $p = 0.0093$ ) (Figure AI.2).  $\text{O}_2$  oscillations imposed on capillaries between 100 – 200  $\mu\text{ms}$  away from the micro-outlet edge caused a significant change in  $\text{SO}_2$  at 12% GEC [ $\text{O}_2$ ],  $57.86 \pm 18.40\%$  compared to baseline 7% GEC [ $\text{O}_2$ ],  $52.14 \pm 17.79\%$  ( $p = 0.0019$ ) (Figure AI.2).

Oxygen ( $\text{O}_2$ ) oscillation data utilizing 1000  $\mu\text{m}$  micro-outlets for hemodynamic measurements consisted of a total of 316 capillaries across 7 animals. A total of 183 capillaries were analyzed directly overlying the window and 133 capillaries were measured

outside the outlet edge. With respect to capillaries measured outside the outlet edge, 26 were measured less than 100  $\mu\text{ms}$  away, 35 were between 100 – 200  $\mu\text{ms}$  away, and 72 greater than 200  $\mu\text{ms}$  away.

$\text{O}_2$  oscillations imposed on capillaries directly overlying 1000  $\mu\text{m}$  diameter micro-outlets caused significant changes in capillary hematocrit at 12% GEC [ $\text{O}_2$ ],  $17.45 \pm 10.74\%$ , and 2% GEC [ $\text{O}_2$ ],  $23.46 \pm 8.59\%$ , compared to baseline 7% GEC [ $\text{O}_2$ ]  $19.37 \pm 8.91\%$  ( $p < 0.0144$ ) (Figure AI.3).  $\text{O}_2$  oscillations caused no significant changes to capillary hematocrit in vessels at various distances from the outlet edge.

$\text{O}_2$  oscillations imposed on capillaries directly overlying 1000  $\mu\text{m}$  diameter micro-outlets caused significant changes in capillary velocity at 12% GEC [ $\text{O}_2$ ],  $137.90 \pm 82.8 \mu\text{m/s}$ , and 2% GEC [ $\text{O}_2$ ],  $207.80 \pm 131.10 \mu\text{m/s}$ , compared to baseline 7% GEC [ $\text{O}_2$ ],  $155.0 \pm 97.71 \mu\text{m/s}$  and 12% GEC [ $\text{O}_2$ ] compared to 2% GEC [ $\text{O}_2$ ] ( $p < 0.0022$ ) (Figure AI.5).  $\text{O}_2$  oscillations imposed on capillaries between 100 – 200  $\mu\text{ms}$  away from the micro-outlet edge caused a significant change at 2% GEC [ $\text{O}_2$ ],  $189.0 \pm 97.70 \mu\text{m/s}$ , compared to baseline 7% GEC [ $\text{O}_2$ ],  $165.9 \pm 78.51$  ( $p = 0.0099$ ).  $\text{O}_2$  oscillations imposed on capillaries greater than 200  $\mu\text{m}$  away from the micro-outlet edge caused a significant change at 2% GEC [ $\text{O}_2$ ],  $184.0 \pm 109.8 \mu\text{m/s}$ , and 7% GEC [ $\text{O}_2$ ],  $187.8 \pm 119.6 \mu\text{m/s}$  compared to baseline 7% GEC [ $\text{O}_2$ ],  $172.8 \pm 112.3 \mu\text{m/s}$  ( $p < 0.0179$ ) (Figure AI.6).

$\text{O}_2$  oscillations imposed on capillaries directly overlying 1000  $\mu\text{m}$  micro-outlets caused significant changes in capillary supply rate at 12% GEC [ $\text{O}_2$ ],  $5.98 \pm 5.87 \text{ cells/s}$ , 2% GEC [ $\text{O}_2$ ],  $13.45 \pm 11.18 \text{ cells/s}$ , and 7% GEC [ $\text{O}_2$ ],  $9.98 \pm 8.57 \text{ cells/s}$  compared to

baseline 7% GEC [O<sub>2</sub>]  $8.011 \pm 6.854$  cells/s and at 12% compared to 2% ( $p < 0.0001$ ) (Figure AI.7). O<sub>2</sub> oscillations imposed on capillaries between 100 – 200 μm away the micro-outlet edge caused a significant change in supply rate at 2% GEC [O<sub>2</sub>],  $11.58 \pm 6.38$  cells/s, compared to baseline 7% GEC [O<sub>2</sub>],  $9.91 \pm 5.74$  cells/s. O<sub>2</sub> oscillations imposed on capillaries greater than 200 μm away from the micro-outlet edge caused a significant change in supply rate at 2% GEC [O<sub>2</sub>],  $10.55 \pm 7.52$  cells/s, and 7% GEC [O<sub>2</sub>],  $10.45 \pm 7.47$  cells/s compared to baseline 7% GEC [O<sub>2</sub>],  $9.43 \pm 7.24$  cells/s ( $p < 0.006$ ) (Figure AI.8).

#### 1000 μm Micro-Outlet Oxygen Challenge Data

Oxygen (O<sub>2</sub>) challenge data utilizing 1000 μm diameter micro-outlets for oxygen saturation (SO<sub>2</sub>) measurements consisted of a total of 116 capillaries for 7-12% and 98 capillaries for 7-2% across 7 animals. A total of 71 in high O<sub>2</sub> challenges (7-12%) and 61 in low O<sub>2</sub> challenges (7-2%) capillaries were analyzed directly overlying the window. With respect to capillaries measured outside the outlet edge for high oxygen challenges, 9 were measured less than 100 μm away, 15 were between 100 – 200 μm away, and 21 were greater than 200 μm away. With respect to capillaries measured outside the outlet edge for low oxygen challenges, 10 were measured less than 100 μm away, 16 were between 100 – 200 μm away, and 11 were greater than 200 μm away.

O<sub>2</sub> challenges imposed on capillaries directly overlying 1000 μm micro-outlets caused significant changes in capillary SO<sub>2</sub> at 12% GEC [O<sub>2</sub>],  $88.03 \pm 9.16\%$ , compared to baseline 7% GEC [O<sub>2</sub>],  $65.40 \pm 13.18\%$  ( $p < 0.0001$ ) (Figure AI.9). O<sub>2</sub> challenges imposed

on capillaries directly overlying 1000  $\mu\text{m}$  micro-outlets caused significant changes in capillary  $\text{SO}_2$  at 2% GEC [ $\text{O}_2$ ],  $45.73 \pm 19.75\%$ , compared to baseline 7% GEC [ $\text{O}_2$ ],  $71.15 \pm 15.28\%$  ( $p < 0.0001$ ) (Figure AI.11). Both high and low  $\text{O}_2$  challenges imposed on capillaries caused no significant change in  $\text{SO}_2$  on capillaries outside the micro-outlet edge (Figure AI.10, AI.12).

Oxygen ( $\text{O}_2$ ) challenge data utilizing 1000  $\mu\text{m}$  micro-outlets for paired hemodynamic measurements consisted of a total of 200 capillaries across 6 animals. A total of 72 for high and 73 capillaries for low  $\text{O}_2$  challenges were analyzed directly overlying the window. With respect to capillaries measured outside the outlet edge during high challenges, 5 were measured less than 100  $\mu\text{ms}$  away, 12 were between 100 – 200  $\mu\text{ms}$  away, and 25 were greater than 200  $\mu\text{ms}$  away. With respect to capillaries measured outside the outlet edge during low challenges, 7 were measured less than 100  $\mu\text{ms}$  away, 13 were between 100 – 200  $\mu\text{ms}$  away, and 16 were greater than 200  $\mu\text{ms}$  away.

$\text{O}_2$  challenges imposed on capillaries directly overlying 1000  $\mu\text{m}$  micro-outlets caused significant changes in capillary hematocrit at 12% GEC [ $\text{O}_2$ ],  $20.40 \pm 12.29\%$ , compared to baseline 7% GEC [ $\text{O}_2$ ],  $22.55 \pm 12.12\%$  ( $p < 0.0001$ ) (Figure AI.13).  $\text{O}_2$  challenges imposed on capillaries directly overlying 1000  $\mu\text{m}$  micro-outlets caused significant changes in capillary hematocrit at 2% GEC [ $\text{O}_2$ ],  $25.81 \pm 9.12\%$ , compared to baseline 7% GEC [ $\text{O}_2$ ],  $19.34 \pm 10.04\%$  ( $p < 0.0001$ ) (Figure AI.15). Neither high nor low  $\text{O}_2$  challenges caused significant changes in capillary hematocrit for vessels outside the outlet edge (Figure AI.14, AI.16).

O<sub>2</sub> challenges imposed on capillaries directly overlying 1000 μm micro-outlets caused significant changes in capillary velocity at 12% GEC [O<sub>2</sub>], 121.9 ± 107.0 μm/s, compared to baseline 7% GEC [O<sub>2</sub>], 153.0 ± 115.8 μm/s ( $p < 0.0001$ ) (Figure AI.17). O<sub>2</sub> challenges imposed on capillaries directly overlying 1000 μm micro-outlets caused significant changes in capillary velocity at 2% GEC [O<sub>2</sub>], 261.2 ± 177.0 μm/s, compared to baseline 7% GEC [O<sub>2</sub>], 166.6 ± 123.7 μm/s ( $p < 0.0001$ ) (Figure AI.19). O<sub>2</sub> challenges caused significant changes in capillary velocity in vessels less than 100 μms away from the outlet edge at 2% GEC [O<sub>2</sub>], 136.2 ± 89.07 μm/s, compared to baseline 7% GEC [O<sub>2</sub>], 114.4 ± 88.25 μm/s ( $p = 0.0469$ ). Vessels between 100 – 200 μms away from the outlet edge experienced significant changes in capillary velocity as well at 2% GEC [O<sub>2</sub>], 196.1 ± 100.7 μm/s, compared to baseline 7% GEC [O<sub>2</sub>], 161.2 ± 92.51 μm/s ( $p = 0.0005$ ) (Figure AI.20).

O<sub>2</sub> challenges imposed on capillaries directly overlying 1000 μm micro-outlets caused significant changes in capillary supply rate at 12% GEC [O<sub>2</sub>], 6.80 ± 7.56 cells/s, compared to baseline 7% GEC [O<sub>2</sub>], 8.99 ± 8.67 cells/s ( $p < 0.0001$ ) (Figure AI.21). O<sub>2</sub> challenges imposed on capillaries directly overlying 1000 μm micro-outlets caused significant changes in capillary supply rate at 2% GEC [O<sub>2</sub>], 16.80 ± 12.70 cells/s, compared to baseline 7% GEC [O<sub>2</sub>], 8.23 ± 7.40 cells/s ( $p < 0.0001$ ) (Figure AI.23). O<sub>2</sub> challenges imposed on capillaries directly overlying 1000 μm micro-outlets caused no significant changes in capillary supply rate in vessels outside the outlet edge at 12% GEC [O<sub>2</sub>]. O<sub>2</sub> challenges imposed on capillaries directly overlying 1000 μm micro-outlets caused significant changes in capillary supply rate in vessels less than 100 μms away from the

outlet edge at 2% GEC [O<sub>2</sub>],  $9.24 \pm 6.31$  cells/s, compared to baseline 7% GEC [O<sub>2</sub>],  $7.04 \pm 5.77$  cells/s ( $p = 0.031$ ) (Figure AI.24). Vessels between 100 – 200  $\mu\text{ms}$  away from the outlet edge experienced significant changes in capillary supply rate at 2% GEC [O<sub>2</sub>],  $13.90 \pm 13.99$  cells/s, compared to baseline 7% GEC [O<sub>2</sub>],  $10.69 \pm 9.77$  cells/s ( $p = 0.0034$ ). Capillaries greater than 200  $\mu\text{ms}$  away showed significant changes in supply rate at 2% GEC [O<sub>2</sub>],  $13.52 \pm 12.36$  cells/s, compared to baseline 7% GEC [O<sub>2</sub>],  $10.85 \pm 9.07$  cells/s ( $p = 0.0443$ ) (Figure AI.24).

#### 600 $\mu\text{m}$ Micro-Outlet Oxygen Oscillation Data

Oxygen (O<sub>2</sub>) oscillation data utilizing 600  $\mu\text{m}$  diameter micro-outlets for oxygen saturation (SO<sub>2</sub>) measurements consisted of a total of 273 capillaries across 11 animals. 148 capillaries were analyzed directly overlying the window, and 125 were analyzed outside the outlet edge. Concerning capillaries measured outside the outlet edge, 37 were measured less than 100  $\mu\text{ms}$  away, 50 were between 100 – 200  $\mu\text{ms}$  away, and 38 were greater than 200  $\mu\text{ms}$  away.

O<sub>2</sub> oscillations imposed on capillaries directly overlying 600  $\mu\text{m}$  micro-outlets caused significant changes in mean capillary RBC SO<sub>2</sub> at 12% GEC [O<sub>2</sub>],  $84.12 \pm 11.24\%$  and 2% GEC [O<sub>2</sub>],  $42.83 \pm 15.75\%$ , compared to baseline 7% GEC [O<sub>2</sub>],  $66.90 \pm 13.04\%$  ( $p < 0.0001$ ). O<sub>2</sub> oscillations imposed on capillaries directly overlying 600  $\mu\text{m}$  micro-outlets caused significant changes in mean capillary SO<sub>2</sub> at 12% GEC [O<sub>2</sub>],  $84.12 \pm 11.24\%$ , compared to 2% GEC [O<sub>2</sub>],  $42.83 \pm 15.75\%$  ( $p < 0.0001$ ) (Figure AI.25). O<sub>2</sub> oscillations caused no significant changes in SO<sub>2</sub> in capillaries outside the micro-outlet edge (Figure AI.26).

Oxygen (O<sub>2</sub>) oscillation data utilizing 600 µm micro-outlets for hemodynamic measurements comprised a total of 270 capillaries across 11 animals. A total of 110 capillaries were analyzed directly overlying the window, and 160 were analyzed outside the outlet edge. Concerning capillaries measured outside the outlet edge, 40 were measured less than 100 µms away, 56 were between 100 – 200 µms away, and 64 were greater than 200 µms away.

O<sub>2</sub> oscillations imposed on capillaries directly overlying 600 µm micro-outlets caused significant changes in mean capillary hematocrit at 2% GEC [O<sub>2</sub>],  $23.58 \pm 8.75\%$ , and 7% GEC [O<sub>2</sub>],  $22.92 \pm 8.32\%$ , compared to baseline 7% GEC [O<sub>2</sub>],  $21.17 \pm 9.73\%$  ( $p < 0.0013$ ). Significant changes in mean capillary hematocrit were also found at 12% GEC [O<sub>2</sub>],  $19.54 \pm 9.57\%$ , compared to 2% GEC [O<sub>2</sub>],  $23.58 \pm 8.75\%$  ( $p < 0.0001$ ) (Figure AI.27).

O<sub>2</sub> oscillations caused significant changes in mean capillary hematocrit in capillaries less than 100 µms away from the outlet edge at 2% GEC [O<sub>2</sub>],  $26.06 \pm 12.11\%$ , compared to baseline 7% GEC [O<sub>2</sub>],  $23.43 \pm 11.96\%$  and between 12% GEC [O<sub>2</sub>],  $23.74 \pm 11.37\%$  and 2% GEC [O<sub>2</sub>],  $26.06 \pm 12.11\%$  ( $p = 0.0256$ ). O<sub>2</sub> oscillations caused significant changes in mean capillary hematocrit in capillaries 100 to 200 µms away from the outlet edge at 2% GEC [O<sub>2</sub>],  $18.74 \pm 8.62\%$ , compared to baseline 7% GEC [O<sub>2</sub>]  $16.93 \pm 8.37\%$  and between 12% GEC [O<sub>2</sub>],  $17.15 \pm 8.83\%$  and 2% GEC [O<sub>2</sub>],  $18.74 \pm 8.62\%$  ( $p = 0.0406$ ). O<sub>2</sub> oscillations did not cause significant changes in mean capillary hematocrit in capillaries greater than 200 µms away from the outlet edge (Figure AI.28).

O<sub>2</sub> oscillations imposed on capillaries directly overlying 600 μm micro-outlets caused significant changes in capillary velocity at 12% GEC [O<sub>2</sub>], 196.9 ± 111.5 μm/s, and 2% GEC [O<sub>2</sub>], 277.3 ± 143.8 μm/s, and 7% GEC [O<sub>2</sub>], 252.1 ± 133.5 μm/s, compared to baseline 7% GEC [O<sub>2</sub>], 214.7 ± 122.5 μm/s and at 12% GEC [O<sub>2</sub>], 196.9 ± 111.5 μm/s, compared to 2% GEC [O<sub>2</sub>], 277.3 ± 143.8 μm/s ( $p < 0.0464$ ) (Figure AI.29).

O<sub>2</sub> oscillations imposed on capillaries directly overlying 600 μm micro-outlets caused significant changes in capillary velocity in vessels less than 100 μms away from the outlet edge at 12% GEC [O<sub>2</sub>], 233.0 ± 123.3 μm/s, compared to 2% GEC [O<sub>2</sub>], 264.7 ± 140.1 μm/s, ( $p = 0.0032$ ). Capillaries 100 to 200 μms away from the outlet edge also experienced significant changes in velocity at 2% GEC [O<sub>2</sub>], 238.9 ± 145.5 μm/s, compared to baseline 7% GEC [O<sub>2</sub>], 217.4 ± 142.3 μm/s, and at 12% GEC [O<sub>2</sub>], 220.3 ± 136.4 μm/s, compared to 2% GEC [O<sub>2</sub>], 238.9 ± 145.5 μm/s, ( $p < 0.0035$ ) (Figure AI.30). Capillaries 200 μms away from the outlet edge also experienced significant changes in velocity at 2% GEC [O<sub>2</sub>], 260.7 ± 149.9 μm/s, and at 7% GEC [O<sub>2</sub>], 269.2 ± 153.2 μm/s, compared to baseline 7% GEC [O<sub>2</sub>], 238.2 ± 133.8 μm/s ( $p < 0.0017$ ) (Figure AI.30).

O<sub>2</sub> oscillations imposed on capillaries directly overlying 600 μm micro-outlets caused significant changes in capillary supply rate at 12% GEC [O<sub>2</sub>], 9.58 ± 8.15 cells/s, 2% GEC [O<sub>2</sub>], 16.69 ± 12.29 cells/s, and 7% GEC [O<sub>2</sub>], 14.63 ± 10.73 μm/s, compared to baseline 7% GEC [O<sub>2</sub>], 11.45 ± 9.14 cells/s and at 12% GEC [O<sub>2</sub>], 9.58 ± 8.15 cells/s, compared to 2% GEC [O<sub>2</sub>], 16.69 ± 12.29 cells/s ( $p < 0.0175$ ) (Figure AI.31).

O<sub>2</sub> oscillations imposed on capillaries directly overlying 600 µm micro-outlets caused significant changes in capillary supply rate in vessels less than 100 µms away from the outlet edge at 2% GEC [O<sub>2</sub>], 17.73 ± 12.35 cells/s, compared to baseline 7% GEC [O<sub>2</sub>], 14.41 ± 9.71 cells/s, and 12% GEC [O<sub>2</sub>], 13.84 ± 9.40 cells/s, compared to 2% GEC [O<sub>2</sub>], 17.73 ± 12.35 cells/s, (*p*<0.0146). Capillaries 100 to 200 µm away from the outlet edge experienced significant changes in supply rate at 2% GEC [O<sub>2</sub>], 10.53 ± 6.90 cells/s, compared to baseline 7% GEC [O<sub>2</sub>], 8.76 ± 6.25 cells/s, and at 12% GEC [O<sub>2</sub>], 8.97 ± 6.72 cells/s, compared to 2% GEC [O<sub>2</sub>], 10.53 ± 6.90 µm/s, (*p* < 0.0001). Capillaries greater than 200 µms away from the outlet edge showed significant changes in supply rate at 2% GEC [O<sub>2</sub>], 12.60 ± 8.09 cells/s, and 7% GEC [O<sub>2</sub>], 11.96 ± 7.54 cells/s, compared to baseline 7% GEC [O<sub>2</sub>], 10.44 ± 6.87 cells/s (*p* < 0.0098) (Figure AI.32).

#### 600 µm Micro-Outlet Oxygen Challenge Data

Oxygen (O<sub>2</sub>) challenge data utilizing 600 µm diameter micro-outlets for oxygen saturation measurements consisted of a total of 145 capillaries for 7-12 and 132 capillaries for 7-2 across 8 animals. A total of 83 in high O<sub>2</sub> challenges (7-12%) and 79 in low O<sub>2</sub> challenges (7-2%) capillaries were analyzed directly overlying the window. With respect to capillaries measured outside the outlet edge for high oxygen challenges, 21 were measured less than 100 µms away, 22 were between 100 – 200 µms away, and 19 were greater than 200 µms away. Concerning capillaries measured outside the outlet edge for low oxygen challenges, 15 were measured less than 100 µms away, 21 were between 100 – 200 µms away, and 17 were greater than 200 µms away.

O<sub>2</sub> challenges imposed on capillaries directly overlying 600 μm micro-outlets caused significant changes in capillary RBC SO<sub>2</sub> at 12% GEC [O<sub>2</sub>], 86.61 ± 10.57%, compared to baseline 7% GEC [O<sub>2</sub>], 67.98 ± 13.32% (*p* < 0.0001) (Figure AI.33). O<sub>2</sub> challenges imposed on capillaries directly overlying 600 μm micro-outlets caused significant changes in capillary RBC SO<sub>2</sub> at 2% GEC [O<sub>2</sub>], 50.22 ± 18.33%, compared to baseline 7% GEC [O<sub>2</sub>], 72.36 ± 11.26% (*p* < 0.0001) (Figure AI.35). Both high and low O<sub>2</sub> challenges imposed on capillaries caused no significant change in SO<sub>2</sub> on capillaries outside the micro-outlet edge (Figure AI.34, AI.36).

Oxygen (O<sub>2</sub>) challenge data utilizing 600 μm diameter micro-outlets for hemodynamic measurements consisted of a total of 280 capillaries across 8 animals. A total of 49 for high and 93 capillaries for low O<sub>2</sub> challenges were analyzed directly overlying the window. With respect to capillaries measured outside the outlet edge during high challenges, 28 were measured less than 100 μms away, 22 were between 100 – 200 μms away, and 33 were greater than 200 μms away. With respect to capillaries measured outside the outlet edge during low challenges, 18 were measured less than 100 μms away, 25 were between 100 – 200 μms away, and 30 were greater than 200 μms away.

O<sub>2</sub> challenges imposed on capillaries directly overlying 600 μm micro-outlets caused significant changes in capillary hematocrit at 2% GEC [O<sub>2</sub>], 25.54 ± 10.82%, compared to baseline 7% GEC [O<sub>2</sub>], 21.36 ± 10.93% (*p* < 0.0001) but not at 12% GEC [O<sub>2</sub>] compared to baseline 7% GEC [O<sub>2</sub>] (Figure AI.37, AI.39). O<sub>2</sub> challenges imposed on capillaries directly overlying 600 μm micro-outlets did not cause significant changes in capillary hematocrit in vessels outside at various distances from the outlet edge.

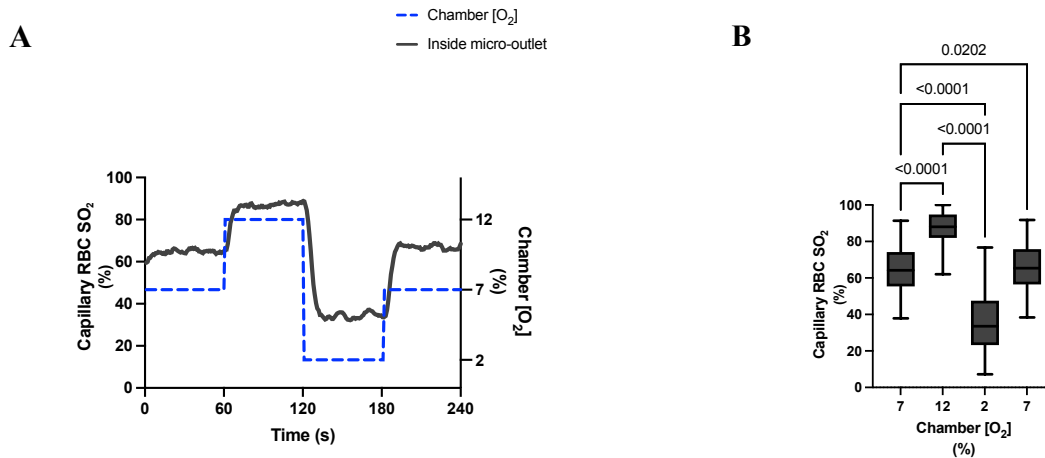
O<sub>2</sub> challenges imposed on capillaries directly overlying 600 μm micro-outlets caused significant changes in capillary velocity at 12% GEC [O<sub>2</sub>], 205.8 ± 147.7 μm/s, compared to baseline 7% GEC [O<sub>2</sub>], 239.3 ± 145.0 μm/s (*p* = 0.0018) (Figure AI.41). O<sub>2</sub> challenges imposed on capillaries less than 100 μm away from the 600 μm micro-outlets caused significant changes in capillary velocity at 12% GEC [O<sub>2</sub>], 224.9 ± 142.7 μm/s, compared to baseline 7% GEC [O<sub>2</sub>], 273.4 ± 156.4 μm/s and greater than 200 μm away at 12% GEC [O<sub>2</sub>], 270.7 ± 153.1 μm/s, compared to baseline 7% GEC [O<sub>2</sub>], 252.9 ± 127.9 μm/s (*p* = 0.0230) (Figure AI.42).

O<sub>2</sub> challenges imposed on capillaries directly overlying 600 μm micro-outlets caused significant changes in capillary velocity at 2% GEC [O<sub>2</sub>], 291.1 ± 182.7 μm/s, compared to baseline 7% GEC [O<sub>2</sub>], 218.1 ± 149.4 μm/s (*p* < 0.0001) (Figure AI.43). O<sub>2</sub> challenges imposed on capillaries directly overlying 600 μm micro-outlets did not cause significant changes in capillary velocity in vessels less than 200 μm away from the outlet edge but did in vessels 200 μm away at 2% GEC [O<sub>2</sub>], 280.3 ± 161.2 μm/s, compared to baseline 7% GEC [O<sub>2</sub>], 264.0 ± 151.3 μm/s (*p* = 0.0405) (Figure AI.44).

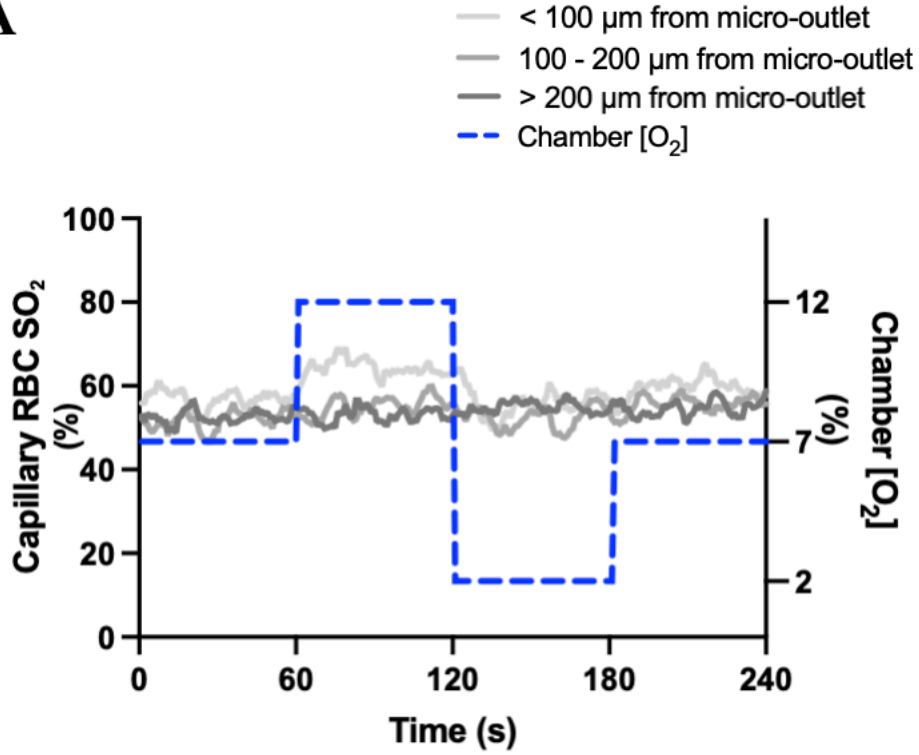
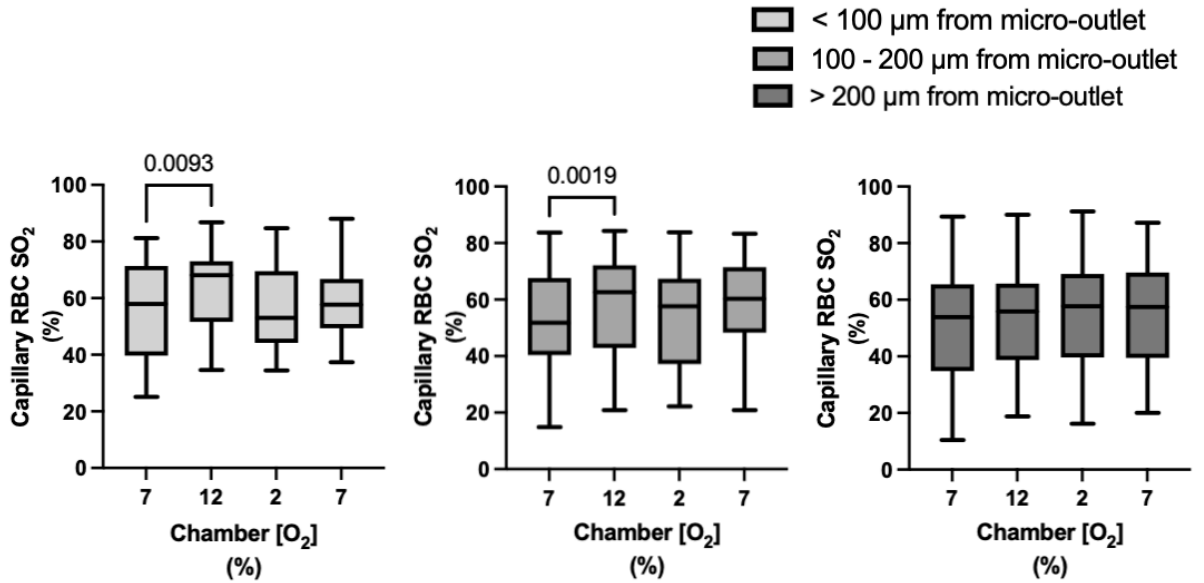
O<sub>2</sub> challenges imposed on capillaries directly overlying 600 μm micro-outlets caused significant changes in capillary supply rate at 12% GEC [O<sub>2</sub>], 12.04 ± 9.81 cells/s, compared to baseline 7% GEC [O<sub>2</sub>], 14.19 ± 9.72 cells/s (*p* = 0.0091) (Figure AI.45). O<sub>2</sub> challenges imposed on capillaries directly overlying 600 μm micro-outlets caused significant changes in capillary supply rate in vessels less than 100 μm away from the outlet edge at 12% GEC [O<sub>2</sub>] 15.80 ± 7.73 cells/s compared to baseline 7% GEC [O<sub>2</sub>] 12.52 ± 7.39 cells/s (*p* < 0.0012) and in vessels 200 μm away at 12% GEC [O<sub>2</sub>], 15.80 ± 12.85

cells/s, compared to baseline 7% GEC [O<sub>2</sub>], 13.68 ± 10.72 cells/s ( $p = 0.0098$ ) (Figure AI.46).

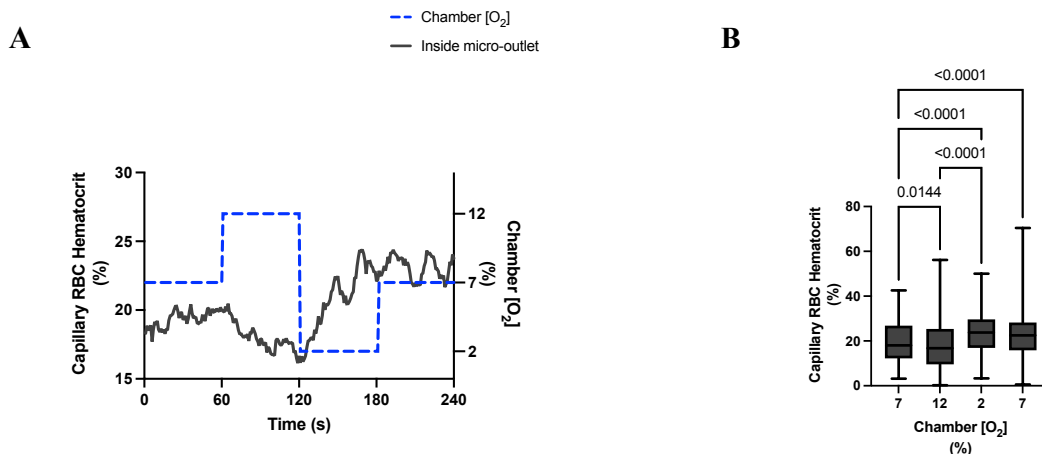
O<sub>2</sub> challenges imposed on capillaries directly overlying 600 μm micro-outlets caused significant changes in capillary supply rate at 2% GEC [O<sub>2</sub>], 18.41 ± 14.79 cells/s, compared to baseline 7% GEC [O<sub>2</sub>], 12.26 ± 11.91 cells/s ( $p < 0.0001$ ) (Figure AI.47). O<sub>2</sub> challenges imposed on capillaries directly overlying 600 μm micro-outlets caused significant changes in capillary supply rate in vessels less than 100 μm away from the outlet edge at 2% GEC [O<sub>2</sub>] 19.93 ± 17.06 cells/s compared to baseline 7% [O<sub>2</sub>] 16.38 ± 14.38 cells/s ( $p < 0.0237$ ) (Figure AI.48).



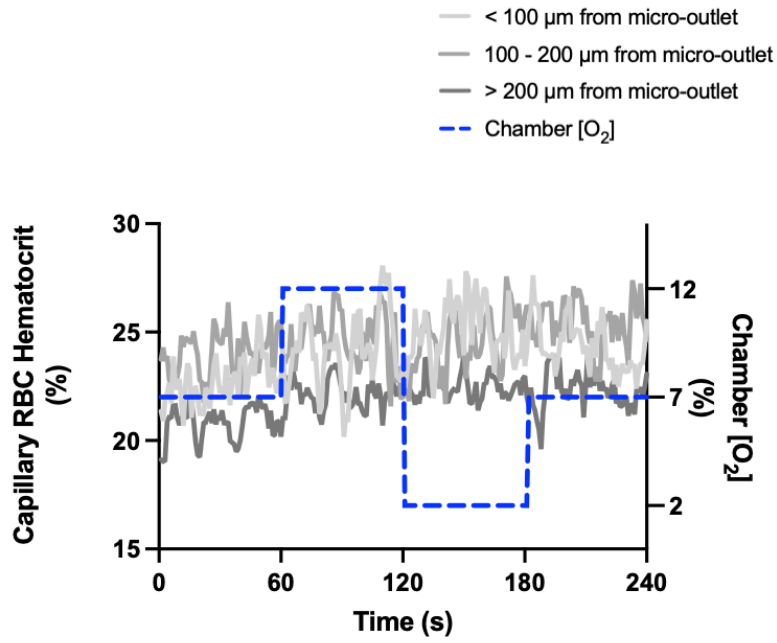
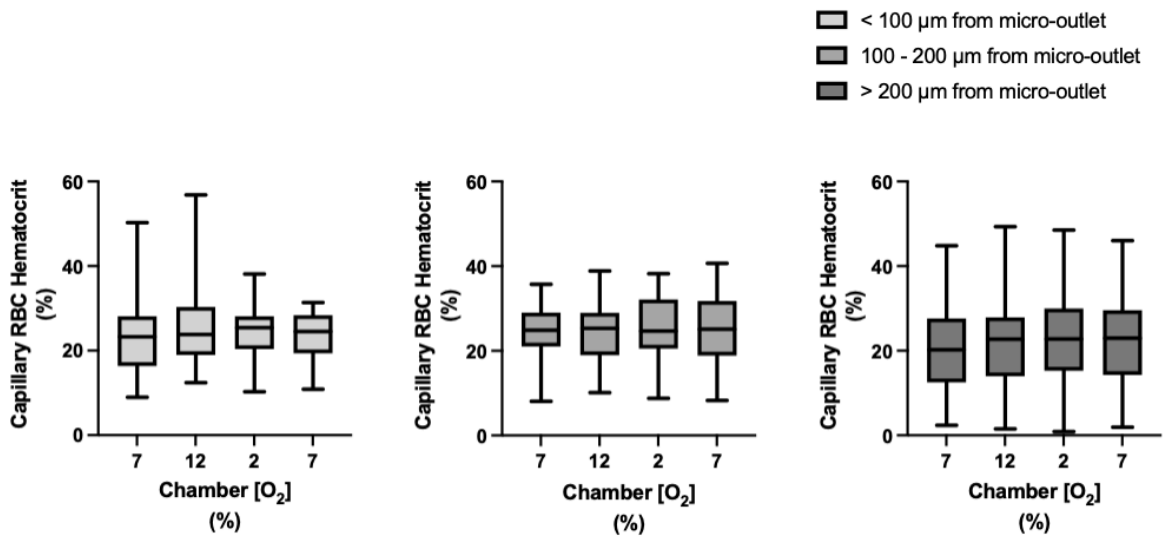
**Figure AI.1 Capillary RBC oxygen saturation in response to oxygen oscillations for capillaries directly overlying the 1000  $\mu\text{m}$  micro-outlet.** A) Time series plot showing the mean capillary RBC oxygen saturation ( $\text{SO}_2$ ) in capillaries overlying the 1000  $\mu\text{m}$  micro-outlet edge across the 4-minute  $\text{O}_2$  oscillation (7-12-2-7%). B) The micro-outlet gas exchange device perturbs oxygen concentrations within the gas exchange chamber from 7%, 12%, 2%, and 7% for one minute each over a 4-minute period. Mean values are taken from the first entire minute at baseline and the last 15 seconds at 12%, 2%, and 7% ( $n = 150$  capillaries).  $p$  values are based on Tukey's multiple comparisons test after significant repeated measures ANOVA and are indicated in the figure with a  $p < 0.05$  considered to be significant. Box and whisker plots show minimum, median, maximum, and associated quartiles.

**A****B**

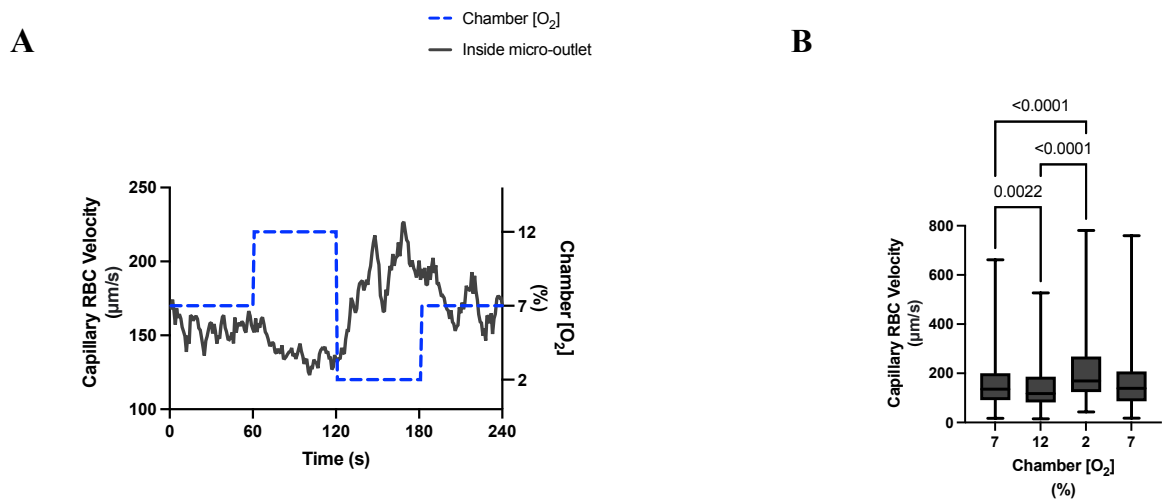
**Figure AI.2 Capillary RBC oxygen saturation responses in capillaries at various distances outside the 1000  $\mu\text{m}$  micro-outlet edge.** A) Time series plot showing the mean capillary RBC oxygen saturation ( $\text{SO}_2$ ) in capillaries at various distance ranges outside the 1000  $\mu\text{m}$  micro-outlet edge across the 4-minute  $\text{O}_2$  oscillation (7-12-2-7%). B) The micro-outlet gas exchange device imposes 4-minute oxygen oscillations for one minute at a baseline concentration of 7%, one minute at 12%, one minute at 2%, and one minute at 7%. Panel B shows capillary  $\text{SO}_2$  within 100  $\mu\text{m}$  of the micro-outlet edge ( $n = 26$  capillaries), capillary  $\text{SO}_2$  in vessels between 100 – 200  $\mu\text{m}$  from the outlet edge ( $n = 33$  capillaries), and capillary  $\text{SO}_2$  in vessels greater than 200  $\mu\text{m}$  from the outlet edge ( $n = 57$  capillaries) respectively.  $p$  values based on Tukey's multiple comparisons test after significant repeated measures ANOVA are indicated in the figure with a  $p < 0.05$  considered to be significant. Box and whisker plots show minimum, median, maximum, and associated quartiles.



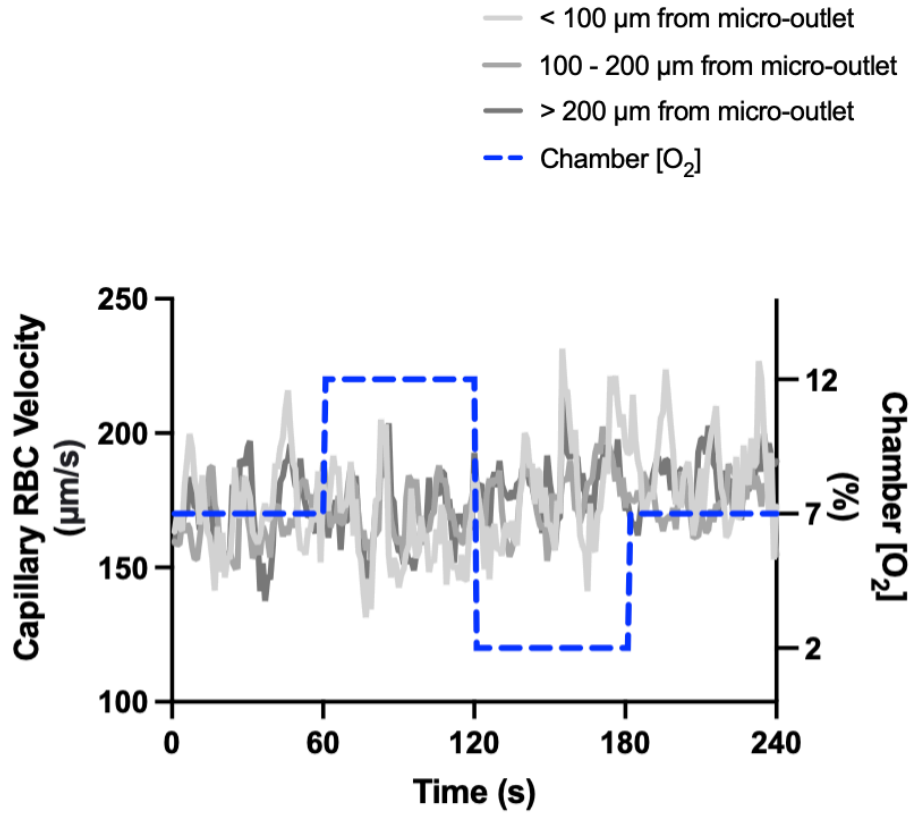
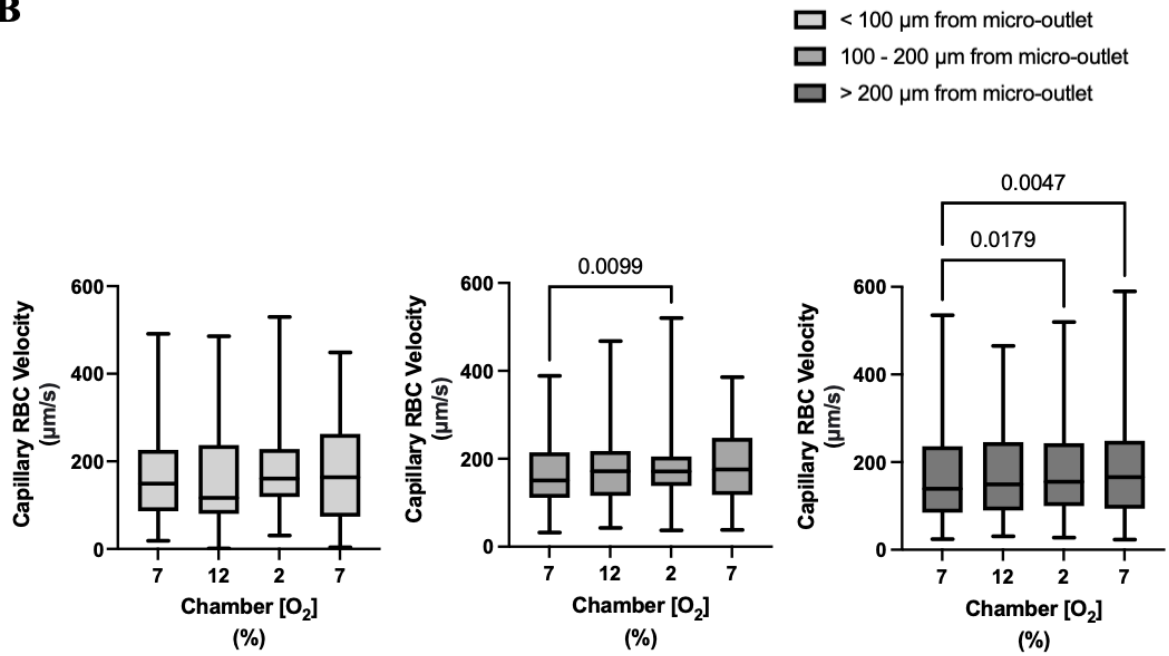
**Figure AI.3 Capillary hematocrit levels in response to oxygen oscillations for capillaries directly overlying the 1000  $\mu\text{m}$  micro-outlet.** A) Time series plot showing the mean capillary hematocrit in capillaries overlying the 1000  $\mu\text{m}$  micro-outlet across the 4-minute  $\text{O}_2$  oscillation (7-12-2-7%). B) The micro-outlet gas exchange device imposes 4-minute oxygen oscillations for one minute at a baseline concentration of 7%, one minute at 12%, one minute at 2%, and one minute at 7%. Mean hematocrit values are taken from the first entire minute at baseline and the last 15 seconds at 12%, 2%, and 7% ( $n = 183$  capillaries).  $p$  values based on Dunn's multiple comparisons test after significant Friedman test are indicated in the figure with a  $p < 0.05$  considered to be significant.

**A****B**

**Figure AI.4 Capillary hematocrit values in capillaries at various distances outside the 1000  $\mu\text{m}$  micro-outlet edge.** A) Time series plot showing the mean capillary hematocrit in capillaries outside the 1000  $\mu\text{m}$  micro-outlet edge across the 4-minute  $\text{O}_2$  oscillation (7-12-2-7%). B) The micro-outlet gas exchange device imposes 4-minute oxygen oscillations for one minute at a baseline concentration of 7%, one minute at 12%, one minute at 2%, and one minute at 7%. Mean hematocrit values are taken from the first entire minute at baseline and the last 15 seconds at 12%, 2%, and 7%. Panel B shows capillaries within 100  $\mu\text{m}$  from the micro-outlet edge ( $n = 26$  capillaries), capillaries between 100 – 200  $\mu\text{m}$  from the outlet edge ( $n = 35$  capillaries), and capillaries greater than 200  $\mu\text{m}$  from the outlet edge ( $n = 72$  capillaries) respectively.  $p$  values based on Dunn's multiple comparisons test after significant Friedman test are indicated in the figure and no significant differences were found.

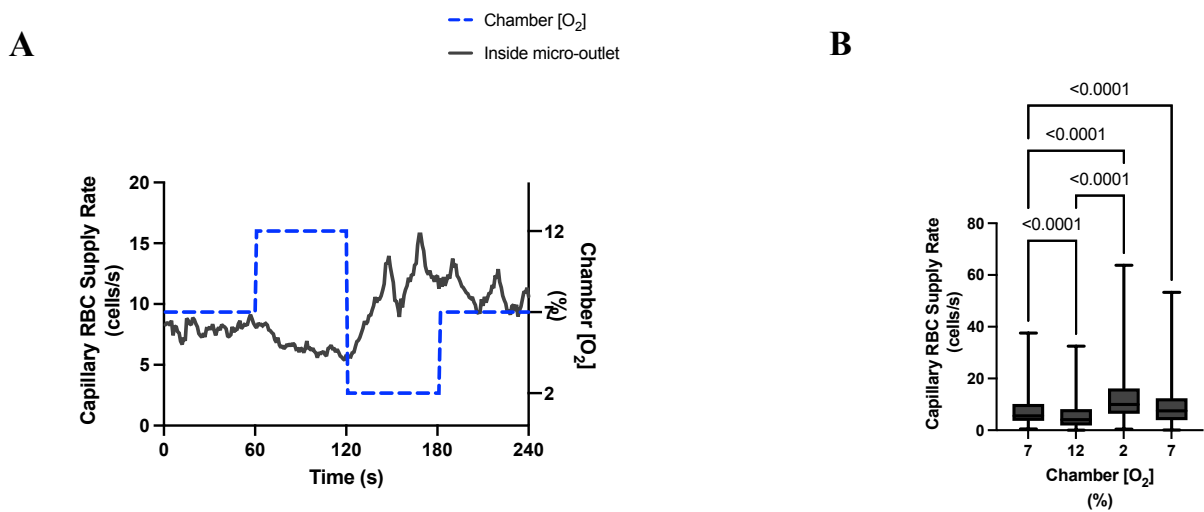


**Figure AI.5 Capillary RBC velocity for capillaries overlying the 1000  $\mu\text{m}$  micro-outlet following 4-minute oxygen oscillations.** A) Time series plot showing the mean RBC velocity for capillaries overlying the 1000  $\mu\text{m}$  micro-outlet across the 4-minute  $\text{O}_2$  oscillation (7-12-2-7%). B) Oxygen oscillations consisted of one minute at a baseline oxygen concentration of 7% and one minute at 12%, 2%, and 7% oxygen concentration. The mean was calculated for the entire first minute at a baseline 7% and the last 15 seconds of each of the following oxygen concentrations at 12%, 2%, and 7% ( $n = 183$  capillaries).  $p$  values based on Dunn's multiple comparisons test after the significant Friedman test are indicated in the figure with a  $p < 0.05$  considered to be significant. Box and whisker plots show minimum, median, maximum, and associated quartiles.

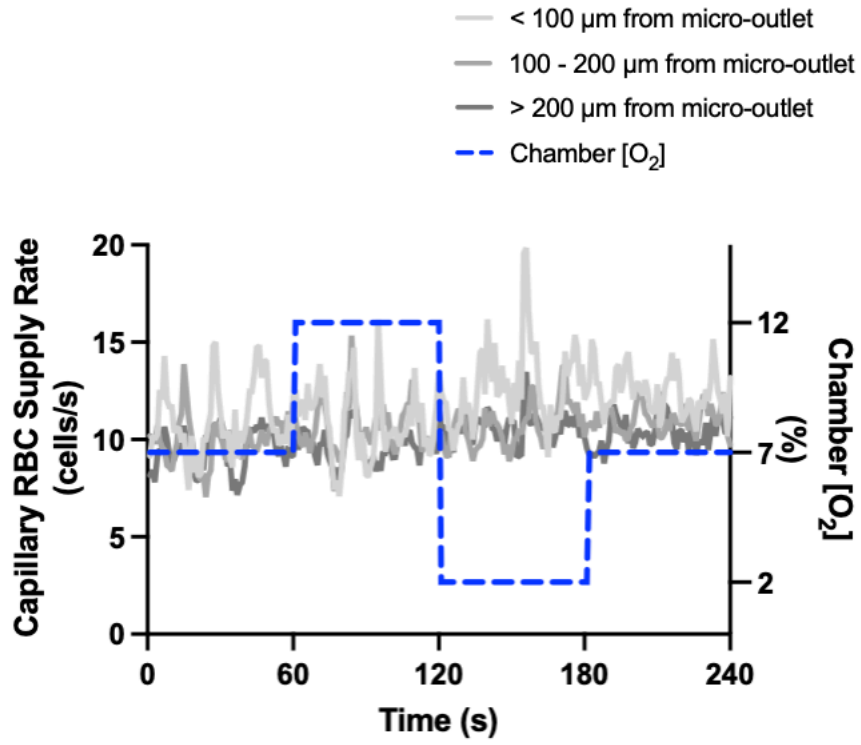
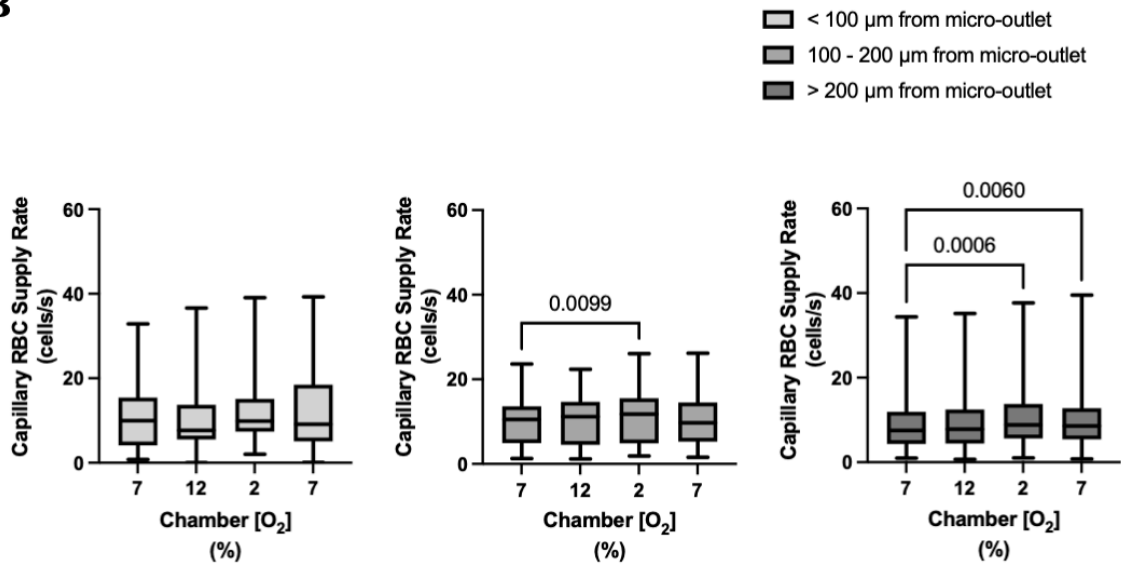
**A****B**

**Figure AI.6 Capillary RBC velocity for capillaries outside the 1000  $\mu\text{m}$  micro-outlet at varying distances from the outlet edge following 4-minute oxygen oscillations. A)**

Time series plot showing the mean RBC velocity for capillaries outside the 1000  $\mu\text{m}$  micro-outlet at varying distances across the 4-minute  $\text{O}_2$  oscillation (7-12-2-7%). B) Oscillations consisted of one minute at a baseline oxygen concentration of 7% followed by one minute at 12%, 2%, and 7% oxygen concentration. The mean was calculated for the entire first minute at 7% and the last 15 seconds of the following oxygen concentrations of 12%, 2%, and 7%. Panel A shows capillaries within 100  $\mu\text{m}$  from the micro-outlet edge ( $n = 26$  capillaries), panel B shows capillaries between 100 – 200  $\mu\text{m}$  from the outlet edge ( $n = 35$  capillaries), and panel C shows capillaries greater than 200  $\mu\text{m}$  from the outlet edge ( $n = 72$  capillaries).  $p$  values based on Dunn's multiple comparisons test after the significant Friedman test are indicated in the figure with a  $p < 0.05$  considered to be significant. Box and whisker plots show minimum, median, maximum, and associated quartiles.



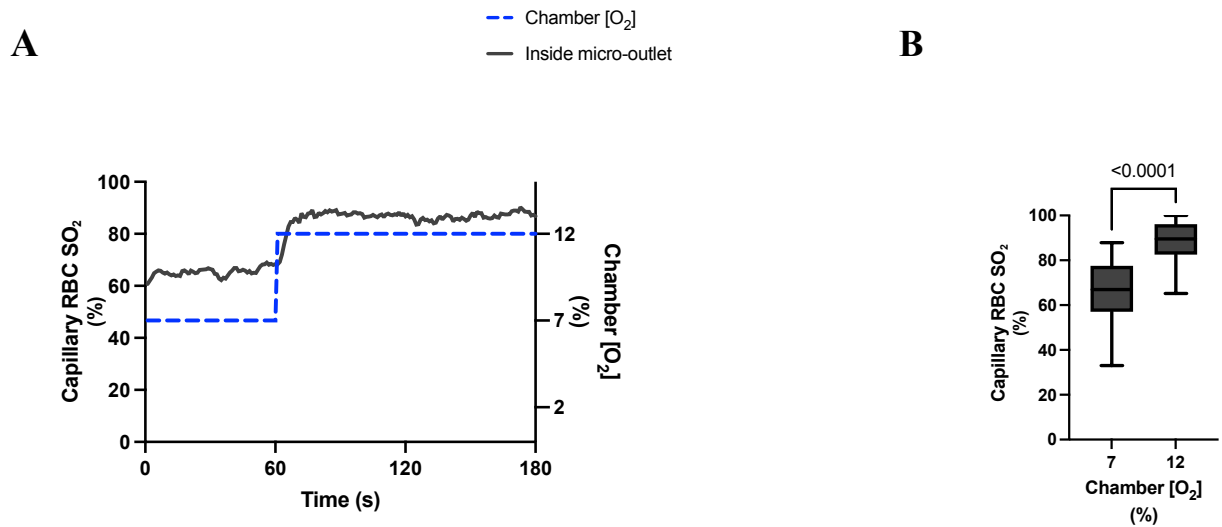
**Figure AI.7 Capillary RBC supply rate for capillaries overlying the 1000  $\mu\text{m}$  micro-outlet following 4-minute oxygen oscillations.** A) Time series plot showing mean RBC supply rate for capillaries overlying the 1000  $\mu\text{m}$  micro-outlet across the 4-minute  $\text{O}_2$  oscillation (7-12-2-7%). B) Oxygen oscillations consisted of one minute at a baseline oxygen concentration of 7% and one minute at 12%, 2%, and 7% oxygen concentration. The mean was calculated for the entire first minute at a baseline 7% and the last 15 seconds of each of the following oxygen concentrations at 12%, 2%, and 7% ( $n = 183$  capillaries).  $p$  values based on Dunn's multiple comparisons test after the significant Friedman test are indicated in the figure with a  $p < 0.05$  considered to be significant. Box and whisker plots show minimum, median, maximum, and associated quartiles.

**A****B**

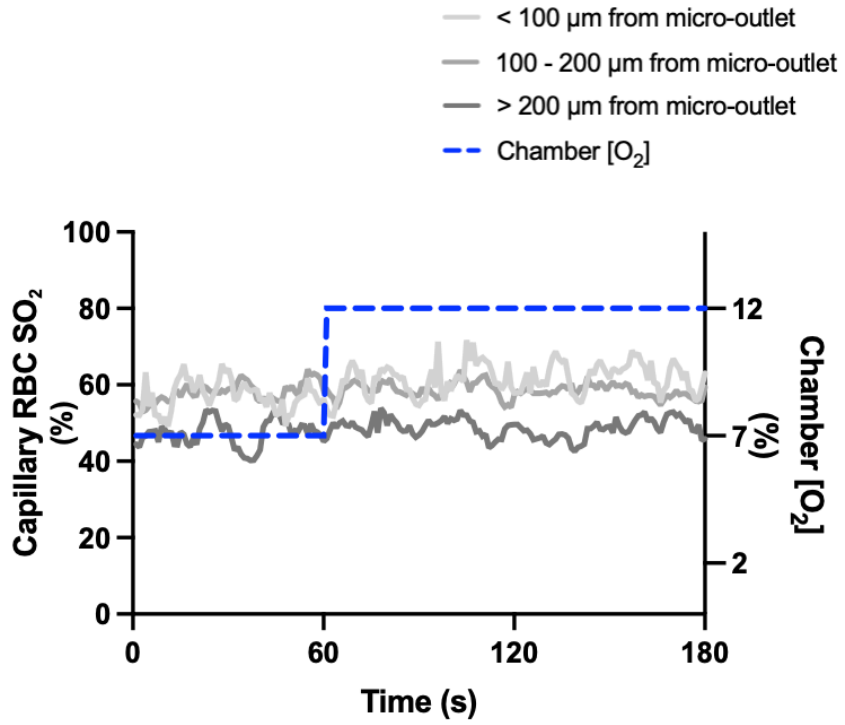
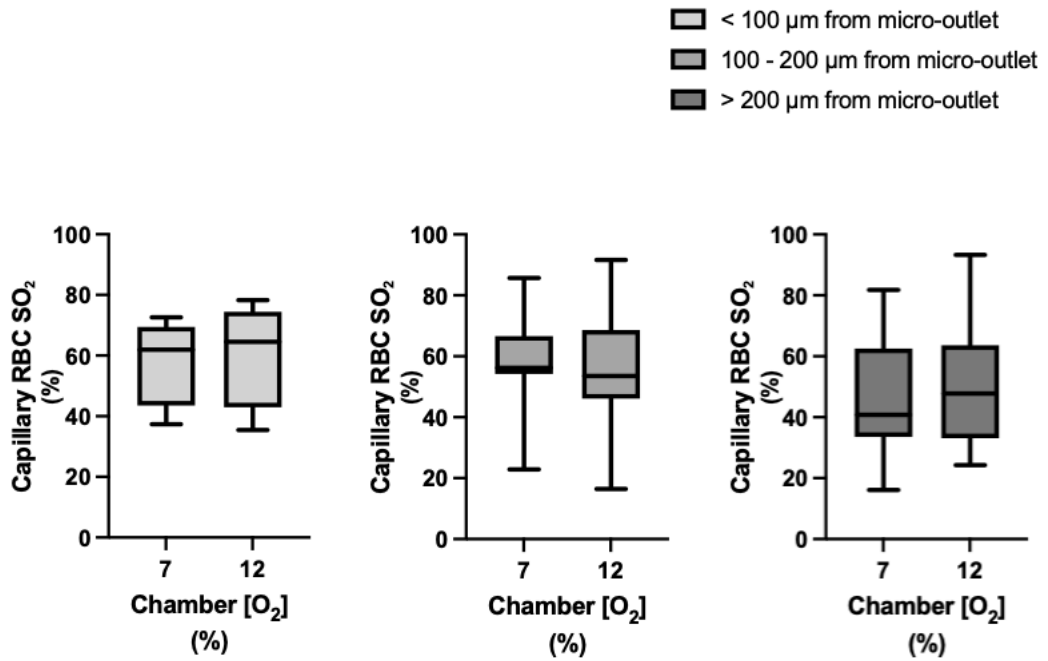
**Figure AI.8 Capillary RBC supply rate for capillaries outside the 1000  $\mu\text{m}$  micro-outlet at varying distances from the outlet edge following 4-minute oxygen oscillations.**

A) Time series plot showing mean RBC supply rate for capillaries outside the 1000  $\mu\text{m}$  micro-outlet at varying distances across the 4-minute  $\text{O}_2$  oscillation (7-12-2-7%). B) Oscillations consisted of one minute at a baseline oxygen concentration of 7% followed by one minute at 12%, 2%, and 7% oxygen concentration. The mean was calculated for the entire first minute at 7% and the last 15 seconds of the following oxygen concentrations of 12%, 2%, and 7%. Panel B shows capillaries within 100  $\mu\text{m}$  from the micro-outlet edge ( $n = 26$  capillaries), capillaries between 100 – 200  $\mu\text{m}$  from the outlet edge ( $n = 35$  capillaries), and capillaries greater than 200  $\mu\text{m}$  from the outlet edge respectively ( $n = 72$  capillaries).  $p$  values based on Dunn's multiple comparisons test after significant Friedman test are indicated in the figure with a  $p < 0.05$  considered to be significant. Box and whisker plots show minimum, median, maximum, and associated quartiles.

## 1000 $\mu\text{m}$ Micro-Outlet Oxygen Challenge Data



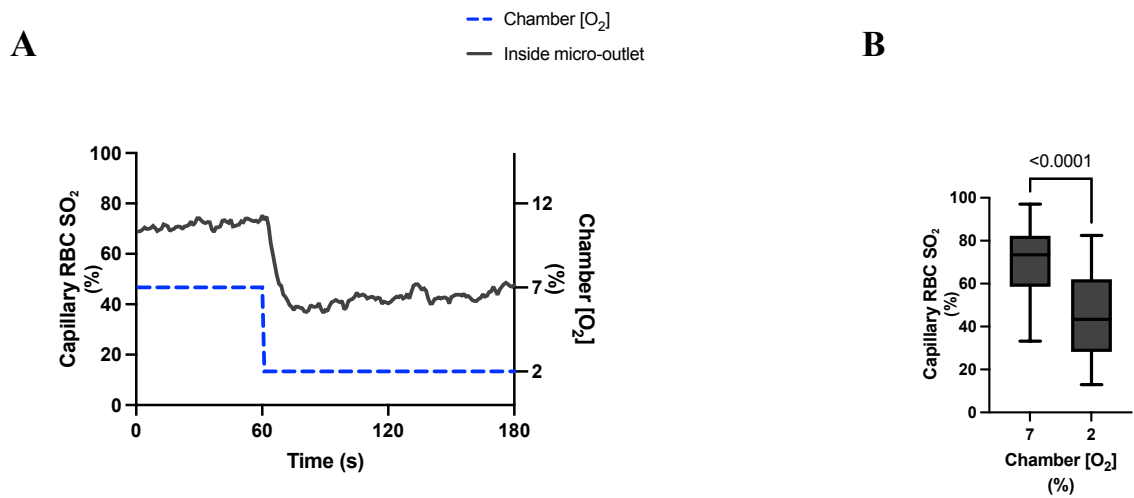
**Figure AI.9 Capillary RBC oxygen saturation in response to high oxygen challenges for capillaries directly overlying the 1000  $\mu\text{m}$  micro-outlet.** A) Time series plot showing mean capillary RBC oxygen saturation ( $\text{SO}_2$ ) for capillaries overlying the micro-outlet in response to high (7-12%) oxygen challenges. B) Oxygen challenges consisted of one minute at a baseline oxygen concentration of 7% followed by two minutes at 12%. The mean was calculated for the entire first minute at 7% and the last 15 seconds at 12% oxygen concentration ( $n = 71$  capillaries).  $p$  values based on paired  $t$  tests and values indicated in the figure with a  $p < 0.05$  considered to be significant. Box and whisker plots show minimum, median, maximum, and associated quartiles.

**A****B**

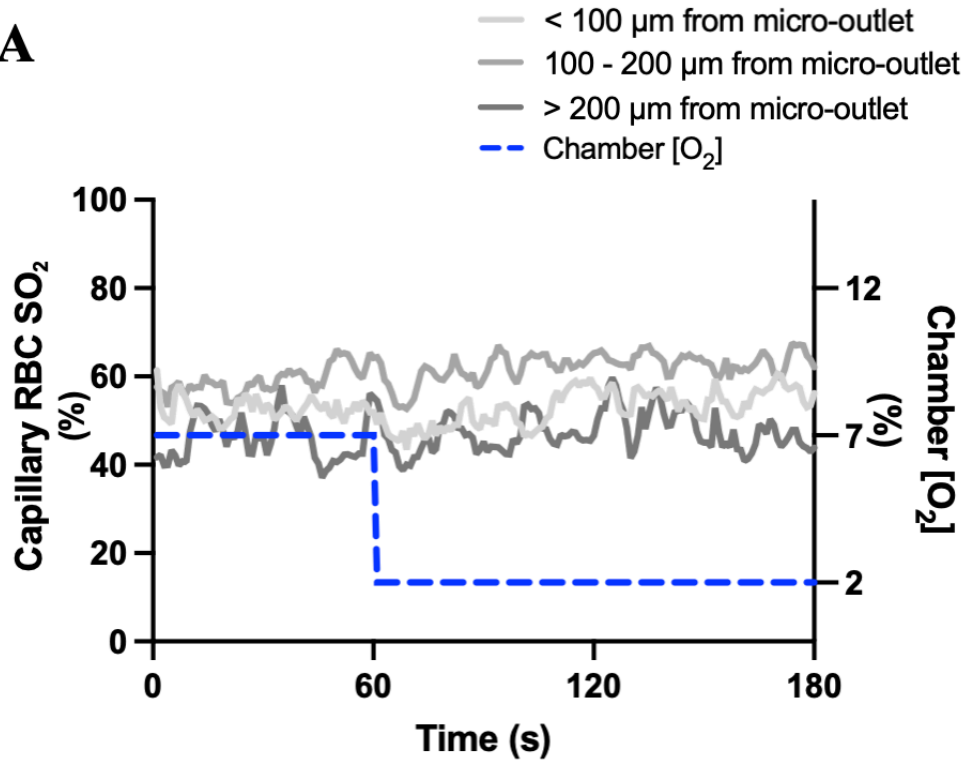
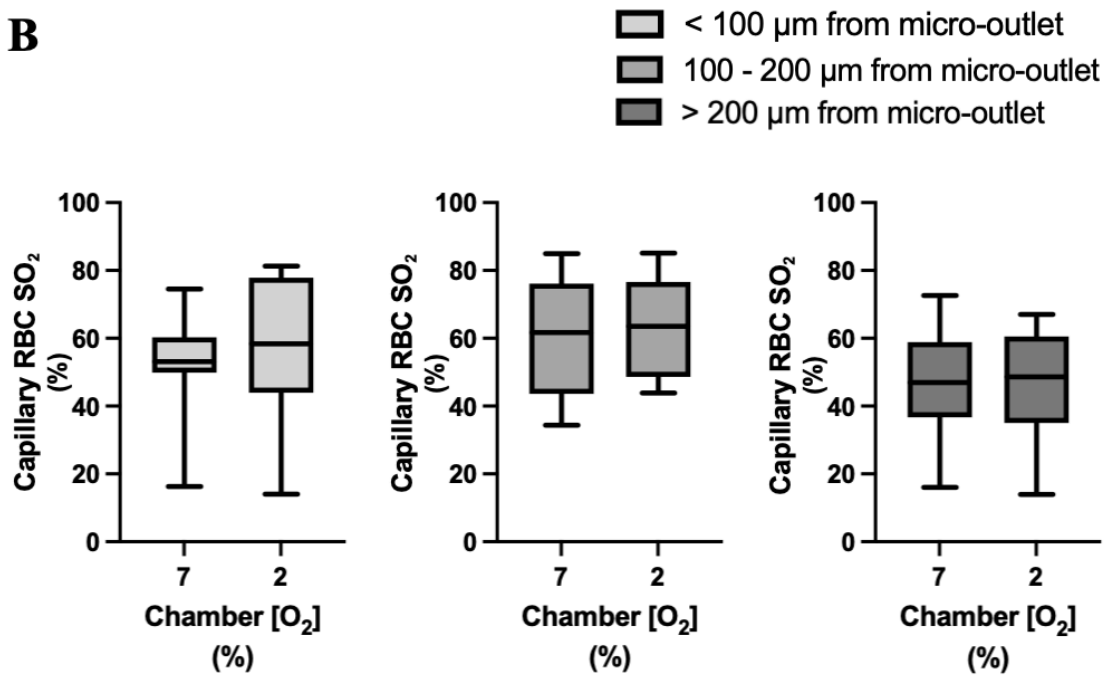
**Figure AI.10 Capillary RBC oxygen saturation responses in capillaries at various distances outside the 1000  $\mu\text{m}$  micro-outlet edge in response to high oxygen challenges.**

A) Time series plot showing mean capillary RBC oxygen saturation ( $\text{SO}_2$ ) for capillaries outside the micro-outlet edge at varying distances during high (7-12%) oxygen challenges.

B) Oxygen challenges consisted of one minute at a baseline oxygen concentration of 7% followed by one minute at 12%. The mean was calculated for the entire first minute at 7% and the last 15 seconds at a 12% oxygen concentration. Panel B shows capillaries within 100  $\mu\text{m}$  from the micro-outlet edge ( $n = 9$  capillaries), capillaries between 100 – 200  $\mu\text{m}$  from the outlet edge ( $n = 15$  capillaries), and capillaries greater than 200  $\mu\text{m}$  from the outlet edge ( $n = 21$  capillaries) respectively.  $p$  values based on paired t-tests and values indicated in the figure with a  $p < 0.05$  are significant. Box and whisker plots show minimum, median, maximum, and associated quartiles.



**Figure AI.11 Capillary RBC oxygen saturation in response to low oxygen challenges for capillaries directly overlying the 1000  $\mu\text{m}$  micro-outlet.** A) Time series plot showing mean capillary RBC oxygen saturation ( $\text{SO}_2$ ) for capillaries overlying the micro-outlet during low (7-2%) oxygen challenges. B) Oxygen challenges consisted of one minute at a baseline oxygen concentration of 7% followed by two minutes at 2%. The mean was calculated for the entire first minute at 7% and the last 15 seconds at a 2% oxygen concentration ( $n = 61$  capillaries).  $p$  values based on paired t-tests and values indicated in the figure with a  $p < 0.05$  are significant. Box and whisker plots show minimum, median, maximum, and associated quartiles.

**A****B**

**Figure AI.12 Capillary RBC oxygen saturation responses in capillaries at various distances outside the 1000  $\mu\text{m}$  micro-outlet edge in response to low oxygen challenges.**

A) Time series plot showing mean capillary RBC oxygen saturation ( $\text{SO}_2$ ) for capillaries outside the micro-outlet edge at varying distances during low (7-2%) oxygen challenges.

B) Oxygen challenges consisted of one minute at a baseline oxygen concentration of 7% followed by two minutes at 2%. The mean was calculated for the entire first minute at 7% and the last 15 seconds at a 2% oxygen concentration. Panel B shows capillaries within 100  $\mu\text{m}$  from the micro-outlet edge ( $n = 10$  capillaries), capillaries between 100 – 200  $\mu\text{m}$  from the outlet edge ( $n = 16$  capillaries), and capillaries greater than 200  $\mu\text{m}$  from the outlet edge ( $n = 11$  capillaries), respectively.  $p$  values based on paired t-tests and values indicated in the figure with a  $p < 0.05$  are significant. Box and whisker plots show minimum, median, maximum, and associated quartiles.

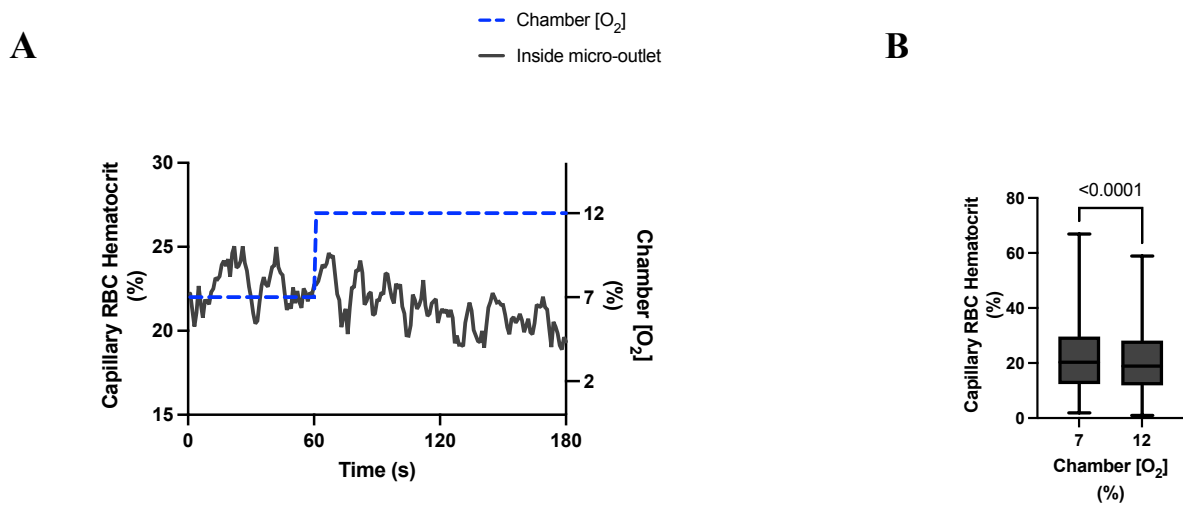


**Figure AI.13 Capillary hematocrit levels in response to high oxygen challenges for capillaries directly overlying the 1000  $\mu\text{m}$  micro-outlet.** A) Time series plot showing mean capillary hematocrit levels for capillaries overlying the micro-outlet during high (7-12%) oxygen challenges. B) Oxygen challenges consisted of one minute at a baseline oxygen concentration of 7% followed by two minutes at 12%. The mean was calculated for the entire first minute at 7% and the last 15 seconds at a 12% oxygen concentration ( $n = 72$  capillaries).  $p$  values based on paired Wilcoxon t test and values indicated in the figure with a  $p < 0.05$  considered to be significant. Box and whisker plots show minimum, median, maximum, and associated quartiles.

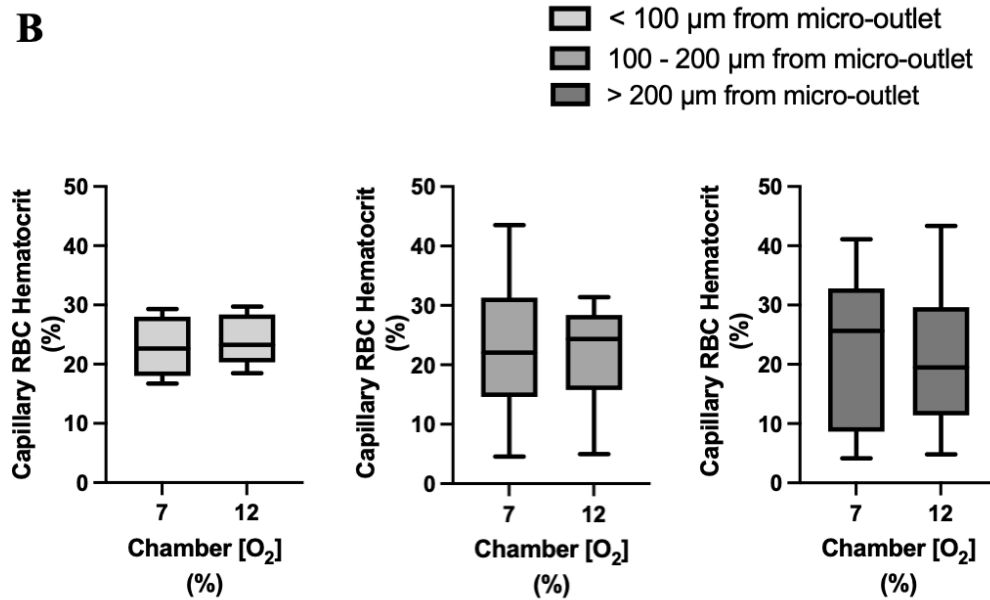
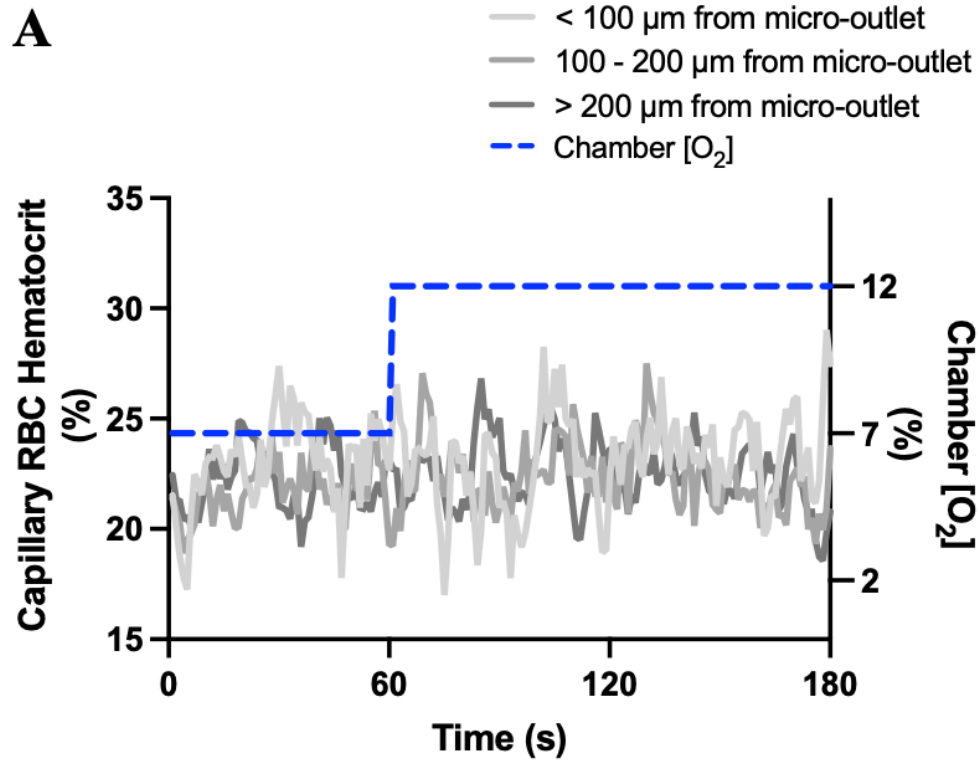


**Figure AI.14 Capillary hematocrit levels in capillaries at various distances outside the 1000  $\mu\text{m}$  micro-outlet edge in response to high oxygen challenges.** A) Time series plot showing mean capillary hematocrit levels for capillaries outside the micro-outlet at varying distances during high (7-12%) oxygen challenges. B) Oxygen challenges consisted of one minute at a baseline oxygen concentration of 7% followed by two minutes at 12%. The mean was calculated for the entire first minute at 7% and the last 15 seconds at a 12% oxygen concentration. Panel B shows capillaries within 100  $\mu\text{m}$  from the micro-outlet edge ( $n = 5$  capillaries), capillaries between 100 – 200  $\mu\text{m}$  from the outlet edge ( $n = 12$  capillaries), and capillaries greater than 200  $\mu\text{m}$  from the outlet edge ( $n = 25$  capillaries) respectively  $p$  values based on paired Wilcoxon t test and values indicated in the figure with a  $p < 0.05$  considered to be significant. Box and whisker plots show minimum, median, maximum, and associated quartiles.

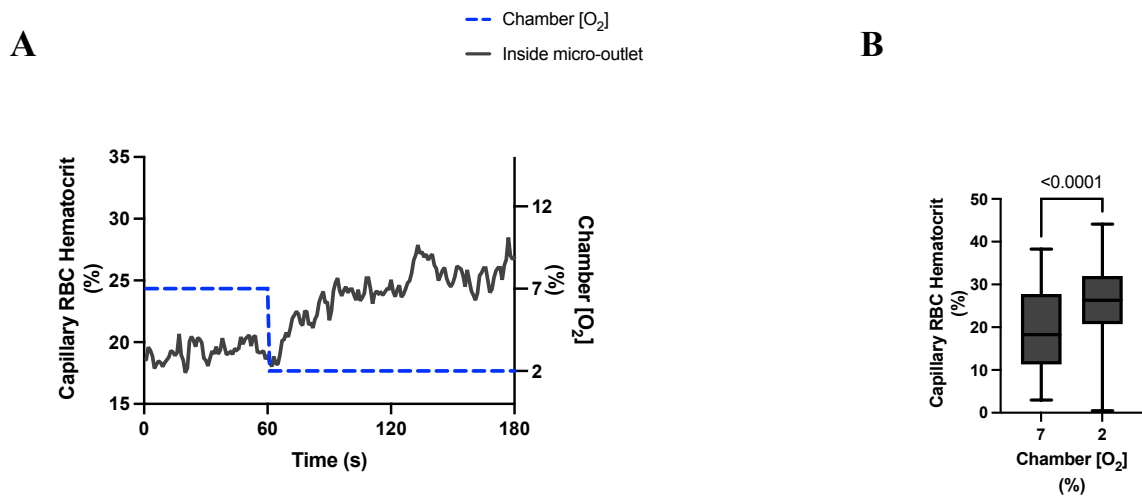
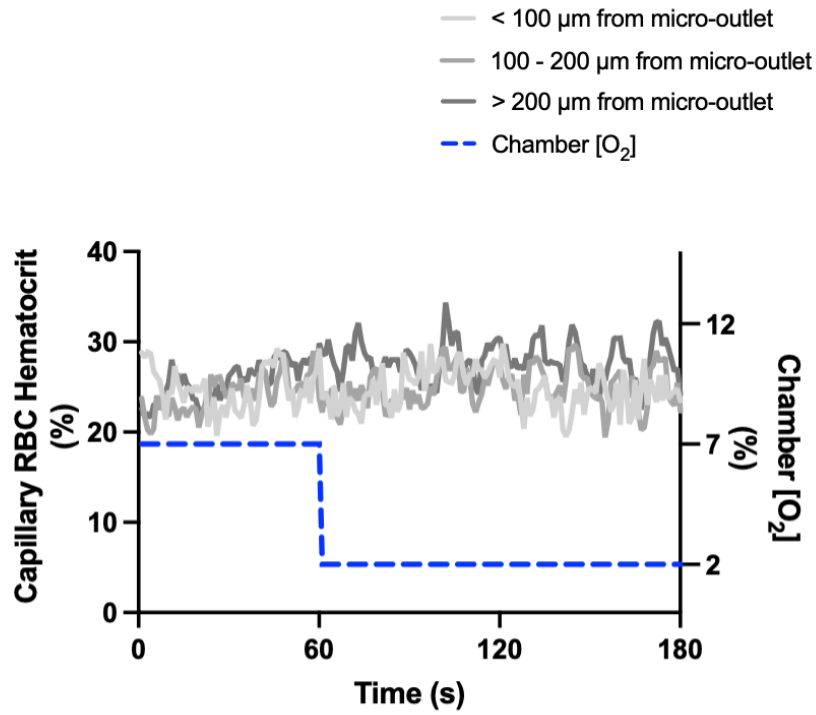
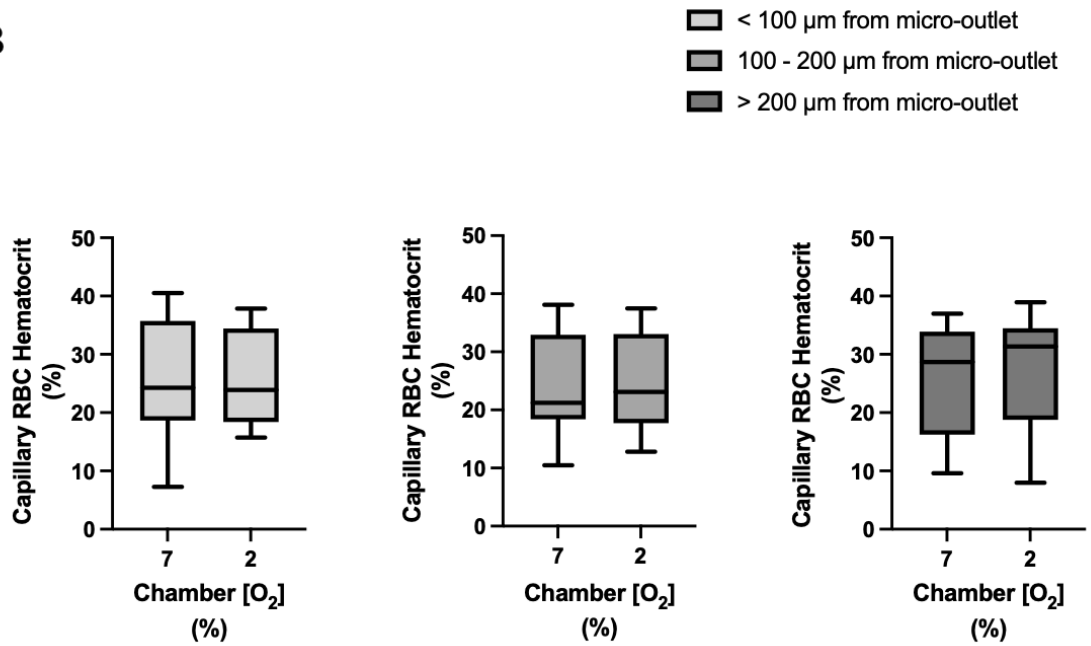


**Figure AI.15 Capillary hematocrit levels in response to low oxygen challenges for capillaries directly overlying the 1000  $\mu\text{m}$  micro-outlet.** A) Time series plot showing mean capillary hematocrit levels for capillaries overlying the micro-outlet during low (7-2%) oxygen challenges. B) Oxygen challenges consisted of one minute at a baseline oxygen concentration of 7% followed by two minutes at 2%. The mean was calculated for the entire first minute at 7% and the last 15 seconds at a 2% oxygen concentration ( $n = 73$  capillaries).  $p$  values based on paired Wilcoxon t test and values indicated in the figure with a  $p < 0.05$  considered to be significant. Box and whisker plots show minimum, median, maximum, and associated quartiles.

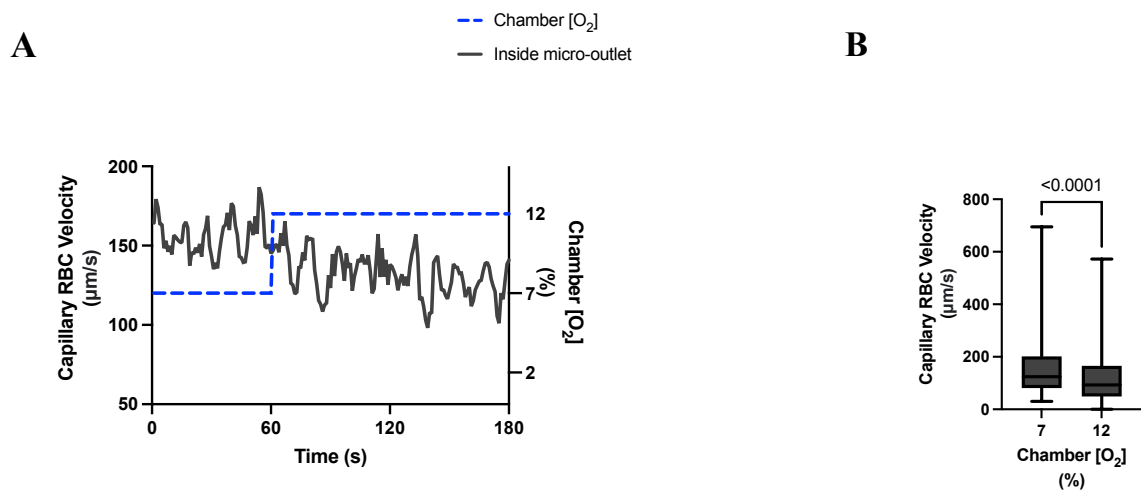
**A**



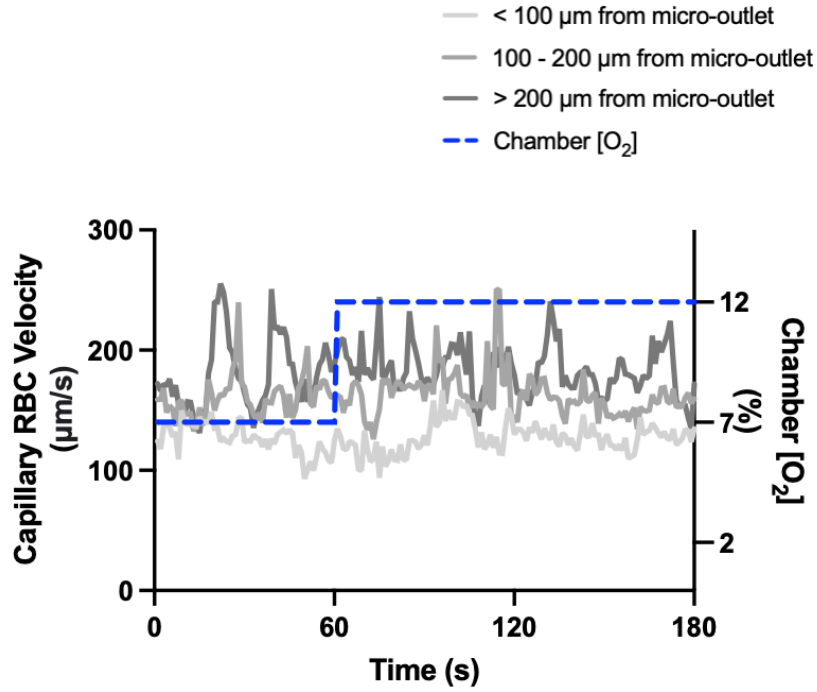
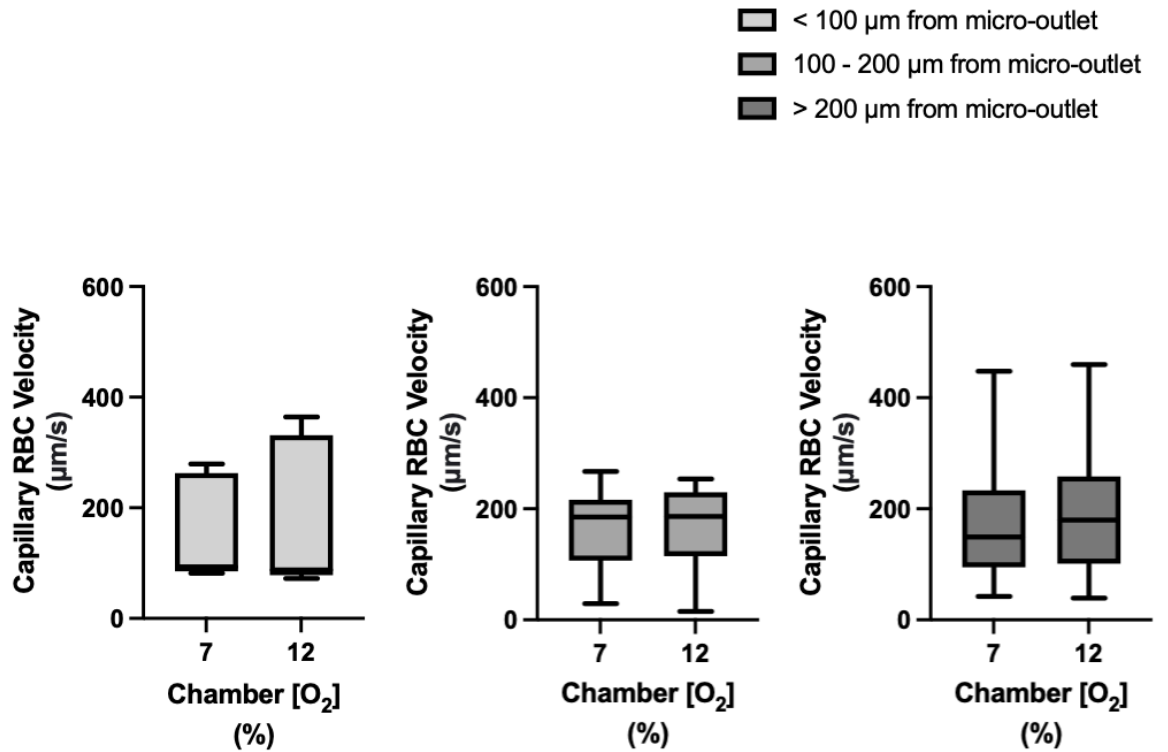
**B**



**Figure AI.16 Capillary hematocrit levels in capillaries at various distances outside the 1000  $\mu\text{m}$  micro-outlet edge in response to low oxygen challenges.** A) Time series plot showing mean capillary hematocrit levels for capillaries outside the micro-outlet at varying distances during low (7-2%) oxygen challenges. B) Oxygen challenges consisted of one minute at a baseline oxygen concentration of 7% followed by two minutes at 2%. The mean was calculated for the entire first minute at 7% and the last 15 seconds at a 2% oxygen concentration. Panel B shows capillaries within 100  $\mu\text{m}$  from the micro-outlet edge ( $n = 7$  capillaries), capillaries between 100 – 200  $\mu\text{m}$  from the outlet edge ( $n = 13$  capillaries), and capillaries greater than 200  $\mu\text{m}$  from the outlet edge ( $n = 16$  capillaries) respectively.  $p$  values based on paired Wilcoxon t test and values with a  $p < 0.05$  considered to be significant. Box and whisker plots show minimum, median, maximum, and associated quartiles.



**Figure A1.17 Capillary RBC velocity response to high oxygen challenges for capillaries directly overlying the 1000  $\mu\text{m}$  micro-outlet.** A) Time series plot showing mean capillary RBC velocity for capillaries overlying the micro-outlet during high (7-12%) oxygen challenges. B) Oxygen challenges consisted of one minute at a baseline oxygen concentration of 7% followed by two minutes at 12%. The mean was calculated for the entire first minute at 7% and the last 15 seconds at a 12% oxygen concentration ( $n = 72$  capillaries). Box and whisker plots show minimum, median, maximum, and associated quartiles.

**A****B**

**Figure AI.18 Capillary RBC velocity levels in capillaries at various distances outside the 1000  $\mu\text{m}$  micro-outlet edge in response to high oxygen challenges.** A) Time series plot showing mean capillary RBC velocity for capillaries outside the micro-outlet at varying distances during high (7-12%) oxygen challenges. B) Oxygen challenges consisted of one minute at a baseline oxygen concentration of 7% followed by two minutes at 12%. The mean was calculated for the entire first minute at 7% and the last 15 seconds at 12% oxygen concentration. Panel B shows capillaries within 100  $\mu\text{m}$  from the micro-outlet edge ( $n = 5$  capillaries), capillaries between 100 – 200  $\mu\text{m}$  from the outlet edge ( $n = 12$  capillaries), and capillaries greater than 200  $\mu\text{m}$  from the outlet edge ( $n = 26$  capillaries) respectively.  $p$  values based on paired Wilcoxon t test and values indicated in the figure with a  $p < 0.05$  considered to be significant. Box and whisker plots show minimum, median, maximum, and associated quartiles.

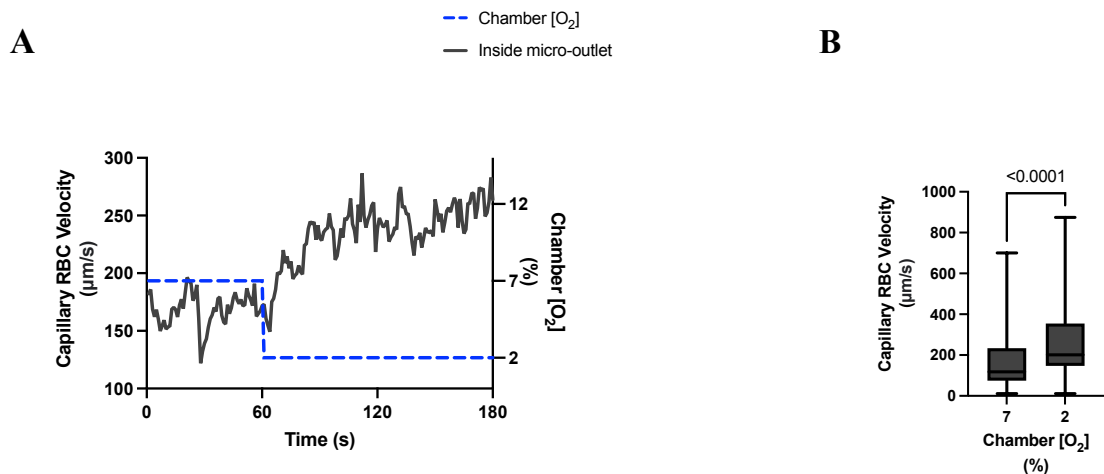
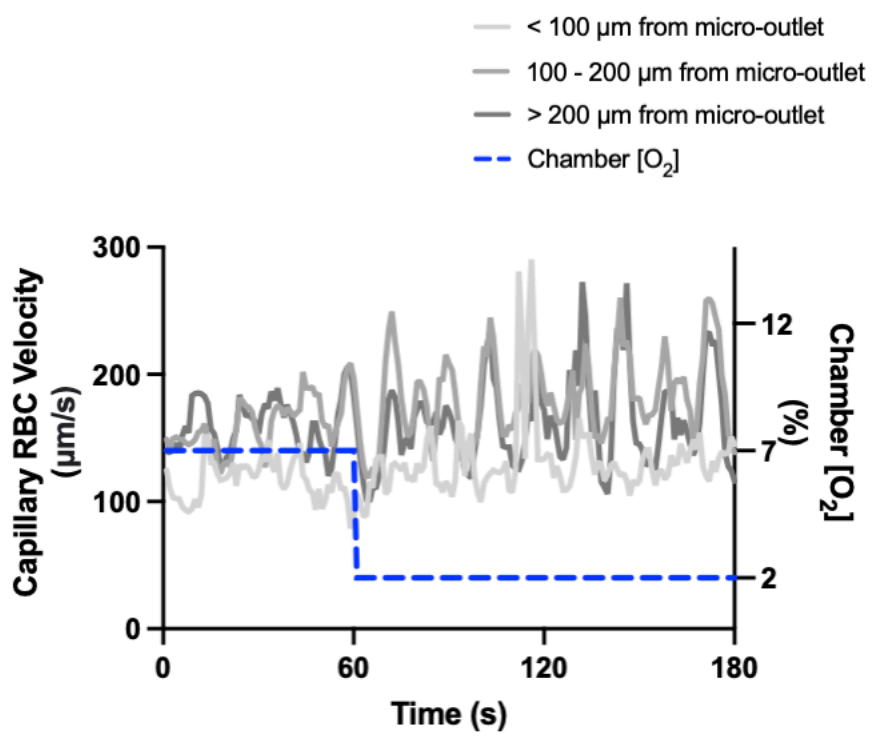
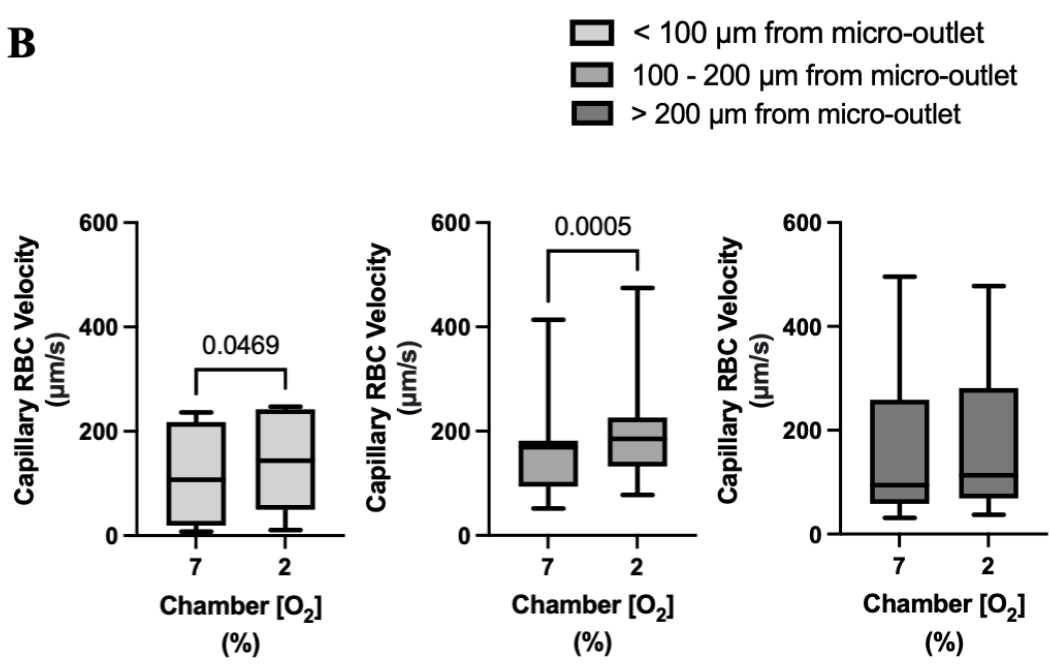


**Figure AI.19 Capillary RBC velocity response to low oxygen challenges for capillaries directly overlying the 1000  $\mu\text{m}$  micro-outlet.** A) Time series plot showing mean capillary RBC velocity for capillaries overlying the micro-outlet during low (7-2%) oxygen challenges. B) Oxygen challenges consisted of one minute at a baseline oxygen concentration of 7% followed by two minutes at 2%. The mean was calculated for the entire first minute at 7% and the last 15 seconds at 2% oxygen concentration ( $n = 73$  capillaries).  $p$  values based on paired Wilcoxon t-test and values indicated in the figure with a  $p < 0.05$  considered to be significant. Box and whisker plots show minimum, median, maximum, and associated quartiles.

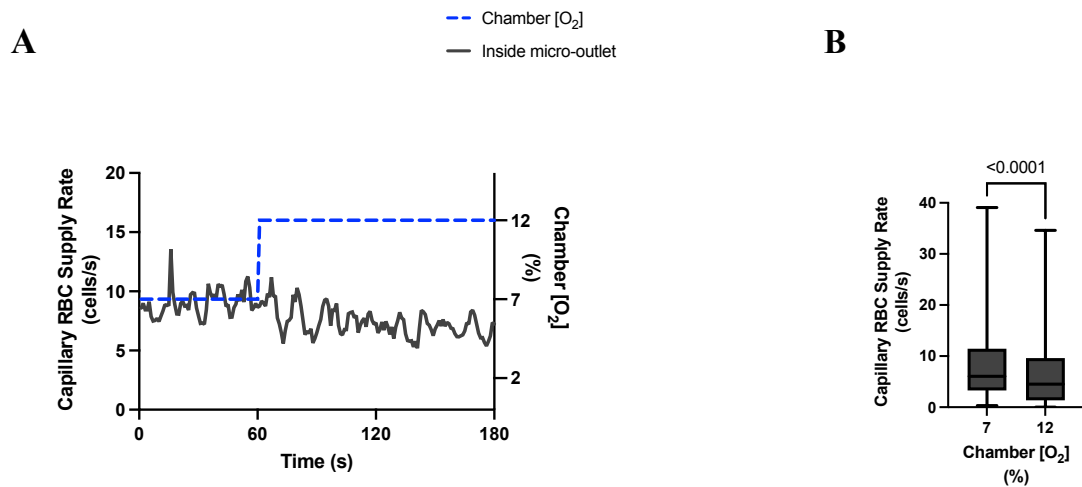
**A**



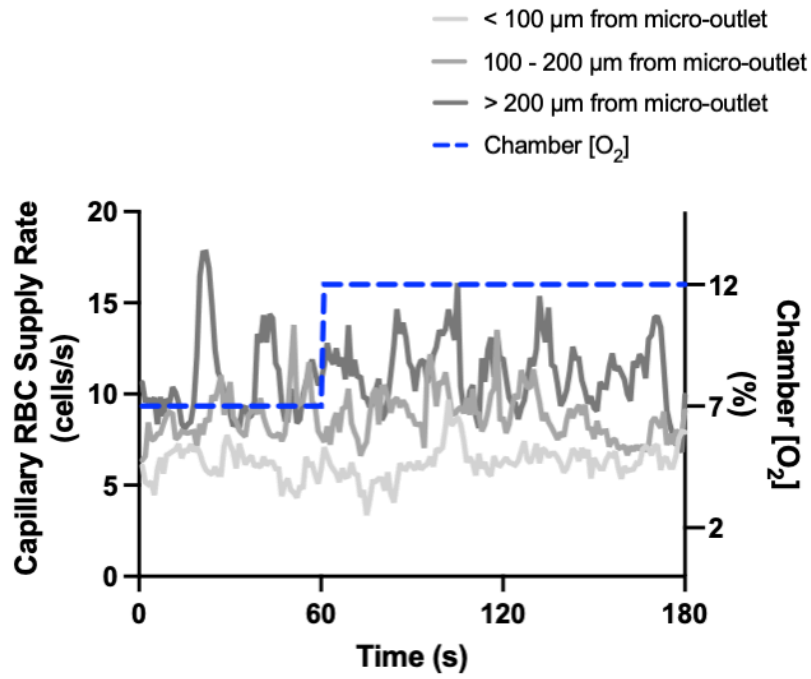
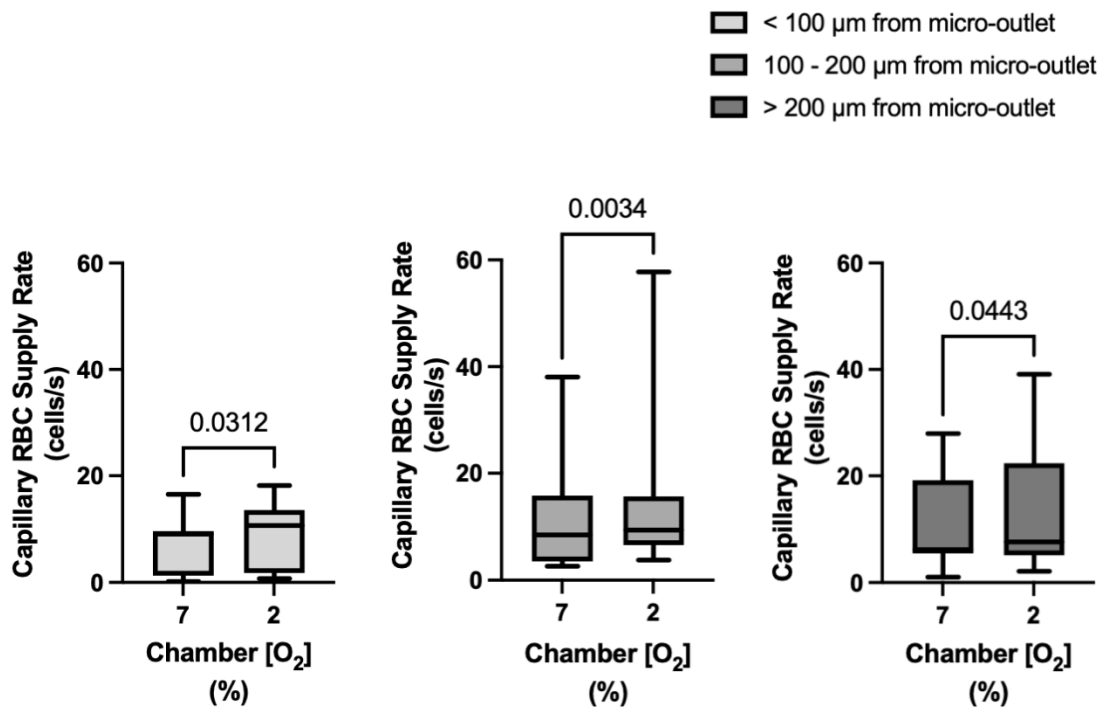
**B**



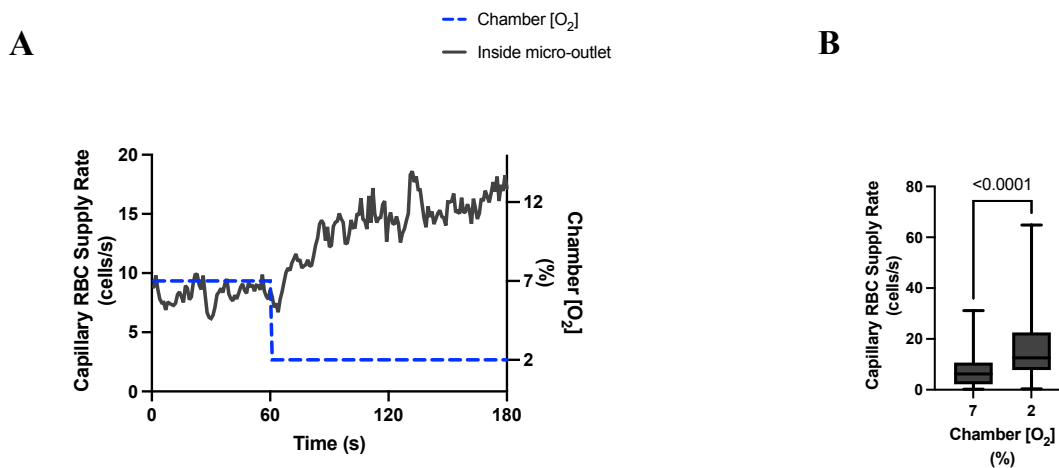
**Figure AI.20 Capillary RBC velocity in capillaries at various distances outside the 1000  $\mu\text{m}$  micro-outlet edge in response to low oxygen challenges.** A) Time series plot showing mean capillary RBC velocity for capillaries outside the micro-outlet at varying distances during low (7-2%) oxygen challenges. B) Oxygen challenges consisted of one minute at a baseline oxygen concentration of 7% followed by two minutes at 2%. The mean was calculated for the entire first minute at 7% and the last 15 seconds at 2% oxygen concentration. Panel B shows capillaries within 100  $\mu\text{m}$  from the micro-outlet edge ( $n = 7$  capillaries), capillaries between 100 – 200  $\mu\text{m}$  from the outlet edge ( $n = 13$  capillaries), and capillaries greater than 200  $\mu\text{m}$  from the outlet edge ( $n = 16$  capillaries) respectively.  $p$  values based on paired Wilcoxon t-test and values indicated in the figure with a  $p < 0.05$  considered to be significant. Box and whisker plots show minimum, median, maximum, and associated quartiles.



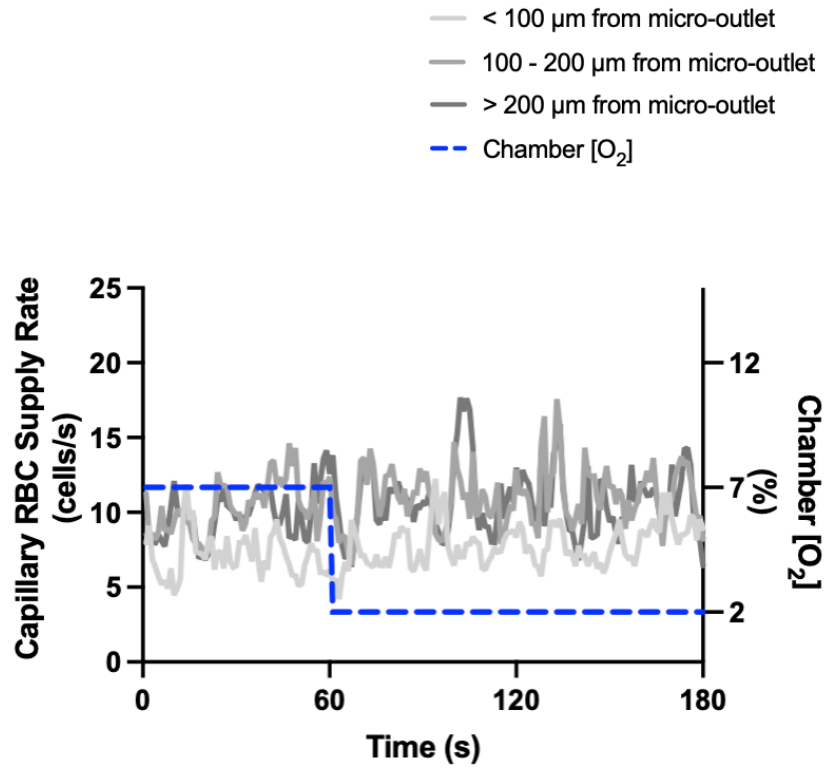
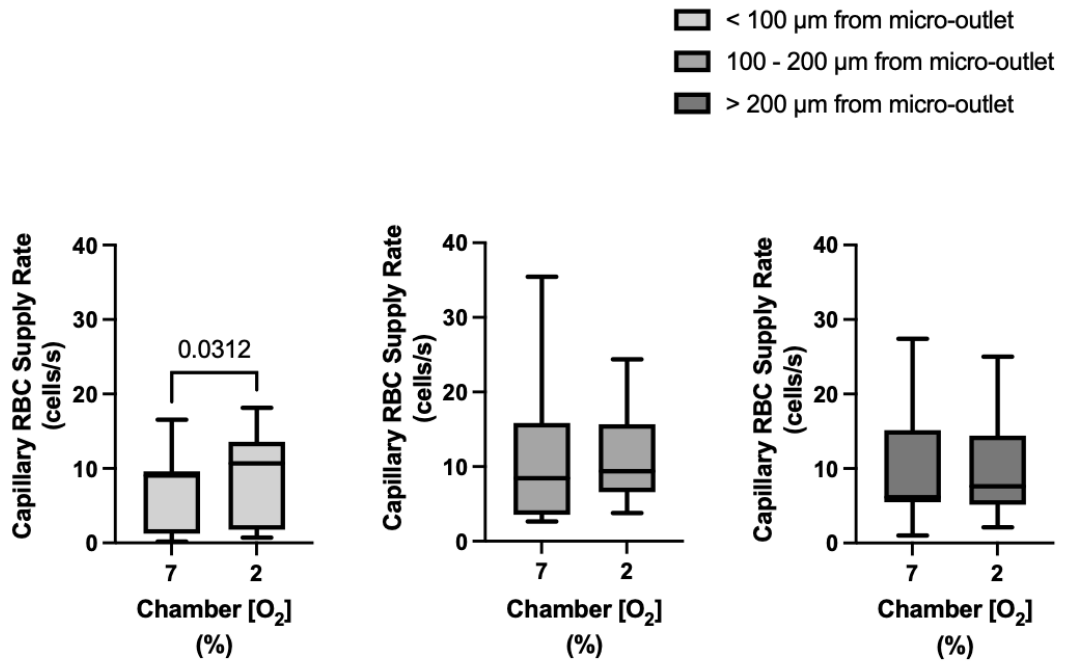
**Figure A1.21 Capillary RBC supply rate response to high oxygen challenges for capillaries directly overlying the 1000  $\mu\text{m}$  micro-outlet.** A) Time series plot showing mean capillary RBC supply rate for capillaries overlying the micro-outlet during high (7-12%) oxygen challenges. B) Oxygen challenges consisted of one minute at a baseline oxygen concentration of 7% followed by two minutes at 12%. The mean was calculated for the entire first minute at 7% and the last 15 seconds at a 12% oxygen concentration ( $n = 72$  capillaries).  $p$  values based on paired Wilcoxon  $t$  test and values indicated in the figure with a  $p < 0.05$  considered to be significant. Box and whisker plots show minimum, median, maximum, and associated quartiles.

**A****B**

**Figure AI.22 Capillary RBC supply rate in capillaries at various distances outside the 1000  $\mu\text{m}$  micro-outlet edge in response to high oxygen challenges.** A) Time series plot showing mean capillary RBC supply rate for capillaries outside the micro-outlet at varying distances during high (7-12%) oxygen challenges. B) Oxygen challenges consisted of one minute at a baseline oxygen concentration of 7% followed by two minutes at 12%. The mean was calculated for the entire first minute at 7% and the last 15 seconds at a 12% oxygen concentration. Panel B shows capillaries within 100  $\mu\text{m}$  from the micro-outlet edge ( $n = 5$  capillaries), capillaries between 100 – 200  $\mu\text{m}$  from the outlet edge ( $n = 12$  capillaries), and capillaries greater than 200  $\mu\text{m}$  from the outlet edge ( $n = 25$  capillaries) respectively.  $p$  values based on paired Wilcoxon t test and values indicated in the figure with a  $p < 0.05$  considered to be significant. Box and whisker plots show minimum, median, maximum, and associated quartiles.



**Figure A1.23 Capillary RBC supply rate in response to low oxygen challenges for capillaries directly overlying the 1000  $\mu\text{m}$  micro-outlet.** A) Time series plot showing mean capillary RBC supply rate for capillaries overlying the micro-outlet during low (7-2%) oxygen challenges. B) Oxygen challenges consisted of one minute at a baseline oxygen concentration of 7% followed by two minutes at 2%. The mean was calculated for the entire first minute at 7% and the last 15 seconds at a 2% oxygen concentration ( $n = 73$  capillaries).  $p$  values based on paired Wilcoxon t test and values indicated in the figure with a  $p < 0.05$  considered to be significant. Box and whisker plots show minimum, median, maximum, and associated quartiles.

**A****B**

**Figure AI.24 Capillary RBC supply rate in capillaries at various distances outside the 1000  $\mu\text{m}$  micro-outlet edge in response to low oxygen challenges.** A) Time series plot showing mean capillary RBC supply rate for capillaries outside the micro-outlet at varying distances during low (7-2%) oxygen challenges. B) Oxygen challenges consisted of one minute at a baseline oxygen concentration of 7% followed by two minutes at 2%. The mean was calculated for the entire first minute at 7% and the last 15 seconds at a 2% oxygen concentration. Panel B shows capillaries within 100  $\mu\text{m}$  from the micro-outlet edge ( $n = 7$  capillaries), capillaries between 100 – 200  $\mu\text{m}$  from the outlet edge ( $n = 13$  capillaries), and capillaries greater than 200  $\mu\text{m}$  from the outlet edge ( $n = 16$  capillaries) respectively.  $p$  values based on paired Wilcoxon t test and values indicated in the figure with a  $p < 0.05$  considered to be significant. Box and whisker plots show minimum, median, maximum, and associated quartiles.

## 600 $\mu\text{m}$ Micro-Outlet Oxygen Oscillation Data

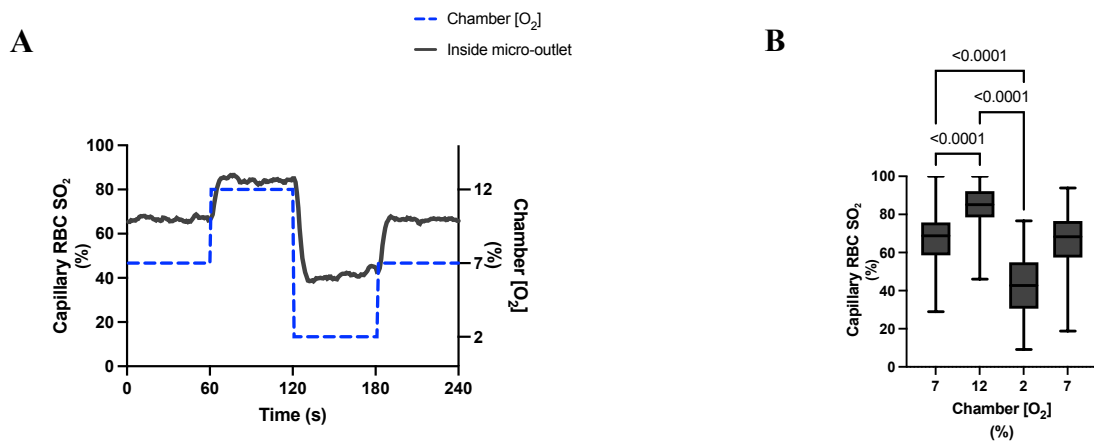
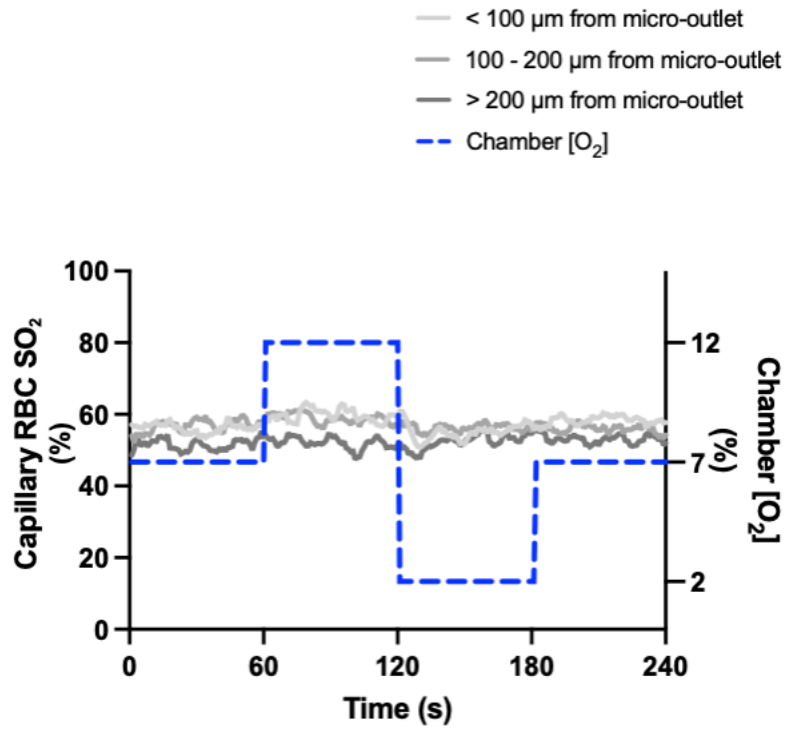


**Figure AI.25 Capillary RBC oxygen saturation in response to oxygen oscillations for capillaries directly overlying the 600  $\mu\text{m}$  micro-outlet.** A) Time series plot showing the mean capillary RBC oxygen saturation (SO<sub>2</sub>) in capillaries overlying the 600  $\mu\text{m}$  micro-outlet edge across the 4-minute O<sub>2</sub> oscillation (7-12-2-7%). B) The micro-outlet gas exchange device imposes 4-minute oxygen oscillations for one minute at a baseline concentration of 7%, 12%, 2%, and 7% respectively. Mean values are taken from the first minute at baseline and the last 15 seconds at 12%, 2%, and 7% (n = 148 capillaries). *p* values are based on the post-hoc Tukey's multiple comparisons test after significant repeated measures ANOVA and are indicated in the figure with a *p* < 0.05 considered to be significant. Box and whisker plots show minimum, median, maximum, and associated quartiles.

**A**



**B**

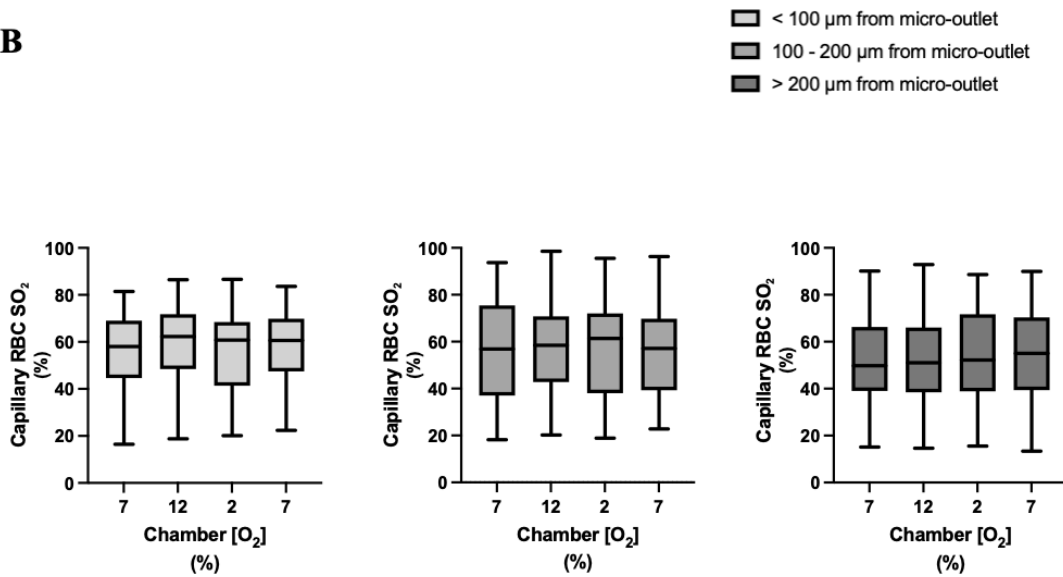


**Figure AI.26 Capillary RBC oxygen saturation responses in capillaries at various distances outside the 600  $\mu\text{m}$  micro-outlet edge.** A) Time series plot showing the mean capillary RBC oxygen saturation ( $\text{SO}_2$ ) in capillaries outside the 600  $\mu\text{m}$  micro-outlet edge across the 4-minute  $\text{O}_2$  oscillation (7-12-2-7%). B) The micro-outlet gas exchange device imposes 4-minute oxygen oscillations across 7 animals for one minute at a baseline concentration of 7%, one minute at 12%, one minute at 2%, and one minute at 7%. Panel B shows capillaries within 100  $\mu\text{m}$  from the micro-outlet edge ( $n = 37$  capillaries), capillaries between 100 – 200  $\mu\text{m}$  from the outlet edge ( $n = 50$  capillaries), and capillaries greater than 200  $\mu\text{m}$  from the outlet edge ( $n = 38$  capillaries) respectively.  $p$  values based on Tukey's multiple comparisons test after significant repeated measures ANOVA are indicated in the figure with a  $p < 0.05$  considered to be significant. Box and whisker plots show minimum, median, maximum, and associated quartile.

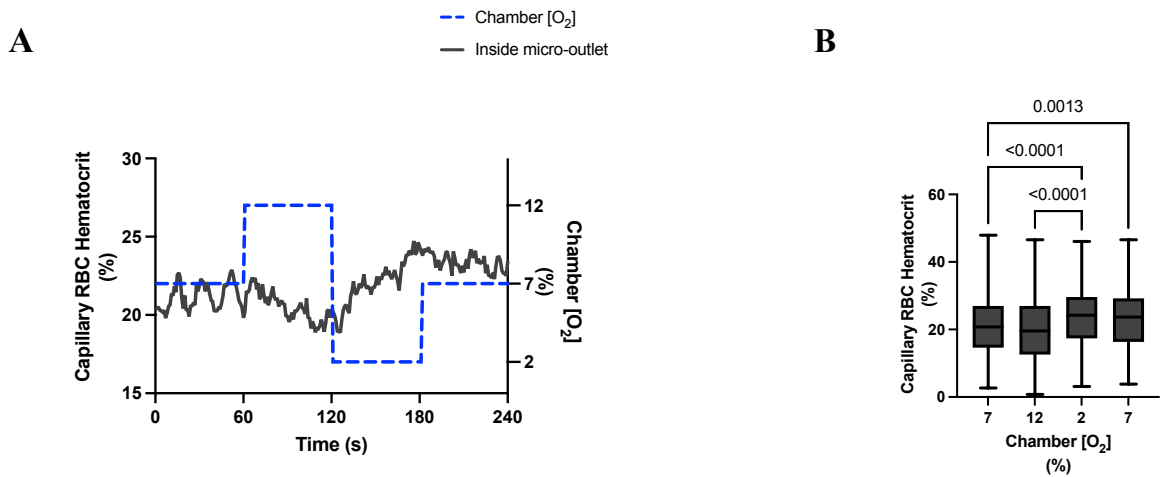
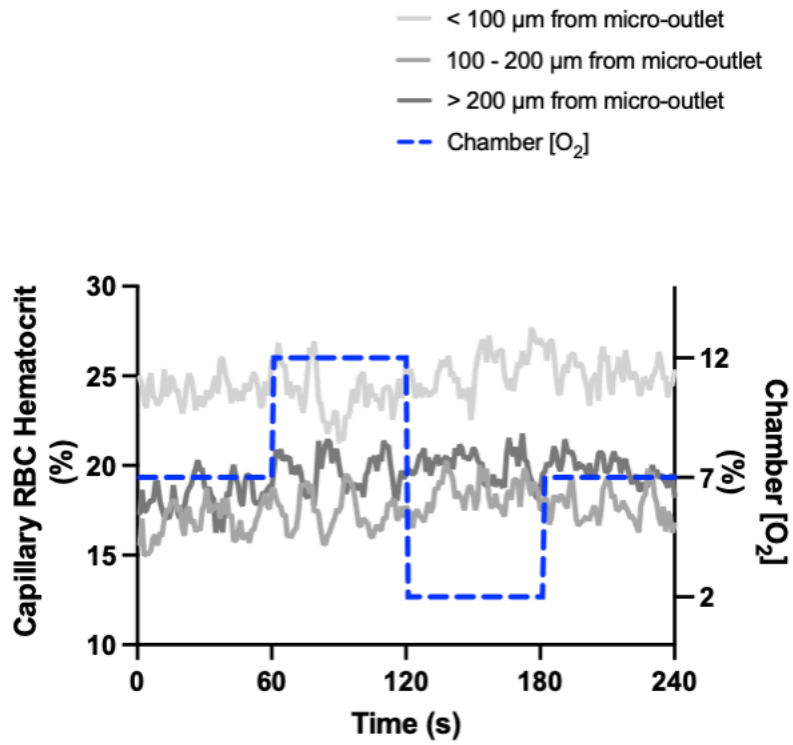
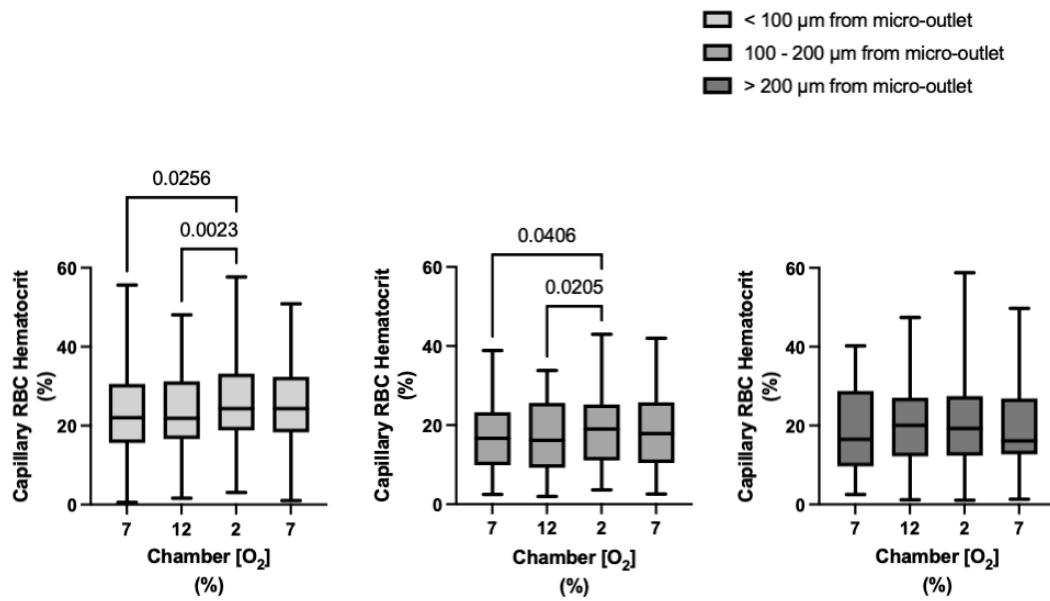


**Figure AI.27 Capillary hematocrit levels in response to oxygen oscillations for capillaries directly overlying the 600  $\mu\text{m}$  micro-outlet.** A) Time series plot showing the mean capillary hematocrit in capillaries overlying the 600  $\mu\text{m}$  micro-outlet across the 4-minute  $\text{O}_2$  oscillation (7-12-2-7%). B) The micro-outlet gas exchange device imposes 4-minute oxygen oscillations for one minute at a baseline concentration of 7%, one minute at 12%, one minute at 2%, and one minute at 7%. Mean hematocrit values are taken from the first entire minute at baseline and the last 15 seconds at 12%, 2%, and 7% ( $n = 110$  capillaries).  $p$  values based on Dunn's multiple comparisons test after significant Friedman test are indicated in the figure with a  $p < 0.05$  considered to be significant.

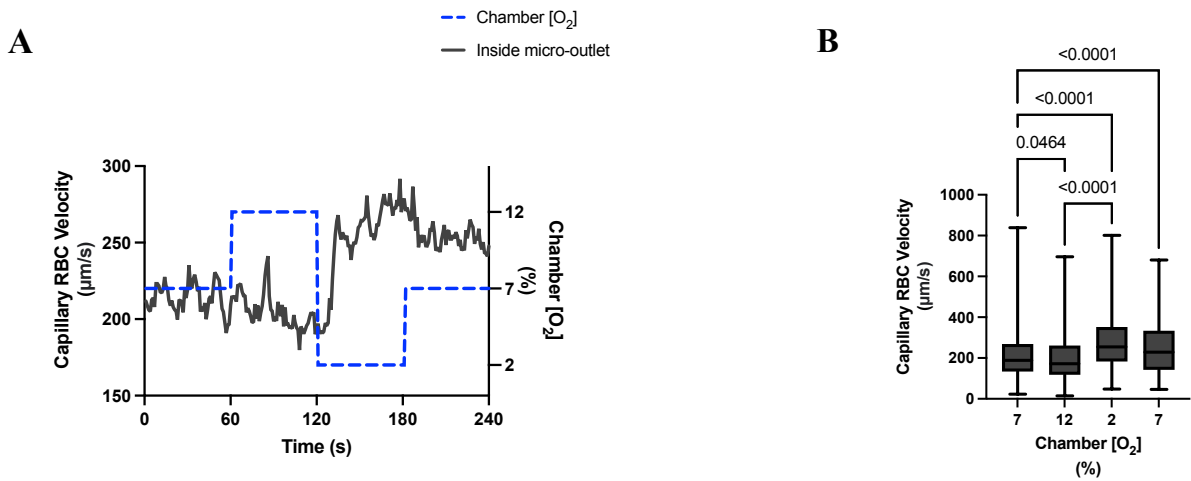
**A**



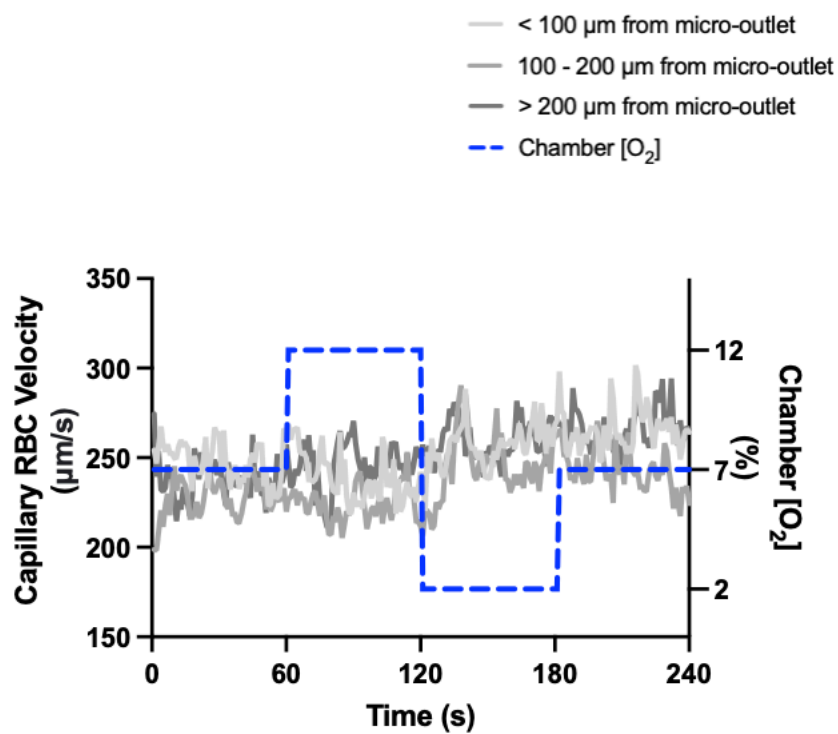
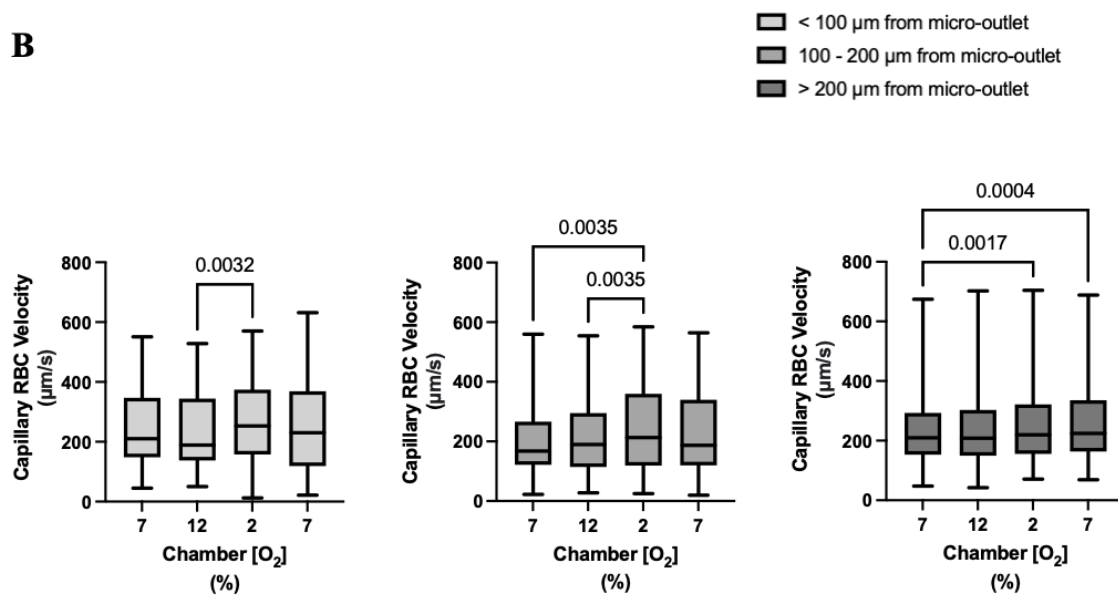
**B**



**Figure AI.28 Capillary hematocrit values in capillaries at various distances outside the 600  $\mu\text{m}$  micro-outlet edge.** A) Time series plot showing the mean capillary hematocrit in capillaries outside the 600  $\mu\text{m}$  micro-outlet edge across the 4-minute  $\text{O}_2$  oscillation (7-12-2-7%). B) The micro-outlet gas exchange device imposes 4-minute oxygen oscillations for one minute at a baseline concentration of 7%, one minute at 12%, one minute at 2%, and one minute at 7%. Mean hematocrit values are taken from the first entire minute at baseline and the last 15 seconds at 12%, 2%, and 7% ( $n = 160$  capillaries). Panel B shows capillaries within 100  $\mu\text{m}$  from the micro-outlet edge ( $n = 40$  capillaries), capillaries between 100 – 200  $\mu\text{m}$  from the outlet edge ( $n = 56$  capillaries), and capillaries greater than 200  $\mu\text{m}$  from the outlet edge ( $n = 64$  capillaries) respectively.  $p$  values based on Dunn's multiple comparisons test after significant Friedman test are indicated in the figure with a  $p < 0.05$  considered to be significant.

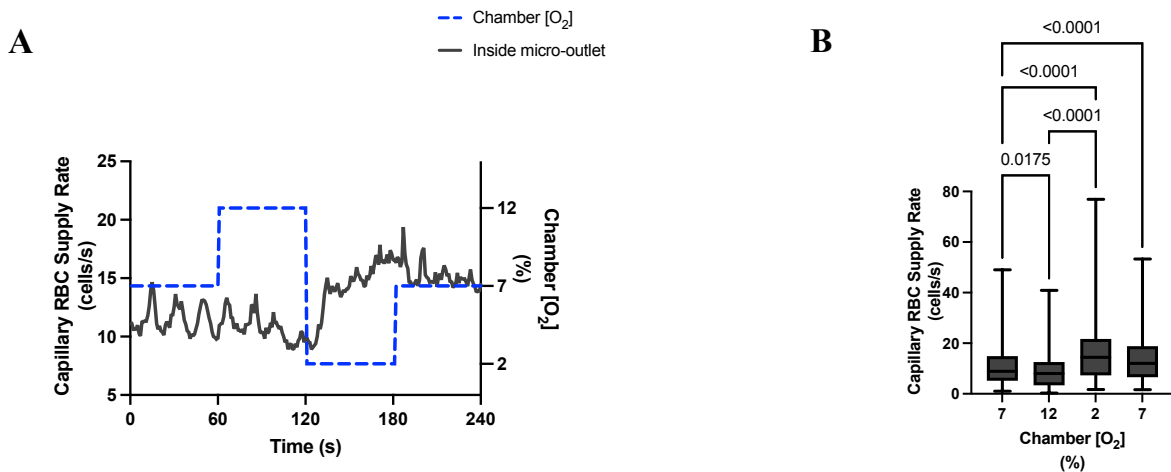


**Figure AI.29 Capillary RBC velocity for capillaries overlying the 600  $\mu\text{m}$  micro-outlet following 4-minute oxygen oscillations.** A) Time series plot showing the mean RBC velocity for capillaries overlying the 600  $\mu\text{m}$  micro-outlet across the 4-minute  $\text{O}_2$  oscillation (7-12-2-7%). B) Oxygen oscillations consisted of one minute at a baseline oxygen concentration of 7% and one minute at 12%, 2%, and 7% oxygen concentration. The mean was calculated for the entire first minute at a baseline 7% and the last 15 seconds of each of the following oxygen concentrations at 12%, 2%, and 7% ( $n = 110$  capillaries).  $p$  values based on Dunn's multiple comparisons test after the significant Friedman test are indicated in the figure with a  $p < 0.05$  considered to be significant. Box and whisker plots show minimum, median, maximum, and associated quartiles.

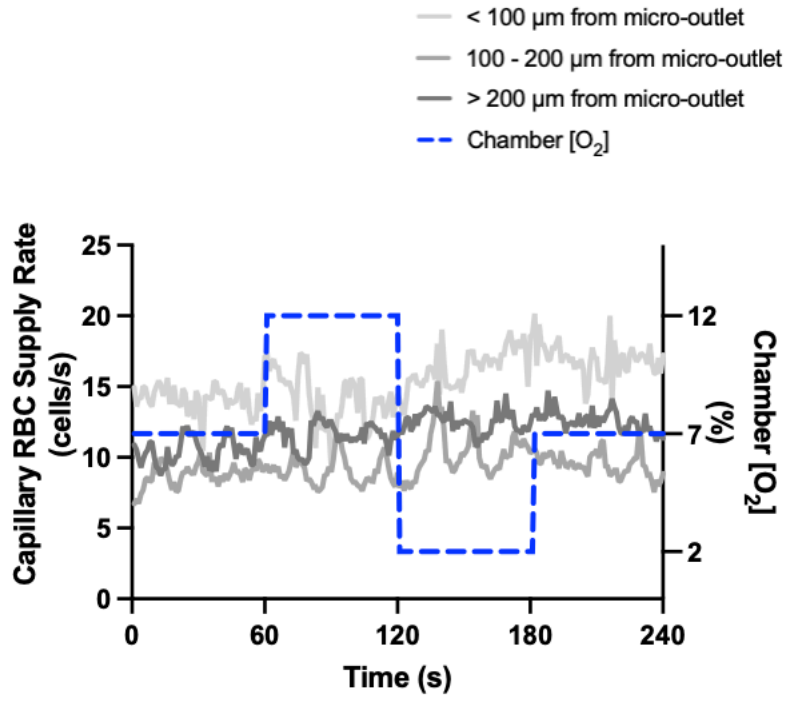
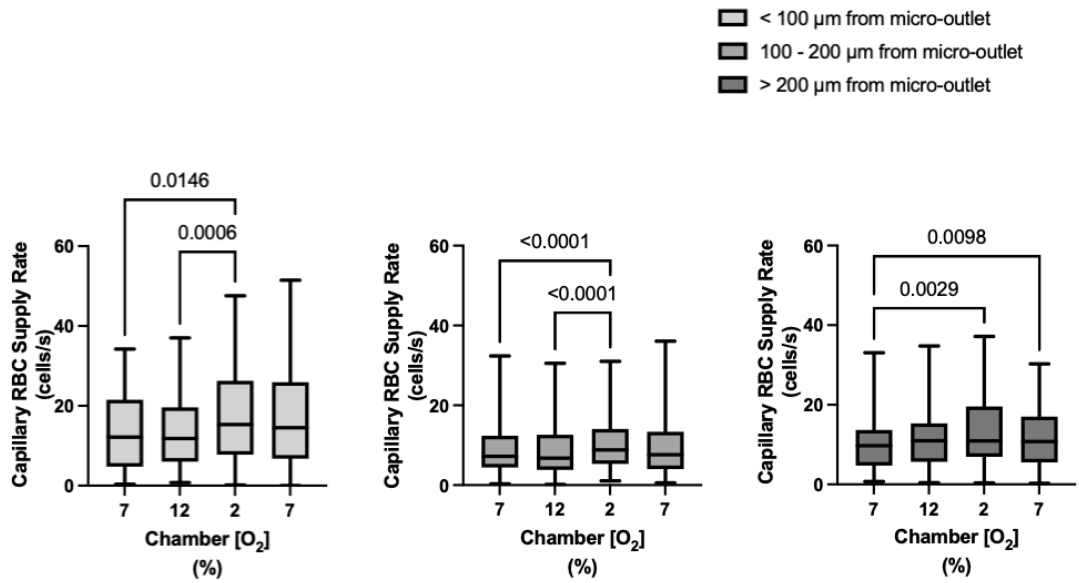
**A****B**

**Figure AI.30 Capillary RBC velocity for capillaries outside the 600  $\mu\text{m}$  micro-outlet at varying distances from the outlet edge following 4-minute oxygen oscillations. A)**

Time series plot showing the mean RBC velocity for capillaries outside the 600  $\mu\text{m}$  micro-outlet at varying distances across the 4-minute  $\text{O}_2$  oscillation (7-12-2-7%). B) Oscillations consisted of one minute at a baseline oxygen concentration of 7% followed by one minute at 12%, 2%, and 7% oxygen concentration. The mean was calculated for the entire first minute at 7% and the last 15 seconds of the following oxygen concentrations of 12%, 2%, and 7%. Panel A shows capillaries within 100  $\mu\text{m}$  from the micro-outlet edge (n = 40 capillaries), panel B shows capillaries between 100 – 200  $\mu\text{m}$  from the outlet edge (n = 56 capillaries), and panel C shows capillaries greater than 200  $\mu\text{m}$  from the outlet edge (n = 64 capillaries). p values based on Dunn's multiple comparisons test after significant Friedman test are indicated in the figure with a  $p < 0.05$  considered to be significant. Box and whisker plots show minimum, median, maximum, and associated quartiles.



**Figure AI.31 Capillary RBC supply rate for capillaries inside the 600  $\mu\text{m}$  micro-outlet following 4-minute oxygen oscillations.** A) Time series plot showing mean RBC supply rate for capillaries inside the 600  $\mu\text{m}$  micro-outlet across the 4-minute  $\text{O}_2$  oscillation (7-12-2-7%). B) Oxygen oscillations consisted of one minute at a baseline oxygen concentration of 7% and one minute at 12%, 2%, and 7% oxygen concentration. The mean was calculated for the entire first minute at a baseline 7% and the last 15 seconds of each of the following oxygen concentrations at 12%, 2%, and 7% ( $n = 110$  capillaries).  $p$  values based on Dunn's multiple comparisons test after the significant Friedman test are indicated in the figure with a  $p < 0.05$  considered to be significant. Box and whisker plots show minimum, median, maximum, and associated quartiles.

**A****B**

**Figure AI.32 Capillary RBC supply rate for capillaries outside the 600  $\mu\text{m}$  micro-outlet at varying distances from the outlet edge following 4-minute oxygen oscillations.**

A) Time series plot showing mean RBC supply rate for capillaries outside the 600  $\mu\text{m}$  micro-outlet at varying distances across the 4-minute  $\text{O}_2$  oscillation (7-12-2-7%). B) Oscillations consisted of one minute at a baseline oxygen concentration of 7% followed by one minute at 12%, 2%, and 7% oxygen concentration. Means were calculated for comparison from the first minute at 7% and the last 15 seconds of the following oxygen concentrations of 12%, 2%, and 7%. Panel B shows capillaries within 100  $\mu\text{m}$  from the micro-outlet edge ( $n = 40$  capillaries), capillaries between 100 – 200  $\mu\text{m}$  from the outlet edge ( $n = 56$  capillaries), and capillaries greater than 200  $\mu\text{m}$  from the outlet edge respectively ( $n = 64$  capillaries).  $p$  values based on Dunn's multiple comparisons test after significant Friedman test are indicated in the figure with a  $p < 0.05$  considered to be significant. Box and whisker plots show minimum, median, maximum, and associated quartiles.

## 600 $\mu\text{m}$ Micro-Outlet Oxygen Challenge Data

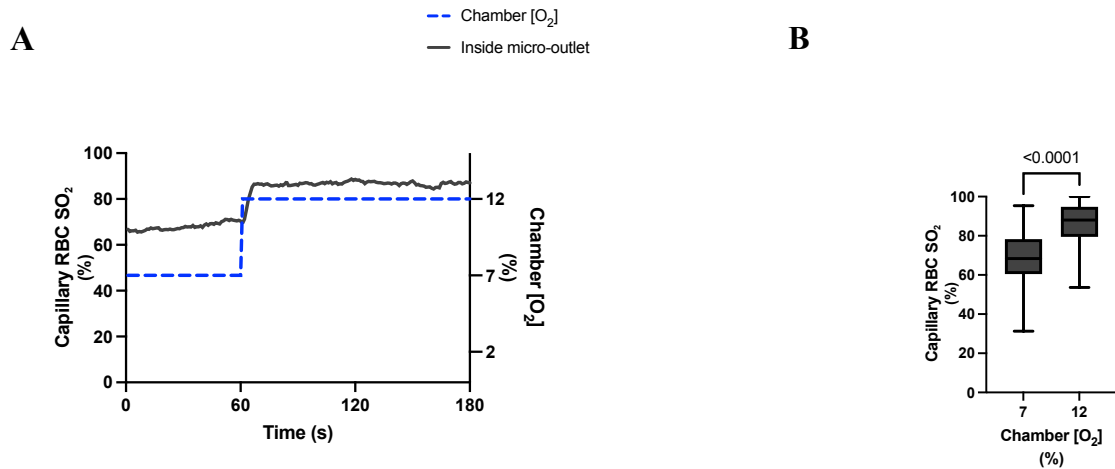
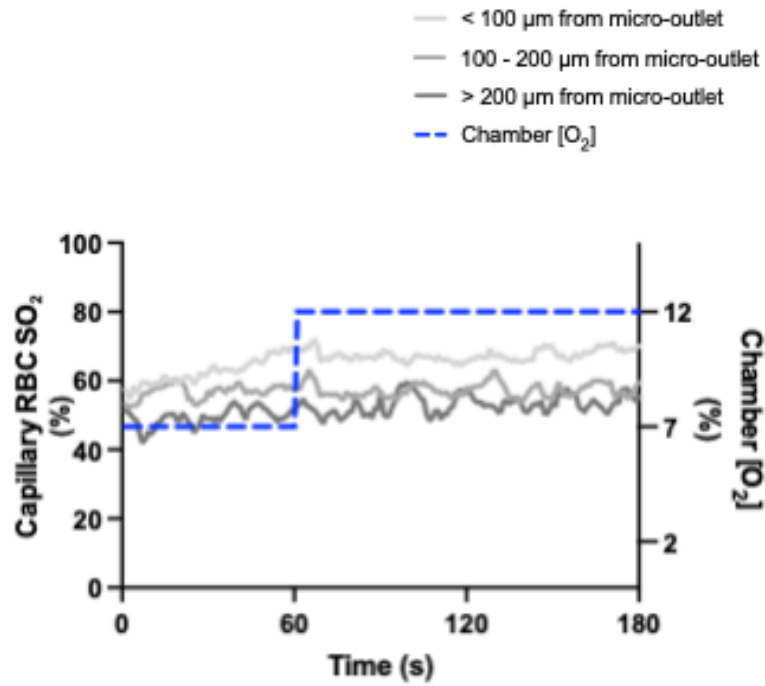
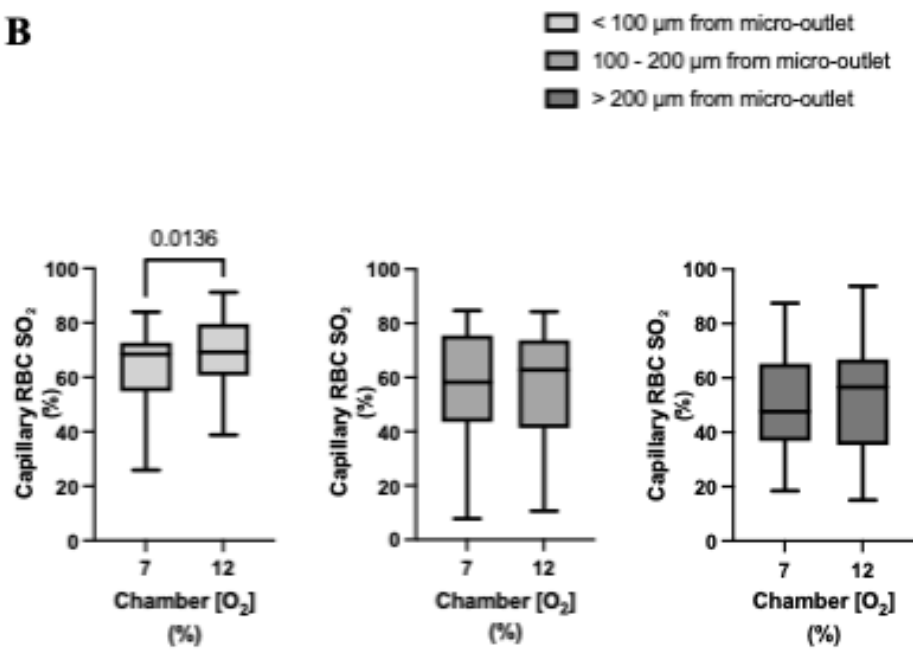


**Figure A1.33 Capillary RBC oxygen saturation (SO<sub>2</sub>) in response to high oxygen challenges for capillaries directly overlying the 600  $\mu\text{m}$  micro-outlet.** A) Time series plot showing mean capillary RBC oxygen saturation for capillaries overlying the micro-outlet in response to high (7-12%) oxygen challenges. B) Oxygen challenges consisted of one minute at a baseline oxygen concentration of 7% followed by two minutes at 12%. The mean was calculated for the entire first minute at 7% and the last 15 seconds at a 12% oxygen concentration ( $n = 83$  capillaries.  $p$  values based on paired t tests and values indicated in the figure with a  $p < 0.05$  considered to be significant. Box and whisker plots show minimum, median, maximum, and associated quartiles.

**A**



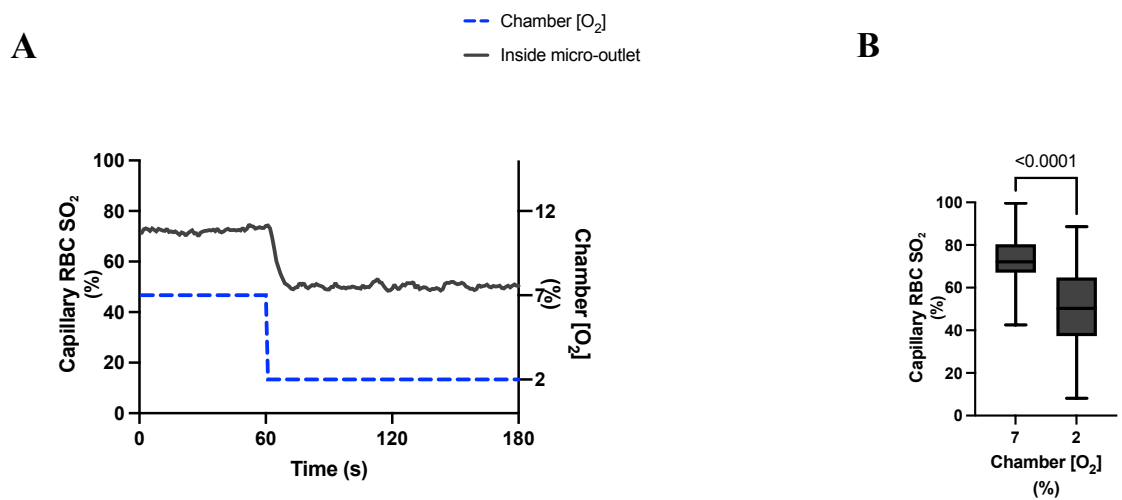
**B**



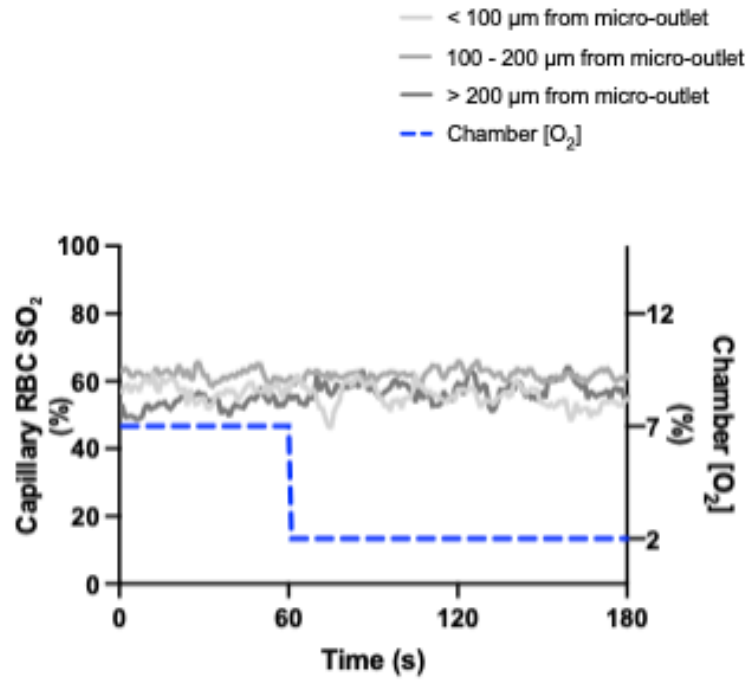
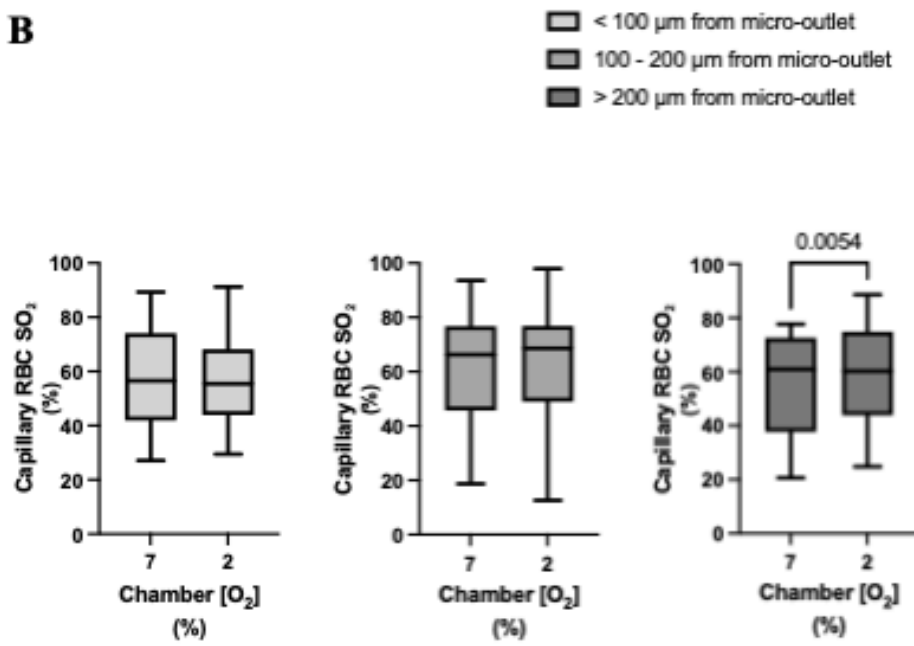
**Figure AI.34 Capillary RBC oxygen saturation responses in capillaries at various distances outside the 600  $\mu\text{m}$  micro-outlet edge in response to high oxygen challenges.**

A) Time series plot showing mean capillary RBC oxygen saturation ( $\text{SO}_2$ ) for capillaries outside the micro-outlet edge at varying distances during high (7-12%) oxygen challenges.

B) Oxygen challenges consisted of one minute at a baseline oxygen concentration of 7% followed by one minute at 12%. The mean was calculated for the entire first minute at 7% and the last 15 seconds at a 12% oxygen concentration. Panel B shows capillaries within 100  $\mu\text{m}$  from the micro-outlet edge ( $n = 21$  capillaries), capillaries between 100 – 200  $\mu\text{m}$  from the outlet edge ( $n = 22$  capillaries), and capillaries greater than 200  $\mu\text{m}$  from the outlet edge ( $n = 19$  capillaries) respectively.  $p$  values based on paired  $t$  tests and values indicated in the figure with a  $p < 0.05$  considered to be significant. Box and whisker plots show minimum, median, maximum, and associated quartiles.



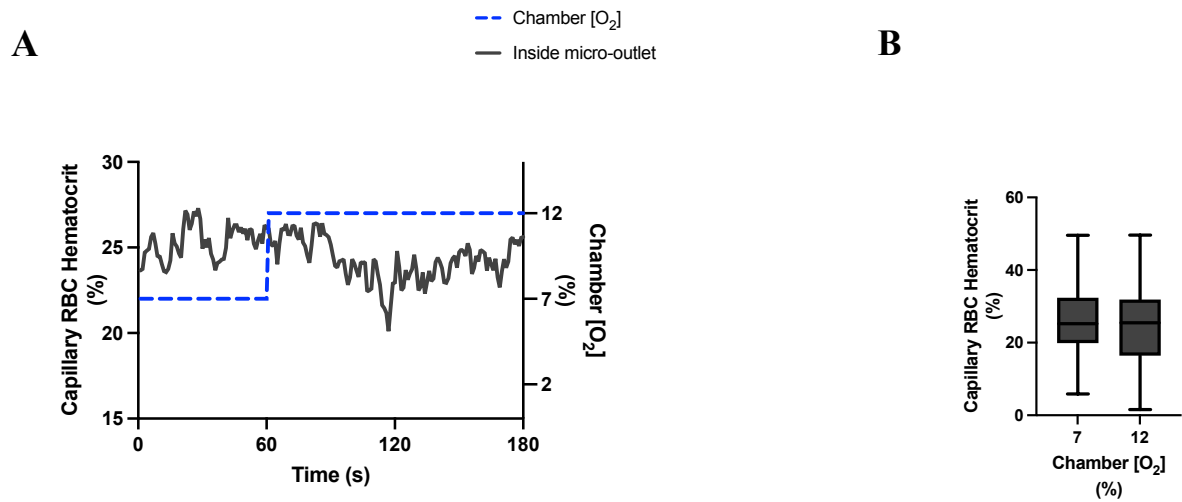
**Figure AI.35 Capillary RBC oxygen saturation in response to low oxygen challenges for capillaries directly overlying the 600  $\mu\text{m}$  micro-outlet.** A) Time series plot showing mean capillary RBC oxygen saturation (SO<sub>2</sub>) for capillaries overlying the micro-outlet during low (7-2%) oxygen challenges. B) Oxygen challenges consisted of one minute at a baseline oxygen concentration of 7% followed by two minutes at 2%. The mean was calculated for the first minute at 7% and the last 15 seconds at a 2% oxygen concentration ( $n = 79$  capillaries).  $p$  values based on paired t-tests and values indicated in the figure with a  $p < 0.05$  are significant. Box and whisker plots show minimum, median, maximum, and associated quartiles.

**A****B**

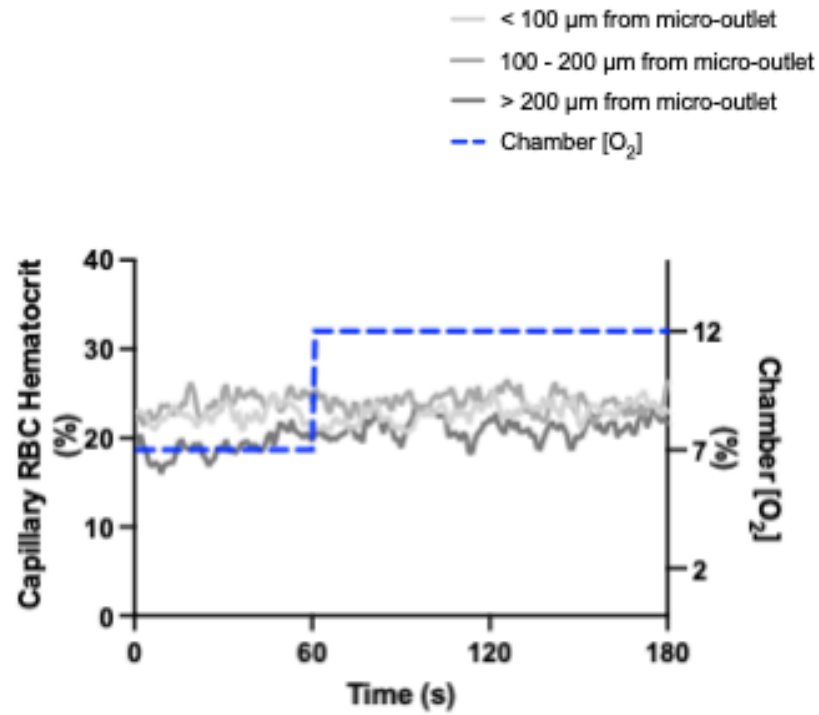
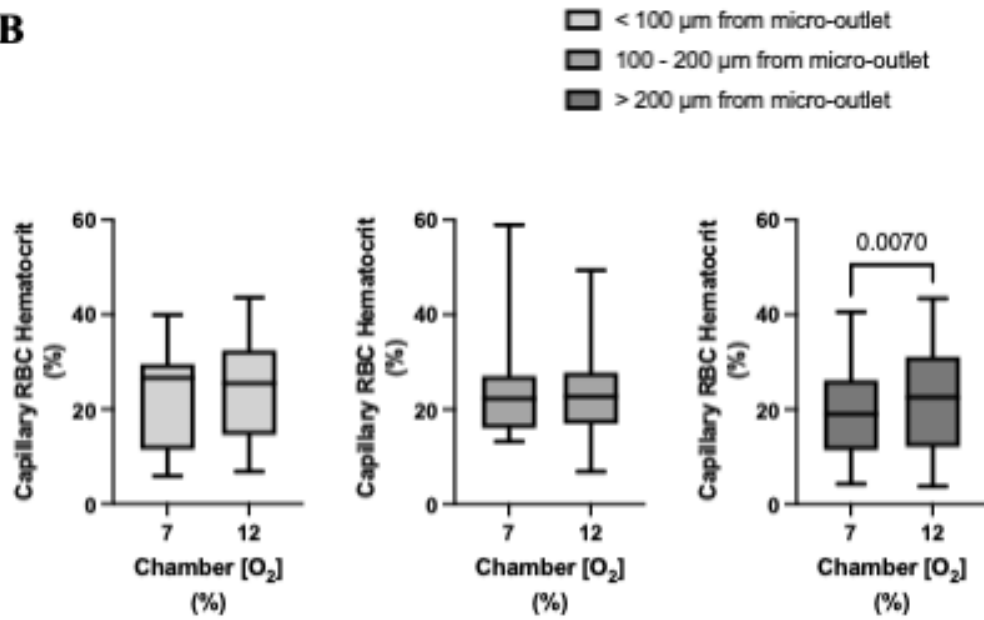
**Figure AI.36 Capillary RBC oxygen saturation responses in capillaries at various distances outside the 600  $\mu\text{m}$  micro-outlet edge in response to low oxygen challenges.**

A) Time series plot showing mean capillary RBC oxygen saturation ( $\text{SO}_2$ ) for capillaries outside the micro-outlet edge at varying distances during low (7-2%) oxygen challenges.

B) Oxygen challenges consisted of one minute at a baseline oxygen concentration of 7% followed by two minutes at 2%. The mean was calculated for the first minute at 7% and the last 15 seconds at a 2% oxygen concentration. Panel B shows capillaries within 100  $\mu\text{m}$  from the micro-outlet edge ( $n = 15$  capillaries), capillaries between 100 – 200  $\mu\text{m}$  from the outlet edge ( $n = 21$  capillaries), and capillaries greater than 200  $\mu\text{m}$  from the outlet edge ( $n = 17$  capillaries), respectively.  $p$  values based on paired t-tests and values indicated in the figure with a  $p < 0.05$  are significant. Box and whisker plots show minimum, median, maximum, and associated quartiles.



**Figure AI.37 Capillary hematocrit levels in response to high oxygen challenges for capillaries directly overlying the 600  $\mu\text{m}$  micro-outlet.** A) Time series plot showing mean capillary hematocrit levels for capillaries overlying the micro-outlet during high (7-12%) oxygen challenges. B) Oxygen challenges consisted of one minute at a baseline oxygen concentration of 7% followed by two minutes at 12%. The mean was calculated for the entire first minute at 7% and the last 15 seconds at a 12% oxygen concentration ( $n = 49$  capillaries).  $p$  values based on paired Wilcoxon  $t$  test and values with a  $p < 0.05$  considered to be significant. Box and whisker plots show minimum, median, maximum, and associated quartiles.

**A****B**

**Figure AI.38 Capillary hematocrit levels in capillaries at various distances outside the 600  $\mu\text{m}$  micro-outlet edge in response to high oxygen challenges.** A) Time series plot showing mean capillary hematocrit levels for capillaries outside the micro-outlet at varying distances during high (7-12%) oxygen challenges. B) Oxygen challenges consisted of one minute at a baseline oxygen concentration of 7% followed by two minutes at 12%. The mean was calculated for the entire first minute at 7% and the last 15 seconds at a 12% oxygen concentration. Panel B shows capillaries within 100  $\mu\text{m}$  from the micro-outlet edge ( $n = 27$  capillaries), capillaries between 100 – 200  $\mu\text{m}$  from the outlet edge ( $n = 22$  capillaries), and capillaries greater than 200  $\mu\text{m}$  from the outlet edge ( $n = 33$  capillaries) respectively  $p$  values based on paired Wilcoxon t test and values indicated in the figure with a  $p < 0.05$  considered to be significant. Box and whisker plots show minimum, median, maximum, and associated quartiles.

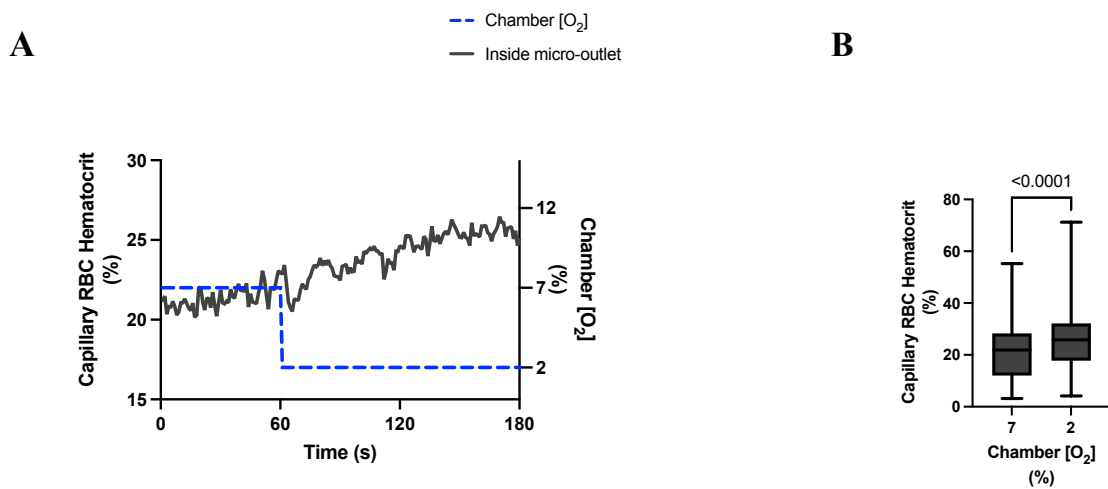
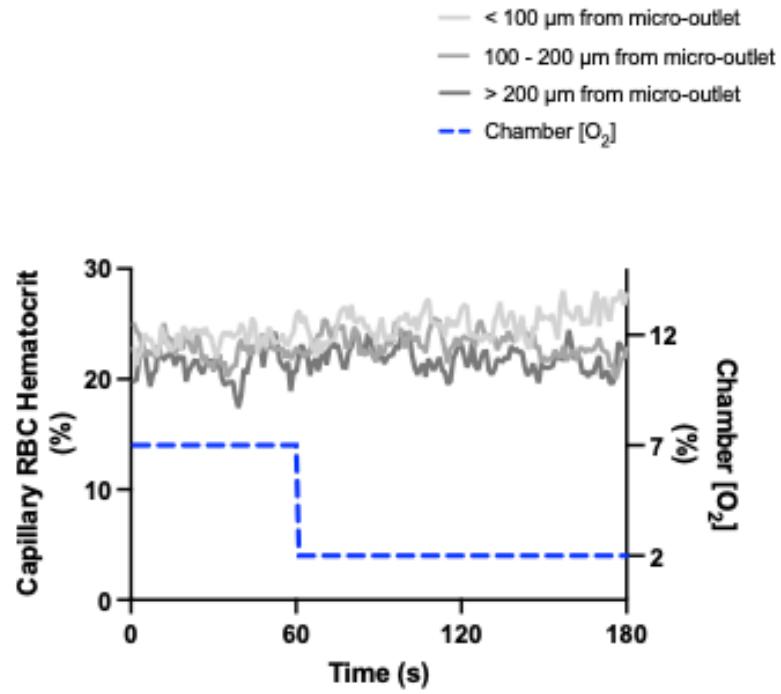
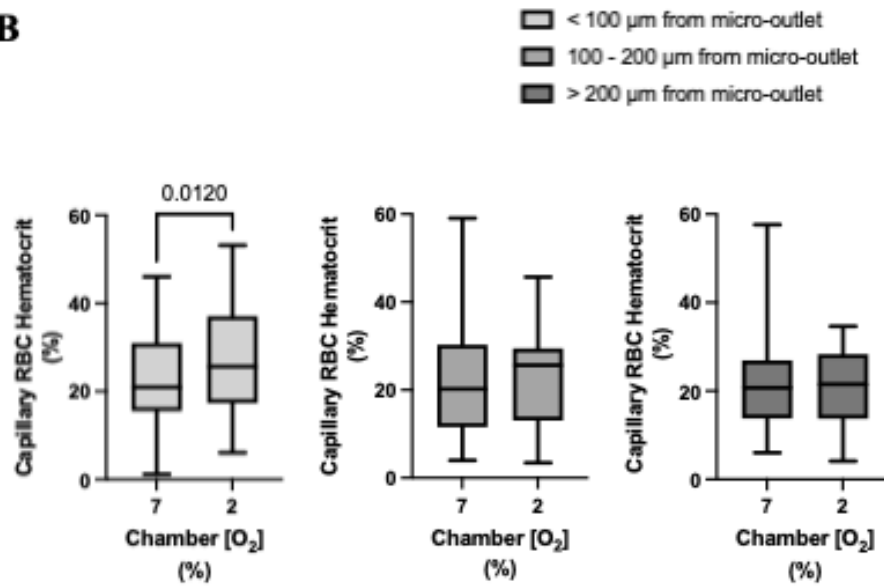


**Figure AI.39 Capillary hematocrit levels in response to low oxygen challenges for capillaries directly overlying the 600  $\mu\text{m}$  micro-outlet.** A) Time series plot showing mean capillary hematocrit levels for capillaries overlying the micro-outlet during low (7-2%) oxygen challenges. B) Oxygen challenges consisted of one minute at a baseline oxygen concentration of 7% followed by two minutes at 2%. The mean was calculated for the first minute at 7% and the last 15 seconds at a 2% oxygen concentration ( $n = 93$  capillaries).  $p$  values based on paired Wilcoxon t test and values indicated in the figure with a  $p < 0.05$  considered to be significant. Box and whisker plots show minimum, median, maximum, and associated quartiles.

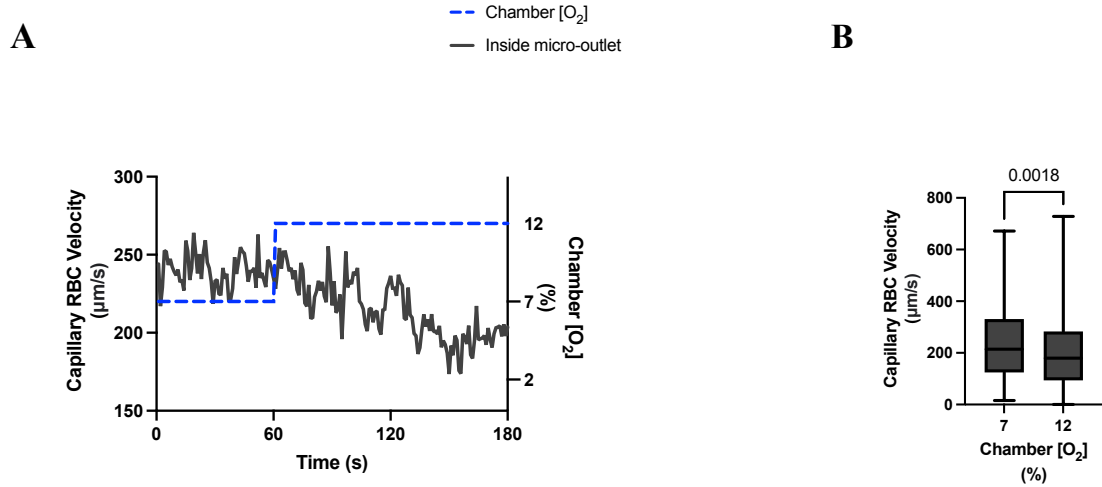
**A**



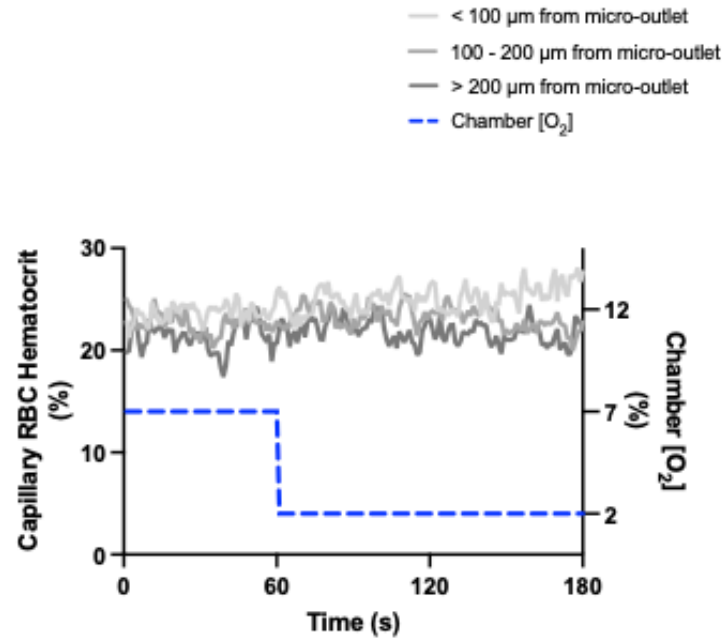
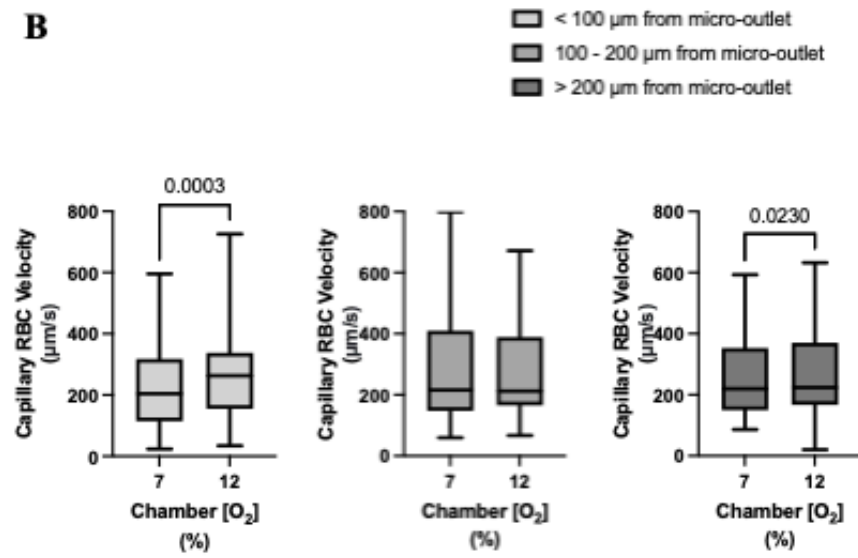
**B**



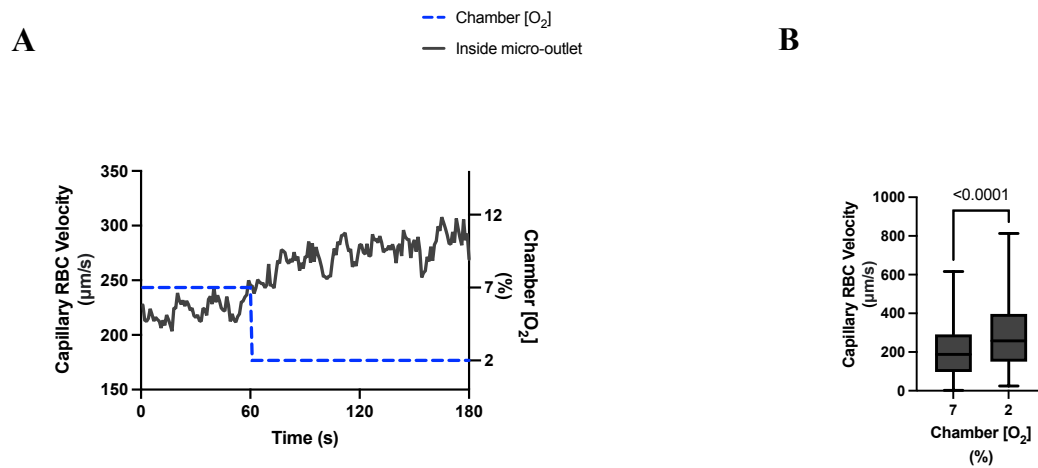
**Figure AI.40 Capillary hematocrit levels in capillaries at various distances outside the 600  $\mu\text{m}$  micro-outlet edge in response to low oxygen challenges.** A) Time series plot showing mean capillary hematocrit levels for capillaries outside the micro-outlet at varying distances during low (7-2%) oxygen challenges. B) Oxygen challenges consisted of one minute at a baseline oxygen concentration of 7% followed by two minutes at 2%. The mean was calculated for the first minute at 7% and the last 15 seconds at a 2% oxygen concentration. Panel B shows capillaries within 100  $\mu\text{m}$  from the micro-outlet edge ( $n = 18$  capillaries), capillaries between 100 – 200  $\mu\text{m}$  from the outlet edge ( $n = 25$  capillaries), and capillaries greater than 200  $\mu\text{m}$  from the outlet edge ( $n = 30$  capillaries) respectively.  $p$  values based on paired Wilcoxon t-test and values indicated in the figure with a  $p < 0.05$  are significant. Box and whisker plots show minimum, median, maximum, and associated quartiles.



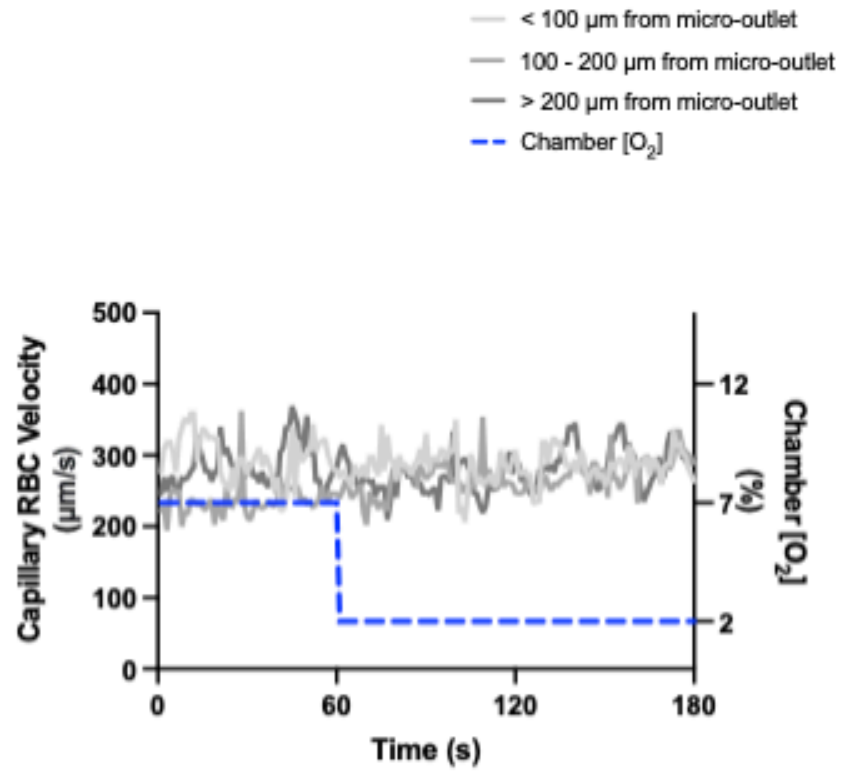
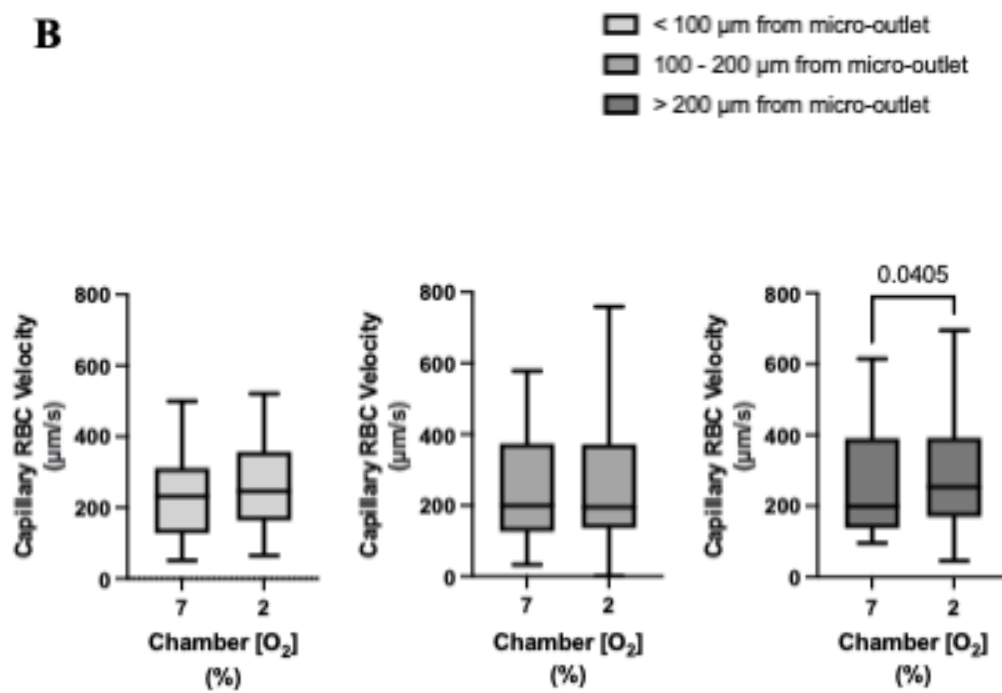
**Figure A1.41 Capillary RBC velocity response to high oxygen challenges for capillaries directly overlying the 600 µm micro-outlet.** A) Time series plot showing mean capillary RBC velocity for capillaries overlying the micro-outlet during high (7-12%) oxygen challenges. B) Oxygen challenges consisted of one minute at a baseline oxygen concentration of 7% followed by two minutes at 12%. The mean was calculated for the first minute at 7% and the last 15 seconds at a 12% oxygen concentration (n = 49 capillaries). Box and whisker plots show minimum, median, maximum, and associated quartiles.

**A****B**

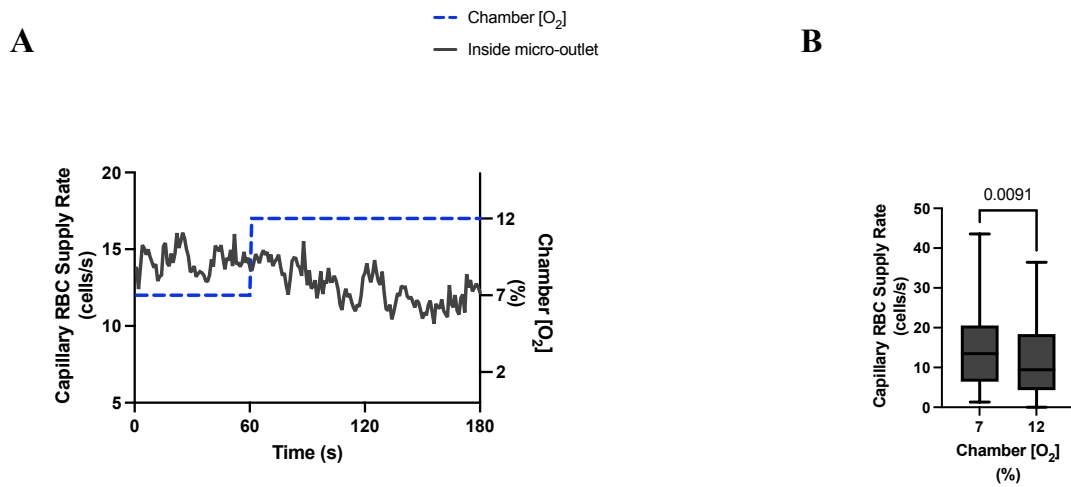
**Figure AI.42 Capillary RBC velocity levels in capillaries at various distances outside the 600  $\mu\text{m}$  micro-outlet edge in response to high oxygen challenges.** A) Time series plot showing mean capillary RBC velocity for capillaries outside the micro-outlet at varying distances during high (7-12%) oxygen challenges. B) Oxygen challenges consisted of one minute at a baseline oxygen concentration of 7% followed by two minutes at 12%. The mean was calculated for the first minute at 7% and the last 15 seconds at 12% oxygen concentration. Panel B shows capillaries within 100  $\mu\text{m}$  from the micro-outlet edge ( $n = 27$  capillaries), capillaries between 100 – 200  $\mu\text{m}$  from the outlet edge ( $n = 22$  capillaries), and capillaries greater than 200  $\mu\text{m}$  from the outlet edge ( $n = 33$  capillaries) respectively.  $p$  values based on paired Wilcoxon t-test and values indicated in the figure with a  $p < 0.05$  are significant. Box and whisker plots show minimum, median, maximum, and associated quartiles.



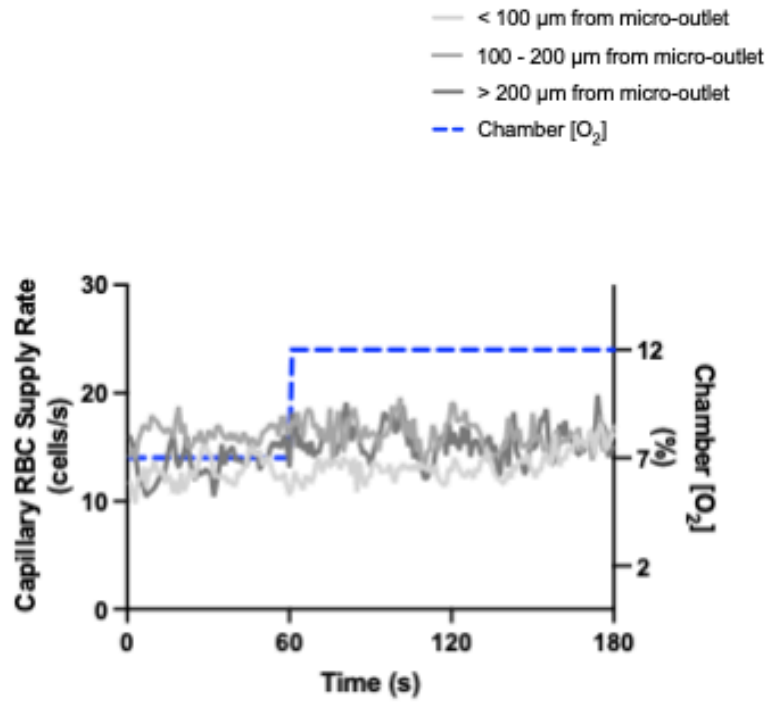
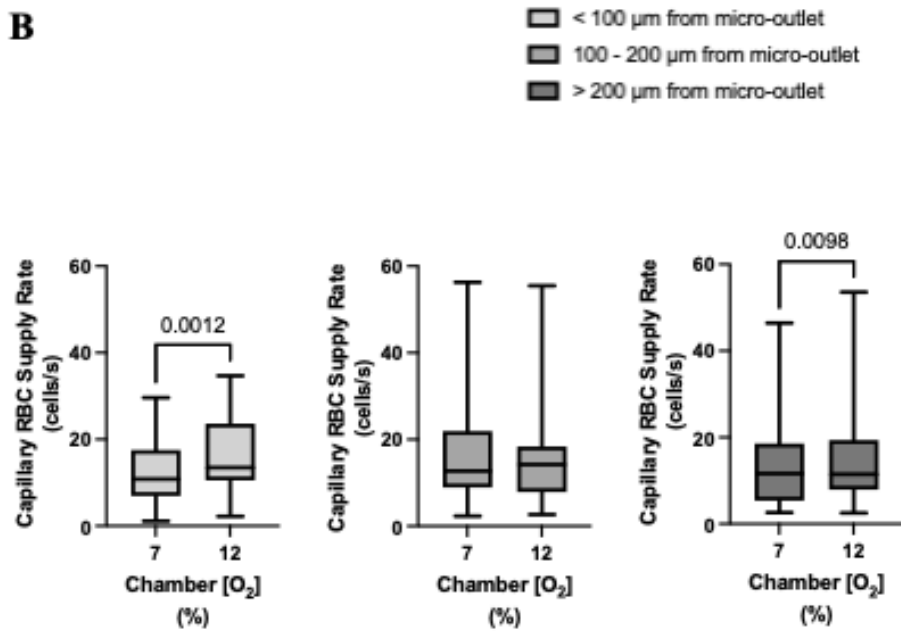
**Figure AI.43 Capillary RBC velocity response to low oxygen challenges for capillaries directly overlying the 600 µm micro-outlet.** A) Time series plot showing mean capillary RBC velocity for capillaries overlying the micro-outlet during low (7-2%) oxygen challenges. B) Oxygen challenges consisted of one minute at a baseline oxygen concentration of 7% followed by two minutes at 2%. The mean was calculated from the entire first minute at 7% and the last 15 seconds at 2% oxygen concentration (n = 93 capillaries). *p* values based on paired Wilcoxon t-test and values indicated in the figure with a *p* < 0.05 are significant. Box and whisker plots show minimum, median, maximum, and associated quartiles.

**A****B**

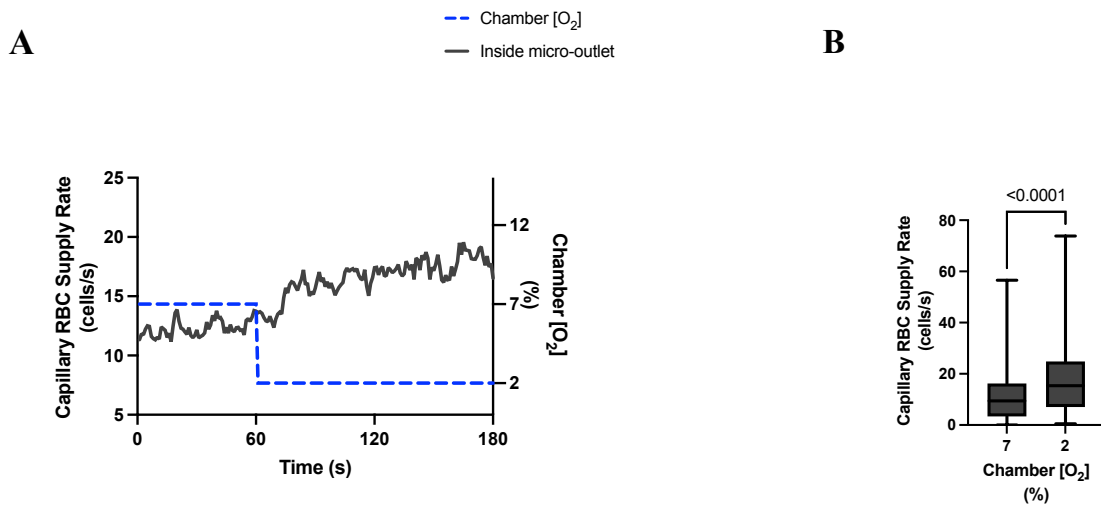
**Figure AI.44 Capillary RBC velocity in capillaries at various distances outside the 600  $\mu\text{m}$  micro-outlet edge in response to low oxygen challenges.** A) Time series plot showing mean capillary RBC velocity for capillaries outside the micro-outlet at varying distances during low (7-2%) oxygen challenges. B) Oxygen challenges consisted of one minute at a baseline oxygen concentration of 7% followed by two minutes at 2%. The mean as calculated from the entire first minute at 7% and the last 15 seconds at a 2% oxygen concentration. Panel B shows capillaries within 100  $\mu\text{m}$  from the micro-outlet edge (n = 18 capillaries), capillaries between 100 – 200  $\mu\text{m}$  from the outlet edge (n = 25 capillaries), and capillaries greater than 200  $\mu\text{m}$  from the outlet edge (n = 30 capillaries) respectively. *p* values based on paired Wilcoxon t-test and values indicated in the figure with a *p* < 0.05 are significant. Box and whisker plots show minimum, median, maximum, and associated quartiles.



**Figure AI.45 Capillary RBC supply rate response to high oxygen challenges for capillaries directly overlying the 600  $\mu\text{m}$  micro-outlet.** A) Time series plot showing mean capillary RBC supply rate for capillaries overlying the micro-outlet during high (7-12%) oxygen challenges. B) Oxygen challenges consisted of one minute at a baseline oxygen concentration of 7% followed by two minutes at 12%. The mean was calculated from the entire first minute at 7% and the last 15 seconds at a 12% oxygen concentration ( $n = 49$  capillaries).  $p$  values based on paired Wilcoxon t-test and values indicated in the figure with a  $p < 0.05$  are significant. Box and whisker plots show minimum, median, maximum, and associated quartiles.

**A****B**

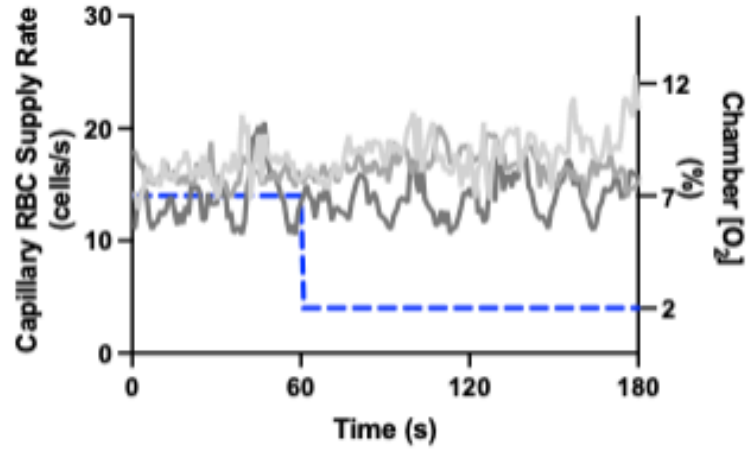
**Figure AI.46 Capillary RBC supply rate in capillaries at various distances outside the 600  $\mu\text{m}$  micro-outlet edge in response to high oxygen challenges.** A) Time series plot showing mean capillary RBC supply rate for capillaries outside the micro-outlet at varying distances during high (7-12%) oxygen challenges. B) Oxygen challenges consisted of one minute at a baseline oxygen concentration of 7% followed by two minutes at 12%. The mean was calculated from the entire first minute at 7% and the last 15 seconds at a 12% oxygen concentration. Panel B shows capillaries within 100  $\mu\text{m}$  from the micro-outlet edge ( $n = 27$  capillaries), capillaries between 100 – 200  $\mu\text{m}$  from the outlet edge ( $n = 22$  capillaries), and capillaries greater than 200  $\mu\text{m}$  from the outlet edge ( $n = 33$  capillaries) respectively.  $p$  values based on paired Wilcoxon t-test and values indicated in the figure with a  $p < 0.05$  are considered significant. Box and whisker plots show minimum, median, maximum, and associated quartiles.



**Figure AI.47 Capillary RBC supply rate in response to low oxygen challenges for capillaries directly overlying the 600  $\mu\text{m}$  micro-outlet.** A) Time series plot showing mean capillary RBC supply rate for capillaries overlying the micro-outlet during low (7-2%) oxygen challenges. B) Oxygen challenges consisted of one minute at a baseline oxygen concentration of 7% followed by two minutes at 2%. The mean was calculated from the entire first minute at 7% and the last 15 seconds at a 2% oxygen concentration ( $n = 93$  capillaries).  $p$  values based on paired Wilcoxon t-test and values indicated in the figure with a  $p < 0.05$  are considered to be significant. Box and whisker plots show minimum, median, maximum, and associated quartiles.

**A**

- < 100  $\mu\text{m}$  from micro-outlet
- 100 - 200  $\mu\text{m}$  from micro-outlet
- > 200  $\mu\text{m}$  from micro-outlet
- - - Chamber  $[\text{O}_2]$

**B**

- < 100  $\mu\text{m}$  from micro-outlet
- ▒ 100 - 200  $\mu\text{m}$  from micro-outlet
- > 200  $\mu\text{m}$  from micro-outlet

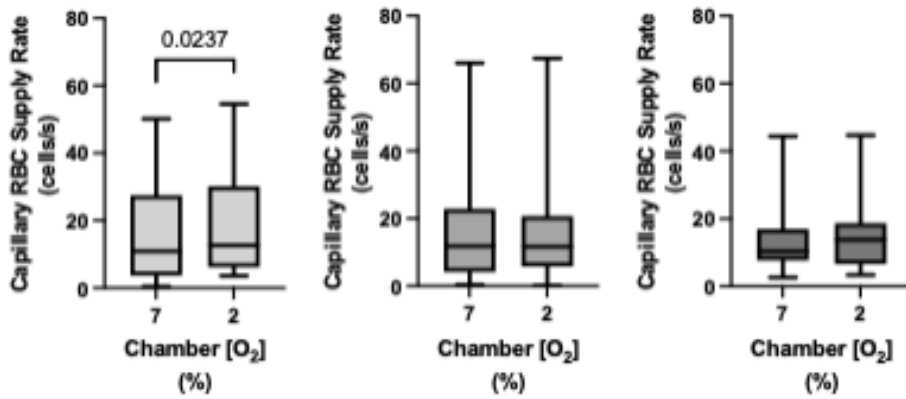


**Figure AI.48 Capillary RBC supply rate in capillaries at various distances outside the 600  $\mu\text{m}$  micro-outlet edge in response to low oxygen challenges.** A) Time series plot showing mean capillary RBC supply rate for capillaries outside the micro-outlet at varying distances during low (7-2%) oxygen challenges. B) Oxygen challenges consisted of one minute at a baseline oxygen concentration of 7% followed by two minutes at 2%. The mean was calculated from the entire first minute at 7% and the last 15 seconds at a 2% oxygen concentration. Panel B shows capillaries within 100  $\mu\text{m}$  from the micro-outlet edge ( $n = 18$  capillaries), capillaries between 100 – 200  $\mu\text{m}$  from the outlet edge ( $n = 25$  capillaries), and capillaries greater than 200  $\mu\text{m}$  from the outlet edge ( $n = 30$  capillaries) respectively.  $p$  values based on paired Wilcoxon t-test and values indicated in the figure with a  $p < 0.05$  considered to be significant. Box and whisker plots show minimum, median, maximum, and associated quartiles.

## Appendix 2



November 13, 2019

Dear: Dr. Graham Fraser, Faculty of Medicine\Division of BioMedical Sciences

Researcher Portal File No.: 20200860

Animal Care File: 19-01-GF

Entitled: (19-01-GF) Microvascular Blood Flow, Regulation, and Insulin Sensitivity in Type 2 Diabetes

Status: Active

**Approval Date: November 13, 2019**

**Annual Report Due: November 13, 2020**

**Ethics Clearance Expires: November 13, 2022**

---

Your Animal Use Protocol (AUP) renewal application to engage in procedures involving animals has been approved for a three-year term. This AUP replaces the previous protocol [[16-01-GF]] as the active ethics clearance associated with this project. Please note the new AUP number when referring to this protocol.

This ethics clearance includes the following Team Members: Dr. Graham Fraser (Principal Investigator)

An Event [Annual Report] will be required following each year of protocol activity.

Should you encounter an unexpected incident that negatively affects animal welfare or the research project relating to animal use, please submit an Event [Incident Report].

Any alterations to the protocol requires prior submission and approval of an Event [Amendment].

Sincerely,

*Anulika Mbakwe*

**ANULIKA MBAKWE | ACC COORDINATOR**

Department of Animal Care Services

Memorial University of Newfoundland

Health Sciences Centre | Room H1848

P: 709-777-6621

E-Mail: [ambakwe@mun.ca](mailto:ambakwe@mun.ca)



## Request to Include Copyright Material

Adobe Reader, minimum version 8, is required to complete this form. Download the latest version at <http://get.adobe.com/reader>. (1) Save the form by clicking on the diskette icon on the upper left side of the screen; (2) Ensure that you are saving the file in PDF format; (3) Specify where you would like to save the file, e.g. Desktop; (4) Review the [How to create and insert a digital signature](#) webpage for step by step instructions; (5) Fill in the required data and save the file; (6) Send the completed form to the copyright holder.

Student Contact Information	
<b>Last name:</b> Kiley	<b>First name:</b> Meghan
<b>Academic Unit:</b> Division of BioMedical Sciences	<b>Degree:</b> MSc
<b>Email Address:</b> mkiley@mun.ca	<b>Telephone No.:</b> 902-388-0144
Copyright Material Request	
<p>I, <u>Meghan Kiley</u>, request that you permit the inclusion of the described material in the thesis/report/practicum listed below and grant an irrevocable, non-exclusive licence to Memorial University of Newfoundland and to Library and Archives Canada to reproduce, lend or sell the material described below as part of my thesis/report/practicum. The title of the thesis/report/practicum is:</p> <p>The development and validation of ultra-thin-film micro-outlet devices for spatially constraining local O<sub>2</sub> perturbations to capillaries</p> <p>to be submitted in partial fulfilment of the requirements for the degree of <u>MSc</u> at Memorial University of Newfoundland.</p>	
Description of the Material to be Included	
<p>Adaptation of a figure showing a visual representation of oxy- and deoxy- hemoglobin molar attenuation coefficient curves and associated visible light spectrum from Figure 1.5 of the thesis:</p> <p>Fraser, G. M. (2012). Modeling Oxygen Transport in Three-Dimensional Capillary Networks. Electronic Thesis and Dissertation Repository. 500. <a href="https://ir.lib.uwo.ca/etd/500">https://ir.lib.uwo.ca/etd/500</a></p>	
Permission of Copyright Holder	
<p>I, <u>Graham Fraser</u>, <small>(Name - type)</small></p>	<p><input checked="" type="checkbox"/> do <input type="checkbox"/> do not grant permission for the indicated use of the material described above.</p>
<p><b>Company/Organization:</b></p>	<p><u>Memorial University of Newfoundland</u></p>
<p><b>Position Title:</b></p>	<p><u>Associate Professor</u></p>
<p><b>Address:</b></p>	<p><u>300 Prince Phillip, Room H-5337</u></p> <p><u>St. John's, NL, A1B3V6</u></p>
<p><b>Signature:</b></p> <p></p>	<p><b>Date:</b> August 26, 2021</p>
<p><i>Note: Signature required on each additional attachment</i></p>	

Memorial University protects privacy and maintains the confidentiality of personal information. The information requested in this form is collected under the general authority of the Memorial University Act (RSNL1990CHAPTERM-7). It is required for administrative purposes of the School of Graduate Studies. If you have any questions about the collection and use of this information please contact the School of Graduate Studies at 709.864.2445 or [sgs@mun.ca](mailto:sgs@mun.ca).

Updated September 2020



## Request to Include Copyright Material

*Adobe Reader, minimum version 8, is required to complete this form.* Download the latest version at <http://get.adobe.com/reader>. (1) Save the form by clicking on the diskette icon on the upper left side of the screen; (2) Ensure that you are saving the file in PDF format; (3) Specify where you would like to save the file, e.g. Desktop; (4) Review the [How to create and insert a digital signature](#) webpage for step by step instructions; (5) Fill in the required data and save the file; (6) Send the completed form to the copyright holder.

Student Contact Information	
<b>Last name:</b> Kiley	<b>First name:</b> Meghan
<b>Academic Unit:</b> Division of BioMedical Sciences	<b>Degree:</b> MSc
<b>Email Address:</b> mkiley@mun.ca	<b>Telephone No.:</b> 902-388-0144
Copyright Material Request	
<p>I, <u>Meghan Kiley</u>, request that you permit the inclusion of the described material in the thesis/report/practicum listed below and grant an irrevocable, non-exclusive licence to Memorial University of Newfoundland and to Library and Archives Canada to reproduce, lend or sell the material described below as part of my thesis/report/practicum. The title of the thesis/report/practicum is:</p> <p style="margin-left: 20px;">The development and validation of ultra-thin-film micro-outlet devices for spatially constraining local O2 perturbations to capillaries</p> <p>to be submitted in partial fulfilment of the requirements for the degree of <u>MSc</u> at Memorial University of Newfoundland.</p>	
Description of the Material to be Included	
<p>Image comparing novel micro-outlets with previous glass designs from Dr. Chris Ellis' laboratory (unpublished images).</p>	
Permission of Copyright Holder	
<p>I, <u>Christopher Ellis</u>, <small>(Name - type)</small> <input checked="" type="checkbox"/> do <input type="checkbox"/> do not grant permission for the indicated use of the material described above.</p>	
<b>Company/Organization:</b>	<u>Western University</u>
<b>Position Title:</b>	<u>Professor Emeritus</u>
<b>Address:</b>	<u>Robarts Research Institute Room 3200</u> <u>London, Ontario, N6A 5C1</u>
<b>Signature:</b> Christopher G Ellis <small>Digitally signed by Christopher G Ellis Location: The University of Western Ontario Date: 2023.09.09 14:15:20 -05'00'</small>	<b>Date:</b> August 26, 2021
<i>Note: Signature required on each additional attachment</i>	

Memorial University protects privacy and maintains the confidentiality of personal information. The information requested in this form is collected under the general authority of the Memorial University Act ([RSNL1990CHAPTERM-7](#)). It is required for administrative purposes of the School of Graduate Studies. If you have any questions about the collection and use of this information please contact the School of Graduate Studies at 709.864.2445 or [sgs@mun.ca](mailto:sgs@mun.ca).

Updated September 2020

JOHN WILEY AND SONS LICENSE  
TERMS AND CONDITIONS

Mar 12, 2023

---

This Agreement between Ms. Meghan Kiley ("You") and John Wiley and Sons ("John Wiley and Sons") consists of your license details and the terms and conditions provided by John Wiley and Sons and Copyright Clearance Center.

License Number 5472110039588

License date Jan 18, 2023

Licensed Content John Wiley and Sons  
Publisher

Licensed Content Acta Physiologica  
Publication

Licensed Content Role of erythrocyte-released ATP in the regulation of microvascular oxygen  
Content Title supply in skeletal muscle

Licensed Content R. S. Sprague, C. G. Ellis, M. L. Ellsworth  
Author

Licensed Content Sep 25, 2015  
Content Date

Licensed Content 216  
Content Volume

Licensed Content 3  
Content Issue

Licensed Content 12  
Content Pages

Type of use Dissertation/Thesis

Requestor type University/Academic

Format Print and electronic

Portion Figure/table

Number of figures/tables 1

Will you be translating? No

Title The development and validation of ultra-thin-film micro-outlet devices for spatially constraining local O<sub>2</sub> perturbations to capillaries

Institution name Memorial University of Newfoundland

Expected presentation date May 2023

Order reference number 1414

Portions figure 2 - Proposed mechanism by which human erythrocytes participate in the sensing of tissue oxygen (O<sub>2</sub>) tension and stimulate increases in blood flow (O<sub>2</sub> delivery) to match that need

Requestor Location Ms. Meghan Kiley  
2 Windsor Drive  
Stratford, PE C1B1N3  
Canada  
Attn: Ms. Meghan Kiley

Publisher Tax ID EU826007151

THE AMERICAN PHYSIOLOGICAL SOCIETY LICENSE  
TERMS AND CONDITIONS

Mar 12, 2023

---

This Agreement between Ms. Meghan Kiley ("You") and The American Physiological Society ("The American Physiological Society") consists of your license details and the terms and conditions provided by The American Physiological Society and Copyright Clearance Center.

License Number 5473070719707

License date Jan 20, 2023

Licensed Content Publisher The American Physiological Society

Licensed Content Publication Am J Physiol- Heart and Circulatory Physiology

Licensed Content Title Capillary communication: the role of capillaries in sensing the tissue environment, coordinating the microvascular, and controlling blood flow

Licensed Content Author Coral L. Murrant, Nicole M. Fletcher

Licensed Content Date Nov 1, 2022

Licensed Content Volume 323

Licensed Content Issue 5

Type of Use Thesis/Dissertation

Requestor type author

Format print and electronic

Portion figures/tables/images

Number of figures/tables/images 1

Will you be translating? no

World Rights no

Order reference number 5678

Title The development and validation of ultra-thin-film micro-outlet devices for spatially constraining local O<sub>2</sub> perturbations to capillaries

Institution name Memorial University of Newfoundland

Expected presentation date May 2023

Order reference number 5678

Portions figure 1A - page H1022

Ms. Meghan Kiley  
2 Windsor Drive